OFFICE OF ONR NAVAL RESEARCH

VISIBILITY OF DISPLAYED INFORMATION
IMAGE DESCRIPTORS FOR DISPLAYS

Curtis R. Carlson and Roger W. Cohen

RCA LABORATORIES
PRINCETON
NEW JERSEY
08540

JULY 1978

FINAL REPORT for the period
10 December 1976 to 31 December 1977

PREPARED FOR THE

NOTICES

Change of Address

Organizations receiving reports on the initial distribution list should confirm correct address. This list is located at the end of the report. Any change of address or distribution should be conveyed to the Office of Naval Research, Code 221, Arlington, Virginia 22217.

Disposition

When this report is no longer needed, it may be transmitted to other authorized organizations. Do not return it to the originator or the monitoring office.

Disclaimer

The findings in this report are not to be construed as an official Department of Defense or Military Department position unless so designated by other official documents.

Reproduction

Reproduction in whole or in part is permitted for any purpose of the United States Government.

UNCLASSIFIED

⑨ *Final rept. 10 Dec 76 - 31 Dec 77*

⑲ REPORT DOCUMENTATION PAGE		READ INSTRUCTIONS BEFORE COMPLETING FORM
1. REPORT NUMBER ⑱ ONR-CR213-120-4F	2. GOVT ACCESSION NO.	3. RECIPIENT'S CATALOG NUMBER
4. TITLE (and Subtitle) ⑥ VISIBILITY OF DISPLAYED INFORMATION.		5. TYPE OF REPORT & PERIOD COVERED Final Report (12-10-76 to 12-31-77)
		6. PERFORMING ORG. REPORT NUMBER ⑭ PRRL-78-CR-34
7. AUTHOR(s) ⑩ Curtis R. Carlson and Roger W. Cohen		8. CONTRACT OR GRANT NUMBER(s) ⑮ N00014-74-C-0184
9. PERFORMING ORGANIZATION NAME AND ADDRESS RCA Laboratories Princeton, NJ 08540		10. PROGRAM ELEMENT, PROJECT, TASK AREA & WORK UNIT NUMBERS ⑫ 274p.
11. CONTROLLING OFFICE NAME AND ADDRESS Office of Naval Research Arlington, VA 22217		12. REPORT DATE ⑪ July 1978
		13. NUMBER OF PAGES 275
14. MONITORING AGENCY NAME & ADDRESS (if different from Controlling Office)		15. SECURITY CLASS. (of this report) Unclassified
		15a. DECLASSIFICATION/DOWNGRADING SCHEDULE N/A

16. DISTRIBUTION STATEMENT (of this Report)

Approved for public release; distribution unlimited.

17. DISTRIBUTION STATEMENT (of the abstract entered in Block 20, if different from Report)

18. SUPPLEMENTARY NOTES

19. KEY WORDS (Continue on reverse side if necessary and identify by block number)

Modulation Transfer Images
Displays Image-Quality Descriptors
Visual Perception Contrast Detection

20. ABSTRACT (Continue on reverse side if necessary and identify by block number)

This report is concerned with the visibility of displayed luminance information, that is, predicting what an observer can see when he views a display. Some of the specific practical problems addressed are: When does a change in display modulation transfer become visible? What are the perceptual effects of sampling and a visible raster structure? How does the perceived information vary with display signal-to-noise

DD _{1 JAN 73} FORM 1473

20.

ratio? What perceptual effect does a change in display luminance have on the perceived information? And, finally, what display conditions are required in order to produce a perceptually "perfect" displayed image?

It is shown in this report that quantitative answers to these questions can be obtained using a nonlinear luminance signal-detection model for the visual system that is based on recent developments in the psychophysics of vision. This model systematically includes such important display parameters as modulation transfer, noise, sampling processes, scene content, mean luminance, and display size. Most importantly, in those display situations tested, this model has accurately predicted the measured results.

An important feature of this report is that the model's predictions are presented in graphic form, with modulation transfer plotted as a function of retinal frequency. In order to use these figures, which are called Discriminable Difference Diagrams (DDDs), it is only necessary to plot on the appropriate diagram the modulation transfer function (MTF) of the display system under investigation. From the diagram it is then possible, by inspection, to determine the total amount of perceived image structure at different retinal frequencies, and also the perceptual effect that results from changes in the system MTF.

This report is organized into two distinct parts: The first part, which includes Sections II and III, is a handbook of DDDs. Section II is a brief outline of the principles of the DDDs along with many examples to illustrate their use. Section III is a catalog of computed DDDs. Included are DDDs for the perception of both signal and noise with the following parameters: signal-to-noise ratio, mean luminance, display size, and various sampling parameters. The second part, which includes Section IV and the Appendices, gives the theory and experimental verification behind the DDDs.

PREFACE

TABLE OF CONTENTS

v

TABLE OF CONTENTS (Continued)

LIST OF ILLUSTRATIONS

Figure   Page

vii

LIST OF TABLES

LIST OF SYMBOLS

d	Width of Gaussian spot profile (Section II.C.2.a)
DDD	Discriminable Difference Diagram
f	Spatial frequency on the display screen
f'	Spatial frequency on the display screen
f_L	Lower cut-off frequency of the ensemble-averaged power spectrum for pictorial scenes [Eq. (33)]. In this report f_L is approximated as $1/w$
f_{max}	Maximum spatial frequency (or cutoff frequency) on the display screen
f_o	Spatial frequency for which $f_o > \frac{1}{2} f_s$ [Eq. (13)]
f_s	Sampling frequency
$\bar{I}$	Mean display luminance
$I(x)$	Luminance pattern
$I_m(x)$	Luminance modulation for pictorial information defined through $I(x) = \bar{I} + I_m(x)$
$\sqrt{\overline{I_m^2}}/\bar{I}$	Normalized rms luminance modulation depth for pictorial information. In this report $\sqrt{\overline{I_m^2}}/\bar{I} = 1/2$
I_{max}	Maximum luminance of an edge transition [Fig. 119]
I_{min}	Minimum luminance of an edge transition [Fig. 119]
$I_o(x)$	Input luminance pattern [Eq. (A-1)]
$\hat{I}_o(f)$	Fourier transform of $I_o(x)$ [Eq. (A-2)]
$I_N(x)$	Noise contribution to the displayed luminance pattern due to sampling processes [Eq. (B-5)]
$I_S(x)$	Signal contribution to the displayed luminance pattern after sampling [Eq. (B-4)]
jnd	Just-noticeable difference: defined here as the change in the input stimulus required for an observer to perceive that change 75% of the time

$J(\nu)$ — Number of distinguishable contrast levels (i.e., jnd's)

$J_{S,N}(\nu)$ — $J_S(\nu)$ represents the total number of jnd's of signal; $J_N(\nu)$ represents the total number of jnd's of noise [Eq. (30)]

$k(\nu)$ — Weber's fraction [Eq. (20)]. Parameter that sets the signal-to-noise ratio of the visual system

$\ell(f)$ — Spatial integration length of the visual system for spatial sinusoids [Eq. 26]

m — Integer index

$m_E(\nu)$ — Equivalent sine-wave contrast for a one-dimensional luminance edge transition [Eq. (A-14) for analog displays; Eq. (B-14) for sampled displays]

$m_{eq}(\nu)$ — Equivalent sine-wave contrast [Eq. (A-13)]

$m_f(\nu)$ — Final equivalent sine-wave contrast [Eq. (25)]

$m_i(\nu)$ — Initial equivalent sine-wine contrast [Eq. (25)]

$m_I(\nu)$ — Equivalent sine-wave contrast for interfering noise term [Eq. 30]

$m_N(\nu)$ — *Equivalent sine-wave contrast for white noise [Eq. (A-16)].* Also equivalent sine-wave contrast for noise due to sampling processes [Eq. (B-15)]

$m_o(\nu)$ — Initial contrast of a sine-wave grating [Eq. (17)]

$m_P(\nu)$ — Equivalent sine-wave contrast for ensemble-averaged pictorial scenes [Eq. (A-15)]

$m_{S,N}(\nu)$ — Equivalent sine-wave contrasts for either signal (S) or noise (N) [Eq. (30)]

$m_T(\nu)$ — Threshold contrast for sine-wave gratings [Eq. (21)]

MTF — Modulation transfer function

n — Integer index

N^2 — Mean-square noise fluctuation [Eq. (A-10)]

N_s — Number of equally spaced sampling locations across a display ($N_s = f_s w$)

N_{TV} — Number of television lines ($N_{TV} = 2fw$)

$N(f)$ — Noise power spectrum with units of mean-square luminance per cycle per cm [Eq. (A-10)]

$N_v(v)$ — Visual-noise spectral power per unit retinal frequency [Eq. (20)]

p — Overall probability of correctly detecting a change in image structure [Eq. (34)]

p_i — Probability of detecting a change in image structure that occurs in the i'th independent frequency-specific channel [Eq. (34)]

$p(v_2-v_1,v_1)$ — Psychometric function defined as the probability of correctly choosing the sharper of two images with bandwidths v_1 and v_2 (where $v_2 > v_1$) at a specific value of v_1 as a function of $v_2 - v_1$

$P(f)$ — Spatially summed power spectrum [Eq. (A-6)]

$P_N(f)$ — Spatially summed power spectrum computed for $I_N(x)$ [Eq. (B-11)]

$P_S(f)$ — Spatially summed power spectrum computed for $I_S(x)$ [Eq. (B-10)]

q — Integer index

r — Viewing distance

r/w — Viewing distance parameter: ratio of viewing distance to display width

$R(f)$ — Display MTF

$R_D(f)$ — MTF for raster/sampled displays [Fig. 14]

$R_J(v)$ — Display modulation transfer necessary to produce the J'th discriminable contrast level in an independent frequency-specific channel [Eq. (31)]

$R_P(f)$ — Prefilter MTF [Fig. 14]

$R_v(v)$ — Overall physical MTF for the visual system [Eq. (19)]

$R_{-1}(v)$ — Value of display MTF from $R(v) = 1$ required to reduce perceived image structure by 1 jnd [Eq. (4)]

s — Sampling width parameter. In this report either $s = 0$ (delta function sampling) or $s = 1$ (full-width sampling)

S/N	Signal-to-noise ratio defined through Eq. (2)
TR1	Reference 1
TR2	Reference 2
TR3	Reference 3
V	Video voltage [Eq. (C-1)]
V_o	Maximum video voltage [Eq. (C-2)]
w	Width of a display
y	Physical vertical length coordinate on the display. Also, a dummy coordinate in Eq. (B-3)
γ	System gamma [Eq. (C-2)]
δI^2	Change in the mean-square luminance of a sine-wave grating [Eqs. (19) and (20)]
ν	Retinal frequency coordinate: $\nu = \pi r f / 180$ (in cycles/degree)
ν_{max}	Maximum retinal frequency defined through $\nu_{max} = \pi r f_{max} / 180$ [Eq. (5)]
$\nu_{1,2}$	Bandwidth parameters. In Section IV.H.1 the display MTF is defined so that $R(\nu_{1,2}) = 1/2$
Δ	Spacing between diffuser plates [Fig. 133]
ΔI	Luminance edge step height [Fig. 119]
ΔJ	Change in the number of jnd's
$\Delta m(\nu)$	Change in the contrast of a sine-wave grating necessary to realize 1 jnd in contrast [Eq. (19)]
$\Delta R_J(\nu)$	Change in display MTF required to produce 1 additional jnd from the J'th level [Eq. (32)]
$\Delta \nu(\nu)$	Bandwidth of the independent frequency-specific channels in the visual system
$\Phi(f)$	Power spectrum of the input scenes to a display with units of mean-square luminance per cycle per cm [Figs. 3 and 14]

LIST OF SYMBOLS (Continued)

$\Phi_{i,f}(f)$ $\Phi_i(f)$ and $\Phi_f(f)$ are, respectively, the initial and final power spectra in the contrast-detection model [Eq. (23)]

SECTION I

INTRODUCTION

It is occasionally said that a "perfect" image is one that looks like a piece of the world viewed through a picture frame. In photography this ideal can be realized, and in some electro-optical displays it can be approached. More often, however, displayed images are noticeably less than perfect. Although in these cases significant improvements in image quality are desirable, they must generally be achieved over strong technical and economic constraints. In such cases, improvements are best achieved by closely matching the performance of the display both to its purpose and to the visual requirements of the observer. As a result, understanding the limitations of the visual system has always been one of the central problems in display research. It is this problem of predicting what an observer can see when he views a display that is the broad subject of this report.

In the design and specification of displays it is important to know what perceptual effects result from a specified set of display conditions. Typical practical questions are: What are the perceptual effects of sampling and a visible raster structure? How can two displays with different modulation transfer functions* (MTFs) and different signal-to-noise ratios be compared? What perceptual effect does a change in mean display luminance have on the perceived information? Equally important issues involve the determination of when a change in a display parameter is perceptually significant and how trade-offs between various display parameters should be made. In particular, what conditions must be satisfied in order to produce the perceptually "perfect" picture mentioned above?

It is shown in this report that answers to these questions can be obtained using a nonlinear luminance signal-detection model for the visual system that is based on recent developments in the psychophysics of vision. This model system-

---

*We shall assume that the reader is familiar with the concept of the modulation transfer function and has a basic knowledge of Fourier analysis. For expositions of these topics, see, for example, W. J. Smith, "Modern Optical Engineering," McGraw-Hill Book Company, NY (1966) and R. Bracewell, "The Fourier Transform and Its Applications," McGraw-Hill Book Company, NY (1965).

atically includes such important display parameters as MTF, noise, sampling processes, scene content, mean luminance, and display size. Most importantly, in those display situations tested, this model has accurately predicted the measured results.

An important feature of this report is that the model's predictions are presented in graphic form, with modulation transfer plotted as a function of retinal frequency. In order to use these figures, which are called Discriminable Difference Diagrams (DDDs), it is only necessary to plot the magnitude of the MTF of the display system under investigation on the appropriate diagram. From the diagram it is then possible, by inspection, to determine the total amount of perceived image structure at different retinal frequencies, and also the perceptual effect that results from changes in the system MTF. When the model is presented in this form, those spatial frequencies most responsible for a discernable change in image structure are easily recognized.

This report is the last of a series [1,2,3] (hereafter referred to as TR1, TR2, and TR3, respectively) in which we have developed a family of mathematical descriptors for the quantitative evaluation of perceived display performance. In TR1 and TR2 the visual model employed in the descriptors relied on a linear spatial-frequency filtering function (i.e., a visual "MTF"), the form of which was taken from either spatial sine-wave contrast sensitivity or contrast matching measurements. Although this heuristic visual model predicts many interesting properties of the display-observer system, it is substantially less powerful than the approach presented here. Also, it provides relatively little insight into the basic processes that mediate the display-observer system. In TR3 a new nonlinear signal-detection model for the visual system was developed, which we consider to be an important advancement over the previous linear filtering model. It is this model that forms the basis of this report. A significant feature of this model is that it clearly shows the dependence of display performance on the properties of both the display and observer. Meaningful standards and specifications for displays can be achieved only when both of these aspects are included.

This report is organized into two distinct parts: The first part, which includes Sections II and III, is a handbook of DDDs. Section II is a brief outline

2

of the principles of the DDDs along with many examples to illustrate their use. Section III is a catalog of computed DDDs. Included are DDDs for the perception of both signal and noise with the following parameters: signal-to-noise ratio, mean luminance, display size, and various sampling parameters. The second part, which includes Section IV and the Appendices, gives the theory and experimental verification behind the DDDs. The interested reader will probably want to read these sections in order to get a better feeling for the meaning and limitations of the DDDs, as well as for potential new applications.

SECTION II

THE USE OF DISCRIMINABLE DIFFERENCE DIAGRAMS: A GUIDE

A. OVERVIEW AND SUMMARY

This section outlines how and when the Discriminable Difference Diagrams
(DDDs) are to be used. The brief summary given here, in conjunction with the
applications and examples that follow, will enable the reader to use the dia-
grams in a wide range of situations. Additional details regarding the meaning
and development of the DDDs can be found in Section IV. All of the DDDs given
in this report are collected in Section III, where they are listed according
to their DDD numbers (Tables 5-9).*

In order to use the DDDs it is only necessary to locate the appropriate
DDD and then plot on it the MTF of the system under investigation as a function
of retinal frequency ν. Here ν is measured in cycles/degree-of-vision and is
given by $\nu = \pi r f/180$, where r is the viewing distance and f is the display spatial
frequency. From the DDD, one can then directly obtain (1) the change in dis-
play MTF required to produce a just-noticeable difference** (jnd) in luminance
image structure, and (2) the total number of jnd's of luminance image structure
contained in any frequency range.

In order to decide which DDD is appropriate for a given problem the fol-
lowing display parameters must be known: mean display luminance $\bar{I}$, viewing
distance r, display size w, signal-to-noise ratio S/N [see Eqs. (1) and (2)],
and whether the display is analog or sampled. From this information the re-
quired DDD can be located in the DDD index given in Section III. If the exact
DDD required is not listed, it is often possible to interpolate between diagrams
to obtain a reasonable estimate for the answer to a problem.

Given the appropriate DDD, the next step is to superimpose the MTF of the
display under consideration directly on the DDD. As a simple example, consider
Fig. 1, which shows a representative DDD (No. 18) along with a hypothetical dis-
play MTF $R(\nu)$. On the diagram each vertical line, located at the key frequencies

_____
*Located on pages 50 through 54.
**A jnd is defined here to be the change in the input stimulus required for an
  observer to perceive that change 75% of the time.

4

MODULATION TRANSFER

1.4
1.2
1.0
0.8
0.6
0.4
0.2
0

R(ν)

0.3   0.5   1.0   1.5   3.0   6.0   12   24   48   10   80

RETINAL FREQUENCY ν = πrf/180 (CYCLES/DEGREE)
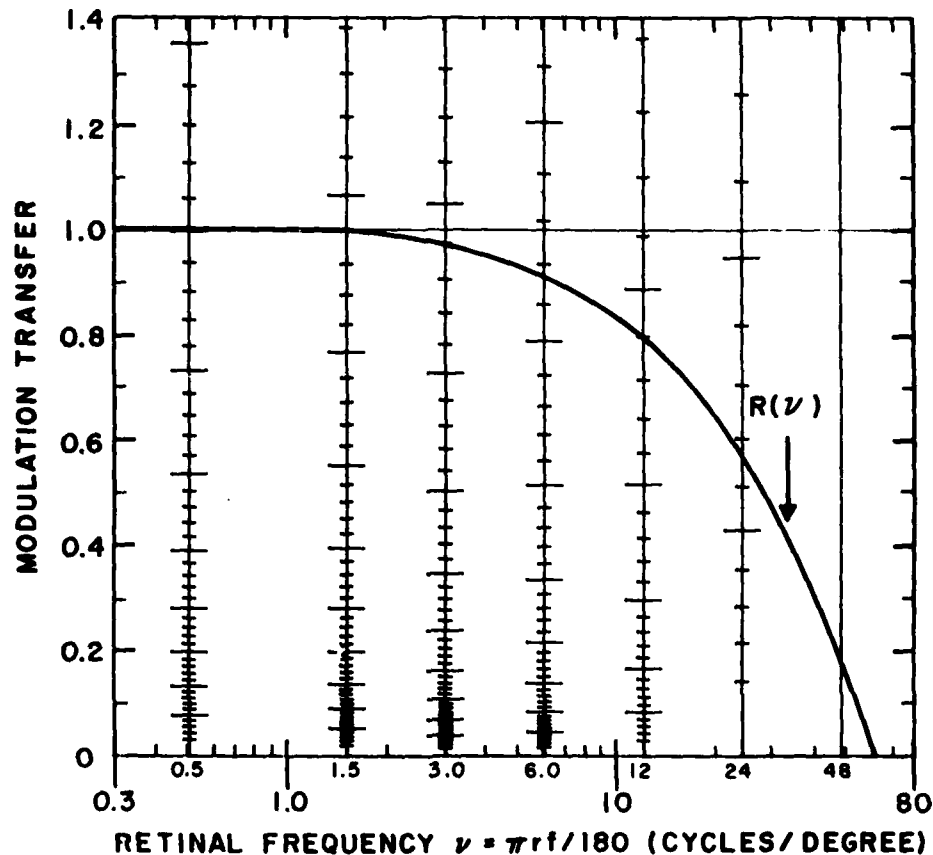
Figure 1.   Example of a typical Discriminable Difference Diagram for sig-
nal levels. The model predicts that when the modulation
transfer R(ν) over any of the key frequencies centered at 0.5,
1.5, 3.0, 6.0, 12, 24, and 48 cycles/degree is increased by
one tick mark, 1 additional jnd in image structure is per-
ceived. For example, the modulation transfer function shown
here must be increased from 0.80 to 0.84 at 12 cycles/degree
for a 1-jnd improvement in image structure. One jnd is de-
fined as the change required for an observer to see that
change 75% of the time. The conversion between display fre-
quency f and retinal frequency ν is: ν = πrf/180, where r
is the viewing distance.

5

of 0.5, 1.5, 3.0, 6.0, 12, 24, and 48 cycles/degree, defines the center of a
frequency-specific channel or band of frequencies. For $\nu \geq 3/2$ cycles/degree,
the width of each channel is one octave, centered about each key frequency.
For $\nu < 3/2$ cycles/degree, the channel width is 1.0 cycle/degree*. At each
channel location the small tick marks on each vertical line indicate the change
in display modulation transfer necessary over that channel for an observer to
perceive a 1-jnd change in displayed image structure. For example, in Fig. 1
it may be seen that, at the channel located at 12 cycles/degree, there are
24 jnd's of perceived image structure between R(12) = 0 and R(12) = 0.80. This
means that as the MTF is increased from 0 to 0.80 over the band of frequencies
between 8 and 16 cycles/degree, an observer will discriminate a change in the
displayed information 24 times. Also, in order to increase the perceived
structure by one additional jnd at this channel location, it is seen from the
figure that the modulation transfer of the display must be increased from 0.80
to 0.84.

The following paragraphs briefly discuss some additional properties of
the DDDs.

(1) When modulation transfer changes occur over more than one channel, the
overall perceptual effect may be computed according to the procedures described
in Section IV.F. To a first approximation, however, jnd's from several channels
may simply be added. For example, a change of 1 jnd in three channels may be
taken as roughly equivalent to a 3-jnd change in a single channel.

(2) The DDDs given in this report apply to scenes that are highly modulated,
a requirement that is often met by pictorial, alphanumeric, and graphic infor-
mation. When the input scenes are not highly modulated, there will be typically
fewer jnd's at each channel location than those shown in the DDDs. A more
complete discussion of this issue is given in Section IV.D.

(3) When two different displays have the same total number of jnd's at the
same frequency-specific channel, that information is equally visible in both
cases. This follows from the fact that equal numbers of jnd's are defined to
have equal probabilities of detection. Consider, for example, two displays,
one of which is limited in performance by low brightness and the other by poor
signal-to-noise ratio. Although the factors determining the amount of perceived

---

*The locations of each channel are given in Table 11 (on page 184).

information on these displays are quite different, if at some spatial-frequency channel the total number of jnd's are the same, then the visibility of that information will be the same. It is this fact that enables the DDDs to be used to compare the absolute performance of displays with different display parameters. If, at a given spatial frequency, the number of jnd's for one display is greater than the number for another display, then the performance of the first is greater than the second in the sense that it can present a larger number of distinguishable contrast levels to an observer.

(4) Jnd's are a measure of the discrimination of a change, not a measure of the appearance or perceptual magnitude of a change. This is an important fact that must be borne in mind. In the example given above in (3) the displays had equal numbers of jnd's, but they would look very different. The low brightness display would appear noise-free with low contrast, while the other display would appear noisy with high contrast. Also, jnd's at one frequency should not be thought of as perceptually equivalent to jnd's at another frequency. For example, a display that produces 5 jnd's in the channel centered at 12 cycles/degree will not appear at all similar to a display that produces 5 jnd's at 1.5 cycles/degree.

(5) The total number of jnd's necessary for the performance of a given task is not presently known.

(6) In discrimination tasks we consider a 1-jnd change to be practically insignificant, a 3-jnd change to be significant, and a 10-jnd change to be substantial. Examples of 3- and 10-jnd changes are shown in Fig. 2. In Figs. 130 and 131* the probability of detecting a change is plotted as a function of number of jnd's, ΔJ.

(7) The DDDs given here can be used for either black-and-white or colored images. The presence of color does not influence the predicted results. This is discussed in Section IV.H.

(8) The diagrams in this report were prepared assuming quasi-static displayed images and noise. That is, it is assumed that both the images and noise change slowly compared with the appropriate time constants of the visual system ($\gtrsim 0.1$ s). This assumption is generally satisfied when applied to displayed information, but for displayed noise it depends on the specific conditions. For example, the visibility of stationary band-limited white noise is roughly

---

*Located on page 187.

7

(a) Original

(b) ΔJ = -3 jnd's   (c) ΔJ = -10 jnd's

Figure 2. Examples of images that differ in their image structure (or
           sharpness) by roughly 3 and 10 jnd's. When viewed at arms
           length there is a 3-jnd difference between Fig. 2(a) and
           Fig. 2(b) and a 10-jnd difference between Fig. 2(a) and Fig.
           2(c). (These values are only approximate due to variations
           in the photographic processes used to make these pictures.)

8

3 dB greater than for nonstationary noise on a TV-like display. For more detail regarding this point, refer to Appendix C.

(9) The DDDs can be used to predict the visibility of MTF changes that occur either isotropically or anisotropically. For most images the *discrimination* of a change in display MTF will not depend strongly on whether it occurs isotropically or anisotropically. However, the total number of jnd's in an image will depend on the full two-dimensional properties of the display systems MTF. The reader is referred to Section IV.G, where these concepts are explained in greater depth.

(10) The ordinate on the Discriminable Difference Diagrams is the *magnitude* of the display system's MTF, $|R(\nu)|$. Therefore, the DDDs cannot be used to predict the perceptual effects due to changes in the spatial *phase* of an image. In addition, when the DDDs are used to predict discernable differences between displays with different MTFs, it is necessary that variations in phase between the displays be small compared with variations in the magnitude of the MTFs. If this condition is not satisfied, it is possible that the perceptual effects due to variations in phase will be seen before those due to variations in the magnitude of the MTFs. In Section IV.B it is explained that these results are a consequence of the contrast-detection model used to construct the DDDs. This model assumes that the relevant psychophysical quantity in constrast-detection experiments is the mean-square luminanc ..e., the signal power) in relatively narrow bands of spatial frequencies. Thus, the phase information is not included in the model. As a simple example of these concepts, consider a sudden, 180-degree phase shift in a displayed one-dimensional sine-wave grating. That is, a change in $R(\nu)$ from 1 to -1. An observer looking at this display could easily see the change in the grating. However, since the magnitude (i.e., $|R(\nu)|$)of the grating was unchanged, the total amount of image structure on the display would also remain unchanged, a result that is correctly predicted by the contrast-detection model.

9

B. APPLICATION OF THE DDDs TO ANALOG DISPLAYS

1. Introduction

In the following paragraphs the use of the analog DDDs will be demonstrated by applying them to practical display problems. In addition, several special cases, not explicitly contained in the DDDs, will be presented. The examples given should be considered as illustrative, not exhaustive.

The analog DDDs in this report were prepared to describe four conditions: The perception of displayed (1) signal levels in the presence of display noise, (2) noise levels on a uniform luminance display, (3) noise levels in the presence of pictorial information, and (4) noise levels near a 100% contrast edge transition. Brief descriptions of each of these cases are given in Table 4* and illustrations of the use of each are given in this section. Detailed information about these diagrams can be found in Section IV.

First, before turning to the examples of this section, we briefly note some definitions used in the construction of the analog DDDs. In Fig. 3 we show the basic elements of the prototypical analog display considered in this

$$\Phi(f) \qquad N(f) \qquad \begin{array}{c} R(f) \\ \overline{I} \\ w \end{array} \qquad r$$
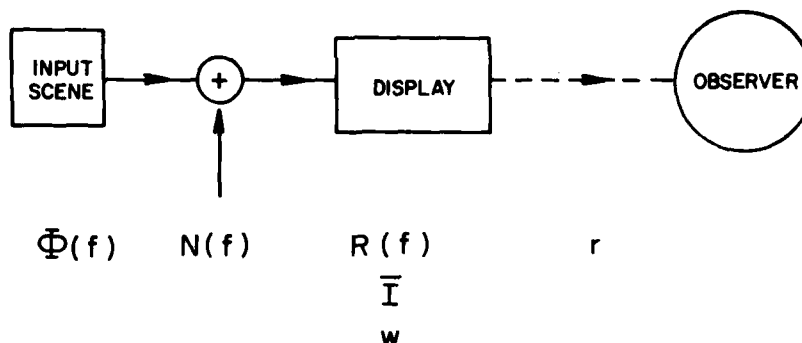
Figure 3. Prototypical analog display considered in this report. The input signal and noise, which are characterized by their respective power spectra $\Phi(f)$ and $N(f)$ [with units of mean-square luminance per cycle per cm], are presented on a display with mean luminance $\overline{I}$ [in mL] and width w [in cm], which is viewed from a distance r [in cm]. It is $R(f)$, plotted as a function of ν ($\nu = \pi r f/180$), that is the ordinate of the DDDs. Note that all the calculations given in this report are for the perceived luminance signals *on the display* (see text).

---

*Located on page 49.

report. The input signal and noise, which are characterized by their respective power spectra $\Phi(f)$ and $N(f)$ [with units of mean-square luminance per cycle per cm], are presented on a display with MTF $R(f)$, width w, and mean luminance $\bar{I}$. It is $R(f)$, plotted as a function of retinal frequency ν ($\nu = \pi r f/180$), that is the ordinate of the DDDs. (See Section IV and Appendix A for detailed discussions of these quantities.)

It should be clearly understood that the calculations given here are for the perceived luminance signals *on the display*. They should not, for example, be confused with those that apply to the video signals in a television system where there are intervening gamma changes between the video voltages and the luminance signals on the screen [4]. As discussed in Appendix C for noise, the effects due to gamma changes must be included separately.

In this report the noise power spectrum for analog displays $N(f)$ is assumed to be white. Thus, for displays with a sharp upper cutoff frequency f_{max} the mean-square noise-luminance fluctuation N^2 is simply

$$N(f) = N^2/f_{max} \qquad \text{for } |f| \le f_{max}$$
$$= 0 \qquad \text{for } |f| > f_{max} \qquad (1)$$

We define the input signal-to-noise ratio to be the ratio of the mean display luminance $\bar{I}$ to the rms noise-luminance fluctuation N as follows

$$S/N = \frac{\bar{I}}{\sqrt{N(f)}} f_{max}^{-\frac{1}{2}} \qquad (2)$$

which can be converted to dB, viz.,

$$S/N(dB) = 20 \log_{10}(S/N) \qquad (3)$$

The parameter $\sqrt{N(f)}/\bar{I}$, in units of $(cm/cycle)^{1/2}$, is used throughout this report to characterize the input display noise, and Eq. (2) is used to compute the input signal-to-noise ratio.

Note that the definition of signal-to-noise ratio given above is different from the one typically used by television engineers. They define the signal-to-noise ratio in the video channel (where the video voltage has been compressed by a gamma of roughly 1/2.2) to be the ratio of the peak-to-peak signal voltage to the rms random-noise voltage [5]. Since, at this point in the video chain the average video voltage is approximately 1/3 the peak voltage (see Section IV.D), it follows that the S/N (peak-to-peak to rms) = S/N (average to rms)

11

+ ∿10 dB. Other factors that affect the comparison of difference signal-to-noise ratios, such as gamma changes, are discussed in Appendix C.

2. Examples

a. *Predicting a Noticeable Difference in Image Structure (or Sharpness)* - In this example the general properties of the DDDs are examined by applying them to the problem of predicting a noticeable change in image structure - a correlate of image sharpness (for additional information on this topic, see ref. 6). Also illustrated in this example are the effects of changes in display modulation transfer on the perception of noise.

Situation:

A technological breakthrough has been achieved at ACR Laboratories in kinescope lens design that increases the modulation transfer of two existing display systems at all spatial frequencies. The first display is an extremely high quality one that may be considered noise-free; the second has an input rms signal-to-noise ratio of roughly 16. Both systems are bright pictorial displays with an upper cutoff frequency of 150 cycles/picture-width. They are normally viewed from a distance of 100 cm, or 3 picture widths. The electrical bandpass in both systems is assumed to be flat up to the cutoff frequency, and zero for frequencies past it.

Management has decided not to incorporate the improved lens in the high-quality display in order to save the capital investment required to make the change. They claim that, since the performance of this display is already so good, further improvements will not be visible. However, they have approved the inclusion of the new lens in the low-quality display. In this case they argue that the display performance is marginal at present; thus, every reasonable effort should be made to improve it. Are management's decisions correct?

Solution:

First, for the noise-free display we select DDD No. 1 from the listed diagrams in Tables 4 and 5*. This diagram is replotted in Fig. 4 along with the two MTFs under consideration. The existing MTF is labeled as A and the improved MTF is labeled as B. Note that, due to the rectangular passband of

---
*Located on pages 49 and 50.

12
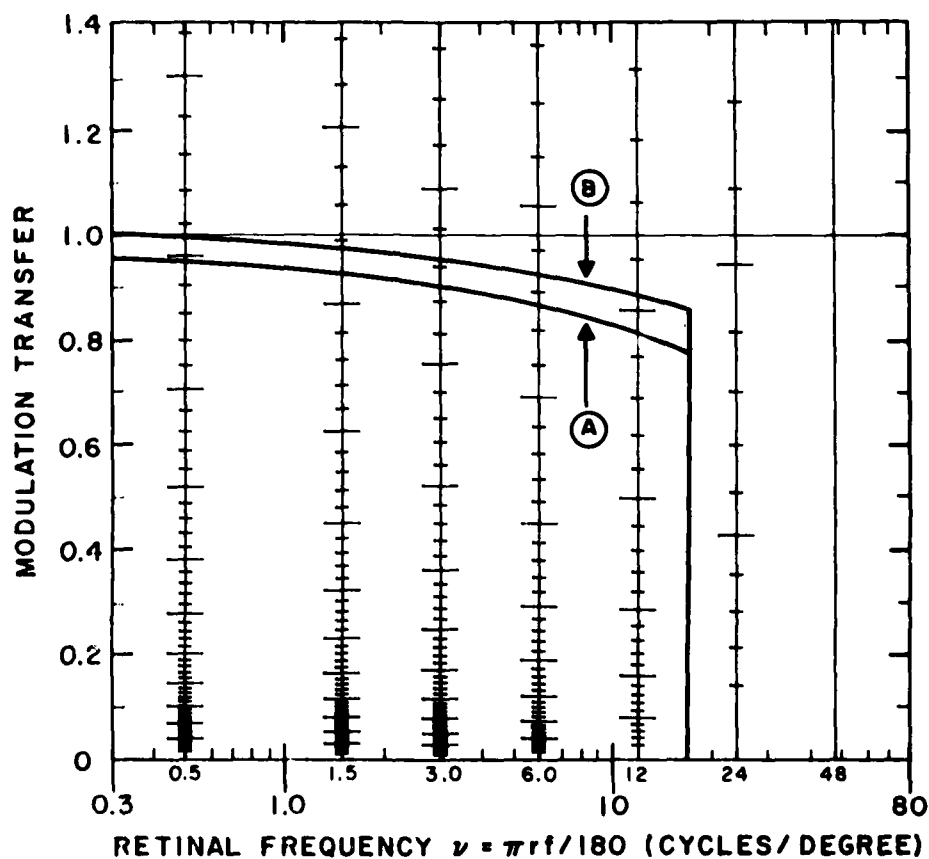
Figure 4. This figure shows the increase in perceived signal levels on a noiseless display when the MTF of the display is increased from A to B (example B.2.a). Here the increase in image structure is approximately 4.2 jnd's. The Diagram is a copy of DDD No. 1 for signal levels: $\sqrt{N(f)}/\bar{I} = 0$, $\bar{I} = 35$ mL, and $r/w = 3$.

the input signals, the overall MTF for these two displays drops to zero at roughly 16 cycles/degree. Since the frequency-specific channel located at 24 cycles/degree begins at 16 cycles/degree (Table 11), it will not contribute to the perceived image structure at this viewing distance.

From Fig. 4 it may be seen that the improvement in modulation transfer in going from MTF A to MTF B is slightly less than one full jnd at each frequency-specific channel location. Nevertheless, the sum of jnd changes at all channel locations is 4.2. This calculation shows that management's prediction was wrong: The improved lens does indeed result in a perceivable, but not over-whelming, difference in the performance of this display.

For the second case, where the display signal-to-noise ratio is 16, we must first determine which DDD to use. From Eq. (3) we find that,* for the specified conditions, a signal-to-noise ratio of 16 corresponds to a value of $\sqrt{N(f)}/\bar{I}$ of approximately 0.03. Therefore, from Table 5 the appropriate diagram to use is No. 11, replotted here as Fig. 5.

Once again, the standard and improved MTFs are shown on the figure as A and B, respectively. However, in this case it may be seen that the increase in modulation transfer in going from MTF A to MTF B results in the perception of no additional signal levels. This result may seem surprising at first, but it can be understood by recognizing that, when the MTF is increased, the perceived display noise increases in direct proportion to the preceived signal. Therefore, since the perceived signal-to-noise level is not increased as the display modulation transfer is increased, no additional signal levels can be perceived.

On the basis of this result one might conclude that incorporating the new lens in this display system is unnecessary, since there is no gain in perfor-mance. In fact, increasing the modulation transfer would actually result in a small reduction in overall display performance. In order to see this, we must consider the effect of the increase in modulation transfer on the number of perceived noise levels (jnd's of noise). We will consider the three cases given in this report: (1) noise on a uniform luminance display, (2) noise in

---

*From Eq. (2), we have $\sqrt{N(f)}/\bar{I} = [(S/N)f_{max}^{\frac{1}{2}}]^{-1} =$

$$\left[16 \times \left(\frac{150 \text{ cycles/picture width}}{33 \text{ cm/picture width}} \right)^{\frac{1}{2}} \right]^{-1} = 0.03.$$
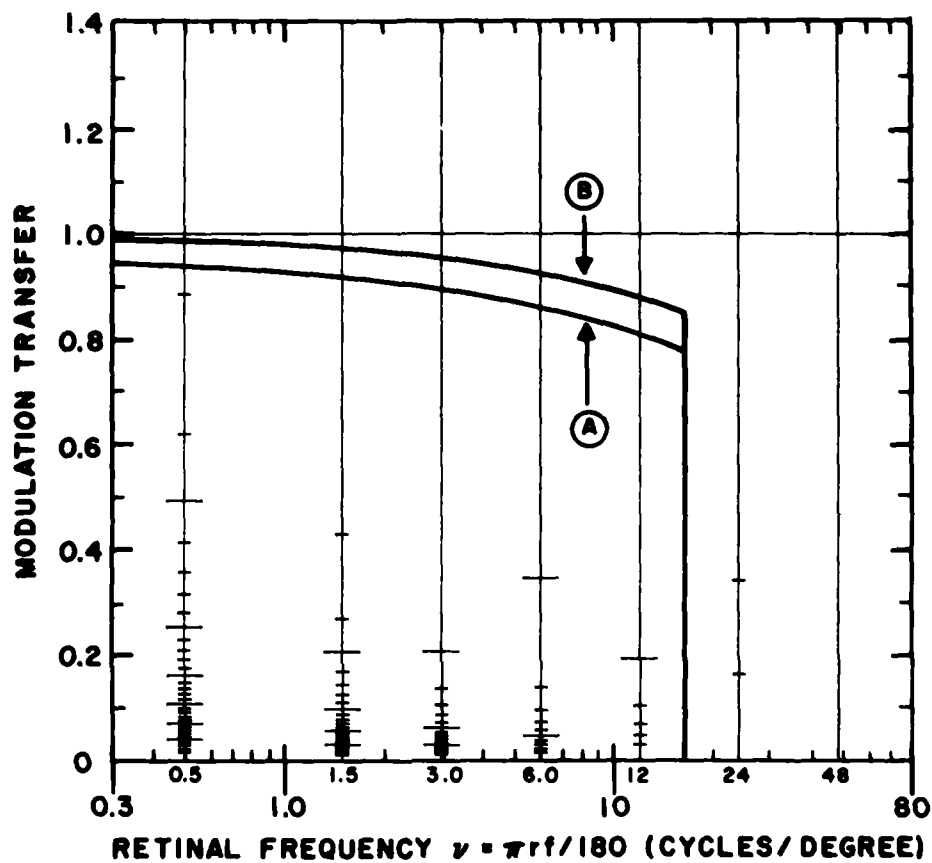
Figure 5. This figure shows the same two display MTFs given in Fig. 4.
Here, however, the S/N = 16 (example B.2.a). In this case
there is essentially no increase in the number of discriminable
signal levels in going from MTF A to MTF B. The Diagram is
No. 11 for signal levels: $\sqrt{N(f)}/\bar{I}$ = 0.03, $\bar{I}$ = 35 mL, and
r/w = 3.

15

the presence of pictorial information, and (3) noise near a 100% contrast luminance edge.

(1) First we consider the perceived noise on a uniform luminance display. This always represents the severest test of noise visibility since there is no pictorial information present to mask the noise. It follows that, in general, this is not a good test of the significance of the noise on a display. Generally one is interested in the noise visibility when the display is presenting information to the observer. Nevertheless, there are pictorial scenes that have large, constant luminance areas so that the most stringent criterion is appropriate. For the conditions of this example we use DDD No. 40, shown in Fig. 6. We find that upon increasing the MTF from curve A to curve B, the visibility of the noise is actually increased by approximately 4.3 jnd's.

(2) The best estimate of the overall perception of noise is given by those DDD's computed using the statistically averaged power spectrum for natural scenes. For this case we use DDD No. 59, shown in Fig. 7. Here the increase in noise visibility in going from MTF A to MTF B is much less than 1 jnd.

(3) Finally, we determine from DDD No. 73, shown in Fig. 8, that there is no increase in noise visibility near a 100% contrast edge input. In this case the noise power is heavily masked at all frequencies by the edge power spectrum.

In summary, we have found that, for this relatively poor signal-to-noise ratio display, increasing the display modulation transfer will not result in an increase in perceived signal. On the other hand, the perceived noise will actually increase slightly. Once again we have found that management's initial decision was incorrect. More importantly, we have shown that the best way to improve the performance of this display is to increase the input signal-to-noise ratio, not the display MTF.

b. *Perceptually Perfect Display* - In many display situations the ultimate goal is to produce an image that is perceptually indistinguishable from the original. In practice the realization of this goal is never possible over the full range of display-observer operating conditions. Nevertheless, it is still useful to determine the conditions required for perfection so that standards of relative performance may be established.
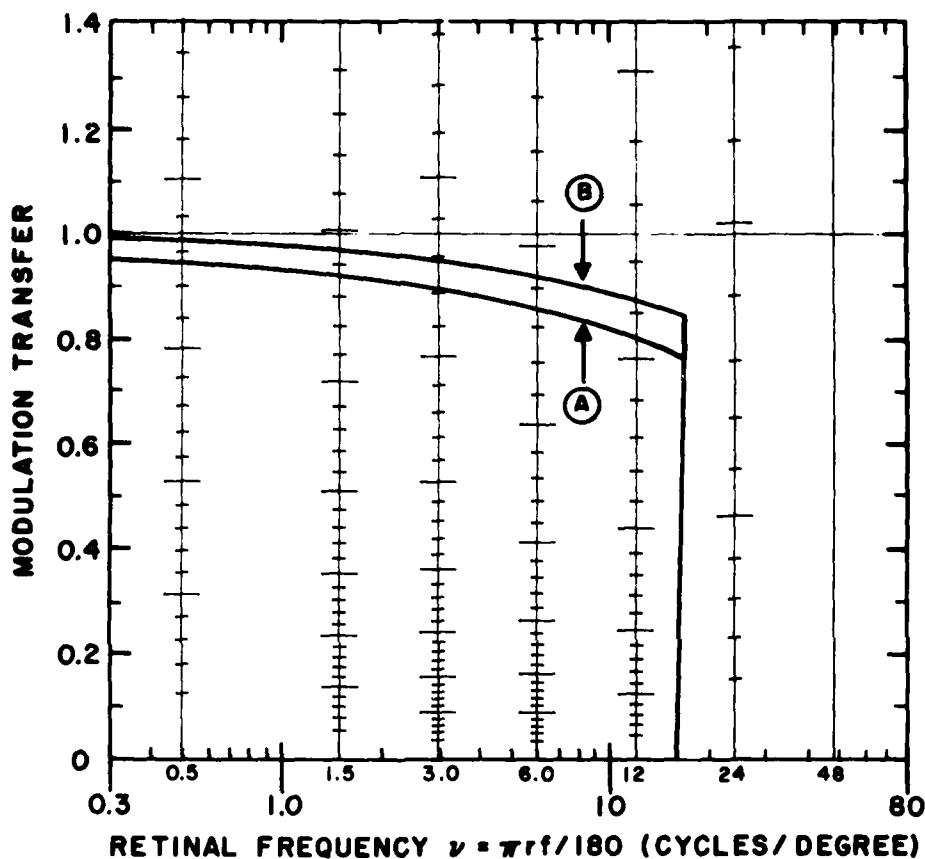
Figure 6.   For the same display conditions of Fig. 5, this figure shows
            the increase in the number of distinguishable *noise* levels on
            a uniform-luminance display when the MTF is increased from
            A to B.   The visibility of the noise increases by roughly
            4.3 jnd's in this case.   The Diagram is No. 40 for the dis-
            tribution of distinguishable noise levels on a uniform-
            luminance display: $\sqrt{N(f)}/\bar{I} = 0.03$, $\bar{I} = 35$ mL, and r/w = 3.

17
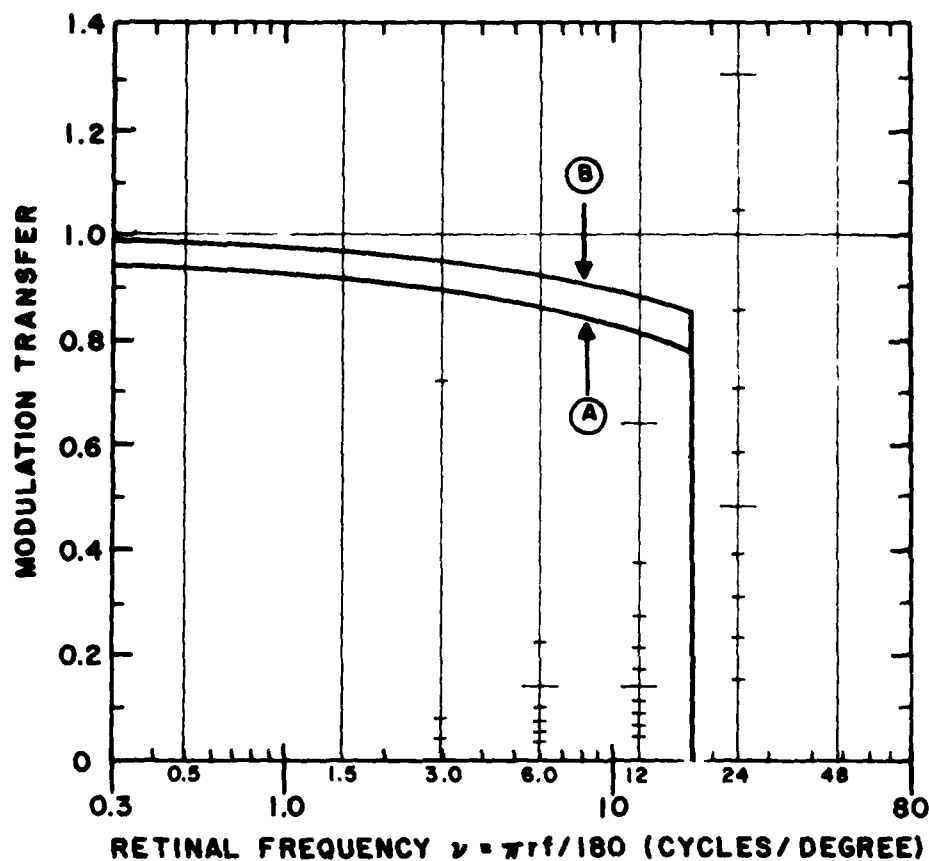
Figure 7. For the same display conditions of Fig. 5, this figure shows
the increase in the number of distinguishable *noise* levels in
the presence of pictorial information when the MTF is in-
creased from A to B. For these conditions there is only a
marginal increase in the visibility of the noise. The Diagram
is No. 59 for the distribution of distinguishable noise
levels in the presence of pictorial information: $\sqrt{N(f)}/\bar{I} =$
0.03, $\bar{I} = 35$ mL, and r/w = 3.

18
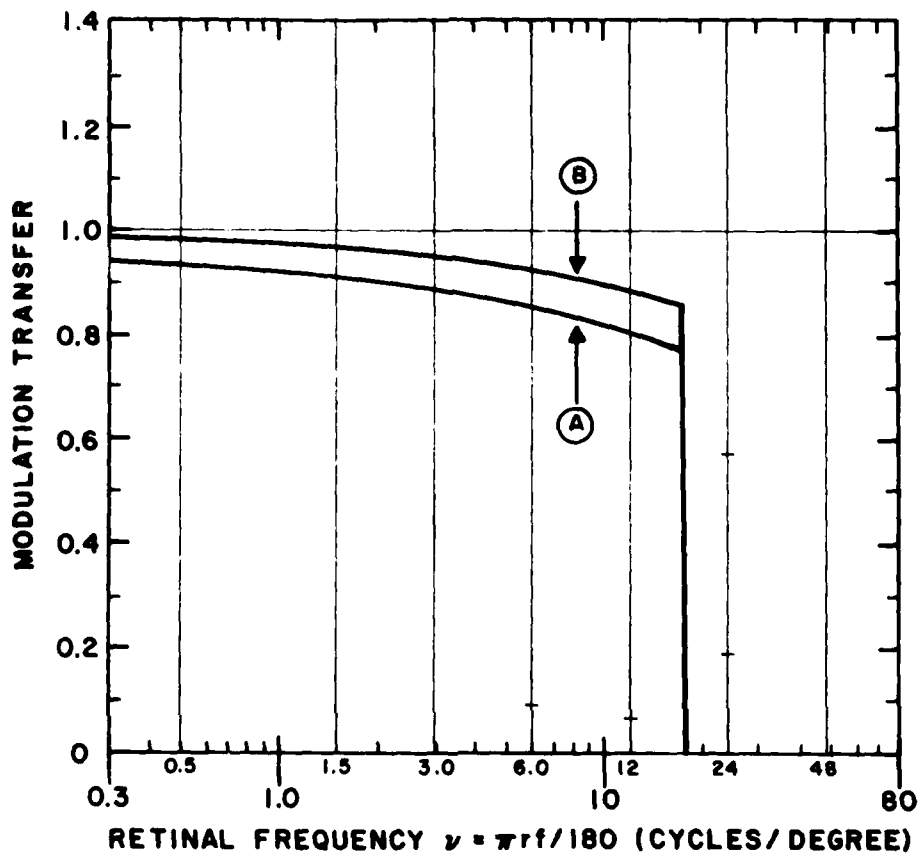
Figure 8. For the same display conditions of Fig. 5, this figure shows the increase in the number of distinguishable *noise* levels near a 100% contrast edge when the MTF is increased from A to B. Here there is essentially no increase in the visibility of the noise. The Diagram is No. 73 for the distribution of distinguishable noise levels in the presence of a 100% contrast luminance edge transition: $\sqrt{N(f)}/\bar{I} = 0.03$, $\bar{I} = 35$ mL, and $r/w = 3$.

In an absolute sense a measurably perfect display must have unity MTF, infinite signal-to-noise ratio, etc. However, these values do not represent realistic standards, since there is always a point past which increases in display performance result in disproportionally small increases in perceived display performance. A more meaningful definition of *effective* display perfection can be obtained by establishing the point at which further improvements result in only one additional discriminable difference in perceived performance. In the following paragraphs we will illustrate the use of this definition for several pertinent cases.

(1) MTF Required for a Perceptually Perfect Display

Situation:

An optical microfilm reader is being designed that must compete with existing systems. The engineer in charge of selecting the projection lens must decide quickly whether an existing lens is suitable for this purpose. She has measured the MTF of this lens on the display screen and found that it is well approximated by $R(f) = e^{-f^2/950}$, where f has the dimensions of cycles/ cm. The average display luminance will be roughly 1 mL, and the viewing distance will be 100 cm away from the 33-cm-wide screen. Can she recommend the use of this lens?

Solution:

From Table 5 we see that, for a mean display luminance of 1.0 mL, the only diagrams given are for r/w = 10, not r/w = 3, as specified above. Nevertheless, for this case these diagrams may be used. This is because, as shown in example d below, the differences between the diagrams with different r/w are primarily at the lower spatial frequencies. Since we are concerned only with the higher spatial frequencies in this example, we can use those diagrams plotted assuming r/w = 10. Finally, we note that neither the MTF nor the signal-to-noise ratio for the microfilms to be projected was given. Since we wish to obtain a conservative estimate of the performance of the lens, we will assume $\sqrt{N(f)}/\bar{I} = 0$. It may be seen from inspecting the DDDs that the presence of noise on the microfilms would make losses in MTF less visible. The MTF for the microfilm will be assumed to be unity, since it has been

20

determined that the microfilms are produced on extremely high contrast film. For these conditions DDD No. 20 is chosen to solve this problem.

In Fig. 9 the MTF of the lens to be evaluated is shown on DDD No. 20. It may be seen that this lens differs from a perfect lens with unity MTF by 0.3 and 0.7 jnd's at the frequency-specific channel locations of 12 and 24 cycles/degree, respectively. Thus, there is only about a 1-jnd difference from perfection, and we conclude that this is an excellent lens for this purpose. Better lenses would give only negligible improvements in the displayed image quality. For these conditions this system may be considered to be perceptually perfect.

We finish this example by giving the general expression for predicting the departure of the modulation transfer from unity necessary to produce one additional jnd in image structure at each frequency-specific channel location for a noiseless display. This expression allows computations similar to the one outlined above to be performed for situations not given in the DDDs. Starting from Eq. (30) (Section IV.B) we find that

$$R_{-1}(\nu) = \left\{ \left[\left(\frac{1 + k(\nu)m_E^2(\nu)/m_T^2(\nu)}{1 + k(\nu)} \right) - 1 \right] \frac{m_T^2(\nu)}{k(\nu)m_E^2(\nu)} \right\}^{1/2} \tag{4}$$

Here $R_{-1}(\nu)$ is the required value of modulation transfer to produce a loss of 1 jnd from $R(\nu) = 1.0$, $m_T(\nu)$ is the sine-wave contrast sensitivity function for the visual system given in Table 11, $m_E(\nu)$ is the equivalent sine-wave contrast for the input signal given by Eq. (27) for the case of a single-edge transition, and $k(\nu)$ is the signal-detection parameter for the visual system given in Table 11. Once again, the retinal frequency ν is related to the display spatial frequency f by the expression $\nu = \pi r f/180$.

For example, consider the case of the microfilm reader described above. Taking $\nu = 12$ cycles/degree, we have, from Table 11 and Eq. (27), the values $m_T(12) = 2.66 \times 10^{-2}$, $m_E(12) = 0.14$ for a 100% contrast edge transition,* and $k(12) = 0.240$. With these values Eq. (4) predicts that $F_{-1}(12) = 0.881$. This value can also be read from Fig. 9 at 12 cycles/degree.

_____
*In the notation employed in Eq. (27), $\Delta I/\bar{I} = 2$ for a 100% contrast edge transition.
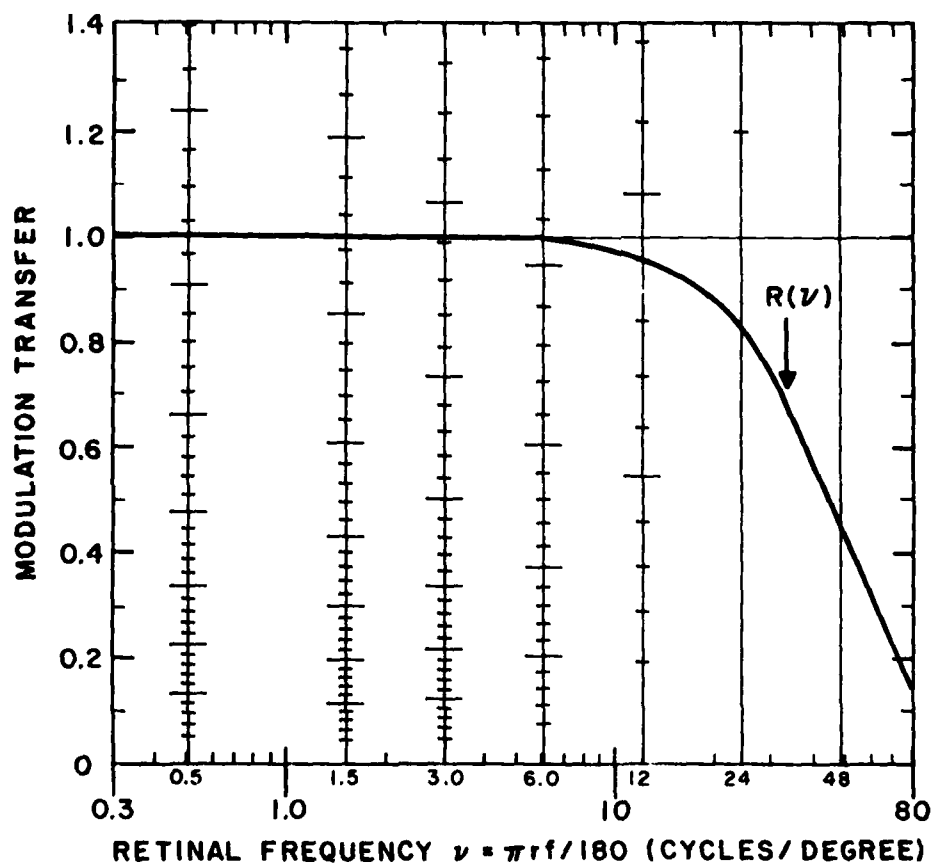
Figure 9. MTF required for a perceptually perfect display (example
B.2.b.i). The MTF shown on the figure is only 1 jnd away
from a perfect display with $R(\nu) = 1.0$. Compared with an
MTF with $R(\nu) = 1$, this MTF results in the loss of 0.3 jnd
at 12 cycles/degree and 0.7 jnd at 24 cycles/degree. The
Diagram used here is No. 20 for signal levels: $\sqrt{N(f)}/\bar{I} = 0$,
$\bar{I} = 1$ mL, and $r/w = 10$.

22

(2) *Conditions necessary for a Noise-Free Display* - A second criterion
necessary to realize excellent image quality is that the displayed images ap-
pear noise-free. (This issue is discussed in greater detail in ref. 7 and
Appendix C.) Once again this condition can be systematically established by
determining the signal-to-noise ratio required to discriminate 1 jnd of
noise -- the threshold of perception for the noise. We will consider the vis-
ibility of noise for three specific cases: (1) noise on a uniform luminance
field, (2) the overall impression of noise in the presence of pictorial scenes,
and (3) the visibility of noise near a high contrast luminance edge. In many
cases the DDDs given in this report can be used to estimate the first jnd of
noise over a wide range of display-observer conditions. Nevertheless, we
first give the analytical expression for predicting the threshold value of
noise. We then apply this expression to several hypothetical examples.

An expression for the perceived rms signal-to-noise ratio for the thres-
hold perception of noise in any frequency-specific channel may be obtained
from the contrast detection model described in Section IV.B, assuming that the
noise power spectrum is white. These equations yield

$$S/N = R(\nu) \left\{ \left(\frac{\nu_{max}}{2\Delta\nu(\nu)} \right) \left(m_T^2(\nu) + k(\nu)m_I^2(\nu) \ R^2(\nu) \right) \right\}^{-1/2} \tag{5}$$

where ν_{max} is the upper cutoff frequency of the noise power spectrum, expressed
in retinal frequency units, and $m_I(\nu)$ is the magnitude of the signal component
that interferes with the visibility of the noise. The quantity $m_I(\nu)$ is given
by Eq. (27) for the case of a luminance edge transition, and by Eq. (28) for
the case of the ensemble-averaged power spectrum of pictorial scenes. For a
uniform luminance display, there is no interfering signal so that $m_I(\nu) = 0$.
The values of the channel width $\Delta\nu(\nu)$ are given in Table 11.

In applying this equation we will assume that the threshold of the noise
is determined by the most sensitive frequency-specific channel. Thus, the
threshold signal-to-noise ratio is computed by maximizing the right side of
Eq. (5). This simplification will not substantially modify the results. (It
is shown in Section IV.F that this approximation is indeed valid at threshold.)

23

Situation:

A Navy display engineer is required to specify signal-to-noise ratio standards for different display systems. The standards should allow minimum visibility of the noise, but they should not be so severe that other aspects of display performance are potentially compromised. Furthermore, since several systems will be used to display different types of information, the standards should reflect these differences. What guidance can he give his suppliers on this question?

Take as a specific case a bright display viewed at a distance of 3 picture widths. The bandwidth of the display, expressed in TV-line numbers $N_{TV} = 2fw$, is 300 lines. Further, assume that $R(\nu) \overset{\sim}{=} 1.0$ and that the input noise power spectrum is white.

Solution:

We shall use Eq. (5) to determine the threshold signal-to-noise ratio required so that only 1 jnd of noise is visible.

Case 1: Threshold Perception of Noise on a Uniform Luminance Display

This case requires the largest signal-to-noise ratio for threshold noise visibility, since there is no signal on the screen to mask the perception of the noise. This value of S/N would apply only to those situations where the displayed information was of extremely low contrast. We present it here in order to determine the maximum value of signal-to-noise that would be required. For most practical cases, as will be shown below, a much smaller value of S/N would be needed.

Solving Eq. (5) with $m_I(\nu) = 0$ and $\nu_{max} = \pi rf/180 = (\pi/360)(N_{TV}r/w) \overset{\sim}{=} 8.0$ cycles/degree, we find that the required S/N is 500 (54 dB), achieved at $\nu \overset{\sim}{=} 6$ cycles/degree (where $\Delta\nu = 4$ cycles/degree), $m_T(6) = 0.002$ from Table 11, and $k(6) = 0.185$ from Table 11).

Case 2: Threshold Perception of Noise in the Presence of the Ensemble-Averaged Power Spectrum of Pictorial Scenes

Here we predict the maximum signal-to-noise ratio required for the important case of white noise in the presence of high-contrast pictorial information. Again using Eq. (5), along with Eq. (28), we find that the maximum required S/N for this situation is 54 (35 dB), which occurs at $\nu = 6$ cycles/ degree (from Table 10 we have taken, as a representative scene modulation

24

depth, $\sqrt{I_m^2/\bar{I}}$ = 1/2 and, from Table 11, k(6) = 0.185). As expected, this signal-to-noise ratio is considerably less than the signal-to-noise ratio required for a uniform luminance display. We feel that this value represents the best estimate for the required S/N on the display under typical operating conditions. (See Appendix C for additional comments on the meaning of this S/N.)

Case 3: Threshold Perception of Noise Near a High-Contrast Edge

Here we assume that the observer is looking directly at a high-contrast luminance edge transition so that the perception of the noise is heavily masked by the edge. This case is most representative of alphanumeric displays where the displayed information consists exclusively of highly modulated edge transitions.

Solving Eq. (5) and using Eq. (27), we obtain a S/N of 17 (25 dB) for the threshold perception of the noise for the case of a 100% contrast edge. This value is considerably less than either the value obtained using the ensemble-averaged power spectrum of pictorial scenes (35 dB) or the value computed assuming a uniform luminance display (54 dB).

These examples illustrate the range of S/N values required for imaging devices displaying different types of information with the constraint that the display noise be at the threshold of perception. Since a single jnd represents a barely perceivable amount of noise, there are many situations where signal-to-noise ratios less than those computed would prove acceptable.

c. *Effect of Display Luminance on Perceived Image Structure* - The effect of the mean display luminance on the DDDs is through the sine-wave contrast sensitivity function of the visual system (refer to Section IV.C). It has been found that for mean luminances below roughly 35 mL, contrast sensitivity increases (i.e., $m_T(\nu)$ becomes smaller) with increasing luminance. But for mean luminances above 35 mL, contrast sensitivity saturates rapidly.

In this report we consider two mean display luminances: 35 mL and 1 mL. The DDDs computed assuming a mean display luminance of 35 mL are suitable for all high-luminance displays, such as conventional home television receivers, airplane cockpit indicators, or radar displays, where the mean display luminance are typically at or above 35 mL. The DDDs computed assuming a luminance

25

of 1 mL indicate the perceptual response for the lowest practical mean display luminance. Even large-screen projection television and 35-mm film theater systems, which must often be viewed in dark ambiances, have mean display luminances between 5 and 10 mL [8].

The influence of the mean display luminance on display performance can be quantified with the aid of the DDDs. As representative examples we show in Fig. 10 (a) and (b) DDD Nos. 18 and 20, which show the signal levels for two noiseless displays with mean luminances of 35 and 1 mL, respectively. The input signal is a single, 100% contrast edge transition. These figures clearly demonstrate the loss in perceived image structure at the lower display luminance. For example, at 3.0 cycles/degree with $R(3) = 1.0$ there are a total of 44 jnd's available for the high-luminance display, and only 29 for the low-luminance display.

The loss in perceived image structure due to low display luminance is shown most dramatically in Fig. 10(a) for the 35-mL display. The curve shown on this figure represents the number of perceived signal levels between $R(\nu) = 0$ and $R(\nu) = 1.0$ for the 1-mL display. That is, the same image structure would be seen on both displays if the 1-mL display had an MTF of unity and the 35-mL display had the MTF shown as the curve on the figure. Yet, the general impression of image quality in these two cases would be quite different. The high-luminance, poor-MTF display would appear washed out or simply unsharp; the low-luminance, unity-MTF display would look relatively good. This subjective comparison would not be a result of relative information transfer in the two cases; the DDDs predict that the information available in the two displays would be identical. Rather, it is an expression of an observer's reaction to the amount of information that is actually presented, relative to what *can* be presented.

It is a common experience that if the luminance of a noisy photographic image is reduced sufficiently, the visibility of the noise will eventually disappear. This is, of course, a direct manifestation of the loss in visual sensitivity described above. We illustrate this effect in Fig. 11(a) and (b) with the aid of DDD Nos. 49 and 52. These figures show the number of perceived noise levels on uniform luminance displays with mean luminances of 35 and 1 mL, respectively. As before, we have plotted the MTF on the high-luminance display

26
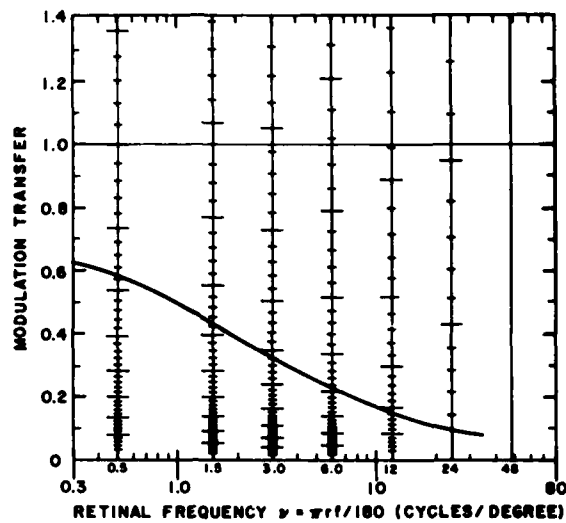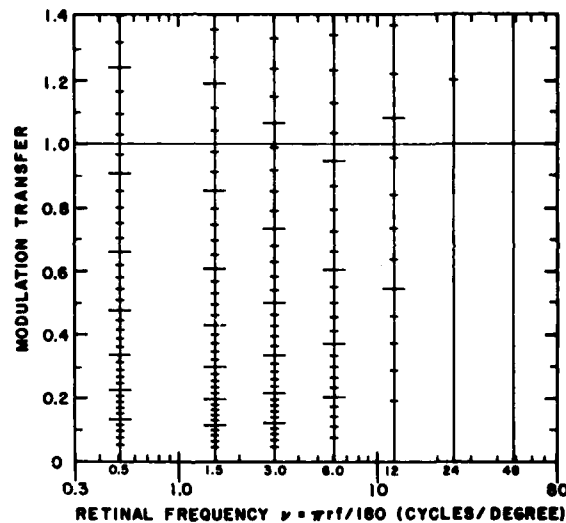
Figure 10. Effect of display luminance on perceived image structure (example B.2.c). These two figures show how the discriminable signal levels change when the mean display luminance is reduced from 35 mL (a) to 1 mL (b). The curve on (a) represents the number of perceived signal levels between $R(\nu) = 0$ and $R(\nu) = 1.0$ for the 1-mL display. Said differently, a display with $\bar{I} = 35$ mL and the MTF shown on (a) will present the same number of distinguishable levels to an observer as a display with $\bar{I} = 1$ mL and $R(\nu) = 1.0$. Figures (a) and (b) are, respectively, copies of DDD Nos. 18 and 20 for the signal levels. In both cases $\sqrt{N(f)}/\bar{I} = 0$ and $r/w = 10$.

27
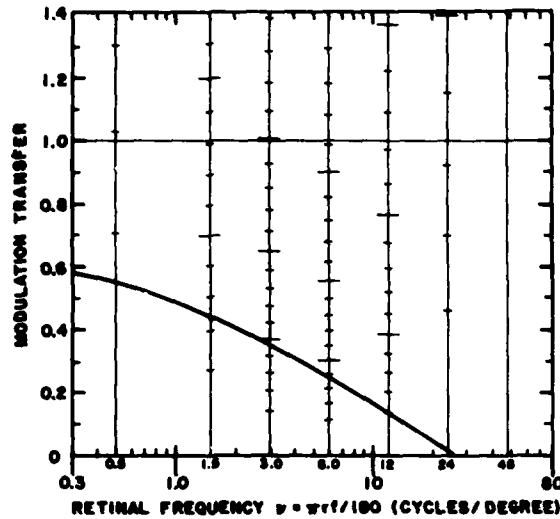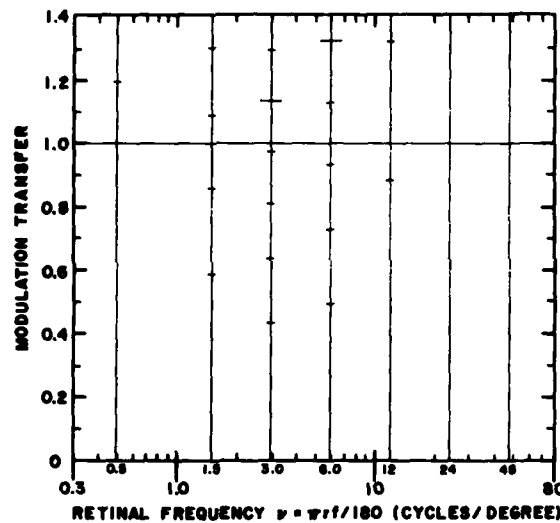
Figure 11. Effect of display luminance on the visibility of display *noise* (example B.2.c). These two figures show how the discriminable noise levels on a uniform luminance display change when the mean display luminance is reduced from 35 mL (a) to 1 mL (b). The curve on (a) represents the number of perceived noise levels between $R(\nu) = 0$ and $R(\nu) = 1.0$ for the 1-mL display. Clearly reducing the display luminance greatly reduces the amount of noise visible. Figures (a) and (b) are, respectively, copies of DDD Nos. 49 and 51. In both cases $\sqrt{N(f)}/\bar{I} = 0.1$, $r/w = 10$, and $r = 100$ cm.

28

that allows the same number of noise levels to be perceived on the low-luminance display when $R(\nu) = 1.0$. As expected, the visibility of the noise on the low-luminance display is greatly diminished.

These demonstrations show that when the total capabilities of different display systems are compared, they should be compared on the basis of absolute performance, and not just their subjective visual impressions. It is clear that any system examined under low-light conditions will have large cosmetic advantages with regard to an overall impression of image quality since noise and MTF losses will be less visible. However, the signal information available in systems viewed under high-luminance conditions is, in general, substantially greater than that available at low-light conditions.

d. Effect of the Viewing Distance Parameter r/w on Perceived Image Structure - In Section IV.C it is shown that the threshold visibility (or contrast sensitivity) of sine-wave gratings decreases with decreasing display size. For the displays of interest here, which are viewed from a distance of 3 to 30 picture widths, Fig. 122 shows that this loss in visibility is almost exclusively at the lower retinal frequencies. Therefore, variations in the DDDs due to different r/w will also occur at the lower retinal frequencies.

In order to illustrate this, we have replotted DDD Nos. 1, 18, and 30 here as Fig. 12(a), (b), and (c), which gives the distribution of perceived signal levels for r/w = 3, 10, and 30, respectively. These DDDs show that over this range of r/w, the largest changes in the discriminable levels are at 0.5 cycle/degree. At higher frequencies the differences between the diagrams decrease, and for frequencies above roughly 12 cycles/degree the diagrams are essentially the same.

The observation that the DDDs are not a strong function of r/w at intermediate to high retinal frequencies will aid in the solution of many problems where the required value of r/w is not provided by a specific DDD. For example, consider the case where r/w = 6, but the MTF of the system under investigation is significantly less than unity only at the higher retinal frequencies. In this case the diagrams for either r/w = 3 or r/w = 10 may be used to predict the loss of image structure due to this MTF.

e. Comparison of the Sharpness of NTSC and PAL Systems - Many international travelers have commented that European television, which uses the PAL system,
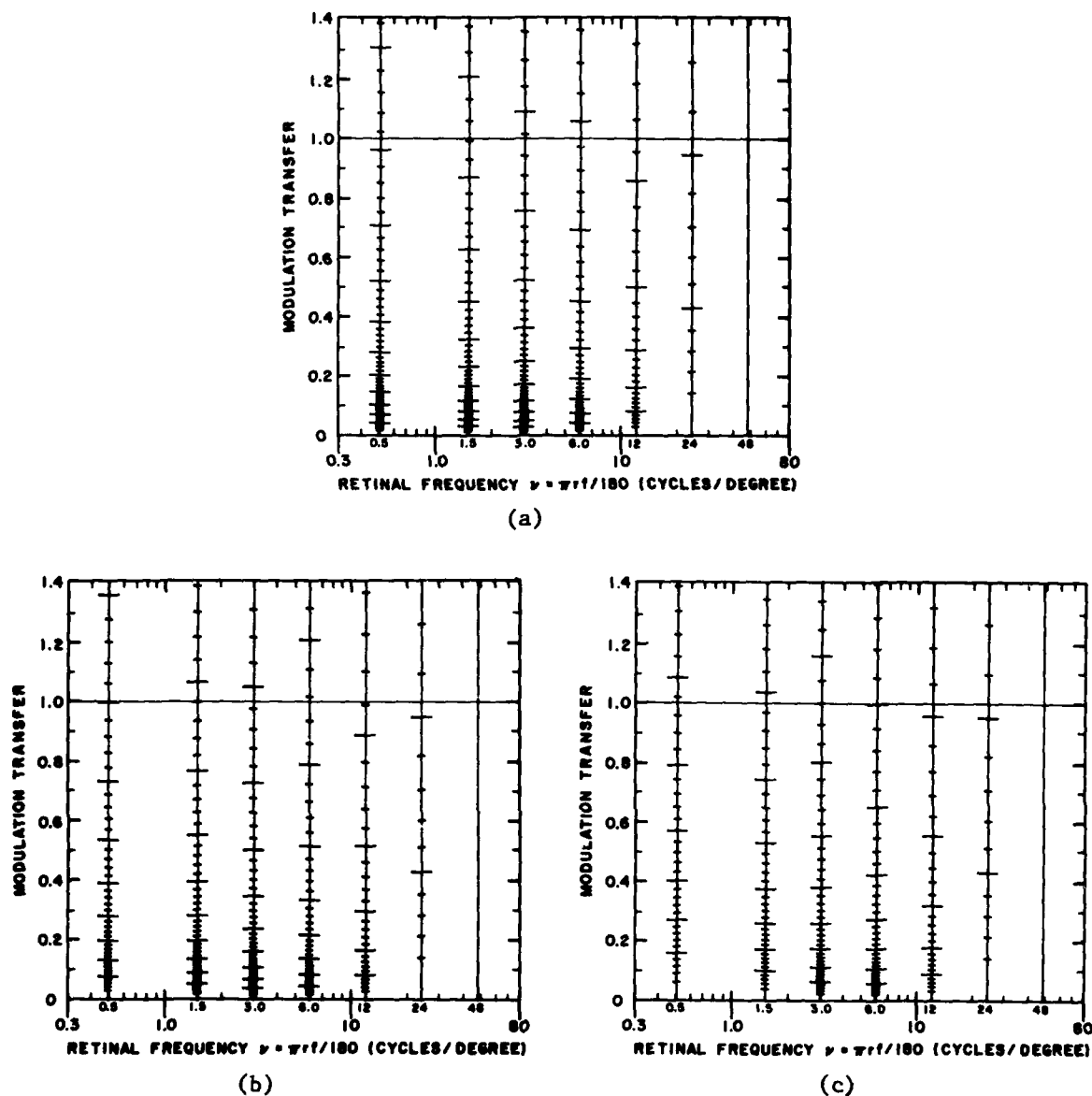
Figure 12. Effect of the viewing distance parameter r/w on the distri-
bution of distinguishable signal levels (example B.2.d).
For the three values given (r/w = 3, 10, and 30), it may be
seen that the primary effect of changing r/w is at the
lowest spatial frequencies. For frequencies above roughly
12 cycles/degree the diagrams are essentially the same for
$3 \le r/w \le 30$. Figures (a), (b), and (c) are, respectively,
copies of DDD Nos. 1, 18, and 30. In all three $\sqrt{N(f)}/\bar{I}$ =
0 and $\bar{I}$ = 35 mL.

30

is considerably sharper than American television, which uses the NTSC system. There are several differences between these two approaches (an example due to sampling will be given later), but one obvious reason for the improved sharpness is that the luminance bandwidth in the horizontal direction is 4.2 MHz for PAL and 3.5 MHz for NTSC. If we assume that noise is not a significant factor, that both systems are presented on high luminance displays, and that the viewing distance is 6 picture widths, we can use DDD No. 1 to estimate the differences in sharpness between these two systems. (For the reasons presented above in example d, this diagram, computed for $r/w = 3$, is appropriate for this case.)

For ease of computation, we will approximate the bandpass characteristic of the NTSC system by a unity MTF up to $N_{TV} = 300$ lines and the PAL system by a similar characteristic with a 360-line cutoff. With these approximations it is simple to represent the two systems on DDD No. 1, as shown in Fig. 13. The upper cutoff frequency for the NTSC system is roughly 16 cycles/degree; for the PAL system it is roughly 19 cycles/degree. It may be seen from the figure that this change in bandwidth results in only a small change in the signal contained within the frequency-specific channel centered about 24 cycles/degree (see Table 11). An estimate of the improvement in image sharpness associated with the PAL system may be obtained if the 12 jnd's in the column centered at 24 cycles/degree are apportioned uniformly within the channel. This computation predicts that there is roughly a 3-jnd difference between the two systems. Although this represents a demonstrable improvement when two displays are examined side by side, it is unlikely that this difference is striking enough to survive in the memories of travelers crossing the Atlantic. However, if the viewing distance is now changed to 2 picture-widths, the difference between the two systems is increased to roughly 10 jnd's. This sharpness advantage in favor of the PAL system is probably great enough to account for some of the enthusiasm its supporters express.

C. APPLICATION OF THE DDDs TO SAMPLED AND RASTER DISPLAYS

1. Introduction

Sampled and raster displays form an important and widely used class of imaging devices for commercial and military applications. Therefore, we
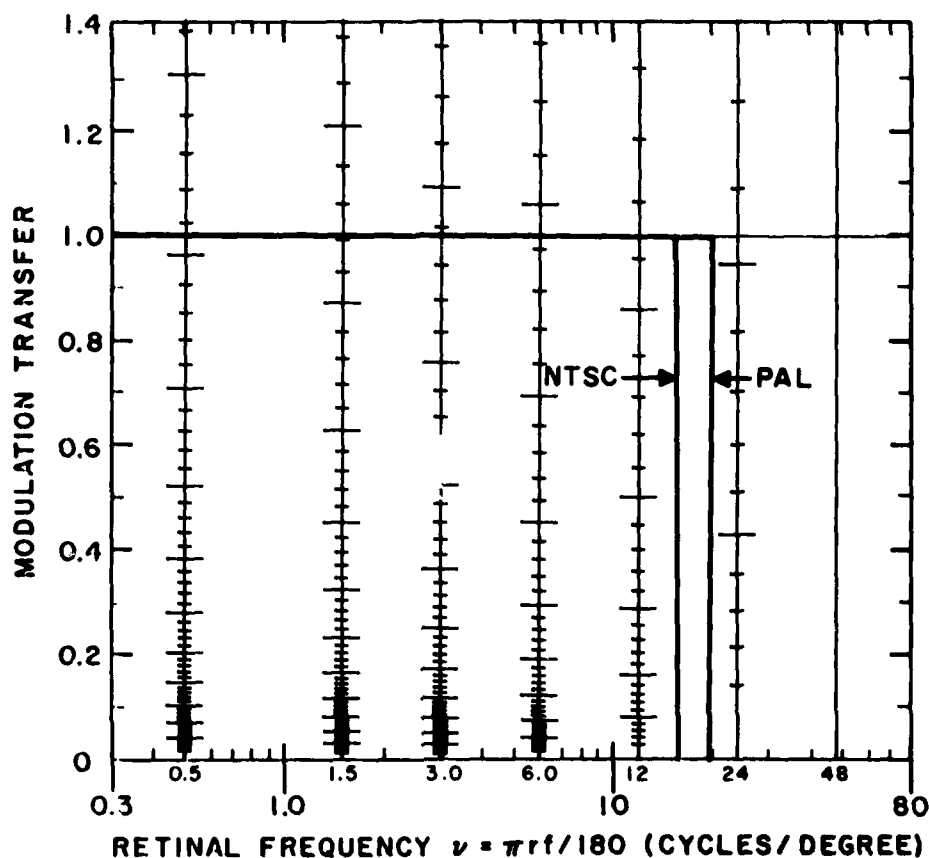
Figure 13. Comparison of the sharpness of NTSC and PAL systems (example
B.2.e). We have plotted on DDD No. 1 for signal levels
$(\sqrt{N(f)}/\bar{I} = 0, \bar{I} = 35$ mL, and $r/w = 3)$ the approximate hori-
zontal rectangular-bandpass characteristics for these two
systems. By simple subdivision of the jnd's in the channel
located at 24 cycles/degree, it is estimated that the PAL
system is roughly 3 jnd's sharper than the NTSC system in
horizontal direction for the conditions explained in the text.

32

include here an expansion and application of the methods described in Section II.B, for the case of analog displays, to selected topics of interest in sampled and raster displays.

a. Parameters for the Sampled/Raster Display Problem - Figure 14 shows a schematic representation of a prototypical sampled display. The various functions and the parameters describing the display system are given below.

Prefilter: In general, the prefiltering process may arise from both optical and electronic sources. The lens of a camera is a common example of pre-filtering. In addition, special circuitry in the display device may pur-posely band-limit the signal in order to reduce or eliminate sampling noise and aliasing. The prefiltering process is described by a transfer function $R_p(f)$, where f is the spatial frequency on the display screen. Two specific cases of interest here are the extreme undersampled display and the Nyquist-sampled display. In the extreme undersampled display, $R_p(f)$ falls off over frequencies that are large compared with the sampling frequency of the display and the characteristic frequency of the visual system. Thus, we may take

$$R_p(f) = 1 \; ; \; \text{Undersampled Display} \tag{6}$$

In the Nyquist-sampled display, the function $R_p(f)$ is specifically chosen to eliminate the possibility of aliasing [9]. The function that simultaneously fulfills the Nyquist criterion for the elimination of aliasing and best pre-serves image quality is a simple low-pass filter with a sharp cutoff at $f = \frac{1}{2} f_s$, where f_s is the sampling frequency:

$$R_p(f) = 1 \; ; \; |f| < \tfrac{1}{2} f_s$$
$$= 0 \; ; \; |f| \geq \tfrac{1}{2} f_s \tag{7}$$

Sample: The sampling process may be carried out either by special electronic circuitry or by the image pickup device itself (e.g., CCD cameras). The prefiltered signal is sampled within N_s equally spaced sampling locations across the display. For a display of width w, the sampling frequency f_s is given by

$$f_s = N_s/w \tag{8}$$

The sampling process consists of taking the average of the prefiltered signal over a fraction s of the width $1/f_s$ of each of the N_s sampling apertures.

33

| INPUT SCENE | → | PREFILTER | → | SAMPLE | → | POSTFILTER & DISPLAY | - - -→ | OBSERVER |

$\Phi(f)$ $R_p(f)$ s $R_D(f)$ r
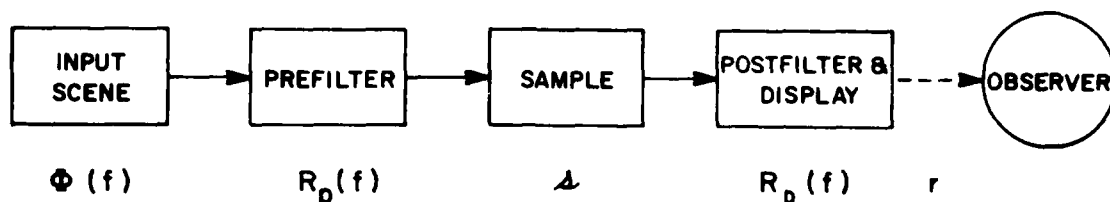
Figure 14.   Prototypical sampled/raster display considered in this re-
port. The input signal, which is represented by its power
spectrum $\Phi(f)$, is first prefiltered by $R_p(f)$, then sampled
by an aperture function s, and finally presented on a dis-
play with MTF $R_D(f)$. In this model $R_D(f)$ also acts as a
postfilter to improve display performance. $Rp(f)$ is
chosen here to give either an extreme undersampled display
or a Nyquist-sampled display, and s is taken to be either
1 (full width sampling) or 0 (delta-function sampling).
The displayed signals are viewed by an observer at a dis-
tance r from the display of width w.

The parameter s is called the sampling width. Two representative values of s
will be considered here. The value s = 0 is called "delta-function sampling";
only the value of the prefiltered signal at the center of the sampling aperture
contributes to the displayed picture. The value s = 1 is called "full-width
sampling." In this case the sampled signal consists of the average of the pre-
filtered signal over each entire sampling aperture. Other values of s may be
handled through the use of the equations presented in Appendix B.

Postfilter and Display: In general, the sampled signal is acted upon by a
postfilter function and displayed on the screen by the use of an appropriate
display device. The combined effect of the postfilter-and-display operation
is represented by a modulation transfer function $R_D(f)$. As will be seen later
in this section, the function $R_D(f)$ is of great importance in determining dis-
play performance.

Observer: The displayed pattern is perceived by an observer located a distance
r from the screen. For the sampled/raster display problem, the natural unit
of viewing distance is the quantity $N_s r/w$. This quantity, when multiplied by
$\pi/180$, gives the retinal frequency, in cycles/degree, corresponding to the
sampling frequency of the display.

b. Discriminable Difference Diagrams for Sampled/Raster Displays - Table 9
lists the Discriminable Difference Diagrams (DDDs) for sampled/raster displays.
The DDDs were constructed using Eqs. (B-14), (B-15), and (31) for the case of

34

a single 100% contrast edge transistion. Table 11 furnished the necessary parameters. (If necessary, the reader can employ these equations to construct DDDs with values of $N_s r/w$, s, and $R_p(f)$ other than those listed in the table.) The meaning and use of the DDD are described in Sections II.B and IV for the case of analog displays. Three differences between the DDDs for sampled/raster displays and those for analog displays are worth noting. First, the DDDs for sampled/raster displays utilize the normalized display frequency f/f_s as the frequency coordinate, rather than the retinal frequency ν. This is because the sampling process provides a natural unit of frequency which can be used to describe the performance of the other components of the display system. As in the case of analog displays, the center frequencies of the visual channels have been set at 0.5, 1.5, 3.0, 6.0, 12, 24, and 48 cycles/degree. Naturally, the relative positions of these key frequencies in the DDDs will depend on the viewing distance. Second, the modulation transfer function displayed in the ordinate of the DDDs is only the postfilter-and-display transfer function $R_D(f)$; the prefilter modulation transfer function $R_p(f)$ is not included. Rather it is treated as a parameter for the DDDs for the two special cases, Eqs. (6) and (7). Last, the noise source for the sampled/raster case is restricted to that arising from the sampling process itself. In Section II.C of TR1, it was shown that the sampling process produces the sum of a signal term and a fluctuating term. The signal term is completely correlated with the input information, whereas the fluctuating term displays the fundamental statistical attributes of noise. In preparing the DDDs, we have employed the partition of the total display output into signal and sampling noise components. Thus, the perceivable noise levels displayed in the appropriate DDDs refer to levels of sampling noise. Similarly, the effect of sampling noise on the distribution of perceivable signal levels was treated in the same way as ordinary noise in analog displays.

2. Examples

The following series of hypothetical examples is offered as illustrative of the use of the model and the DDDs. The examples are not intended to be exhaustive but rather to aid the reader in the application of the model to practical display problems.

35

a. Perception of Raster Lines in a White Field - An engineer charged with the
design of a CRT cockpit display has been told that he must, at all costs,
avoid the perception of raster line structure. Alleged pilot performance de-
gradation arising from confusion of displayed information with raster line
structure is cited as the reason. The engineer wants to know what this
constraint implies for the size of the electron beam spot that is used to scan
the display screen. He knows that the display is to be 15 cm wide and will be
viewed from a distance of about 45 cm. The CRT is to have 480 raster lines
and will be operated at a mean luminance above 35 mL.

The worst case for the perception of raster lines is a simple white field.
Accordingly, we substitute the input spectrum $\hat{I}_o(f) = \bar{I}\delta(f)$ into Eq. (B-1)
[Appendix B] for the displayed intensity pattern of a sampled/raster display
and obtain

$$I(x) = \bar{I}\left\{1 + 2\sum_{m=1}^{\infty} R_D(mf_s)\ \cos(2\pi m f_s x)\right\} \tag{9}$$

This equation states that the displayed intensity pattern is a sum of harmonics
of the sampling frequency with amplitudes determined by the value of the dis-
play modulation transfer function R_D at the appropriate harmonic. For the
case at hand, R_D may be regarded as the Fourier transform of the electron-
beam spot profile. Therefore, we seek a condition on R_D that will render the
raster line structure invisible.

According to the concept of independent frequency-specific channels de-
scribed in Sections IV.A and IV.B, if the amplitude of any one of the harmonics
exceeds the threshold sensitivity function m_T evaluated at the corresponding
retinal frequency $\nu = (\pi/180)mf_s r = (\pi/180)N_s r/w$, the raster lines will be per-
ceived. In our case, the first harmonic corresponds to $\nu = 25.1$ cycles/degree.
Referring to Fig. 122 for $r/w = 3$, it is seen that this frequency lies on the
rapidly decreasing part of the sensitivity curve. Thus, we need consider only
the first harmonic $m = 1$. The condition for the raster line structure to be
invisible is then

$$R_D(f_s) > \tfrac{1}{2}m_T(\pi f_s r/180) \tag{10}$$

Using Fig. 122 for the high-luminance contrast sensitivity function and for
$r/w = 3$, we find $m_T(25.1) = 0.024$ so that the condition [Eq. (10)] is

$$R_D(f_s) > 0.012 \qquad\qquad (11)$$

To proceed further, we must assume an explicit form for $R_D(f)$. It is known that electron beam-addressed displays often exhibit Gaussian spot profiles [10]. Then, taking a spot profile proportional to $\exp[-(2x/d)^2]$, where d is the width of the spot at the 1/e point, we can easily Fourier transform this spot profile to obtain the display MTF $R_D(f) = \exp[-(\pi f d/2)^2]$. Then the condition Eq. (11) becomes

$$(\pi N_s d/2w) > 2.1 \qquad\qquad (12)$$

For the display parameters given, the condition that the raster line structure be invisible is that d be greater than 0.042 cm, or about 1.3 times the width of a raster line.

b. *Elimination of Aliasing* - A CCD camera manufacturer believes that his market will not tolerate a product that produces perceivable aliasing when the camera is exposed to high-frequency periodic patterns. Accordingly, he is planning to attach an optical device to the camera that will effectively pre-filter the signal to eliminate such aliasing. He wants to specify the required values of the modulation transfer function of the device so that the vendor can design and build test models. The camera will consists of a 512 x 512 array, and it is anticipated that the displayed material will generally be viewed at high luminances ($\sim$35 mL) and at viewing distances of about 6 picture widths.

This problem can be easily solved by treating the worst case of an input signal consisting of a 100% modulated sine-wave of frequency $f_o > \frac{1}{2}f_s$ super-imposed on a white field. In general such an input will produce a low-frequency aliased sine-wave. It is convenient to write f_o in the form

$$f_o = f_s [1-(180\nu/\pi)/(N_s r/w)] \qquad\qquad (13)$$

Then the aliased sine-wave will be produced at a display frequency $(f_s - f_o)$, corresponding to a retinal frequency ν. According to Eq. (B-1) [Appendix B] for the displayed intensity pattern of a sampled/raster display, the contrast of the aliased sine-wave is then

$$m = R_D(f_s - f_o) \, R_P(f_o) \, \text{sinc}(sf_o/f_s) \qquad\qquad (14)$$

where $sinc(x) = sin(\pi x)/\pi x$. To be conservative, the camera manufacturer would be wise to assume that the transfer function of the display system that will utilize the camera will have excellent performance over the frequency range $0 \leq f \lesssim f_s$. Thus, we set $R_D = 1$ in Eq. (14). Furthermore, the nature of the CCD imaging device is such that full-width sampling ($s = 1$) is appropriate. With these simplifications, the condition that the aliased sine-wave *not* be perceived is

$$R_P(f_o) < m_T(\nu)/sinc(f_o/f_s) \tag{15}$$

where the display frequency f_o is related to the retinal frequency ν through Eq. (13).

Using Fig. 122 for the high-luminance contrast sensitivity function and the given values $N_s = 512$ and $r/w = 6$, we have computed the required values of the function $R_P(f_o)$ given in Table 1. Only frequencies in the range $0.67f_s \leq f_o \leq f_s$ were considered because, for frequencies below about $0.67f_s$, the input and the aliased sine-wave will lie at frequencies within an octave of each other. In that case, masking of the aliased sine-wave by the input will begin to become important, so that Eq. (15) will be pessimistic. From the entries in the table, it is seen that the camera manufacturer should specify that the optical device should exhibit a frequency response that falls to about 0.02 at or above $0.67f_s$. Naturally, he should also stipulate that

TABLE 1. REQUIRED VALUES OF THE FUNCTION $R_P(f_o)$
FOR THE ELIMINATION OF ALIASING

f_o/f_s	$R_P(f_o)$	ν (cycles/degree)
0.67	0.018	17.5
0.72	0.016	15.0
0.77	0.015	12.5
0.81	0.015	10.0
0.86	0.016	7.5
0.91	0.019	5.0
0.95	0.031	2.5
0.99	0.414	0.5

$R_P(f_o)$ should be as high as possible below $f_o = \frac{1}{2}f_s$ in order to maintain image quality.

c. Effect of Increasing the Display Modulation Transfer Function - An electron optics design engineer working for a television kinescope manufacturer finds that a simple redesign of the electron gun used in the current product will reduce the size of the focused electron beam spot on the kinescope screen by 1/3. He also discovers that, with considerably greater effort and cost of manufacture, he can reduce the size of the beam by another 33%, for a total reduction of 56% from the current product. He wants to know the perceptual effect of these improvements, relative to their cost, so that he can recommend a course of action to his management.

We confine ourselves to the case of a high-contrast edge transition displayed horizontally, i.e., the direction parallel to the scanned raster lines. We take $N_s = 525$, corresponding to the U.S. NTSC standards, and consider a viewing distance of about 5 picture widths in the vertical direction, so that the DDDs for $N_s r/w = 2500$ can be utilized. It is assumed that the image pickup device, presumably a vidicon camera, effectively averages over one scan line, so that the sampling width $s = 1$ is appropriate. Also, since there is no pre-filtering function in the image transmission and receiving system, the display can be regarded as operating in the extreme undersampled limit [Eq. (6)]. Therefore, DDD No. 87 for the signal and DDD No. 99 for the sampling noise can be employed. These figures are reproduced below as Fig. 15(a) and (b) with the display modulation transfer functions for the current product (A), the first redesign (B), and the second redesign (C) indicated in the figures.

Referring to the DDDs, the reader can easily verify by simply summing over the jnd's associated with each of the key frequencies (see Section IV.F), that (1) design B would have an advantage of about 10 jnd's of signal over design A, (2) design C would have an advantage of about 3 jnd's of signal over design B, (3) neither design A or B would produce a single jnd of sampling noise, and (4) design C would produce nearly 2 jnd's of sampling noise. The difference of 10 jnd's of signal between design B and design A is considered extremely significant. However, the difference of 3 jnd's of signal between design B and design C, while still definitely perceivable, is substantially less, even though the physical improvement between the successive redesigns
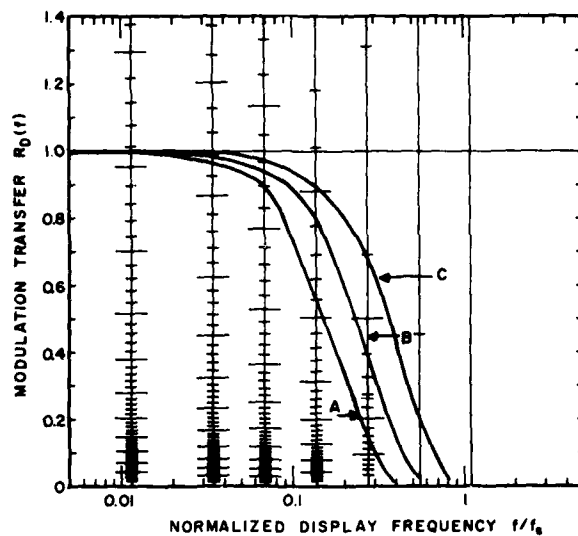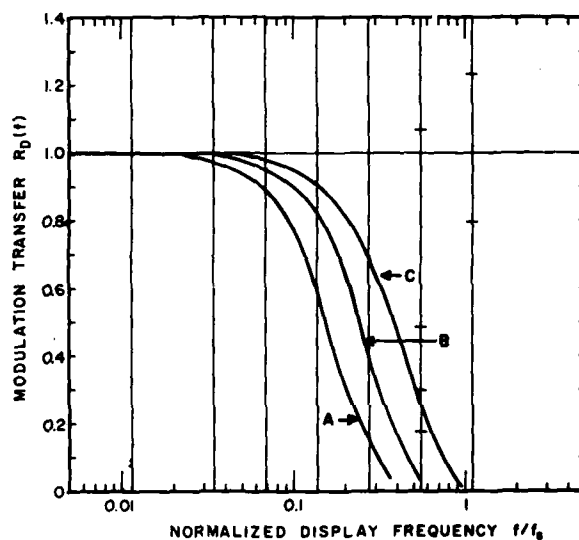
Figure 15. DDDs appropriate for determining the effect of increasing the display modulation transfer function on the signal (a) and the sampling noise (b) of a television display. The current product is indicated by curve A, the first redesign by curve B, and the second redesign by curve C.

40

is identical. Furthermore, the size of the focused spot of design C has become so small that perceivable sampling noise at high contrast edges would be produced. In view of these observations and the additional cost of design C, the engineer might well recommend that his company opt for design B.

d. *Effect of Prefiltering on Signal and Noise jnd's* - A new sampled display system will utilize an array of 256 x 256 sampled picture elements. The only commercially available digital signal-processing system samples the incoming signal at discrete points, so that the sampling width s is effectively zero. No prefiltering of the signal is planned at present because the designers are concerned that any significant prefiltering would produce such a narrow-band system that image quality would suffer. It is anticipated that the display will typically be viewed from a distance of about 5 picture widths. The display is to have a printing-beam profile that is constant over one entire picture element and does not overlap adjacent picture elements. The Fourier transform of such a profile gives the display modulation transfer function

$$R_D(f) = \text{sinc}(f/f_s) \tag{16}$$

where, once again, $\text{sinc}(x) = \sin(\pi x)/\pi x$.

The first prototype displays have been found to exhibit disappointingly poor image quality. Figure 16(a) shows an image formed on a small fraction of the display; Fig. 16(b) shows the same image displayed on an alternative system which utilizes full-width sampling (s = 1). It is apparent that the image of Fig. 16(a) is a less faithful rendition of the original picture than the image of Fig. 16(b). Although the total perceived luminance structure produced by the display of Fig. 16(a) is larger than that of Fig. 16(b), much of this structure appears to be extraneous and uncorrelated with the real picture information. The problem is how to increase the image quality of the display of Fig. 16(a) within the constraints imposed by the s = 0 sampling system.

We consider the effect of adding a Nyquist prefilter to the s = 0 display. DDD Nos. 81 and 93 for the undersampled display and Nos. 82 and 94 for the Nyquist-sampled display are appropriate for this case. These DDDs are reproduced below in Fig. 17, with the magnitude of the display modulation transfer function Eq. (16) superimposed on the diagrams. By simple summation of

41
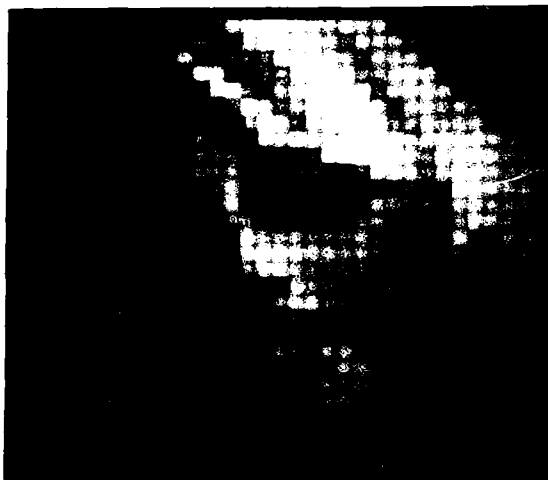
(a) $s = 0$ and $R_p = 1$
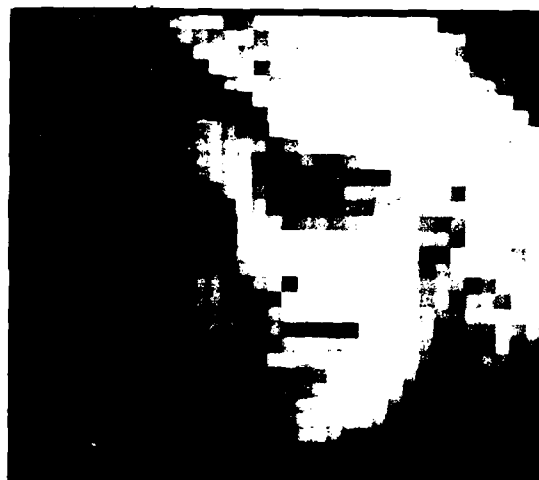
(b) $s = 1$ and $R_p = 1$ (c) $s = 0$ and Nyquist prefiltered

Figure 16.   Images formed on a small fraction of three sampled displays:
(a)   Delta-function sampling ($s = 0$) and no prefiltering
($R_p = 1$), (b)   full-width sampling ($s = 1$) and no prefiltering
($R_p = 1$), and (c)   delta-function sampling ($s = 0$) and a pre-
filter that approximately fulfills the Nyquist criterion
[Eq. (7)].   To approximate the conditions discussed in
example d (Section II.C.2.d), the reader should view the
pictures from a distance of about 40 picture widths.
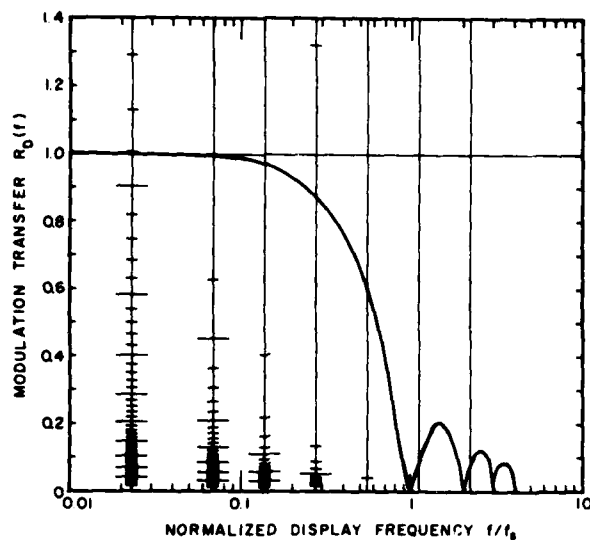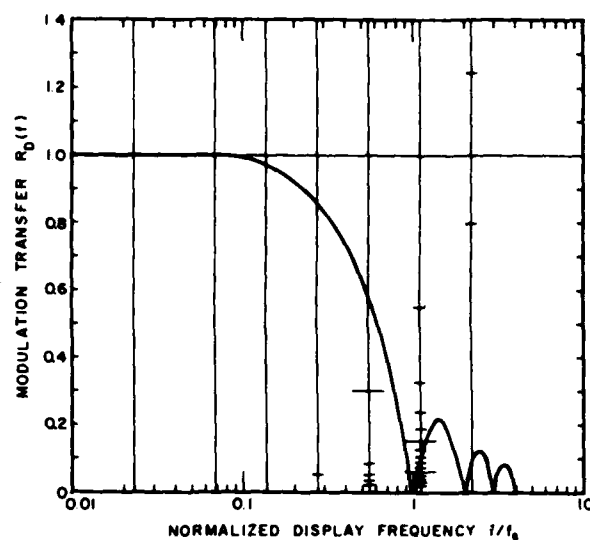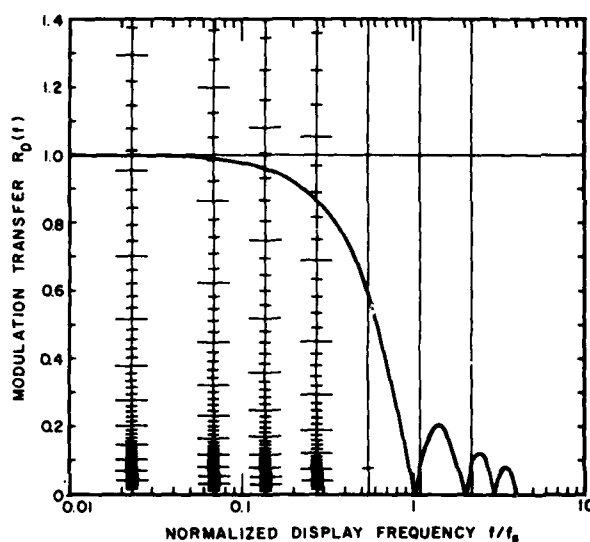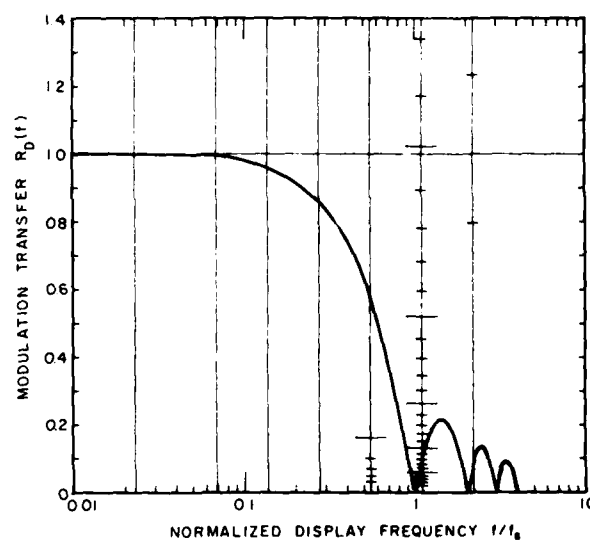
Figure 17.   DDDs appropriate for determining the effect of adding a
Nyquist prefilter to a display with delta-function sampling
(s = 0):   (a) Signal levels and (b) sampling noise levels
for a display with no prefilter (R_p = 1);   (c) signal levels
and (d) sampling noise levels for a display with a Nyquist
prefilter [Eq. (7)].   The magnitude of the display MTF [Eq.
(16)] is superimposed on the diagrams.

43

the appropriate jnd's, one obtains the values of the total number of jnd's of signal, J_S, and of noise, J_N, given in the first two lines of Table 2. These values show that the use of the Nyquist filter produces a dramatic increase in the value of J_S while slightly decreasing the value of J_N. Indeed, the value of J_S exceeds those for displays with full-width sampling, with or without a Nyquist prefilter. Figure 16(c) shows a portion of a display employing both s = 0 sampling and a prefilter that approximates the Nyquist prefilter Eq. (6). The dramatic improvement over the display of Fig. 16(a) is apparent (the reader should view the picture from a distance of about 40 picture widths in order to approximate the condition $N_s r/w = 1250$).

TABLE 2. PARAMETERS FOR DISPLAYS AT VIEWING DISTANCE $N_s r/w = 1250$

Sampling Width(s)	Prefilter	J_S^*	J_N^*
0	None	106	14
0	Nyquist	190	13
1	None	168	13
1	Nyquist	188	15

*With display modulation transfer function $R_D(f) = \text{sinc}(f/f_s)$

The reasons for the great improvement in image quality achieved with the use of the Nyquist prefilter are readily understood. DDD No. 81 shows that nearly all of the jnd's of the original, undersampled display are associated with display frequencies below $\frac{1}{2}f_s$. Therefore, the addition of a Nyquist prefilter certainly cannot have a deleterious influence on image quality because of its band limitation effect, as the designers had originally feared. On the other hand, for frequencies below $\frac{1}{2}f_s$, the effect of the Nyquist pre-filter is to completely eliminate the sampling noise, which masks the perception of the signal information, thereby permitting the full complement of jnd's of signal to be realized.

The effect of the Nyquist prefilter on the value of J_N is the sum of two competing effects. First, the sampling noise spectrum is reduced at all frequencies. This effect, which tends to reduce J_N, is at least partially

offset by the elimination of the signal spectrum present at frequencies above $\frac{1}{2}f_s$. This signal content had served to mask the perception of noise at high frequencies and, therefore, to reduce J_N. In the case at hand, the two effects nearly cancel, so that the value of J_N is little changed by the addition of the Nyquist prefilter.

e. *Change in Sampling Frequency Required to Produce an Improvement in Perceived Image Quality* - Visitors to Europe often return with the impression that European commercial color television has significantly better image quality than the U.S. counterpart. Reasons proposed for this apparent difference include better signal transmission, less sensitivity to phase errors in the chrominance signal processing, wider bandwidth for luminance signals (see example e of Section II.B.2), and a larger number of raster lines (625 for the European PAL system compared with 525 for the U.S. NTSC system). Using the model presented in this report, we can quantitatively evaluate the last of these alleged factors. We shall compute the perceptual effect of a change in the number of raster lines from 525 to 625.

In general, the problem of calculating the change in the sampling frequency required for a perceivable difference in image quality would require that DDDs for a very large number of values of the viewing distance parameter $N_s r/w$ be constructed. Practical considerations rule this out, so that, most often, specific calculations will be needed. This procedure is actually very straightforward. Equation (30) gives the formula for the total number of jnd's J_S and J_N for signal and noise. Table 11 provides the required values of the threshold contrast sensitivity m_T for various viewing conditions and the signal-to-noise fraction k. Equations (B-14) and (B-15) [Appendix B] give the effective sine-wave contrasts m_S and m_N for the signal and noise components of sampled/raster displays, respectively.

For the case at hand, we consider a viewing distance of 6 picture widths in the vertical direction, so that the viewing distance parameter is $N_s r/w = 3150$ for the NTSC system and $N_s r/w = 3750$ for the PAL system. Therefore, the sampling frequency corresponds to a retinal frequency of $(\pi/180)(N_s r/w) = 55.0$ cycles/degree for NTSC and 65.4 cycles/degree for PAL. As in example c above, we take $s = 1$ and $R_p(f) = 1$ for both television systems. Also, since we want to compare *system* capabilities, we assume that the

modulation transfer function of the display (i.e., the electron beam) is essentially unity over the frequency range of interest. Thus, we set $R_D(f) = 1$. Finally, the values of m_T appropriate for typical television viewing are those measured at an average luminance of 35 mL and a viewing distance of 3 picture widths (see Table 11).

In this manner, the entries given in Table 3 for each of the key retinal frequencies are easily generated. From the table, it is seen that the 625-line PAL system enjoys an advantage of about 5 jnd's of signal over the 525-line NTSC system. This difference is considered reasonably significant (see Section II.A). The corresponding advantage of the PAL system in sampling noise is about 2 jnd's, a difference considered to be marginal. Thus, we conclude that at least part of the reputed image quality advantage of the European color television system is indeed due to an intrinsic advantage in perceived sharpness.

TABLE 3. PARAMETERS FOR THE 525-LINE (NTSC)
AND 625-LINE (PAL) SYSTEMS

A. $N_s = 525$

ν(cycles/degree)	f/f_2*	m_S^2	m_N^2	J_S	J_N
0.5	0.0091	5.79×10^{-2}	8.60×10^{-10}	50.8	0
1.5	0.0273	1.93×10^{-2}	2.33×10^{-8}	52.2	0
3.0	0.0546	1.91×10^{-2}	3.77×10^{-7}	48.7	0
6.0	0.1091	1.86×10^{-2}	6.35×10^{-6}	37.8	0
12.0	0.2183	1.65×10^{-2}	1.24×10^{-4}	20.8	0
24.0	0.4365	9.86×10^{-3}	3.72×10^{-3}	4.1	1.1
48.0	0.8731	3.87×10^{-4}	0.866	0	1.3
			Total	214.4	2.4

B. $N_s = 625$

ν(cycles/degree)	f/f_2*	m_S^2	m_N^2	J_S	J_N
0.5	0.0076	5.79×10^{-2}	4.27×10^{-10}	50.8	0
1.5	0.0229	1.93×10^{-2}	1.15×10^{-8}	52.2	0
3.0	0.0458	1.92×10^{-2}	1.87×10^{-7}	48.8	0
6.0	0.0917	1.88×10^{-2}	3.10×10^{-6}	38.5	0
12.0	0.1833	1.73×10^{-2}	5.71×10^{-5}	23.1	0
24.0	0.3667	1.21×10^{-2}	1.47×10^{-3}	6.3	0.4
48.0	0.7334	2.01×10^{-3}	0.115	0	0.2
			Total	219.7	0.6

*For $r/w = 6$

47

SECTION III

COMPUTED DISCRIMINABLE DIFFERENCE DIAGRAMS

A. INDEX

This section contains the computed Discriminable Difference Diagrams (Figs. 18 through 117) listed by their DDD numbers. Table 4 gives a brief description of the analog DDDs contained here. Complete listings of the available analog DDDs are given in Tables 5 through 8. Table 9 is a summary of the sampled and raster display diagrams, along with their DDD numbers.

B. ANALOG DISPLAY DDDs

The analog display DDDs are presented in Figs. 18 through 97.

C. SAMPLED AND RASTER DISPLAY DDDs

The sampled and raster display DDDs are shown in Figs. 98 through 117.

TABLE 4. OUTLINE OF DISCRIMINABLE DIFFERENCE DIAGRAMS FOR ANALOG DISPLAYS

Distinguishable Levels	Description	Parameters	Table No.
Signal Levels	These figures give the distribution of perceived picture information levels as a function of retinal frequency for the indicated display parameters and viewing distances. The input scene is a single 100% contrast luminance edge transition. The noise spectrum is white. For examples of the application of these figures, see Section II.B of the text.	*Display Noise Power N(f) Display Width w Display Mean Luminance $\bar{I}$ Viewing Distance r	5
Noise Levels: On a Uniform Luminance Display	These figures give the distribution of perceived noise levels on a uniform luminance display as a function of retinal frequency for the indicated display parameters and viewing distances. The noise spectrum is white. For examples of the application of these figures, see Section II.B of the text. This situation allows the maximum visibility of the noise.	*Display Noise Power N(f) Display Width w Display Mean Luminance $\bar{I}$ Viewing Distance r	6
Noise Levels: In the Presence of Ensemble- Averaged Pictorial Information	These figures give the distribution of perceived noise levels in the presence of a statistically averaged power spectrum for pictorial scenes as a function of retinal frequency for the indicated display parameters and viewing conditions. The noise spectrum is white. For examples of the application of these figures, see Section II.B of the text. This situation gives the overall impression of noise for the display of pictorial information.	*Display Noise Power N(f) Display Width w Display Mean Luminance $\bar{I}$ Viewing Distance r	7
Noise Levels: Near a 100% Contrast Edge Transition	These figures give the distribution of perceived noise levels in the presence of a 100% contrast luminance edge transition as a function of retinal frequency for the indicated display parameters and viewing conditions. The noise spectrum is white. For examples of the application of these figures, see Section II.B of the text. Due to both the form of the spectrum and the high contrast of the edge assumed, there are fewer noise levels visible in this case, for comparable conditions, than there are in the two cases described above.	*Display Noise Power N(f) Display Width w Display Mean Luminance $\bar{I}$ Viewing Distance r	8

*Equations (1) and (2) should be employed to convert a particular value of the signal-to-noise ratio S/N to the quantity $\sqrt{N(f)}/\bar{I}$ used to index the amount of noise in the calculation of the DDDs.

TABLE 5. DISCRIMINABLE DIFFERENCE DIAGRAMS FOR ANALOG DISPLAYS: SIGNAL LEVELS

SIGNAL LEVELS

DDD No.	r/w	r (cm)	$\bar{I}$ (mL)	$\sqrt{N(f)}/\bar{I}$ $((\text{cycles/cm})^{-1/2})$	Scale*
1	3	--	35	0.0	1.4
2	3	--	35	0.0	0.2
3	3	50	35	0.001	1.4
4	3	50	35	0.003	1.4
5	3	50	35	0.01	1.4
6	3	50	35	0.03	1.4
7	3	50	35	0.1	1.4
8	3	100	35	0.001	1.4
9	3	100	35	0.003	1.4
10	3	100	35	0.01	1.4
11	3	100	35	0.03	1.4
12	3	100	35	0.1	1.4
13	3	200	35	0.001	1.4
14	3	200	35	0.003	1.4
15	3	200	35	0.01	1.4
16	3	200	35	0.03	1.4
17	3	200	35	0.1	1.4
18	10	--	35	0.0	1.4
19	10	--	35	0.0	0.2
20	10	--	1	0.0	1.4
21	10	--	1	0.0	0.2
22	10	50	35	0.01	1.4
23	10	50	35	0.03	1.4
24	10	100	35	0.01	1.4
25	10	100	35	0.03	1.4
26	10	100	1	0.01	1.4
27	10	100	1	0.03	1.4
28	10	200	35	0.01	1.4
29	10	200	35	0.03	1.4
30	30	--	35	0.0	1.4
31	30	--	35	0.0	0.2

* This number is the maximum value of modulation transfer displayed on the DDD.

50

TABLE 6. DISCRIMINABLE DIFFERENCE DIAGRAMS FOR ANALOG DISPLAYS:
NOISE ON A UNIFORM LUMINANCE DISPLAY

DDD No.	r/w	r (cm)	$\bar{I}$ (mL)	$\sqrt{N(f)}/\bar{I}$ $([cycles/cm]^{-1/2})$
32	3	50	35	0.001
33	3	50	35	0.003
34	3	50	35	0.01
35	3	50	35	0.03
36	3	50	35	0.1
37	3	100	35	0.001
38	3	100	35	0.003
39	3	100	35	0.01
40	3	100	35	0.03
41	3	100	35	0.1
42	3	200	35	0.001
43	3	200	35	0.003
44	3	200	35	0.01
45	3	200	35	0.03
46	3	200	35	0.1
47	10	50	35	0.1
48	10	50	35	0.3
49	10	100	35	0.1
50	10	100	35	0.3
51	10	100	1	0.1
52	10	100	1	0.3
53	10	200	35	0.1
54	10	200	35	0.3

TABLE 7. DISCRIMINABLE DIFFERENCE DIAGRAMS FOR ANALOG DISPLAYS: NOISE
IN THE PRESENCE OF ENSEMBLE-AVERAGE PICTORIAL INFORMATION

DDD No.	r/w	r (cm)	$\bar{I}$ (mL)	$\sqrt{N(f)}/\bar{I}$ ($[\text{cycles/cm}]^{-1/2}$)
No Levels	3	50	35	0.001
No Levels	3	50	35	0.003
55	3	50	35	0.01
56	3	50	35	0.03
57	3	50	35	0.1
No Levels	3	100	35	0.001
No Levels	3	100	35	0.003
58	3	100	35	0.01
59	3	100	35	0.03
60	3	100	35	0.1
No Levels	3	200	35	0.001
No Levels	3	200	35	0.003
61	3	200	35	0.01
62	3	200	35	0.03
63	3	200	35	0.1
64	10	50	35	0.01
65	10	50	35	0.03
66	10	100	35	0.01
67	10	100	35	0.03
No Levels	10	100	1	0.01
68	10	100	1	0.03
69	10	200	35	0.01
70	10	200	35	0.03

TABLE 8. DISCRIMINABLE DIFFERENCE DIAGRAMS FOR ANALOG DISPLAYS:
NOISE IN THE PRESENCE OF A 100% CONTRAST EDGE

DDD No.	r/w	r (cm)	$\overline{I}$ (mL)	$\sqrt{N(f)}/\overline{I}$ ($[cycles/cm]^{-1/2}$)
No Levels	3	50	35	0.001
No Levels	3	50	35	0.003
No Levels	3	50	35	0.01
71	3	50	35	0.03
72	3	50	35	0.1
No Levels	3	100	35	0.001
No Levels	3	100	35	0.003
No Levels	3	100	35	0.01
73	3	100	35	0.03
74	3	100	35	0.1
No Levels	3	200	35	0.001
No Levels	3	200	35	0.003
No Levels	3	200	35	0.01
75	3	200	35	0.03
76	3	200	35	0.1
No Levels	10	50	35	0.01
77	10	50	35	0.03
No Levels	10	100	35	0.01
78	10	100	35	0.03
No Levels	10	100	1	0.01
79	10	100	1	0.03
No Levels	10	200	35	0.01
80	10	200	35	0.03

53

TABLE 9. DISCRIMINABLE DIFFERENCE DIAGRAMS FOR SAMPLED AND RASTER DISPLAYS

Distinguish-able Levels	Description	Prefilter	Sampling Width (s)	Viewing Distance ($N_s r/w$)	DDD Number
Signal	These figures give the distribution of perceived picture information levels as a function of the normalized display frequency f/f_s for the indicated display parameters and viewing distances. The input scene is a single 100% contrast edge transition. The display luminance is 35 mL. For examples of the application of these figures, see Section II.C of the text.	None*	0	1250.	81
		Nyquist**	0	1250.	82
		None	1	1250.	83
		Nyquist	1	1250.	84
		None	0	2500.	85
		Nyquist	0	2500.	86
		None	1	2500.	87
		Nyquist	1	2500.	88
		None	0	5000.	89
		Nyquist	0	5000.	90
		None	1	5000.	91
		Nyquist	1	5000.	92
Noise	These figures give the distribution of perceived sampling noise levels as a function of the normalized display frequency f/f_s for the indicated display parameters and viewing distances. The input scene is a single 100% contrast edge transition. The display luminance is 35 mL. For examples of the application of these figures, see Section II.C.of the text.	None	0	1250.	93
		Nyquist	0	1250.	94
		None	1	1250.	95
		Nyquist	1	1250.	96
		None	0	2500.	97
		Nyquist	0	2500.	98
		None	1	2500.	99
		Nyquist	1	2500.	100
		None	0	5000.	No Levels
		Nyquist	0	5000.	No Levels
		None	1	5000.	No Levels
		Nyquist	1	5000.	No Levels

*See Eq. (6)
**See Eq. (7)

MODULATION TRANSFER

1.4

1.2

1.0

0.8

0.6

0.4

0.2

0

RETINAL FREQUENCY $\nu = \pi r f / 180$ (CYCLES/ DEGREE)

0.5   1.5   3.0   6.0   12   24   48

0.3   1.0   10   80
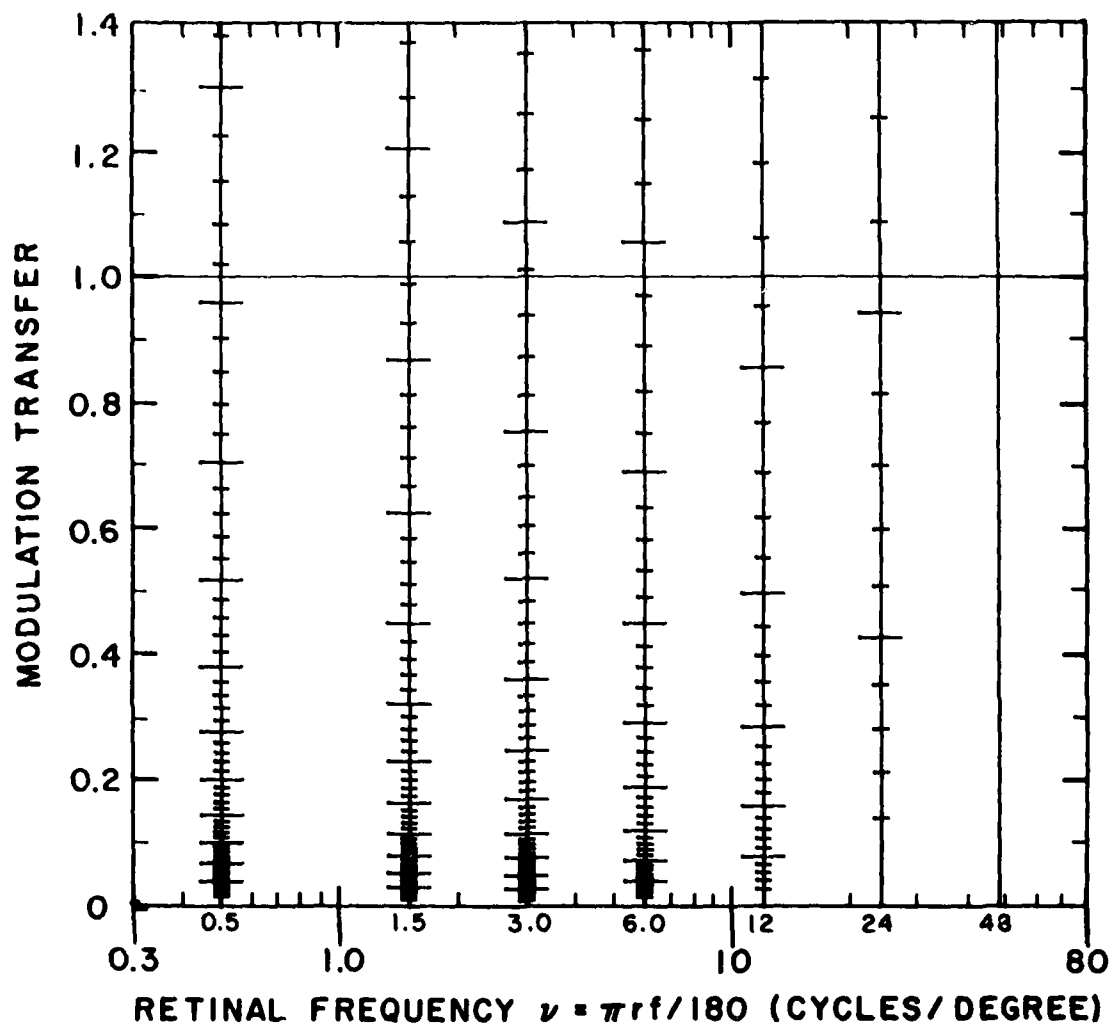
Figure 18.   DDD No. 1.   Discriminable Difference Diagram for signal
levels on an analog display: r/w = 3, $\bar{I}$ = 35 mL, and
$\sqrt{N(f)}/\bar{I}$ = 0.
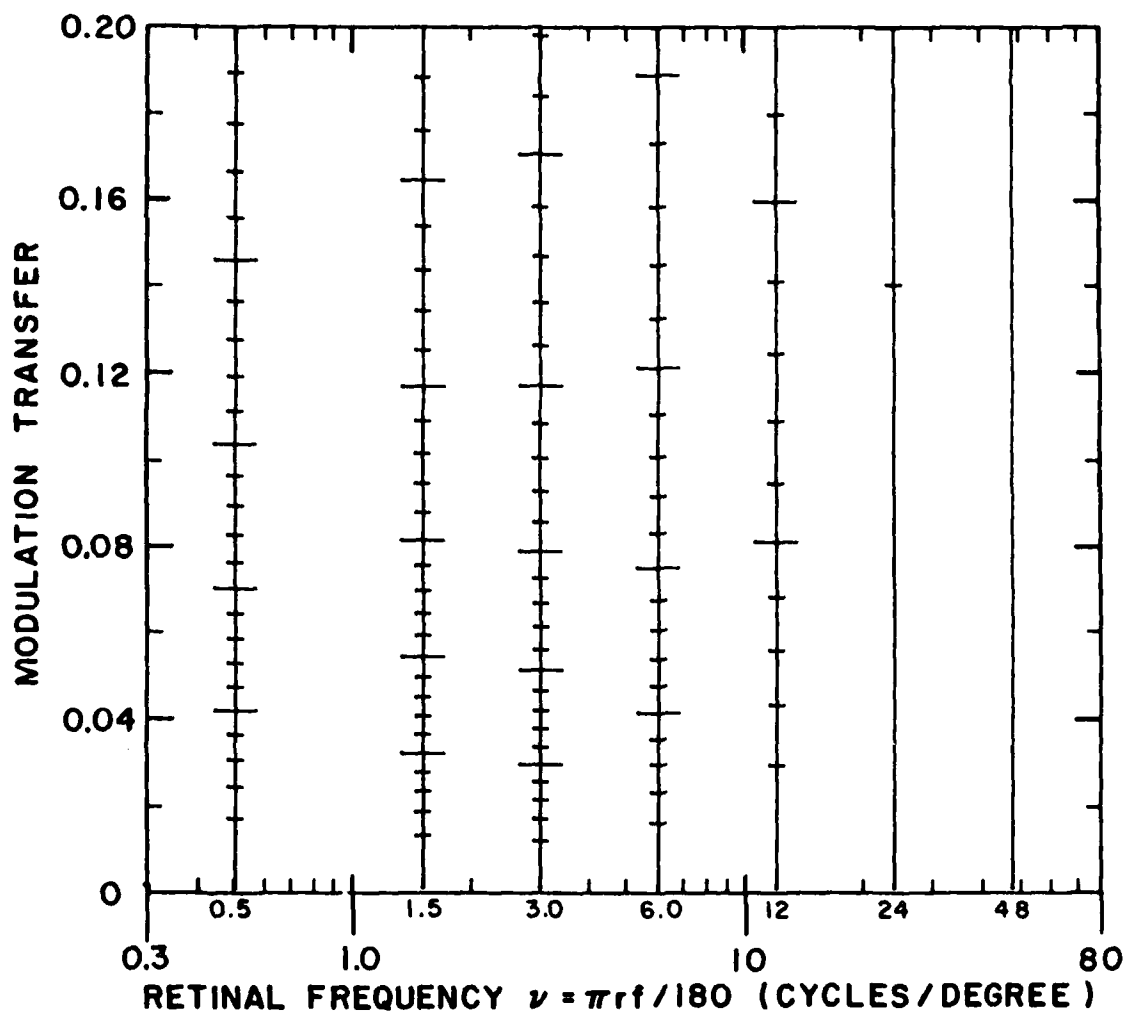
Figure 19. DDD No. 2. Discriminable Difference Diagram for signal
levels on an analog display: r/w = 3, $\overline{I}$ = 35 mL, and
$\sqrt{N(f)}/\overline{I}$ = 0.

56
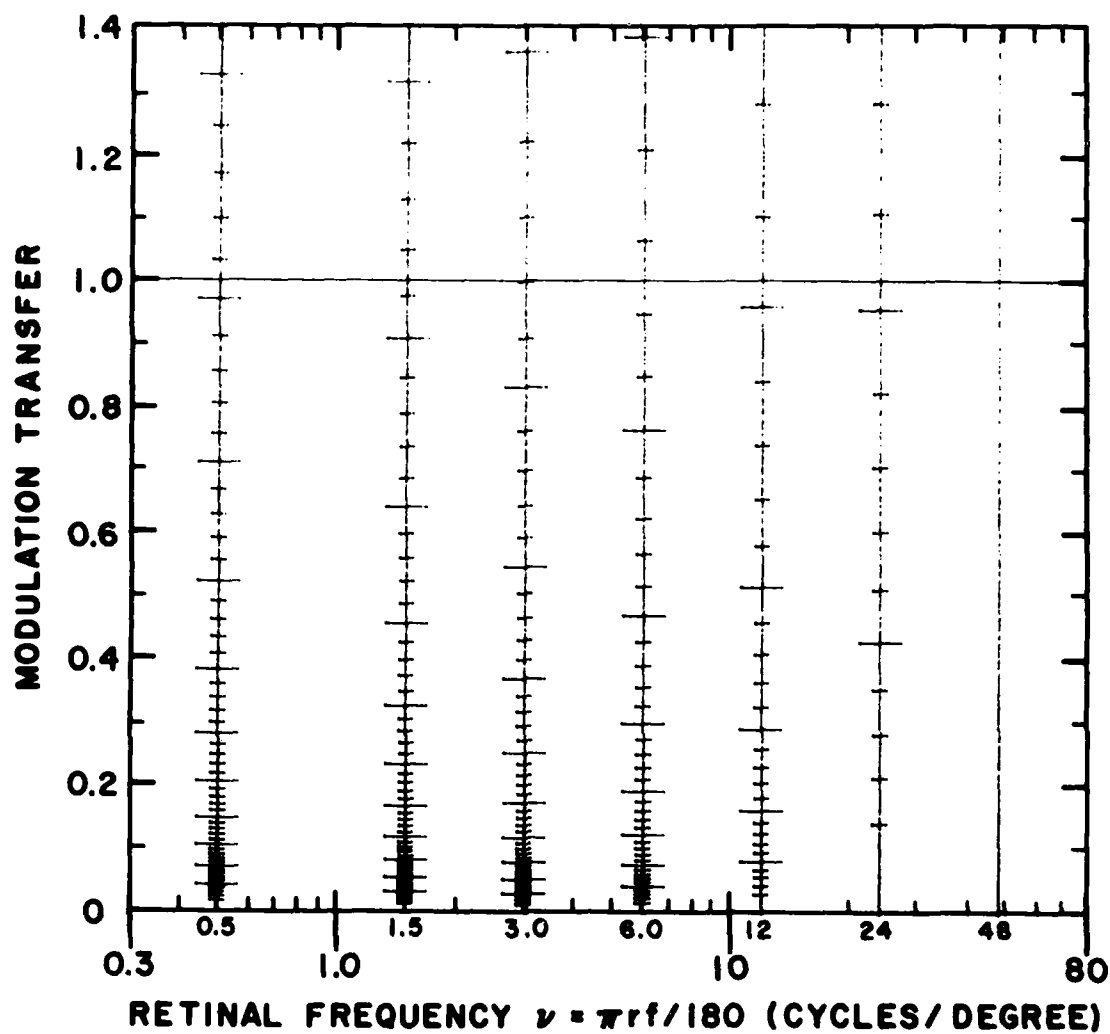
Figure 20. DDD No. 3. Discriminable Difference Diagram for signal levels on an analog display: r/w = 3, r = 50 cm, $\overline{I}$ = 35 mL, and $\sqrt{N(f)}/\overline{I}$ = 0.001.

57
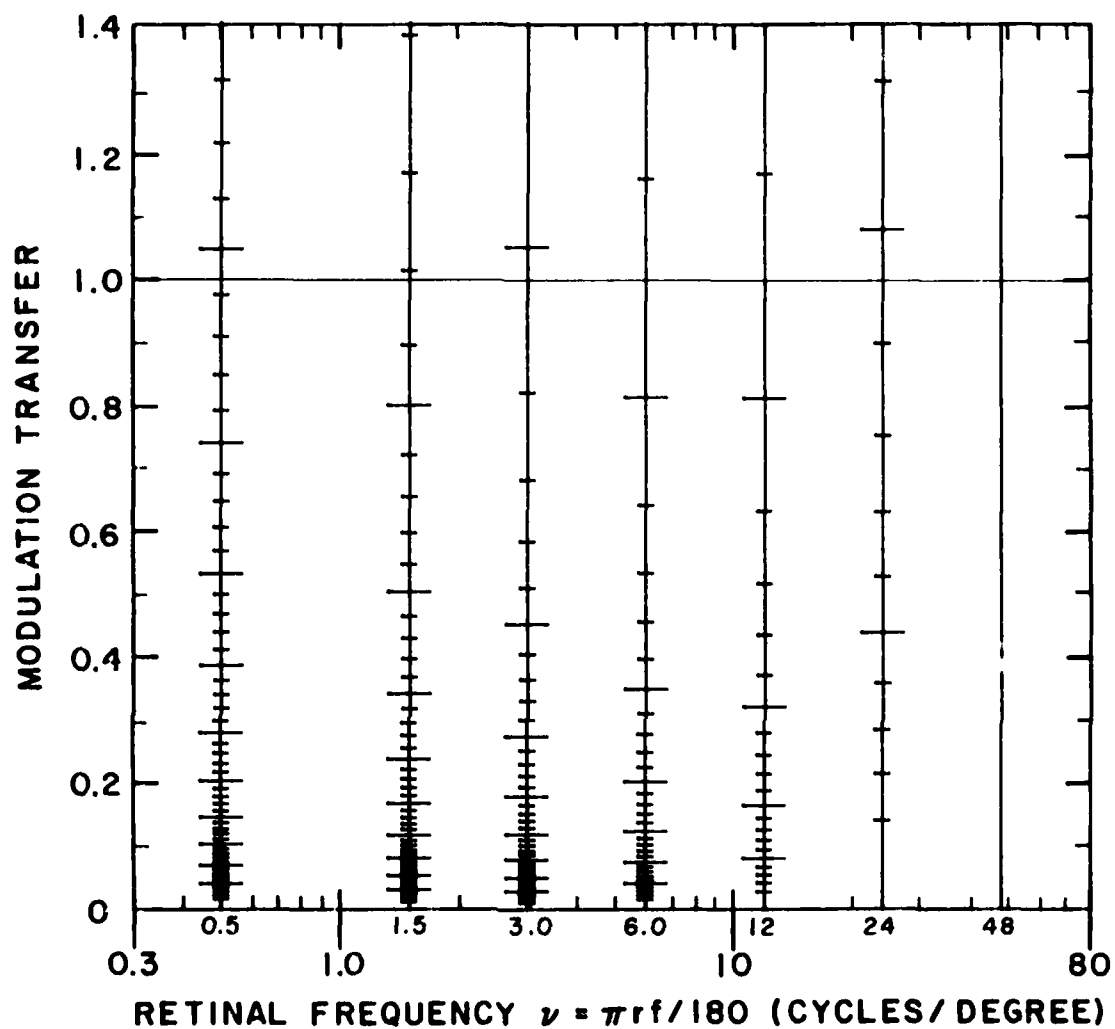
Figure 21. DDD No. 4. Discriminable Difference Diagram for signal
Levels on an analog display: r/w = 3, r = 50 cm,
$\bar{I}$ = 35 mL, and $\sqrt{N(f)}/\bar{I}$ = 0.003.

58
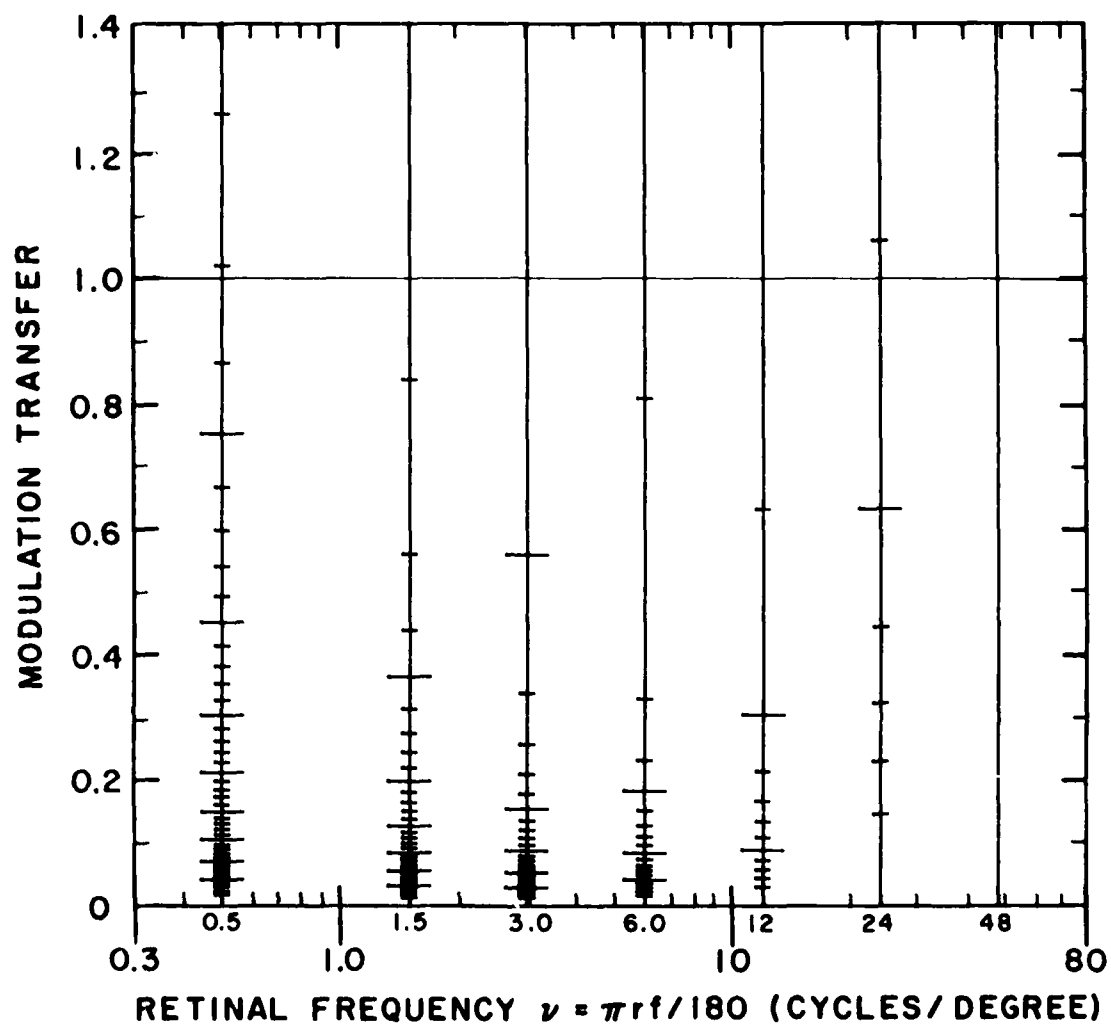
Figure 22.   DDD No. 5.   Discriminable Difference Diagram for signal
            levels on an analog display: r/w = 3, r = 50 cm,
            $\overline{I}$ = 35 mL, and $\sqrt{N(f)}/\overline{I}$ = 0.01.

59
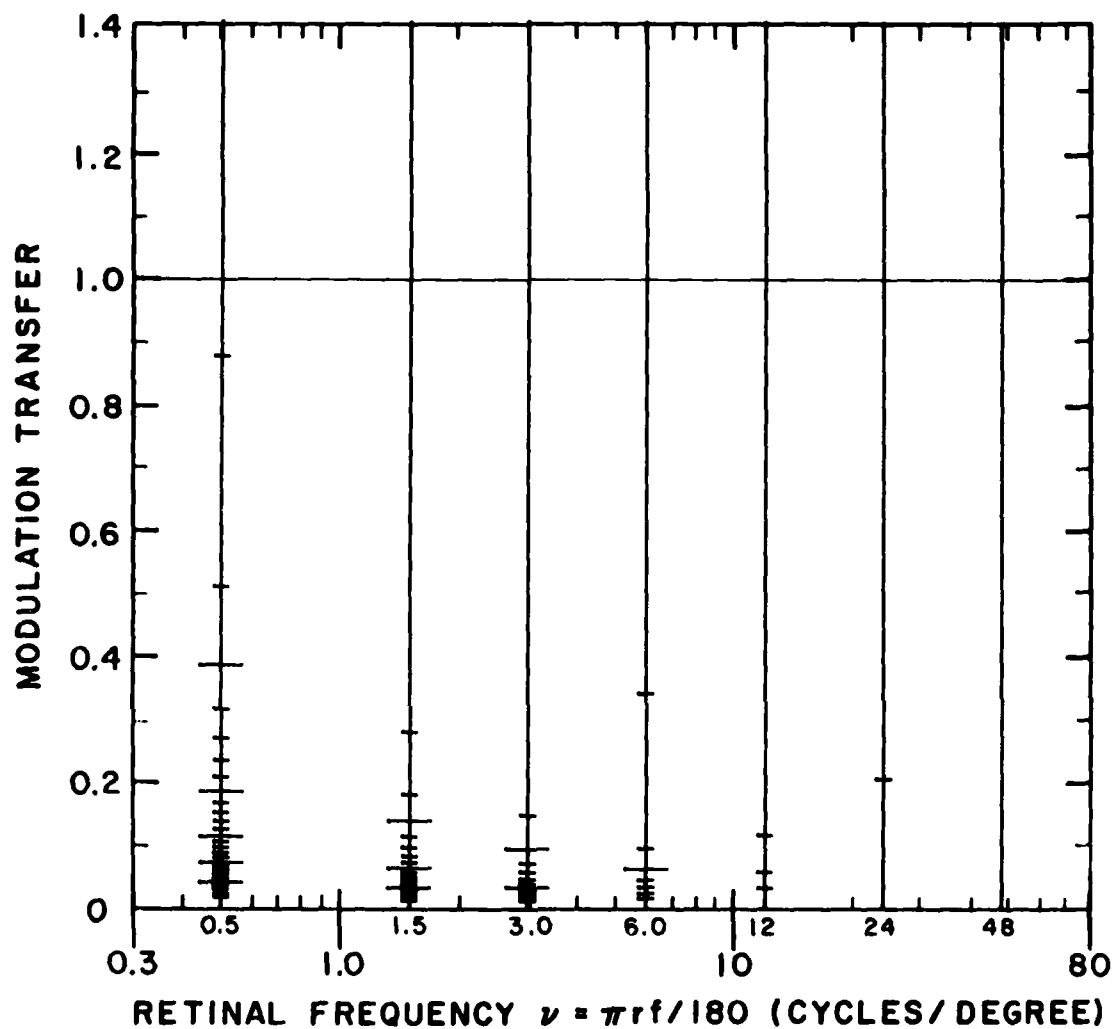
Figure 23.   DDD No. 6.   Discriminable Difference Diagram for signal
            levels on an analog display: r/w = 3, r = 50 cm,
            $\bar{I}$ = 35 mL, and $\sqrt{N(f)}/\bar{I}$ = 0.03.

60
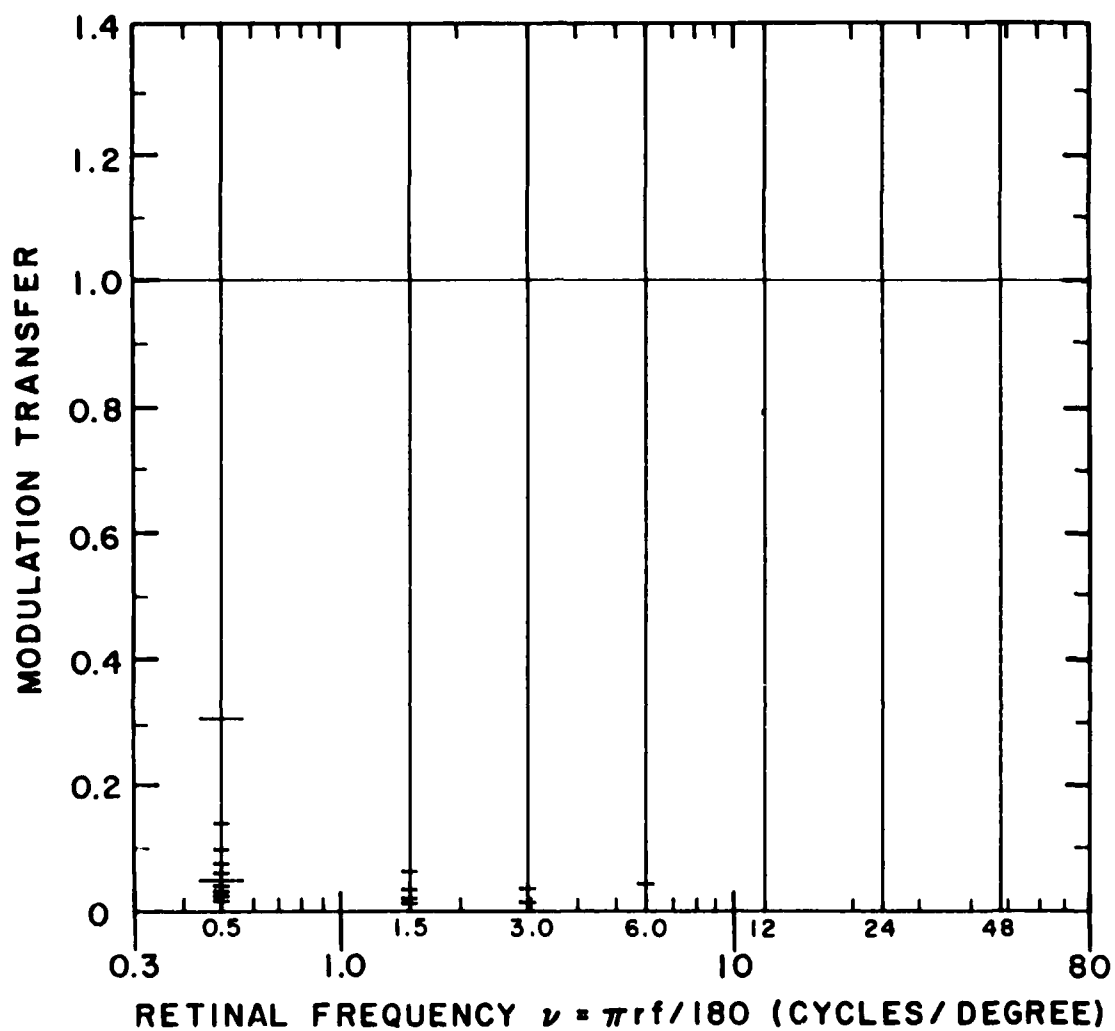
Figure 24. DDD No. 7. Discriminable Difference Diagram for signal
levels on an analog display: r/w = 3, r = 50 cm,
$\bar{I}$ = 35 mL, and $\sqrt{N(f)}/\bar{I}$ = 0.1.

61
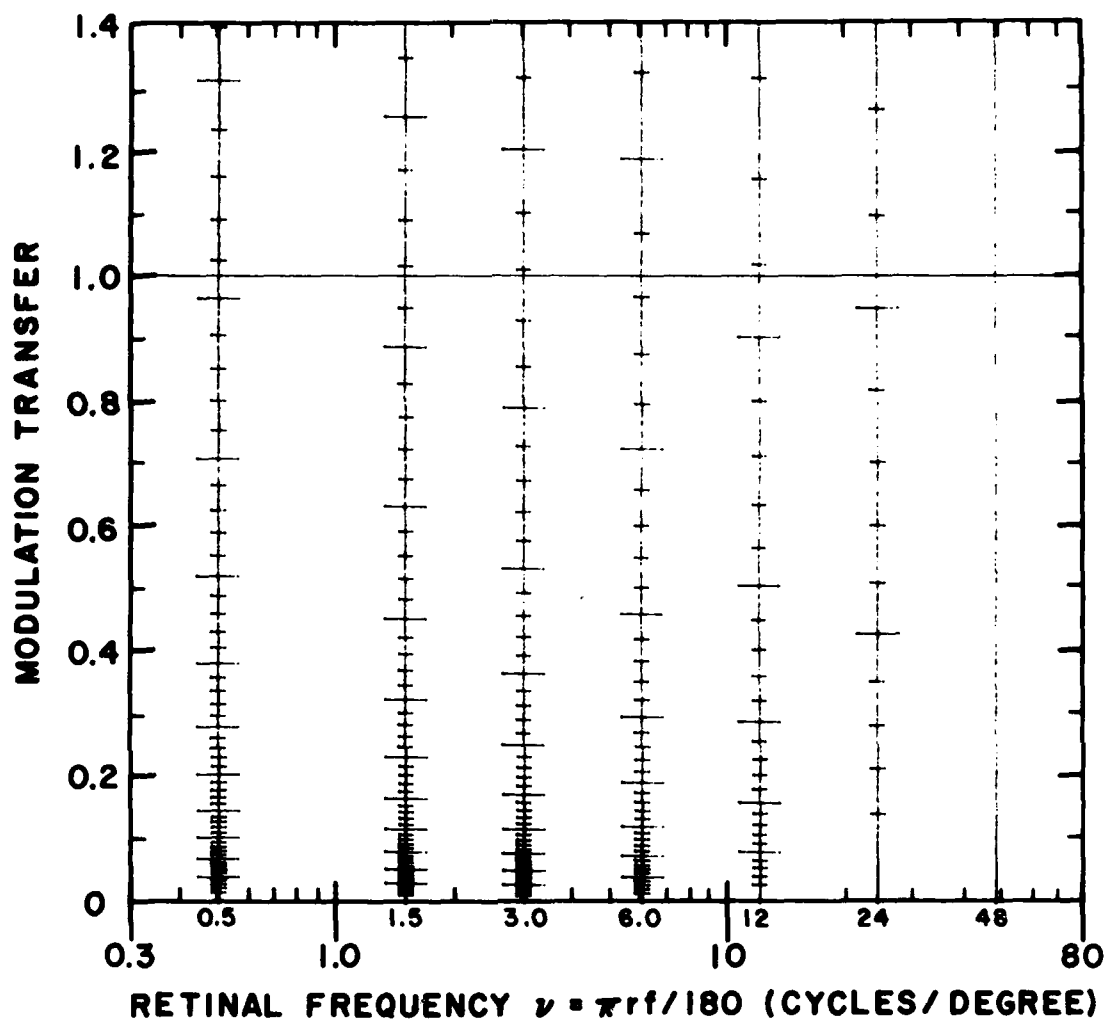
Figure 25. DDD No. 8. Discriminable Difference Diagram for signal
levels on an analog display: r/w = 3, r = 100 cm,
$\overline{I}$ = 35 mL, and $\sqrt{N(f)}/\overline{I}$ = 0.001.
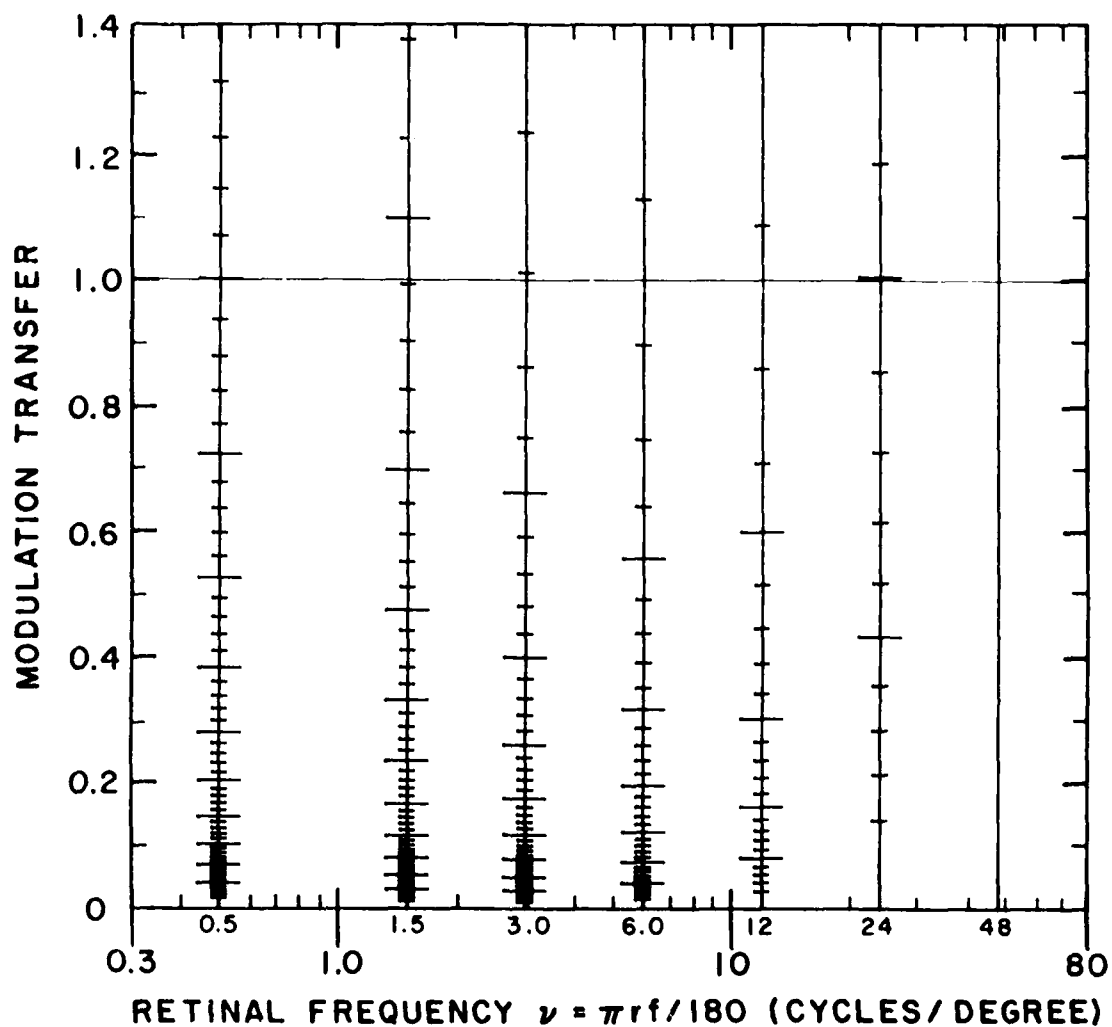
Figure 26. DDD No. 9. Discriminable Difference Diagram for signal
levels on an analog display: $r/w = 3$, $r = 100$ cm,
$\overline{I} = 35$ mL, and $\sqrt{N(f)}/\overline{I} = 0.003$.

63
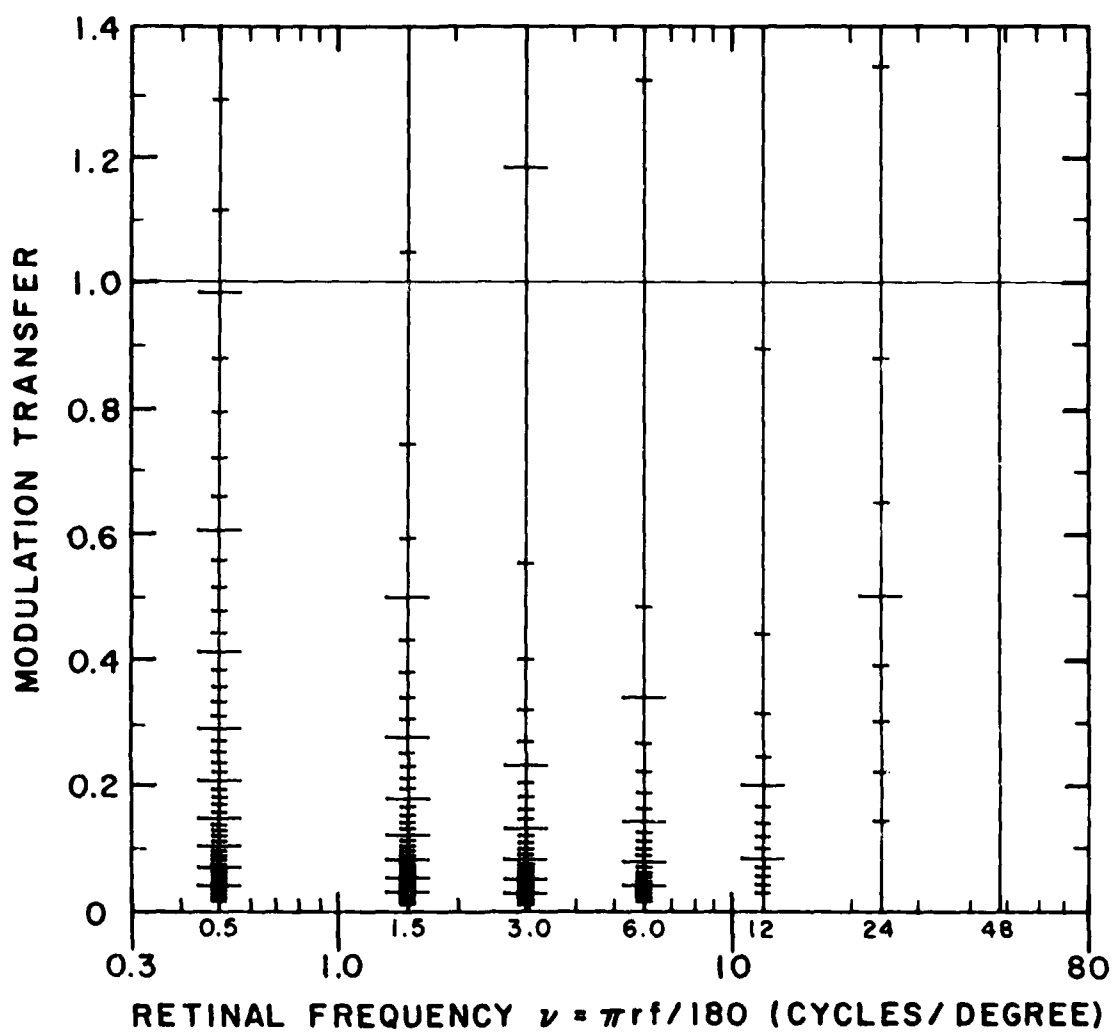
Figure 27.   DDD No. 10.   Discriminable Difference Diagram for signal
              levels on an analog display;   r/w = 3, r = 100 cm,
              $\bar{I}$ = 35 mL, and $\sqrt{N(f)}/\bar{I}$ = 0.01.
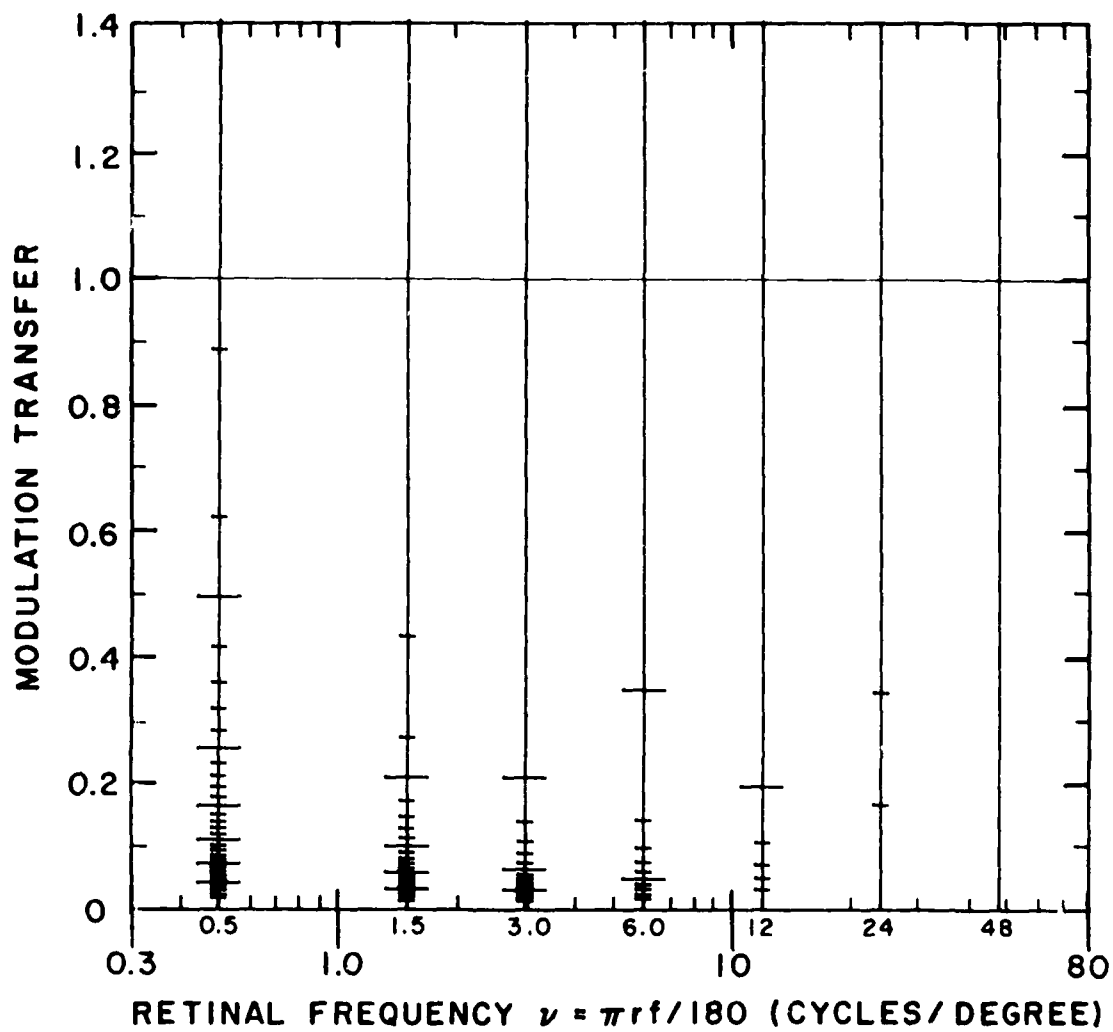
Figure 28. DDD No. 11. Discriminable Difference Diagram for signal
levels on an analog display: r/w = 3, r = 100 cm,
$\overline{I}$ = 35 mL, and $\sqrt{N(f)}/\overline{I}$ = 0.03.
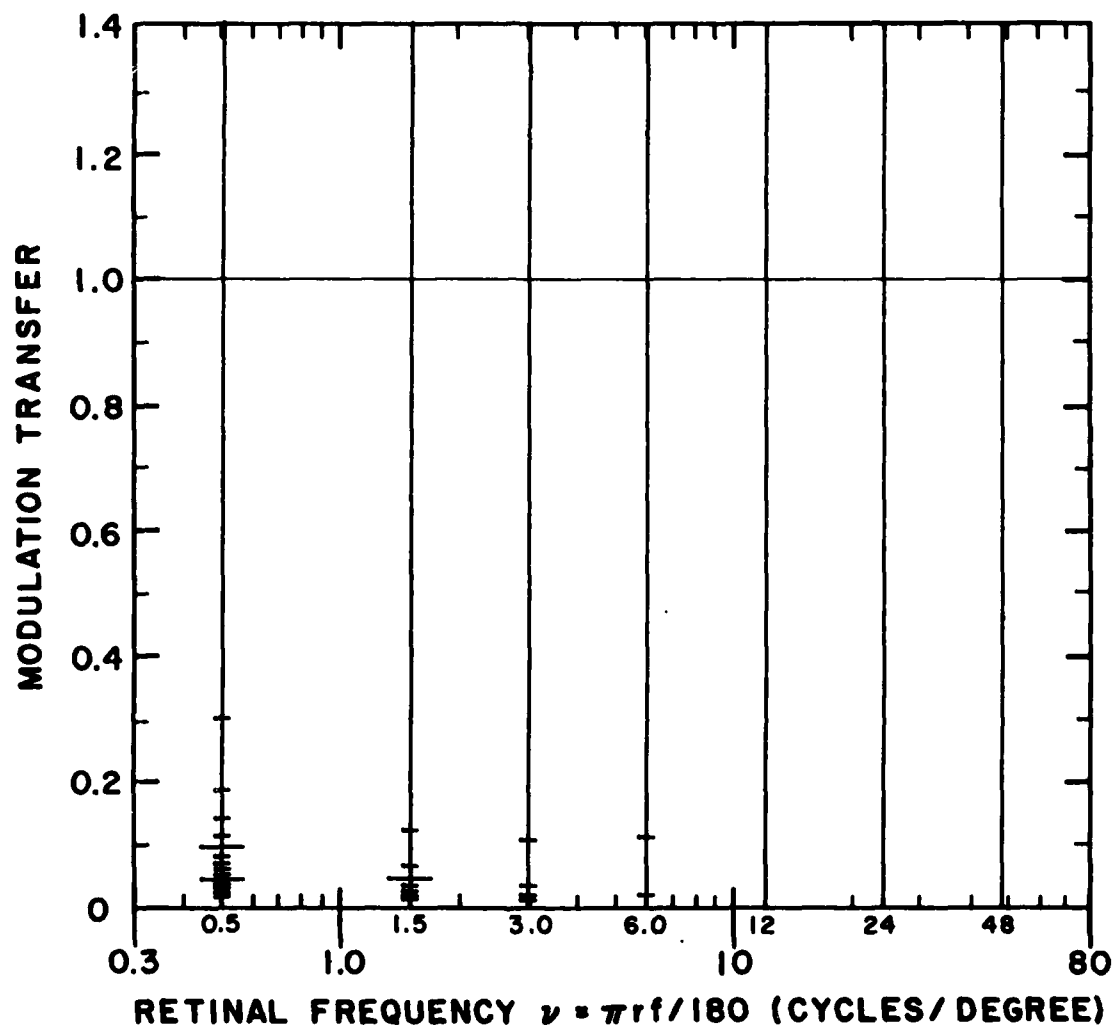
Figure 29. DDD No. 12. Discriminable Difference Diagram for signal
levels on an analog display: r/w = 3, r = 100 cm,
$\bar{I}$ = 35 mL, and $\sqrt{N(f)}/\bar{I}$ = 0.1.
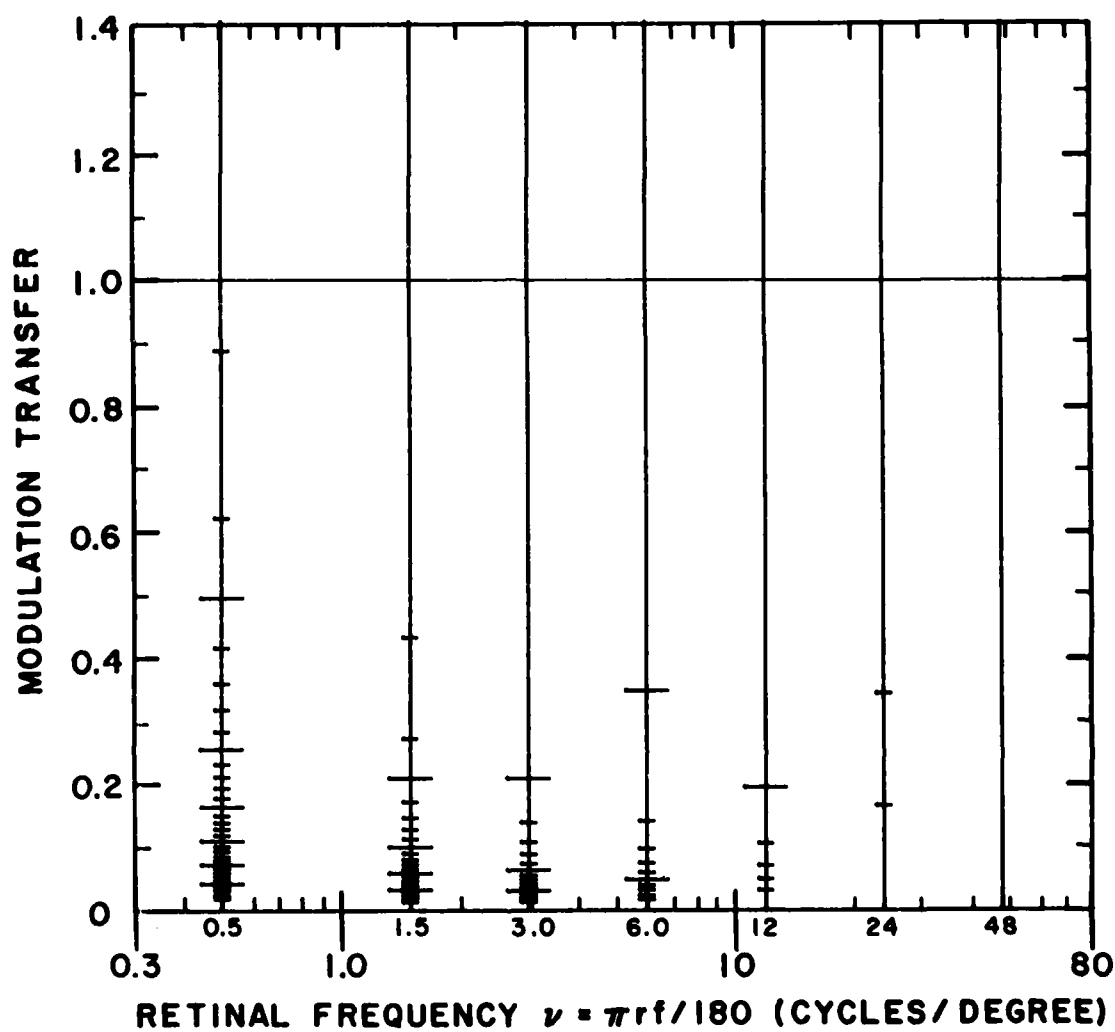
Figure 28. DDD No. 11. Discriminable Difference Diagram for signal
levels on an analog display: r/w = 3, r = 100 cm,
$\bar{I}$ = 35 mL, and $\sqrt{N(f)}/\bar{I}$ = 0.03.
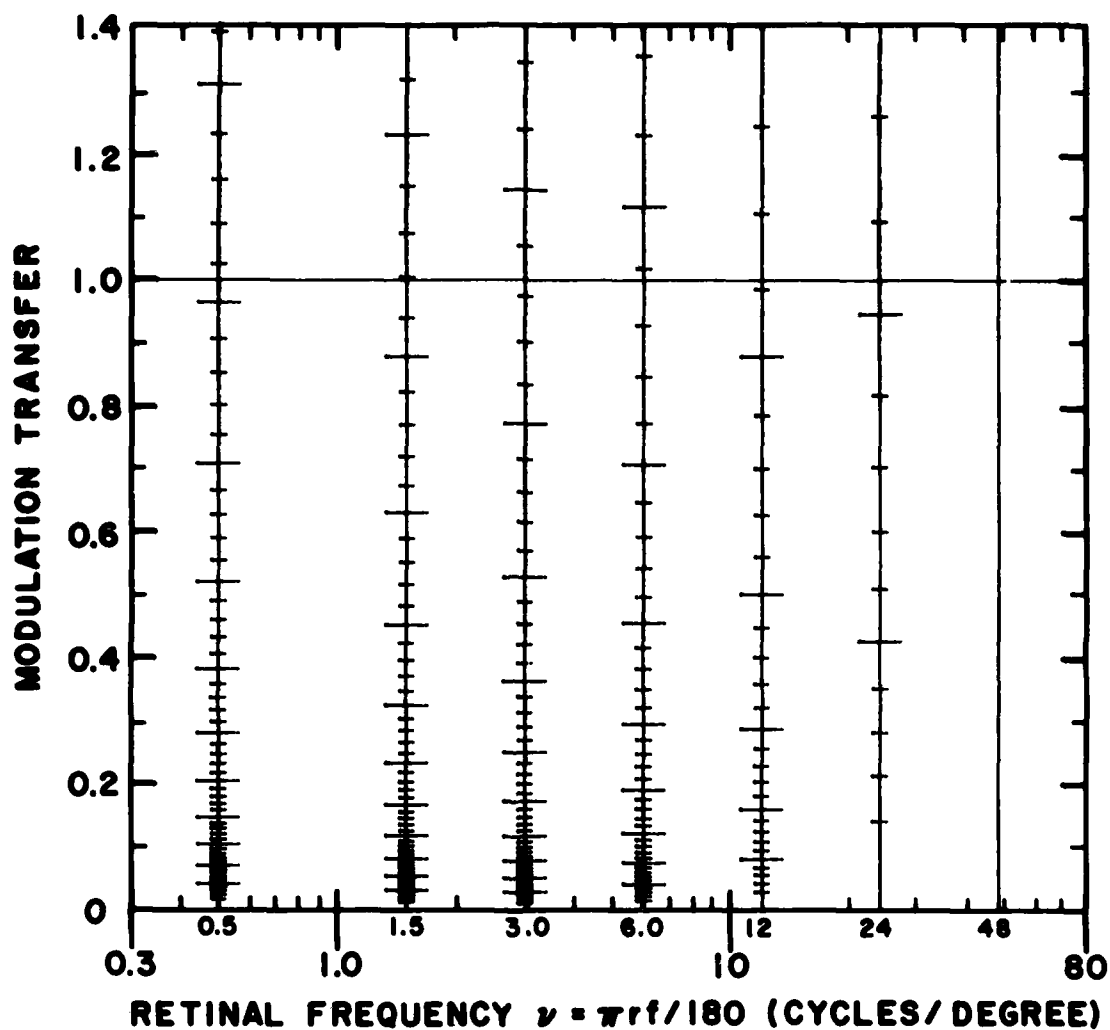
Figure 30. DDD No. 13. Discriminable Difference Diagram for signal
levels on an analog display: $r/w = 3$, $r = 200$ cm,
$\bar{I} = 35$ mL, and $\sqrt{N(f)}/\bar{I} = 0.001$.

67
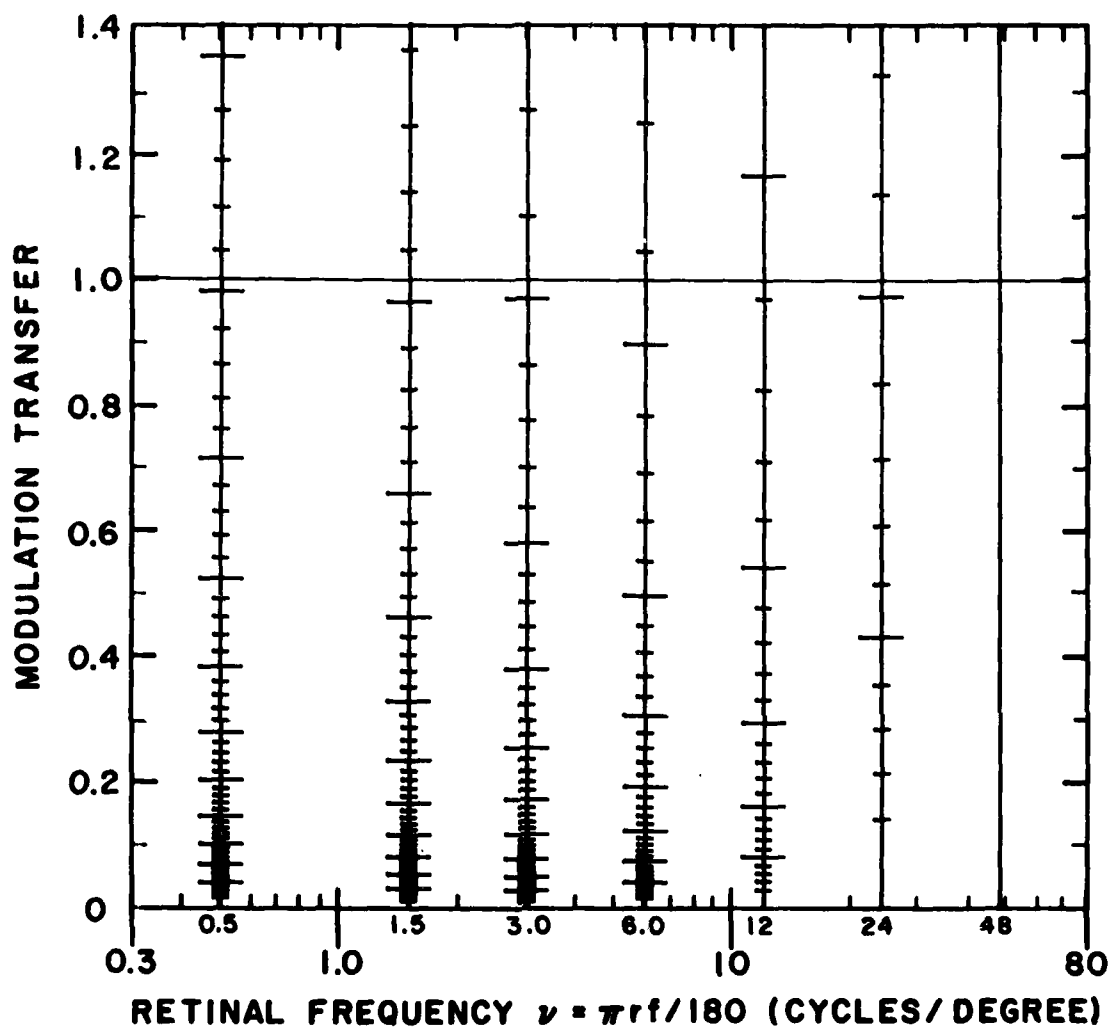
Figure 31. DDD No. 14. Discriminable Difference Diagram for signal
levels on an analog display: r/w = 3, r = 200 cm,
$\bar{I}$ = 35 mL, and $\sqrt{N(f)}/\bar{I}$ = 0.003.

68
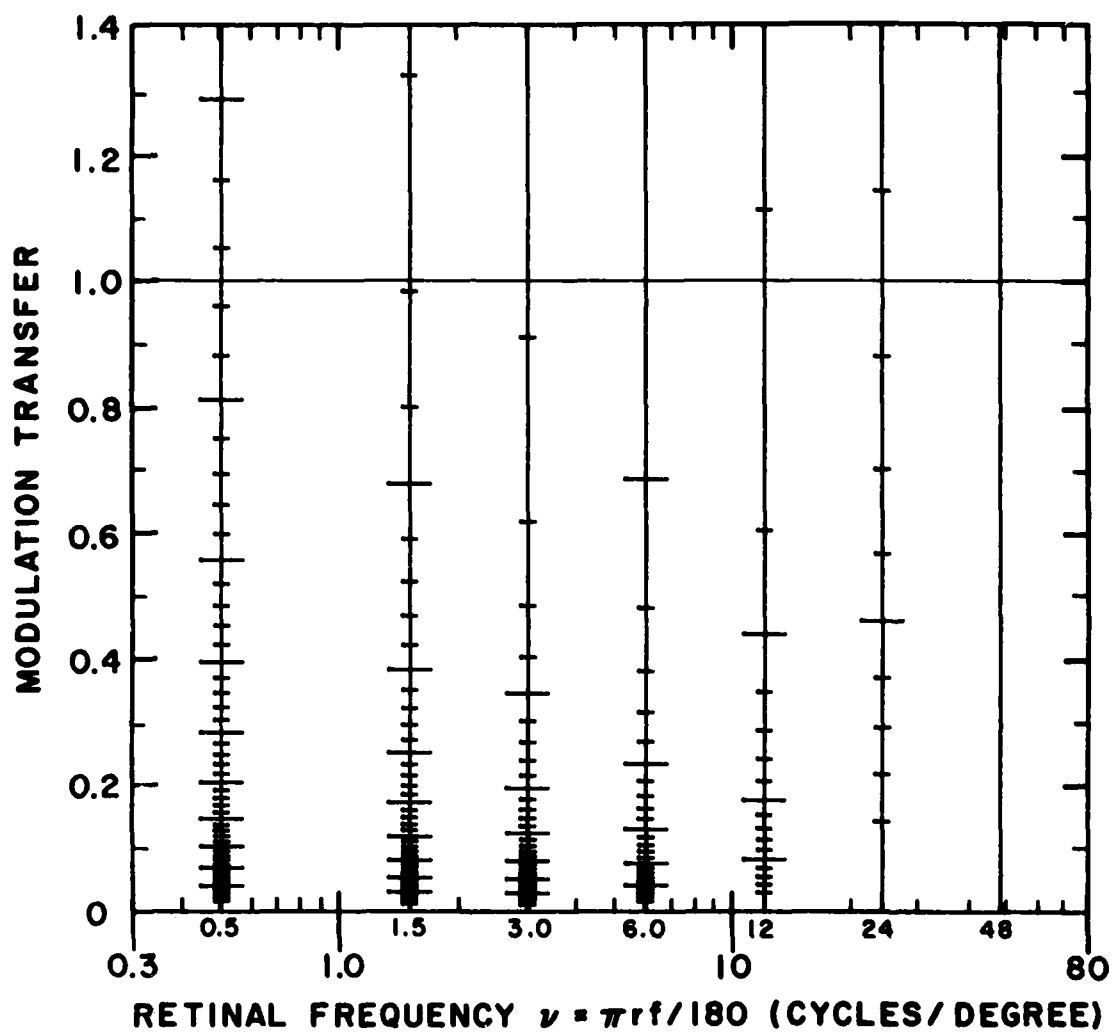
Figure 32. DDD No. 15. Discriminable Difference Diagram for signal levels on an analog display: r/w = 3, r = 200 cm, $\bar{I}$ = 35 mL, and $\sqrt{N(f)}/\bar{I}$ = 0.01.
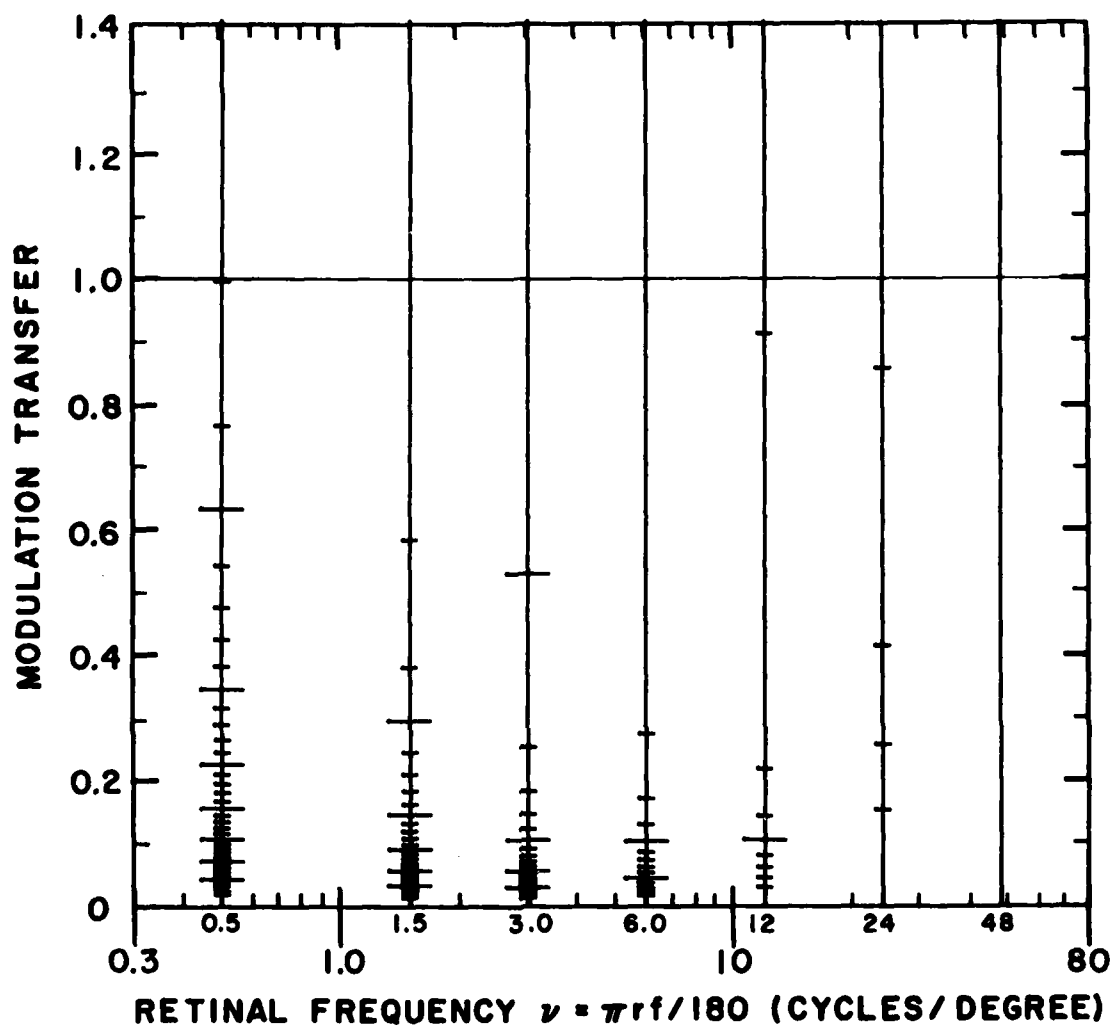
Figure 33. DDD No. 16. Discriminable Difference Diagram for signal
levels on an analog display: r/w = 3, r = 200 cm,
$\bar{I}$ = 35 mL, and $\sqrt{N(f)}/\bar{I}$ = 0.03.

70
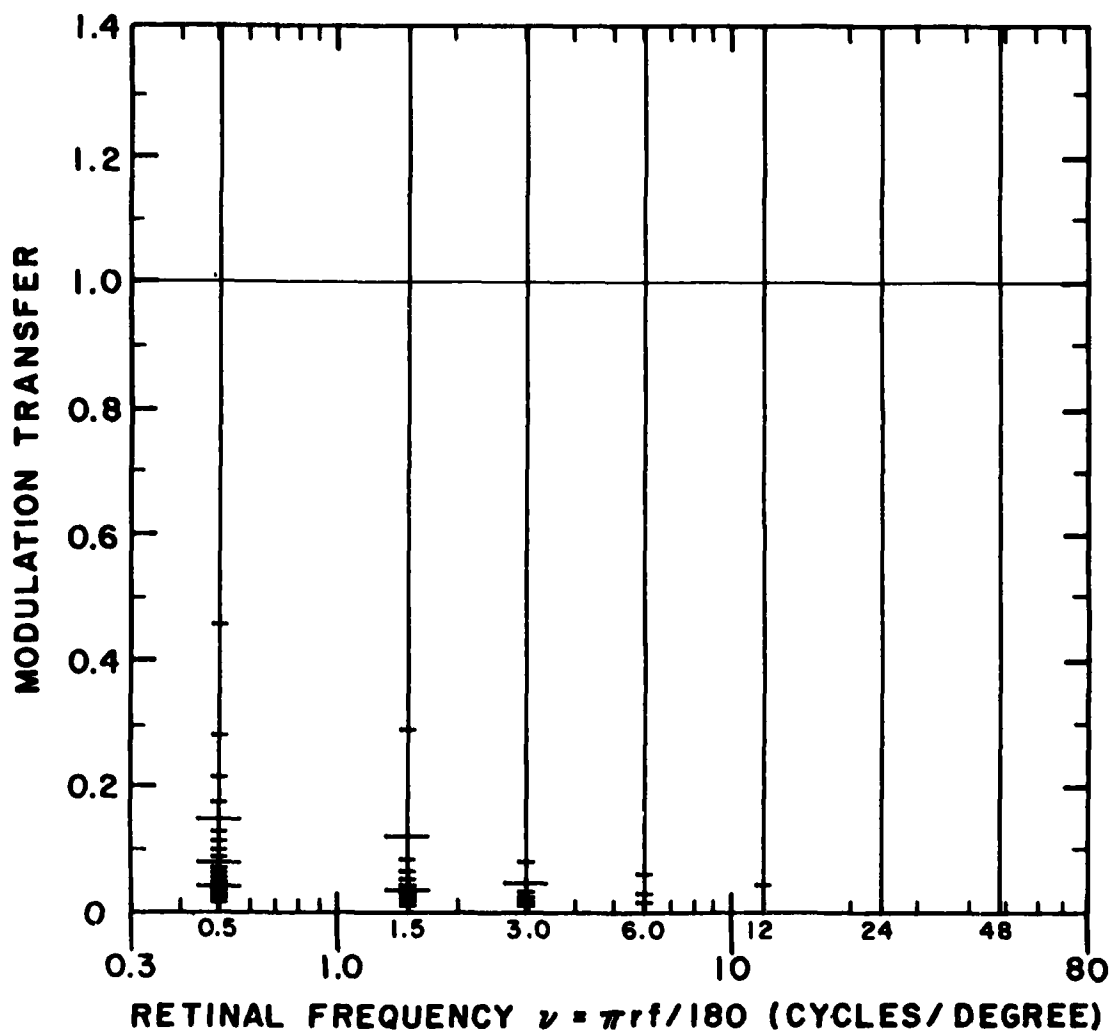
Figure 34. DDD No. 17. Discriminable Difference Diagram for signal levels on an analog display: r/w = 3, r = 200 cm, $\bar{I}$ = 35 mL, and $\sqrt{N(f)}/\bar{I}$ = 0.1.

71
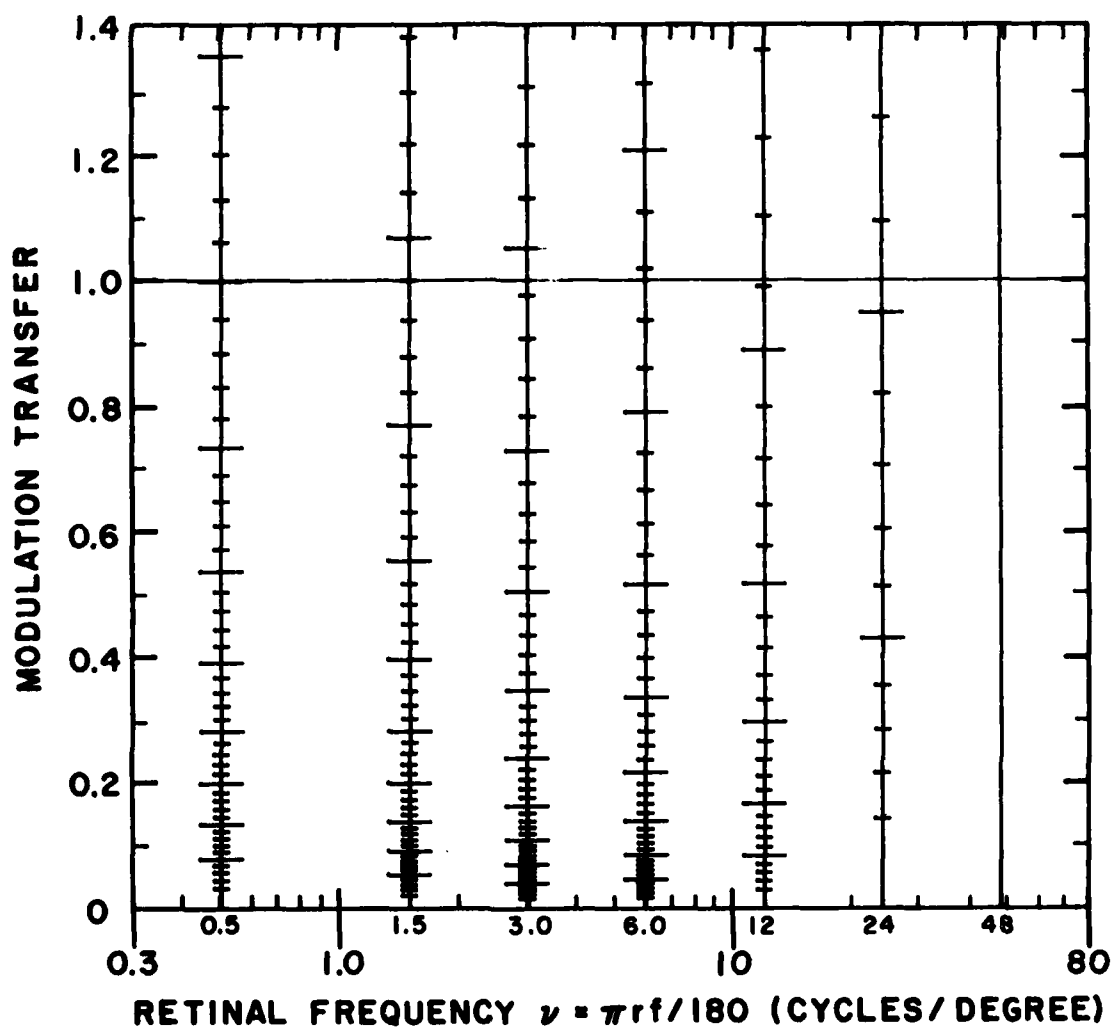
Figure 35. DDD No. 18. Discriminable Difference Diagram for signal levels on an analog display: $r/w = 10$, $\bar{I} = 35$ mL, and $\sqrt{N(f)}/\bar{I} = 0$.

72
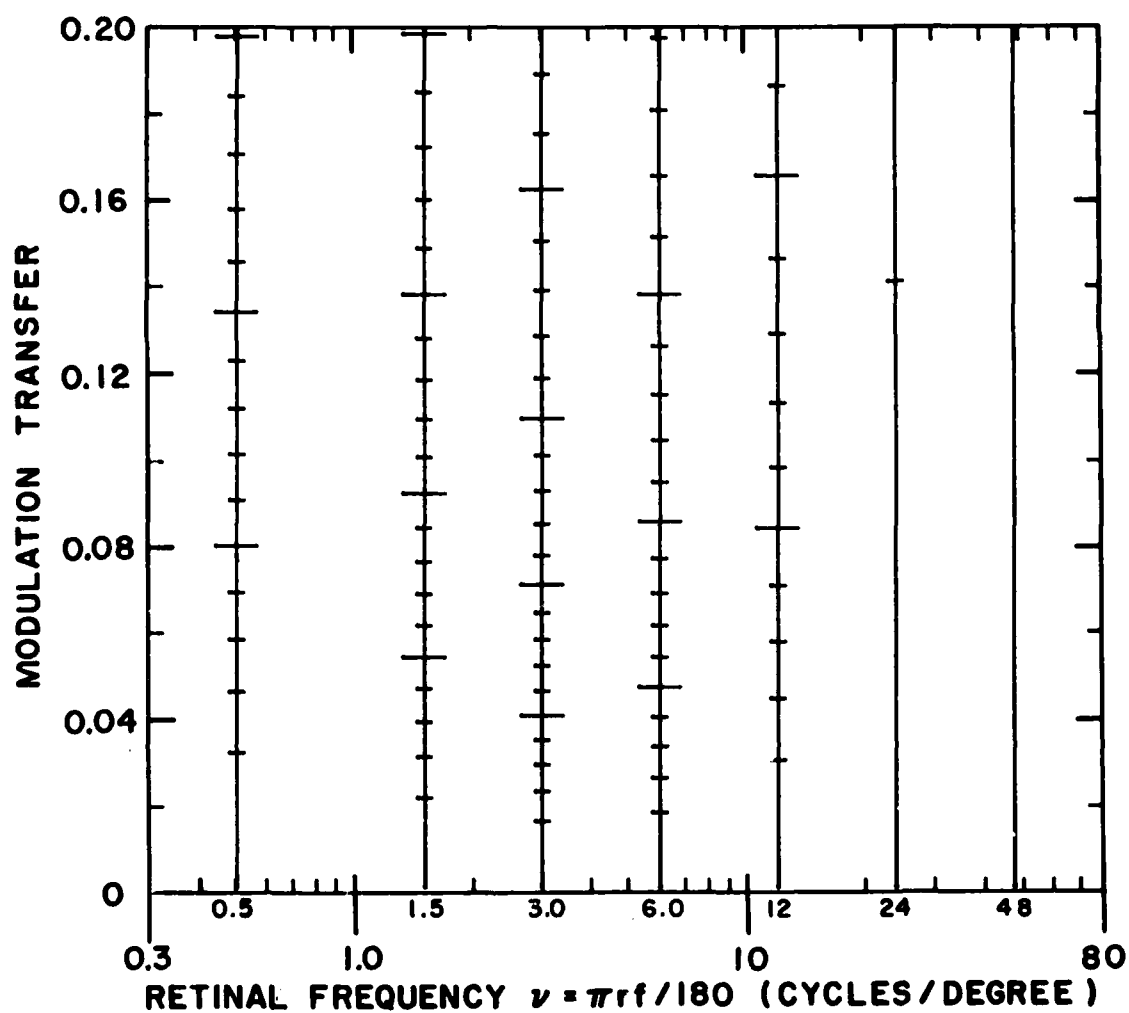
Figure 36. DDD No. 19. Discriminable Difference Diagram for signal
            levels on an analog display: r/w = 10, $\bar{I}$ = 35 mL, and
            $\sqrt{N(f)}/\bar{I} = 0$.
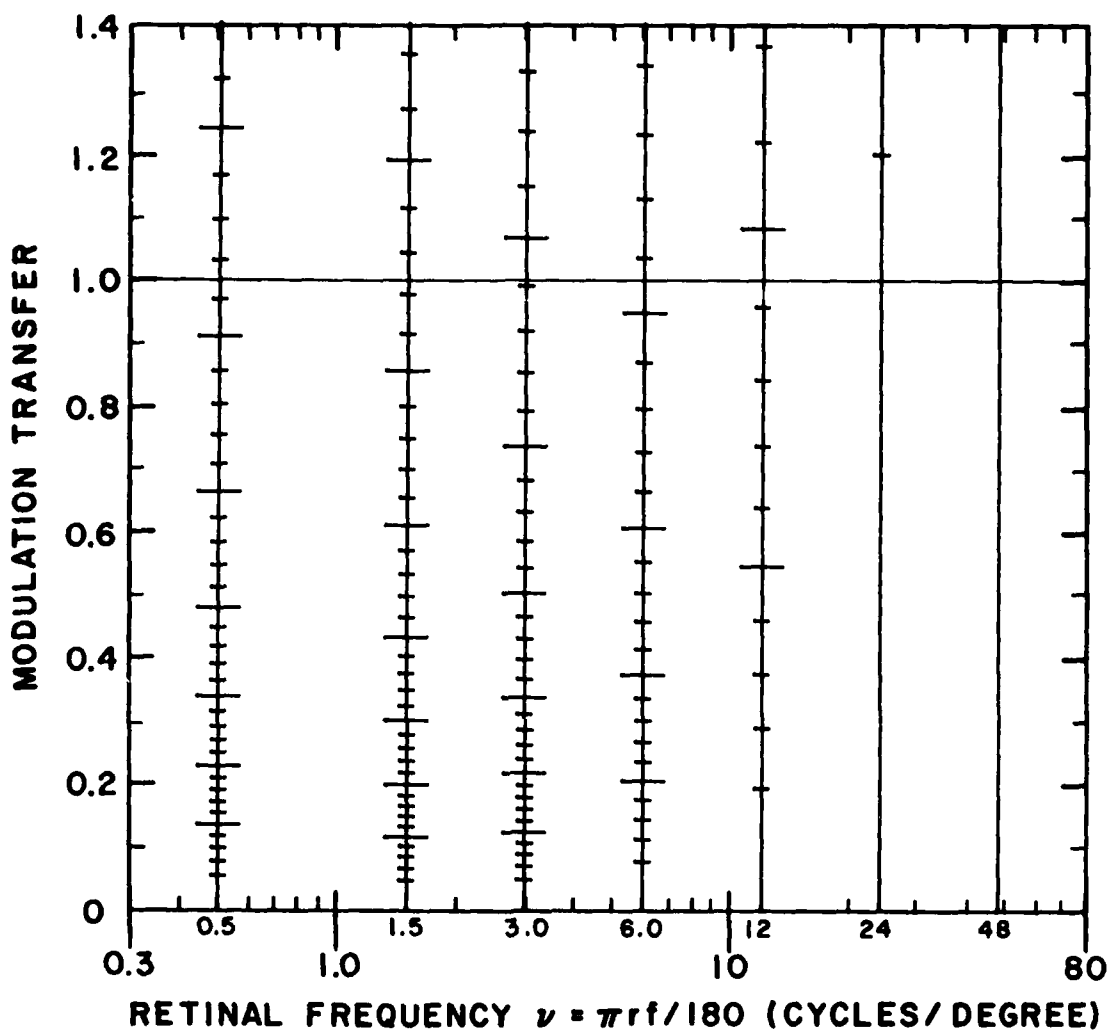
Figure 37. DDD No. 20. Discriminable Difference Diagram for signal levels on an analog display: r/w = 10, $\bar{I}$ = 1 mL, and $\sqrt{N(f)}/\bar{I}$ = 0.
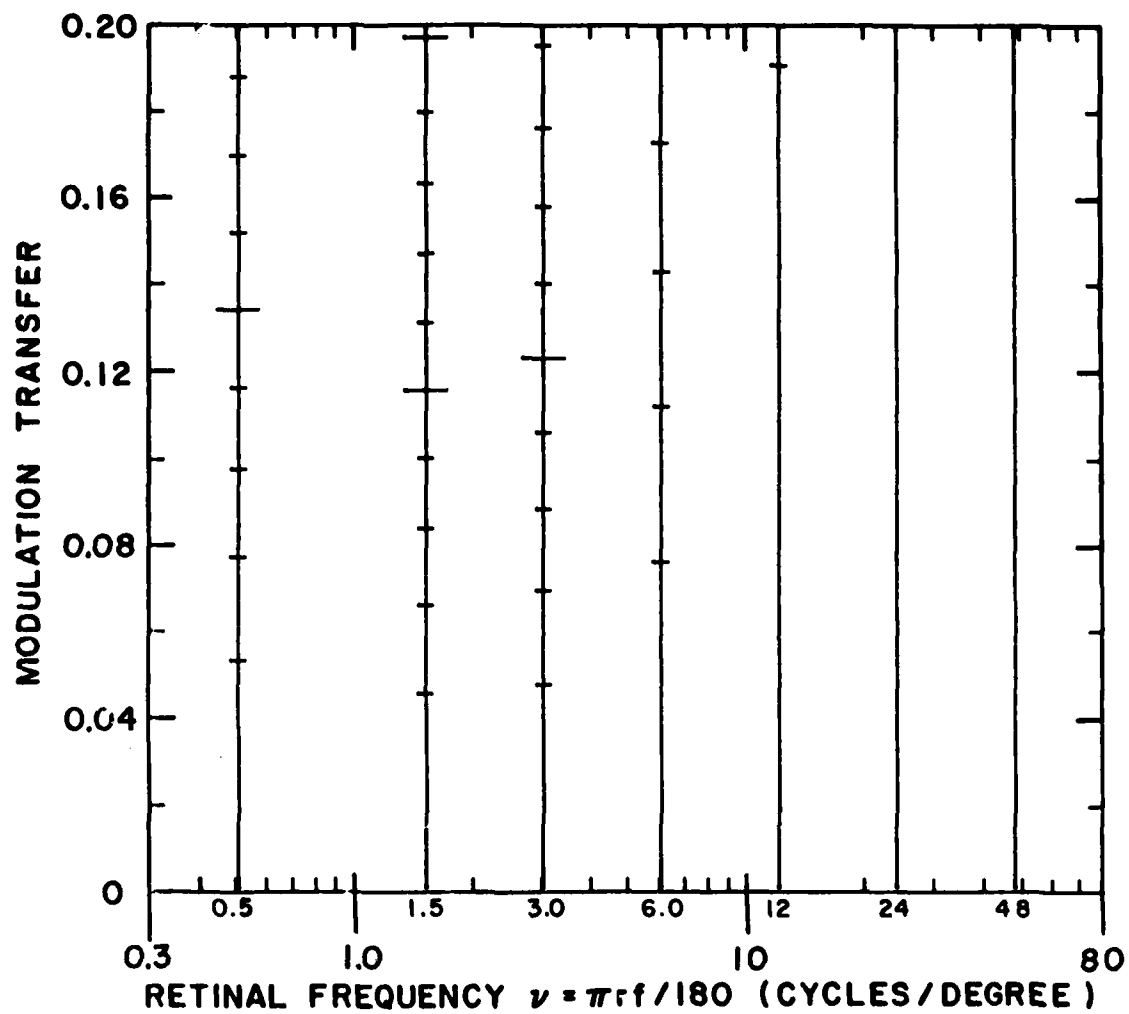
Figure 38. DDD No. 21. Discriminable Difference Diagram for signal levels on an analog display: $r/w = 10$, $\bar{I} = 1$ mL, and $\sqrt{N(f)}/\bar{I} = 0$.

75
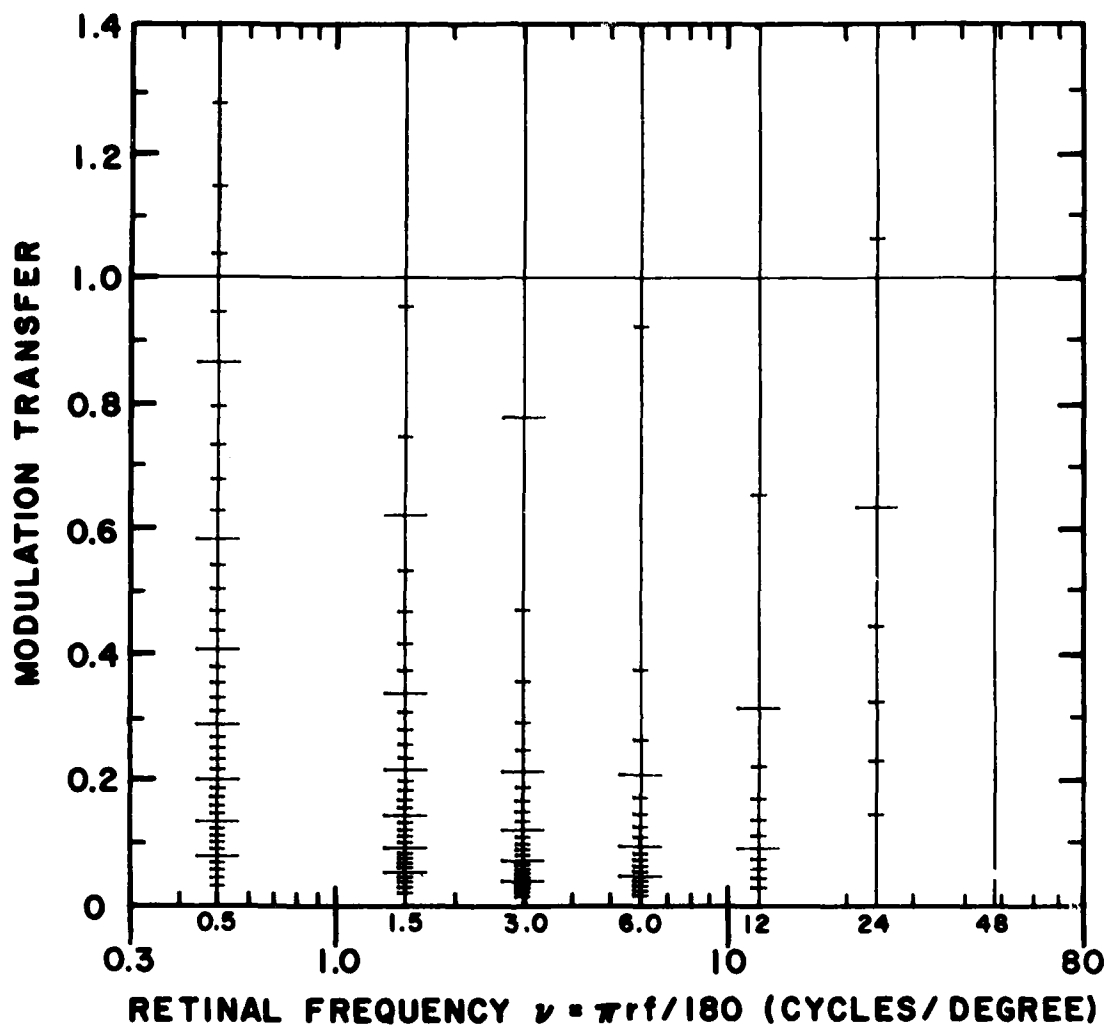
Figure 39.   DDD No. 22.   Discriminable Difference Diagram for signal
levels on an analog display: r/w = 10, r = 50 cm,
I = 35 mL, and $\sqrt{N(f)}/\bar{I}$ = 0.01.
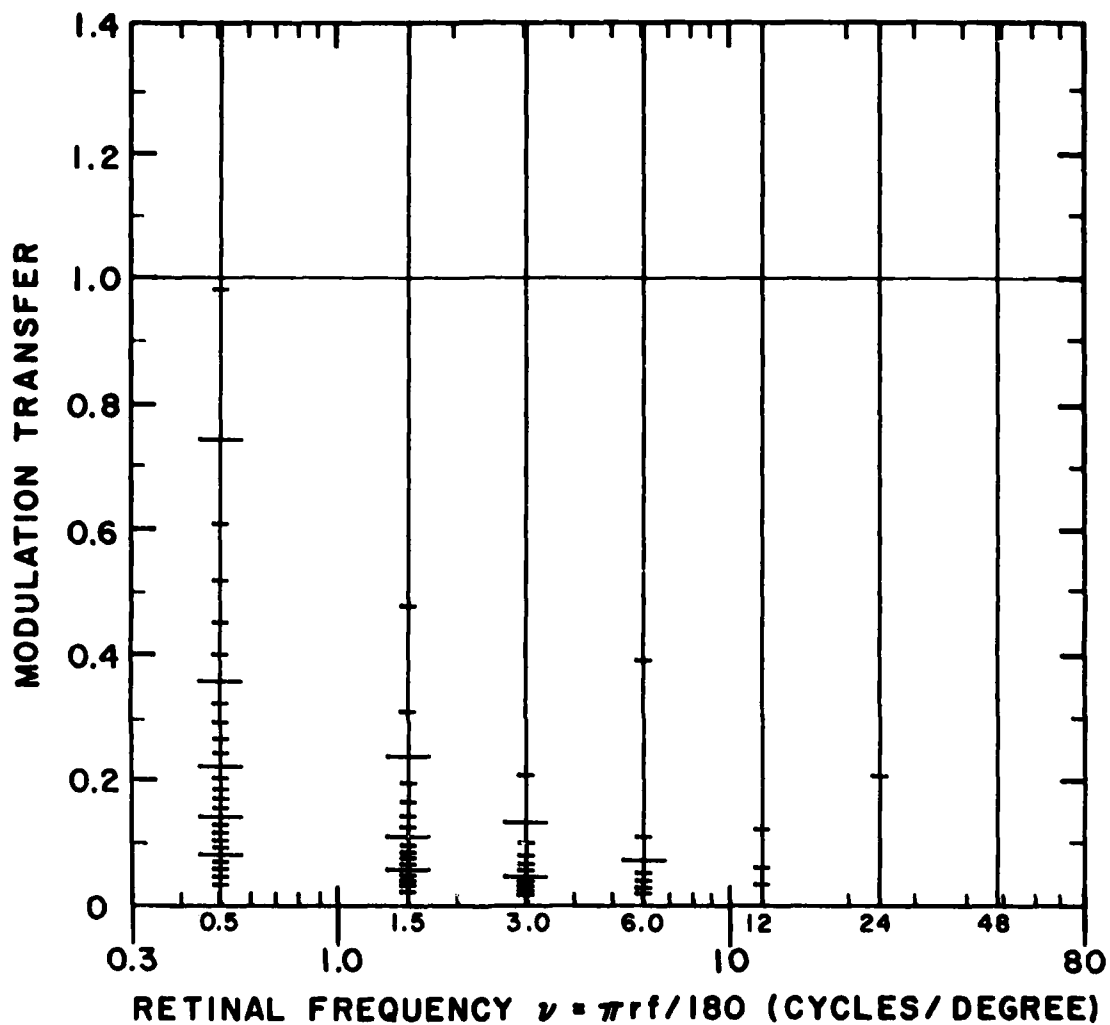
Figure 40. DDD No. 23. Discriminable Difference Diagram for signal levels on an analog display: $r/w = 10$, $r = 50$ cm, $\bar{I} = 35$ mL, and $\sqrt{N(f)}/\bar{I} = 0.03$.
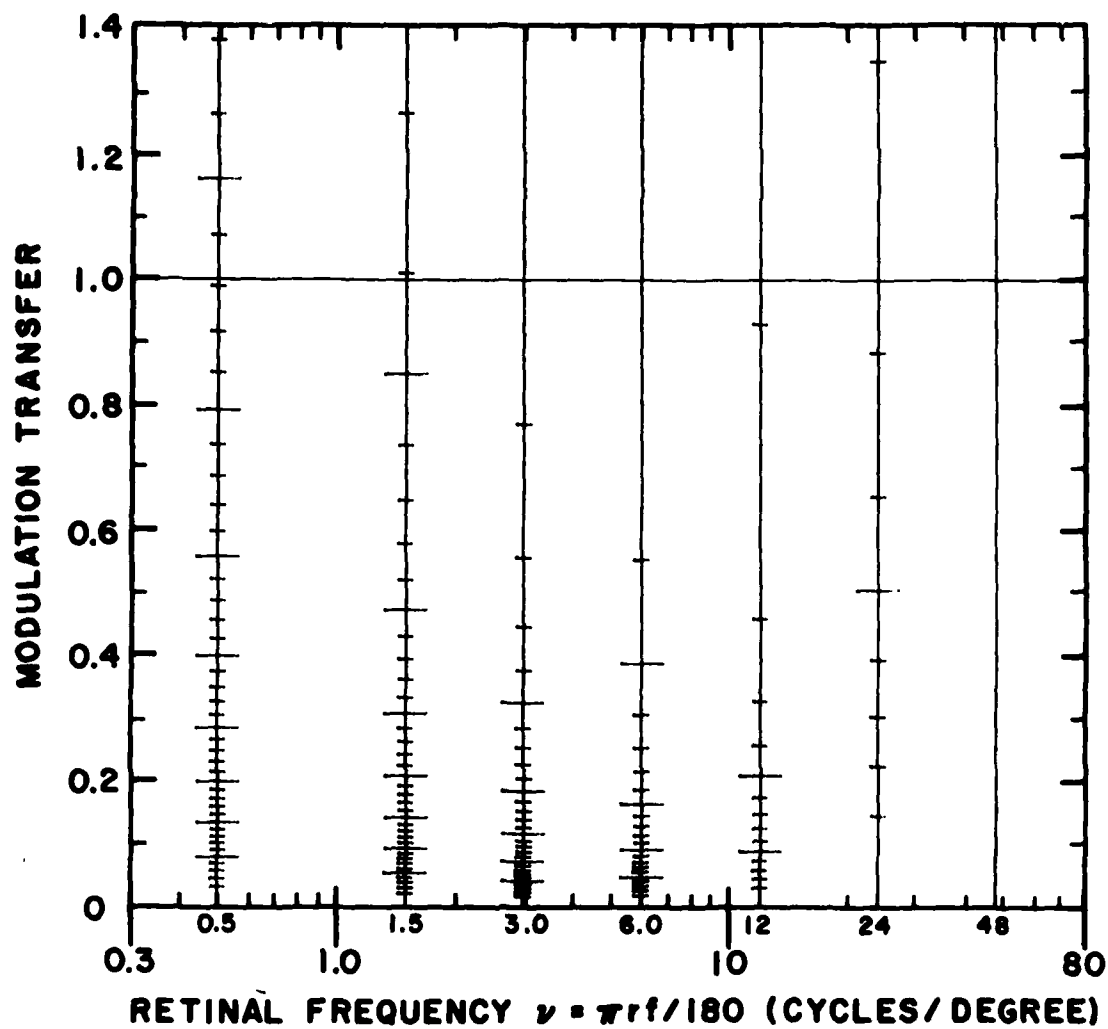
Figure 41.   DDD No. 24.   Discriminable Difference Diagram for signal
levels on an analog display: r/w = 10, r = 100 cm,
$\bar{I}$ = 35 mL, and $\sqrt{N(f)}/\bar{I}$ = 0.01.

78
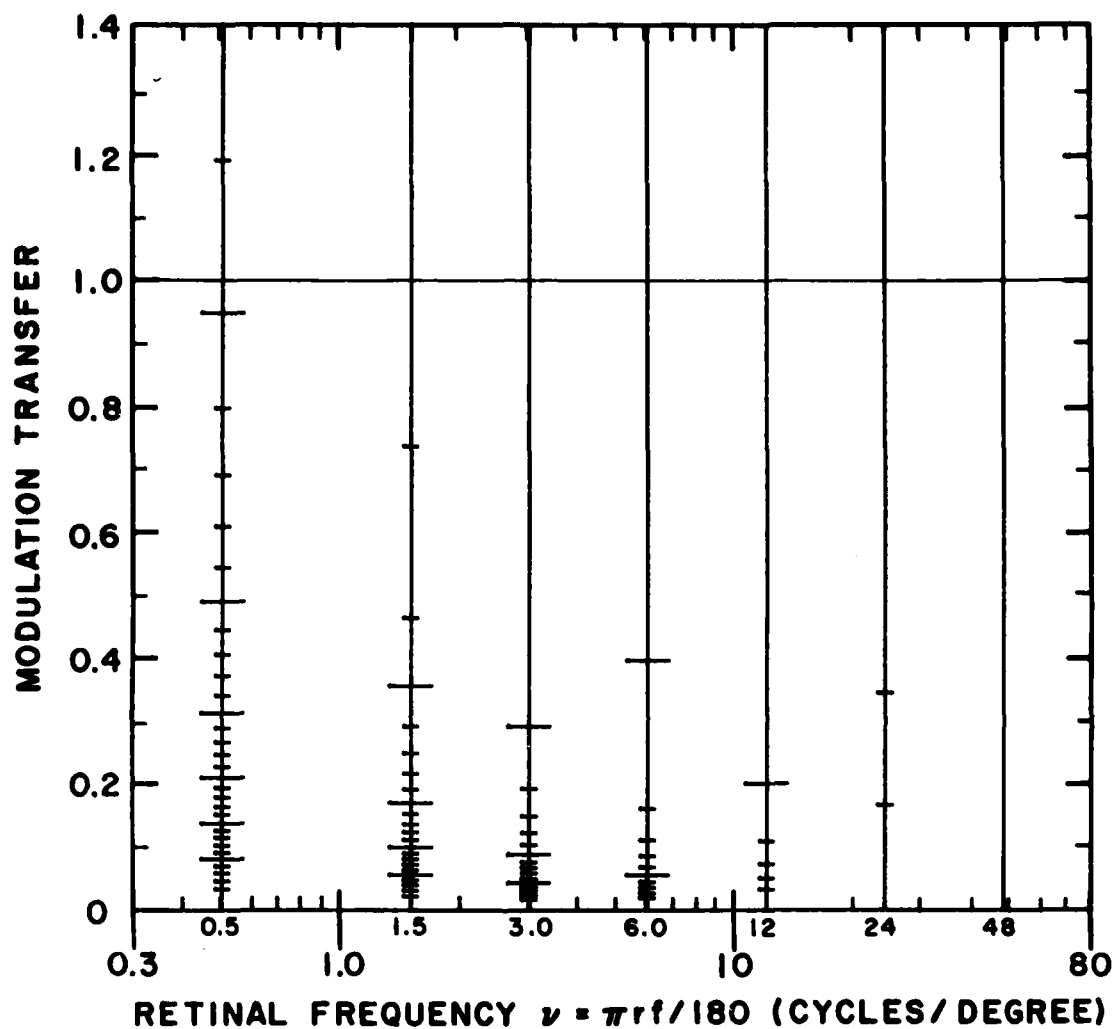
Figure 42.   DDD No. 25.   Discriminable Difference Diagram for signal
levels on an analog display: r/w = 10, r = 100 cm,
$\bar{I}$ = 35 mL, and $\sqrt{N(f)}/\bar{I}$ = 0.03

79
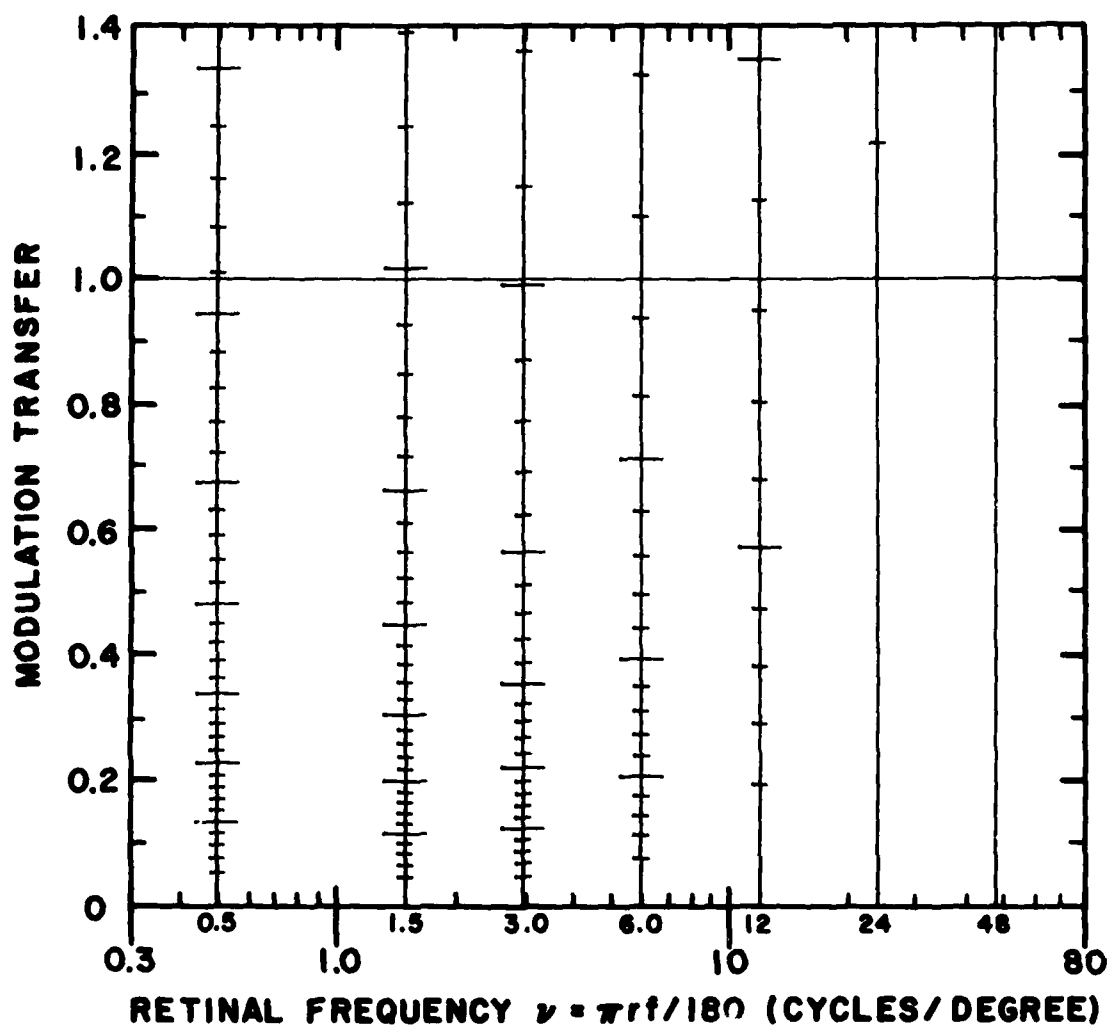
Figure 43. DDD No. 26. Discriminable Difference Diagram for signal
levels on an analog display: $r/w = 10$, $r = 100$ cm,
$\bar{I} = 1$ mL, and $\sqrt{N(f)}/\bar{I} = 0.01$.

80
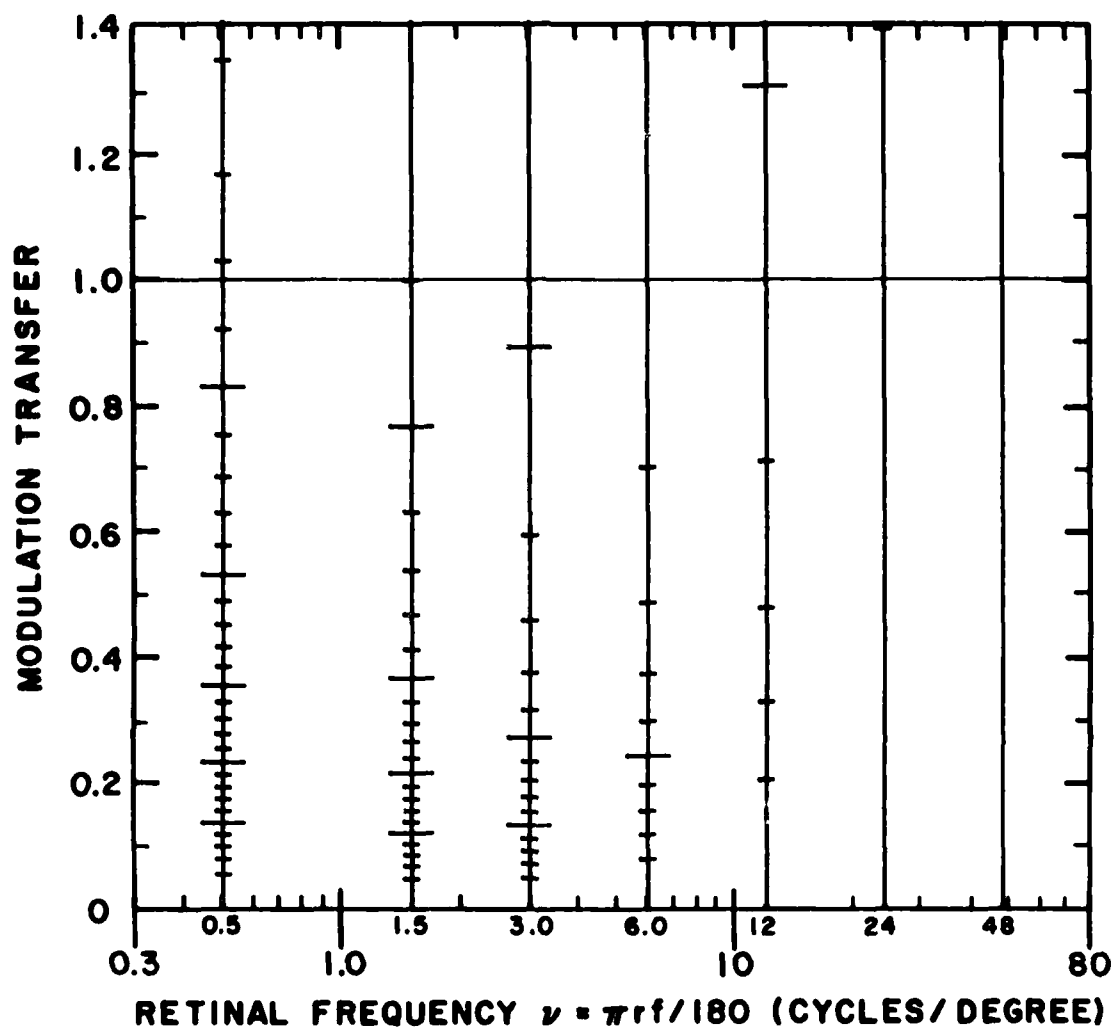
Figure 44. DDD No. 27. Discriminable Difference Diagram for signal
levels on an analog display: r/w = 10, r = 100 cm,
$\overline{I}$ = 1 mL, and $\sqrt{\overline{N(f)}}/\overline{I}$ = 0.03.

81
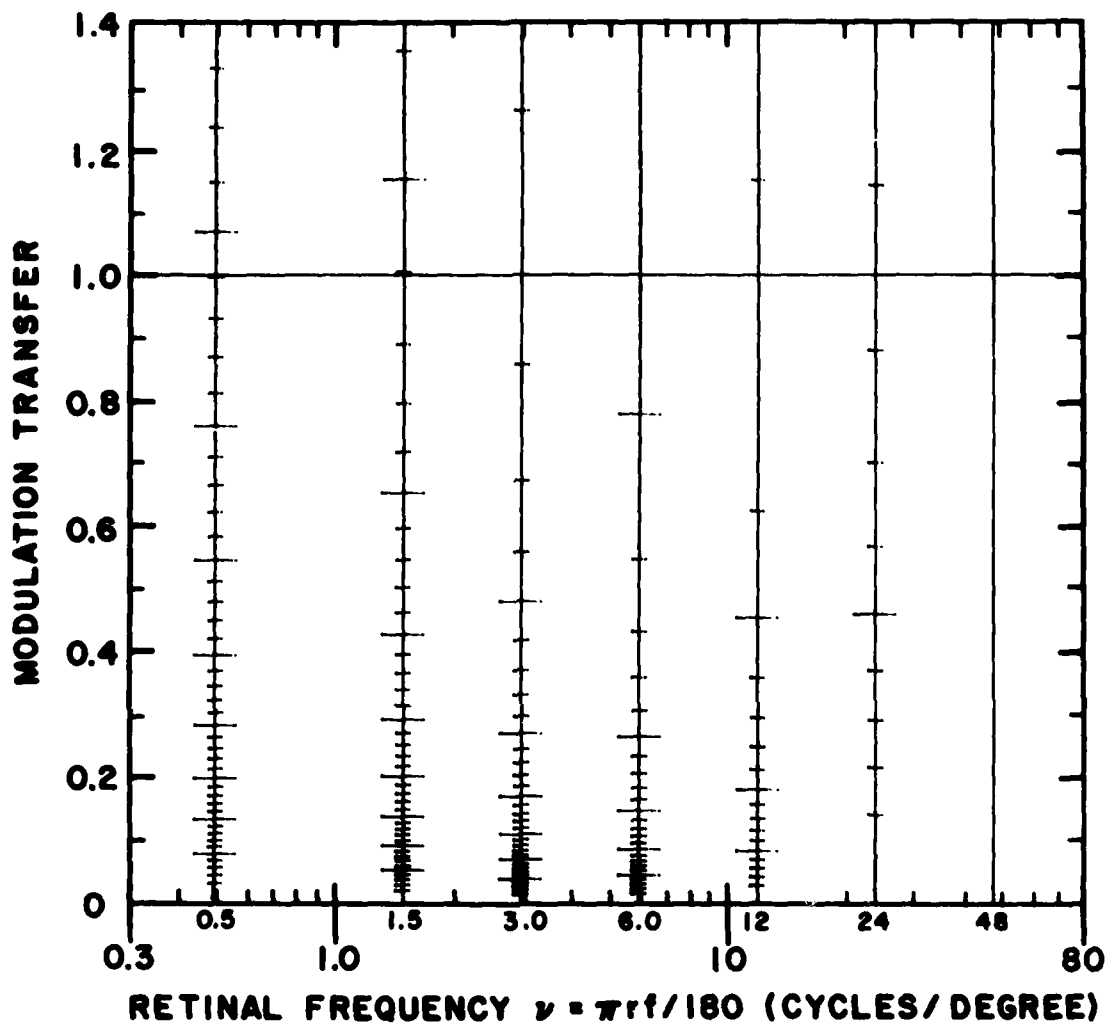
Figure 45. DDD No. 28. Discriminable Difference Diagram for signal levels on an analog display: $r/w = 10$, $r = 200$ cm, $\bar{I} = 35$ mL, and $\sqrt{N(f)}/\bar{I} = 0.01$.

82
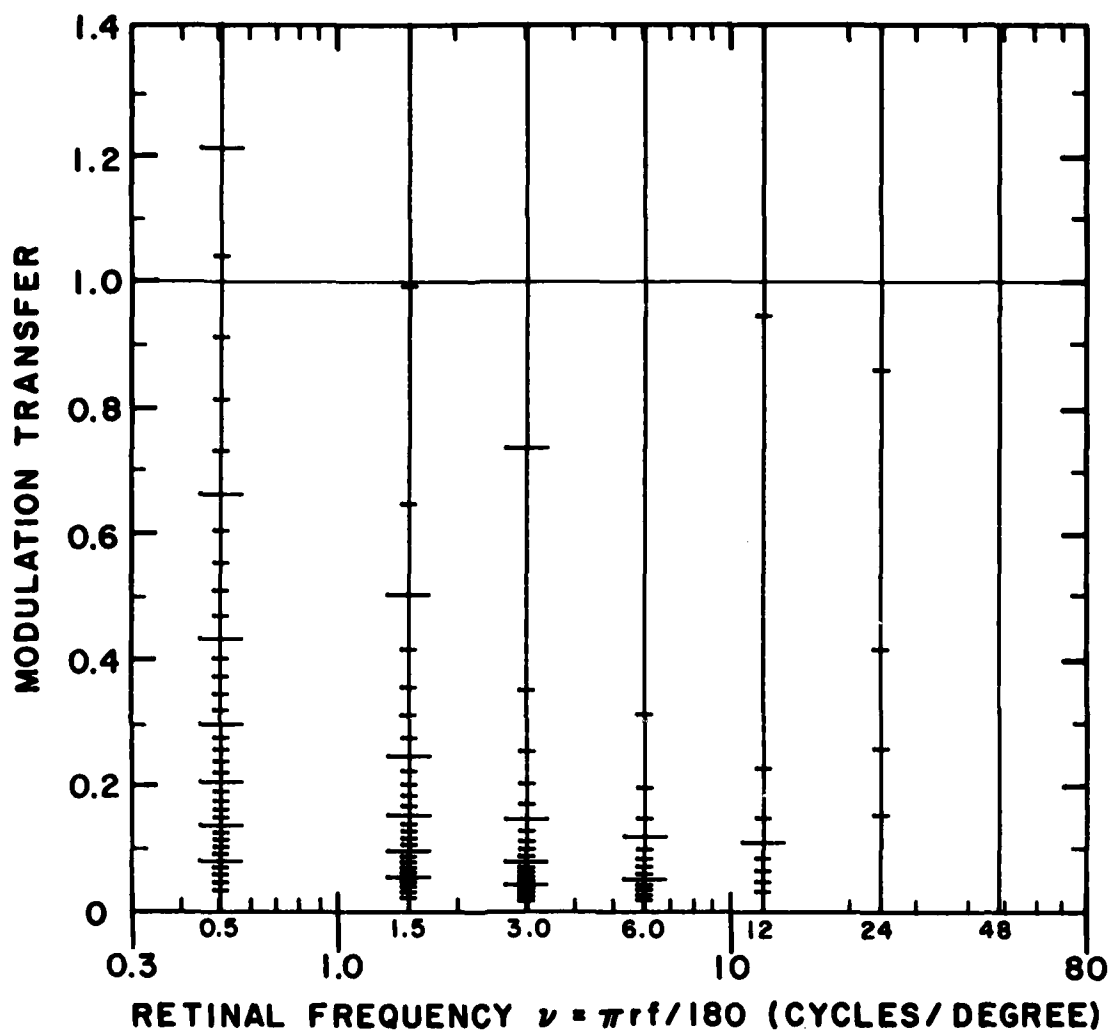
Figure 46.   DDD No. 29.   Discriminable Difference Diagram for signal
              levels on an analog display: r/w = 10, r = 200 cm,
              $\bar{I}$ = 35 mL, and $\sqrt{N(f)}/\bar{I}$ = 0.03.

83
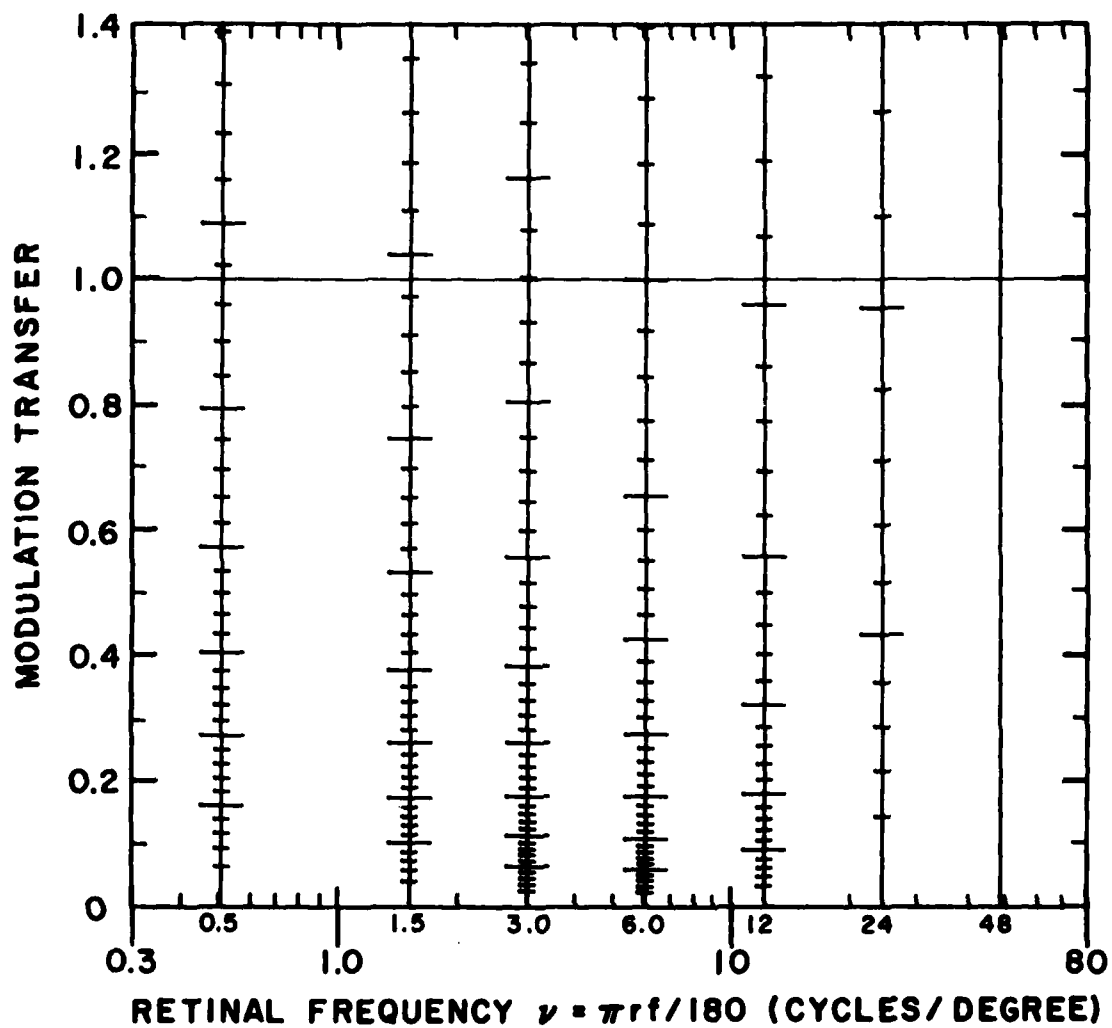
Figure 47.   DDD No. 30.   Discriminable Difference Diagram for signal
            levels on an analog display: r/w = 30, $\overline{I}$ = 35 mL, and
            $\sqrt{N(f)}/\overline{I}$ = 0.
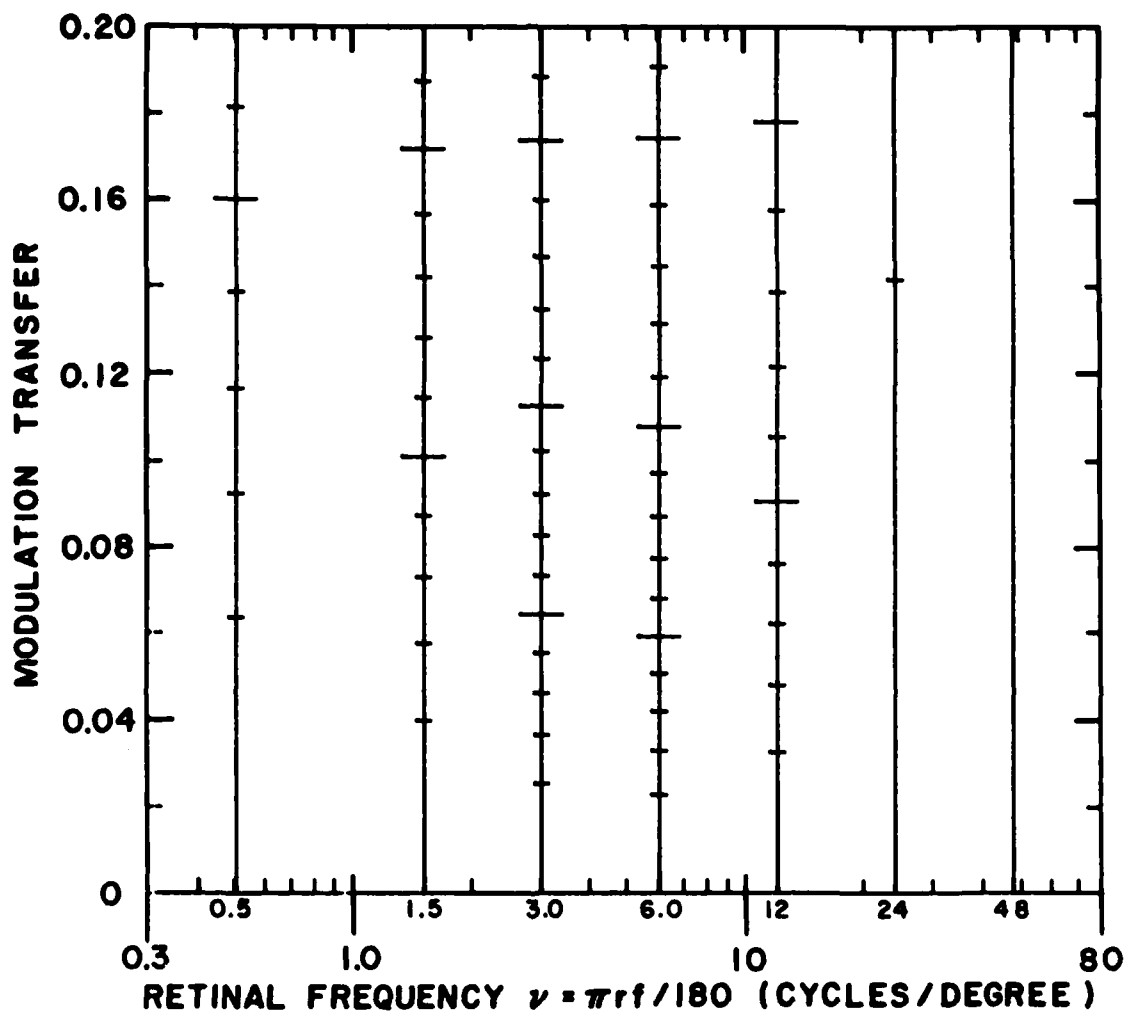
Figure 48. DDD No. 31. Discriminable Difference Diagram for signal levels on an analog display: $r/w = 30$, $\bar{I} = 35$ mL, and $\sqrt{N(f)}/\bar{I} = 0$.
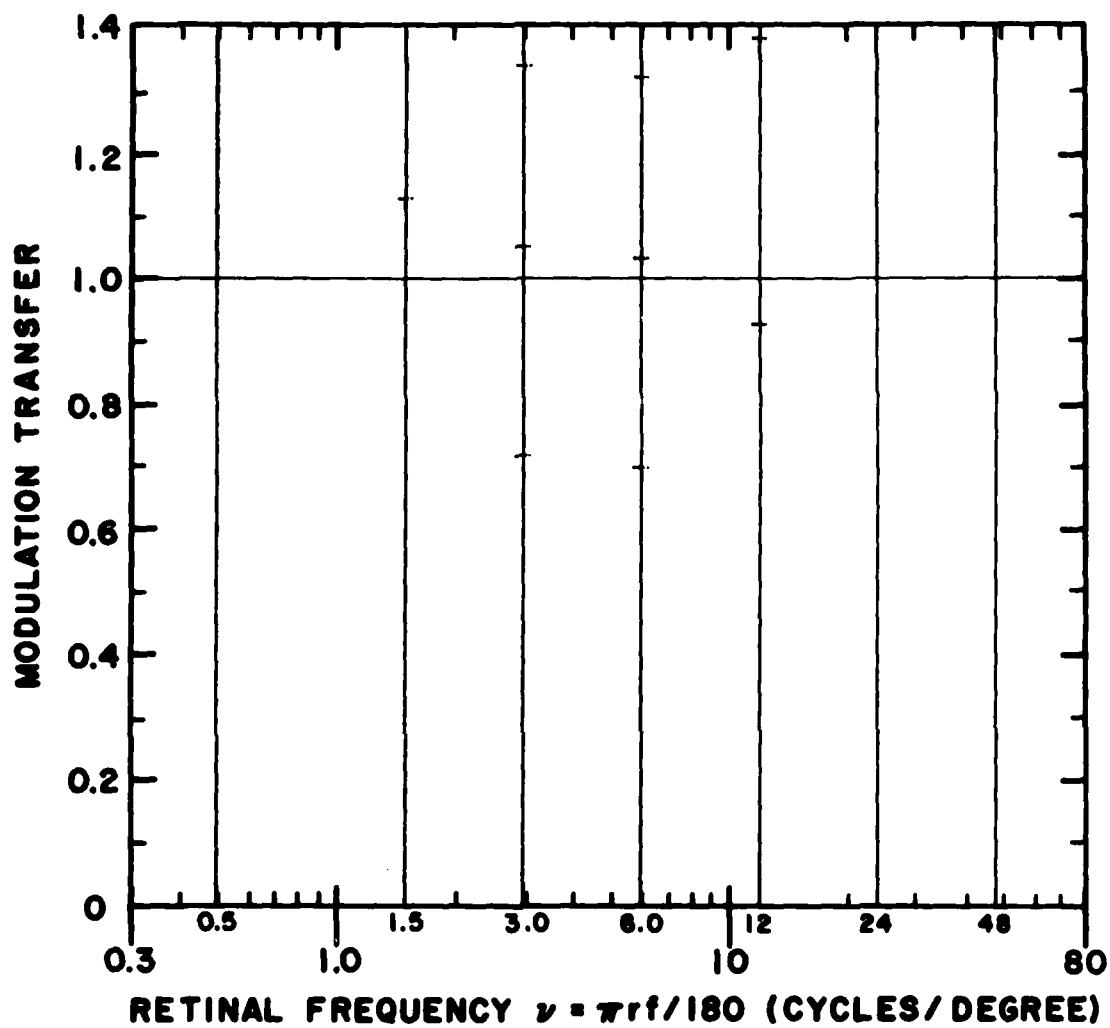
Figure 49.   DDD No. 32.   Discriminable Difference Diagram for noise on a
uniform luminance analog display: r/w = 3, r = 50 cm,
$\overline{I}$ = 35 mL, and $\sqrt{N(f)}/\overline{I}$ = 0.001.
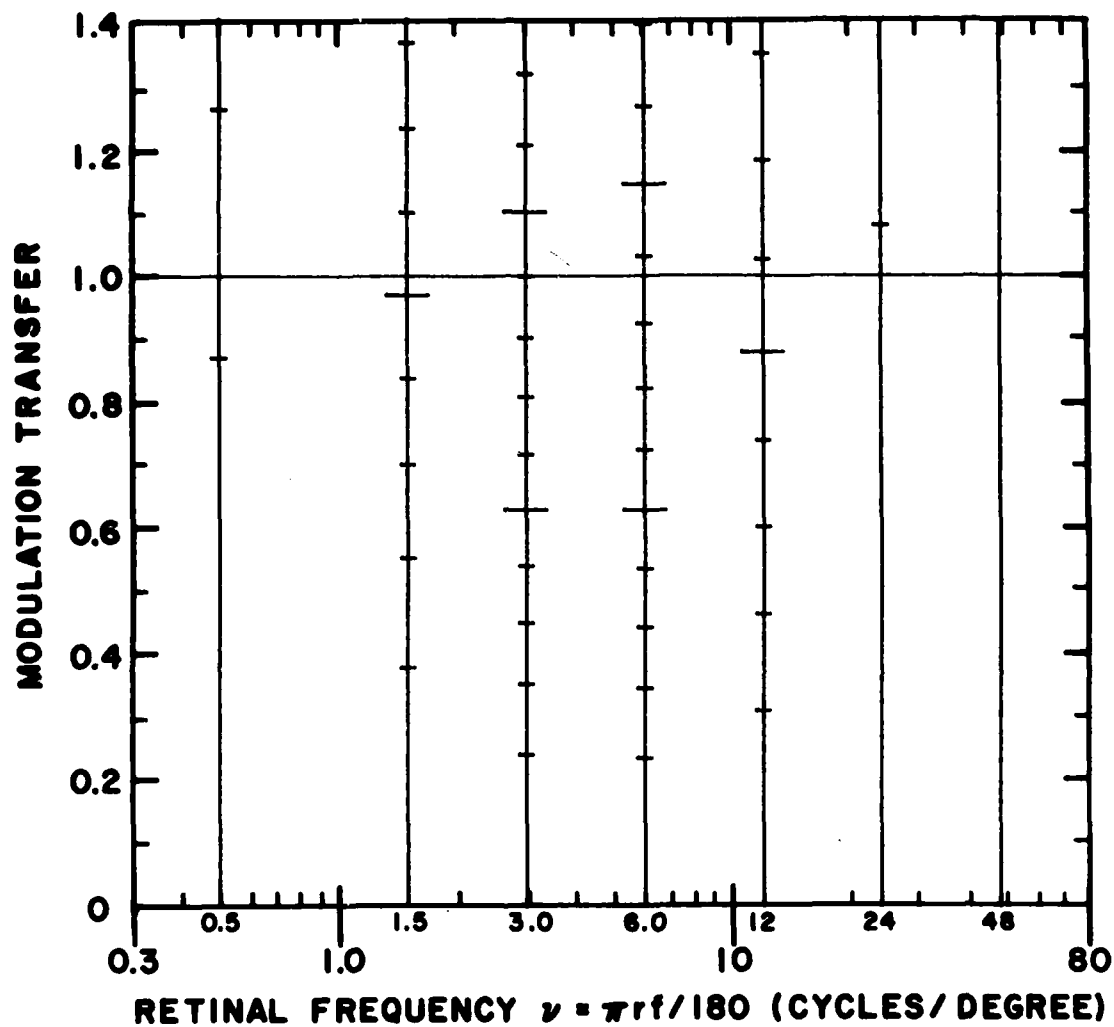
Figure 50. DDD No. 33. Discriminable Difference Diagram for noise on a uniform luminance analog display: r/w = 3, r = 50 cm, $\bar{I}$ = 35 mL, and $\sqrt{N(f)}/\bar{I}$ = 0.003.

87
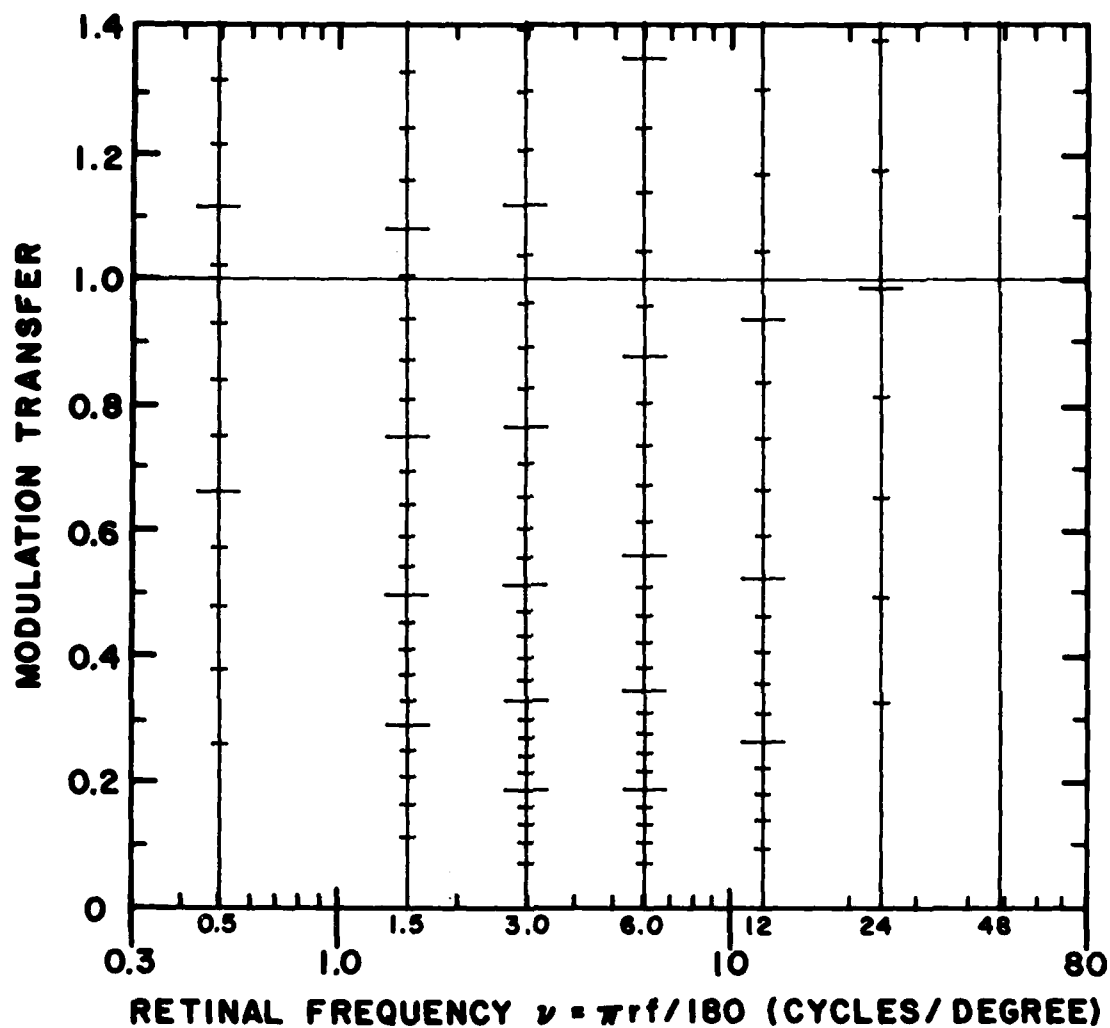
Figure 51. DDD No. 34. Discriminable Difference Diagram for noise on a uniform luminance analog display: r/w = 3, r = 50 cm, $\bar{I}$ = 35 mL, and $\sqrt{N(f)}/\bar{I}$ = 0.01.

88
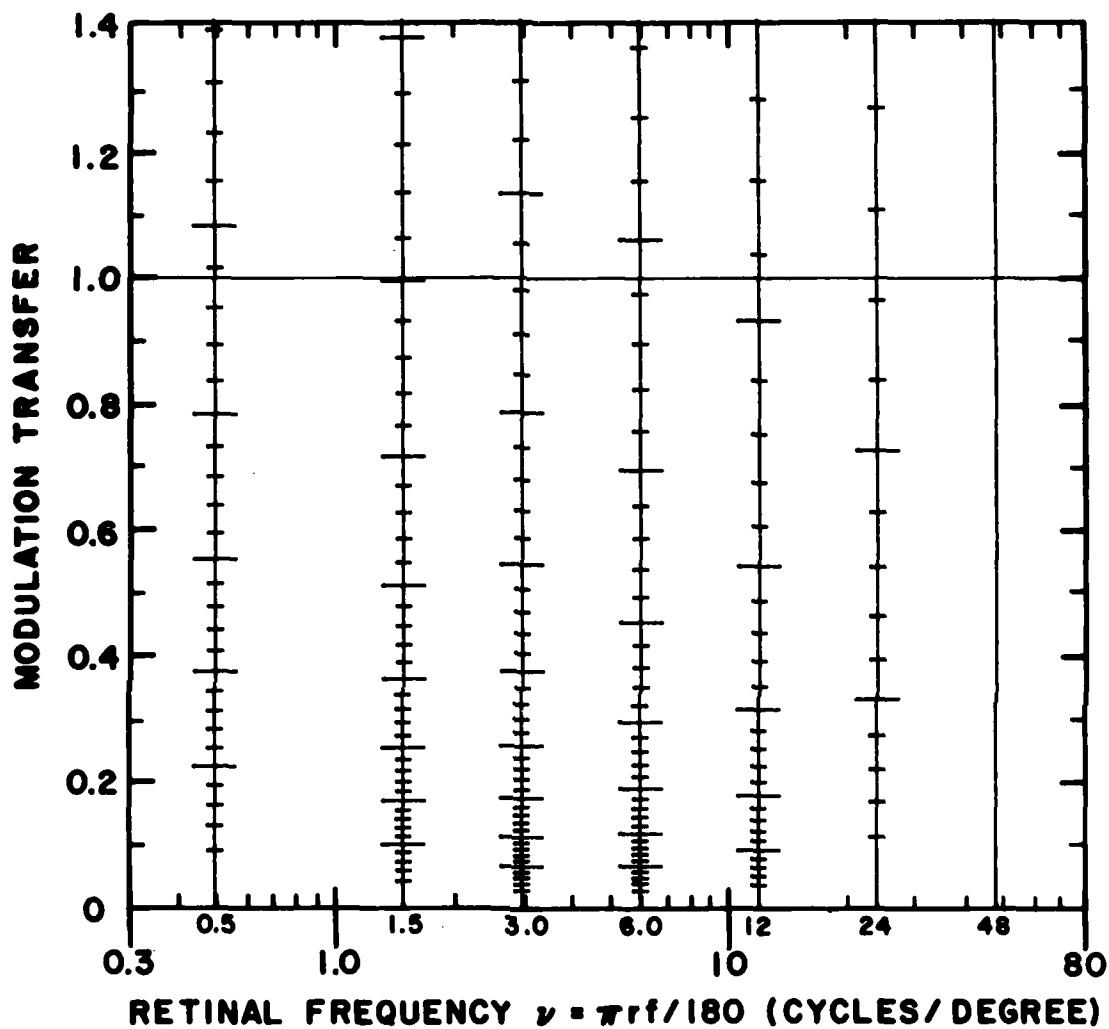
Figure 52.   DDD No. 35.   Discriminable Difference Diagram for noise on a
uniform luminance analog display: r/w = 3, r = 50 cm,
$\bar{I}$ = 35 mL, and $\sqrt{N(f)}/\bar{I}$ = 0.03.
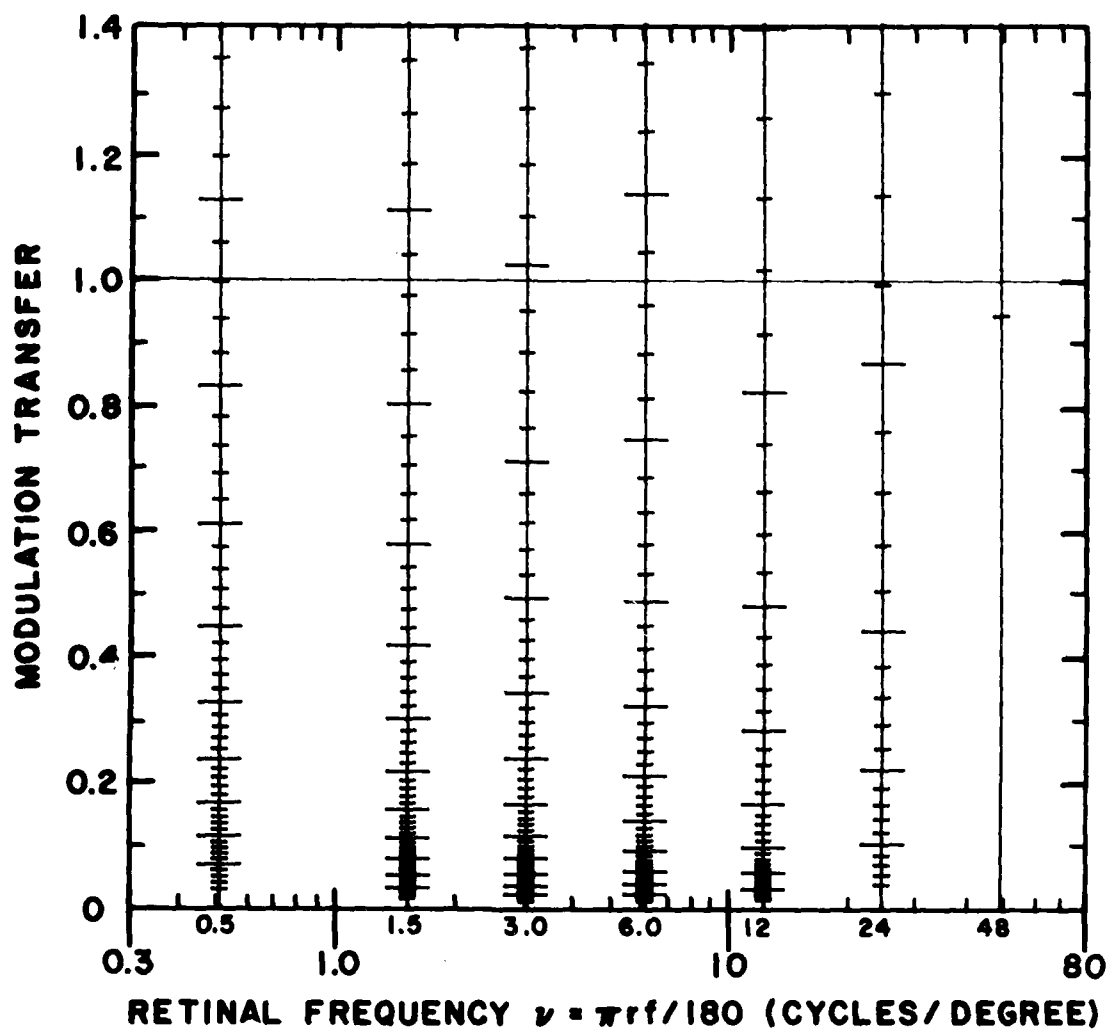
Figure 53. DDD No. 36. Discriminable Difference Diagram for noise on a
uniform luminance analog display: r/w = 3, r = 50 cm,
$\bar{I}$ = 35 mL, and $\sqrt{N(f)}/\bar{I}$ = 0.1.
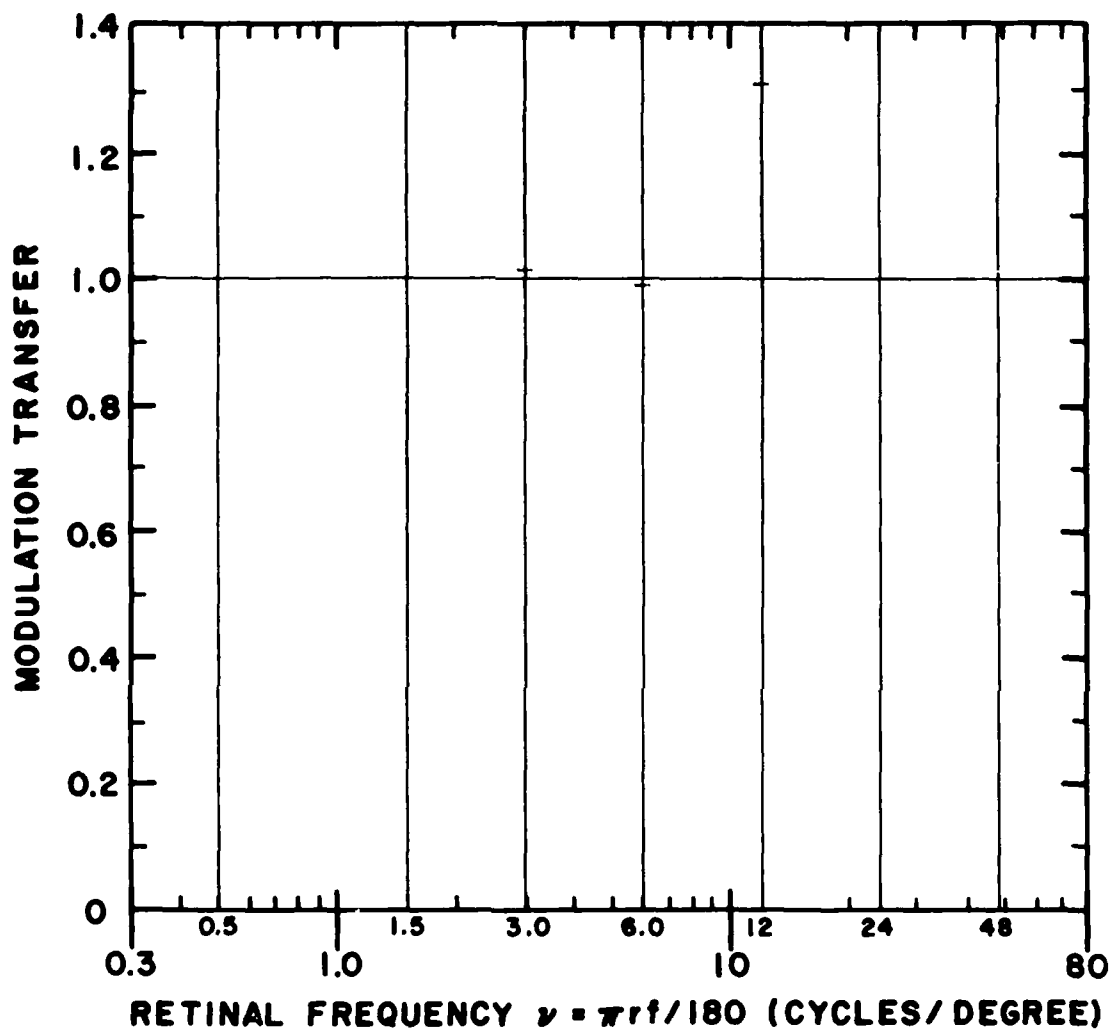
Figure 54. DDD No. 37. Discriminable Difference Diagram for noise on a uniform luminance analog display: $r/w = 3$, $r = 100$ cm, $\bar{I} = 35$ mL, and $\sqrt{N(f)}/\bar{I} = 0.001$.

91
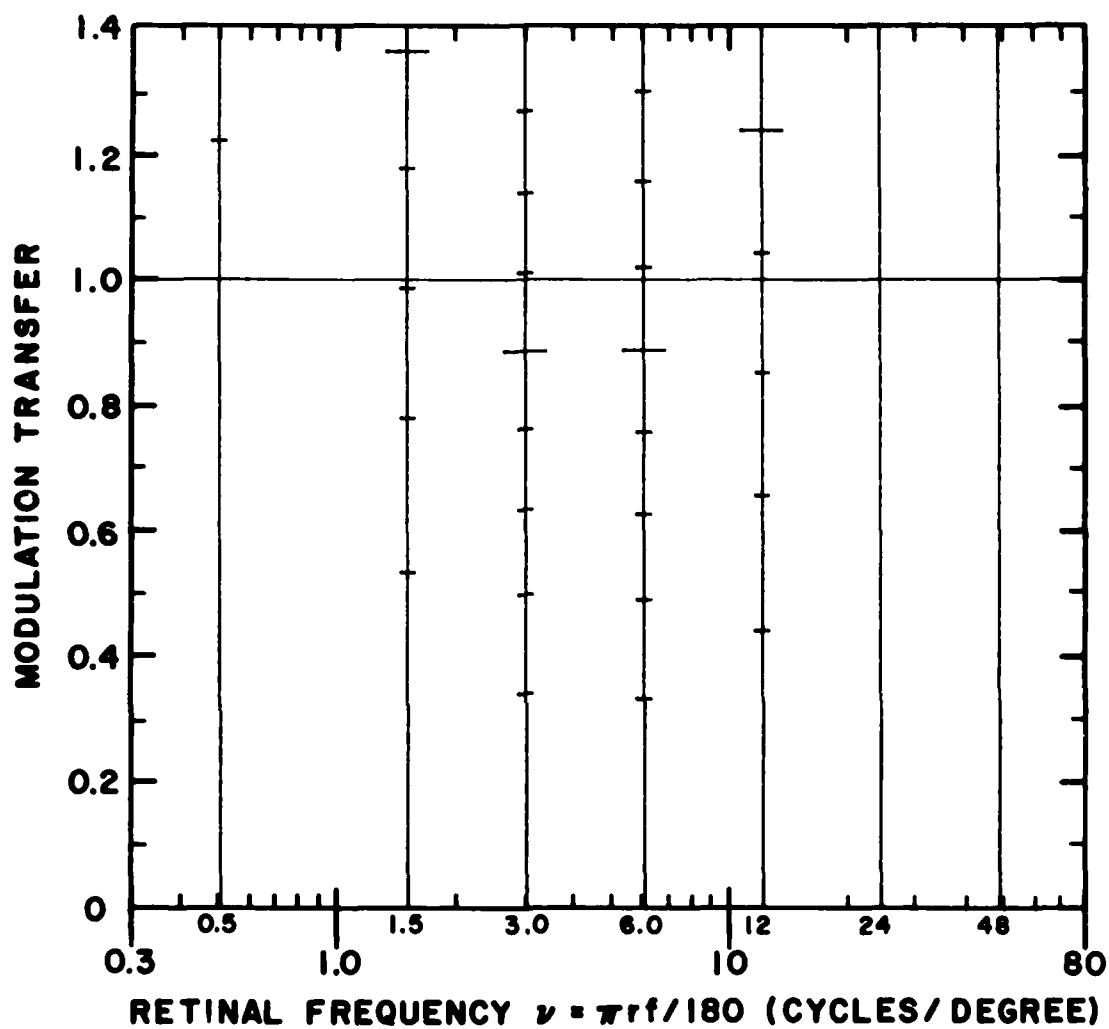
Figure 55. DDD No. 38. Discriminable Difference Diagram for noise on a uniform luminance analog display: $r/w = 3$, $r = 100$ cm, $\bar{I} = 35$ mL, and $\sqrt{N(f)}/\bar{I} = 0.003$.
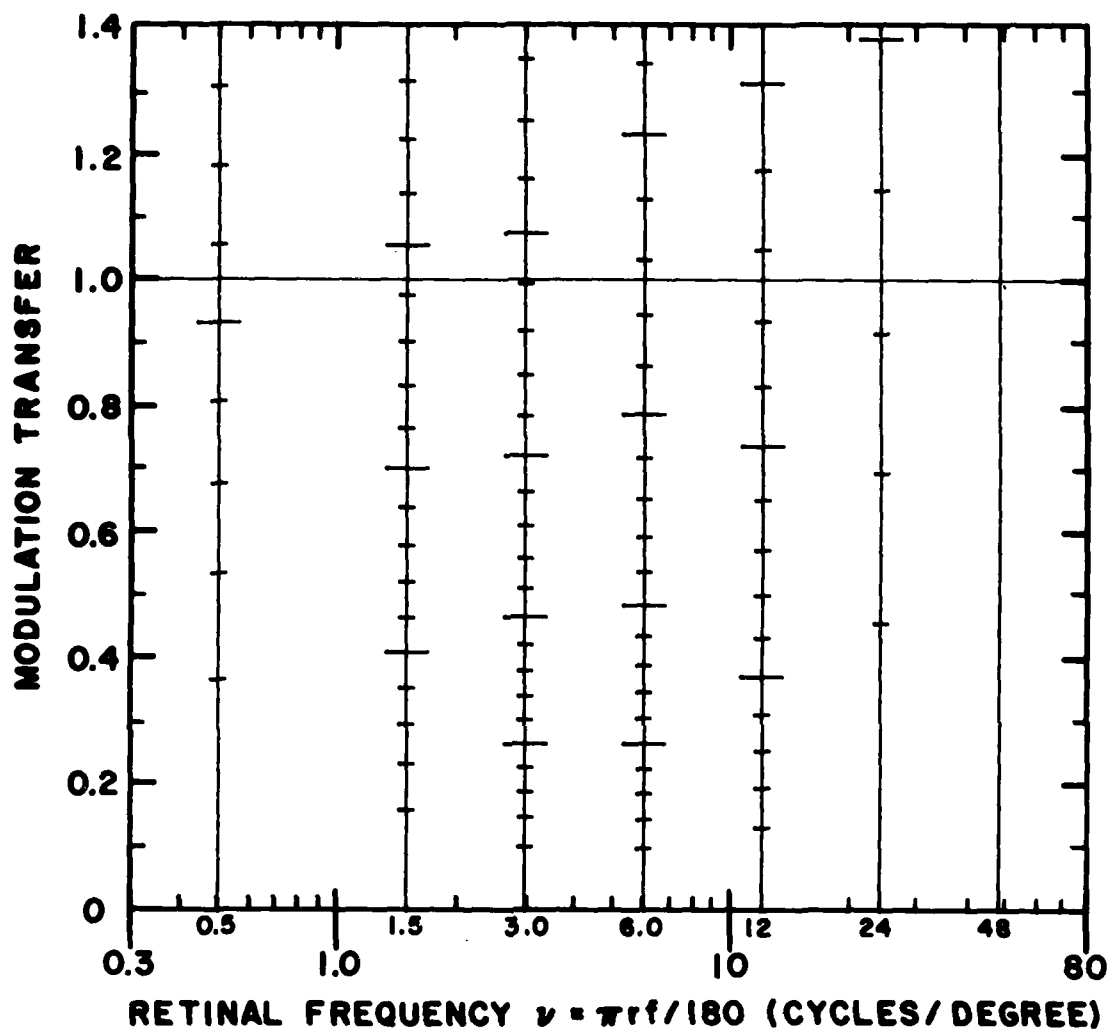
Figure 56. DDD No. 39. Discriminable Difference Diagram for noise on a
uniform luminance analog display: r/w = 3, r = 100 cm,
$\bar{I}$ = 35 mL, and $\sqrt{N(f)}/\bar{I}$ = 0.01.

93
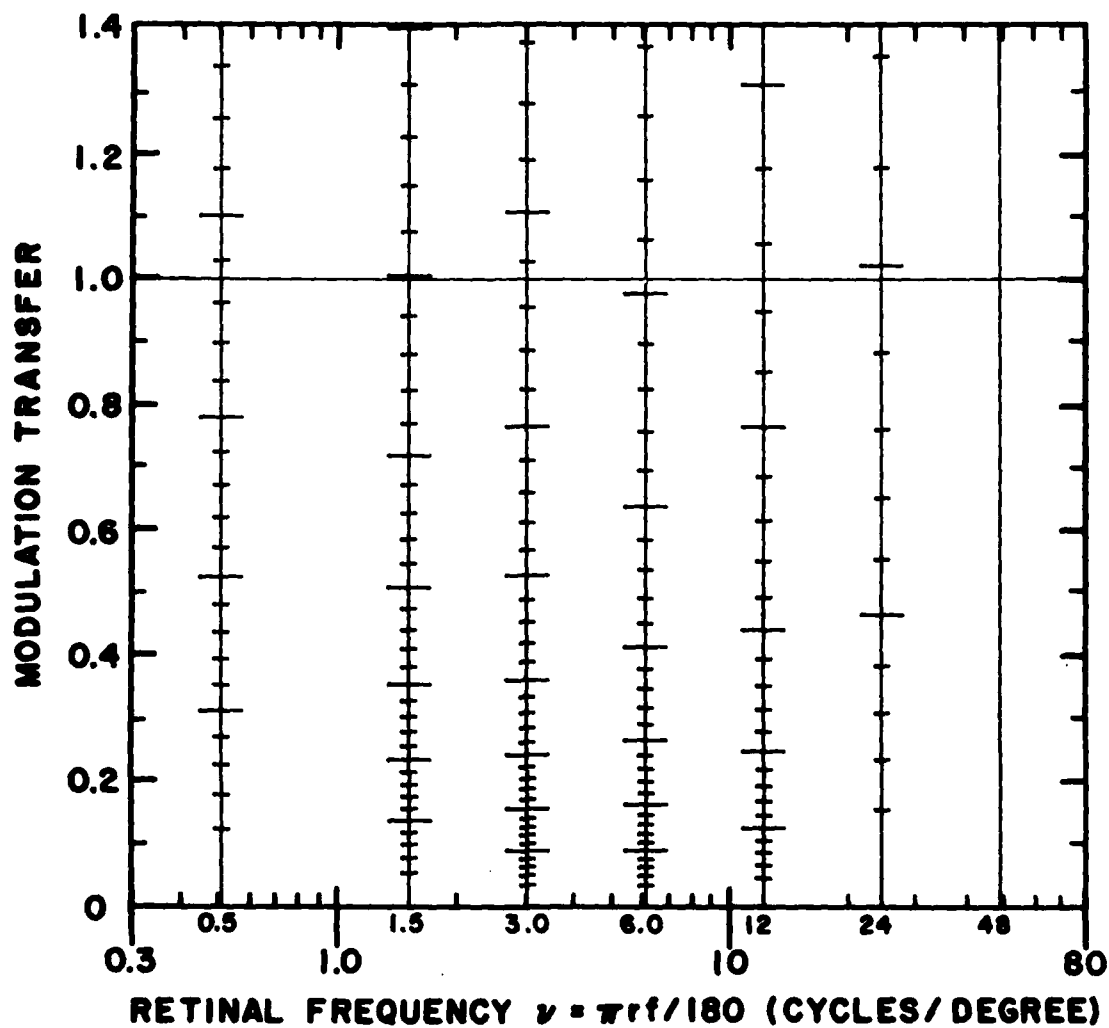
Figure 57. DDD No. 40. Discriminable Difference Diagram for noise on a uniform luminance analog display: $r/w = 3$, $r = 100$ cm, $\bar{I} = 35$ mL, and $\sqrt{N(f)}/\bar{I} = 0.03$.
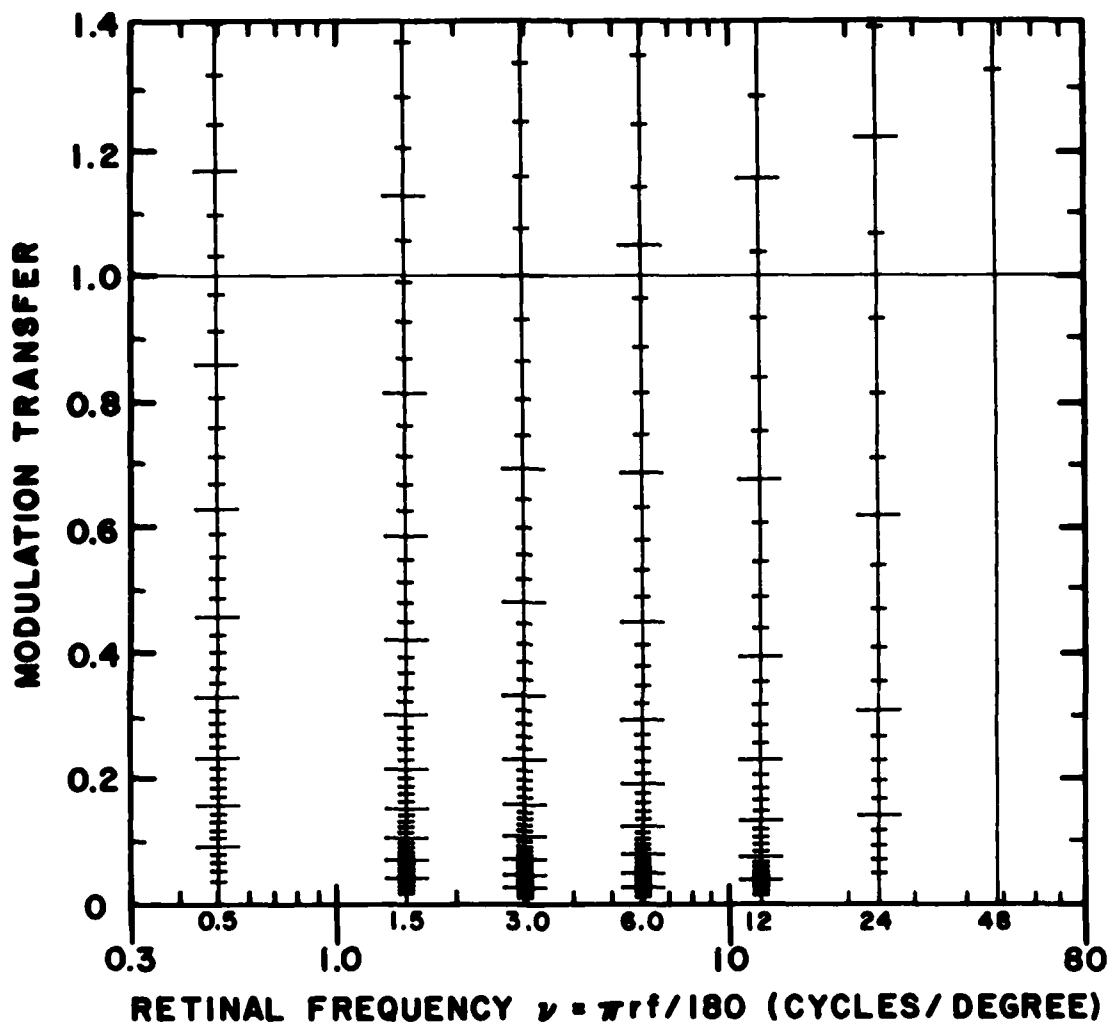
Figure 58. DDD No. 41. Discriminable Difference Diagram for noise on a uniform luminance analog display: $r/w = 3$, $r = 100$ cm, $\bar{I} = 35$ mL, and $\sqrt{N(f)}/\bar{I} = 0.1$.
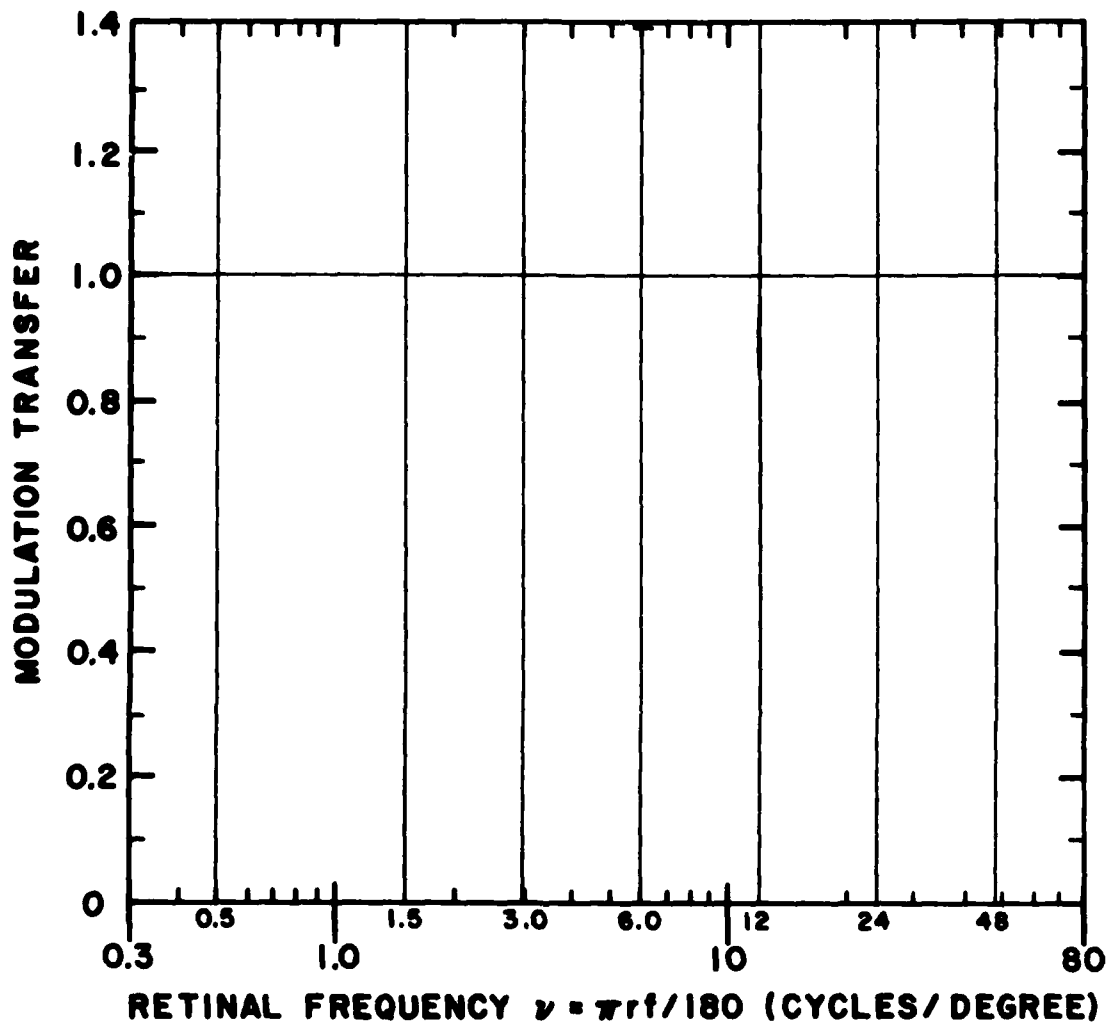
Figure 59. DDD No. 42. Discriminable Difference Diagram for noise on a
uniform luminance analog display: $r/w = 3$, $r = 200$ cm,
$\bar{I} = 35$ mL, and $\sqrt{N(f)}/\bar{I} = 0.001$.
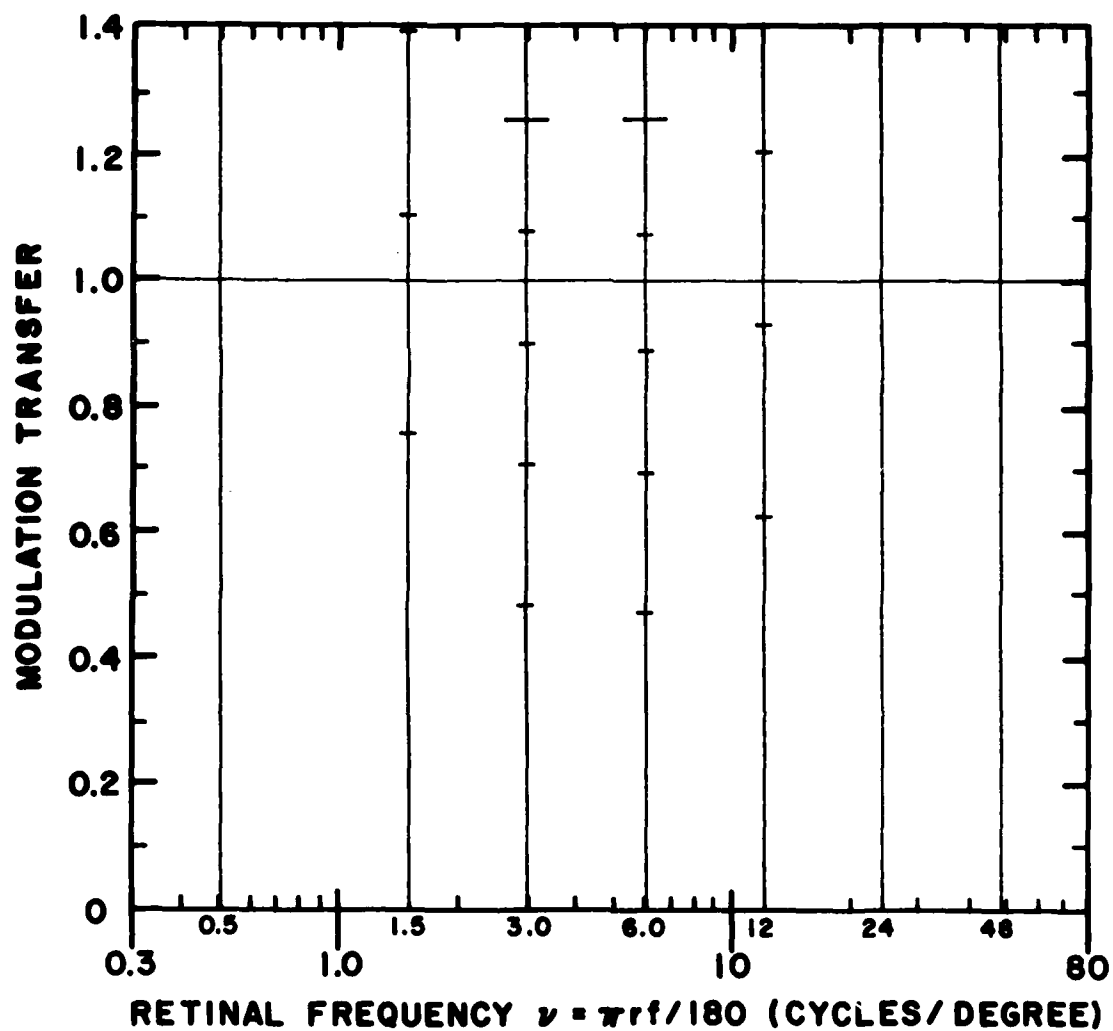
Figure 60. DDD No. 43. Discriminable Difference Diagram for noise on a uniform luminance analog display: $r/w = 3$, $r = 200$ cm, $\bar{I} = 35$ mL, and $\sqrt{N(f)}/\bar{I} = 0.003$.
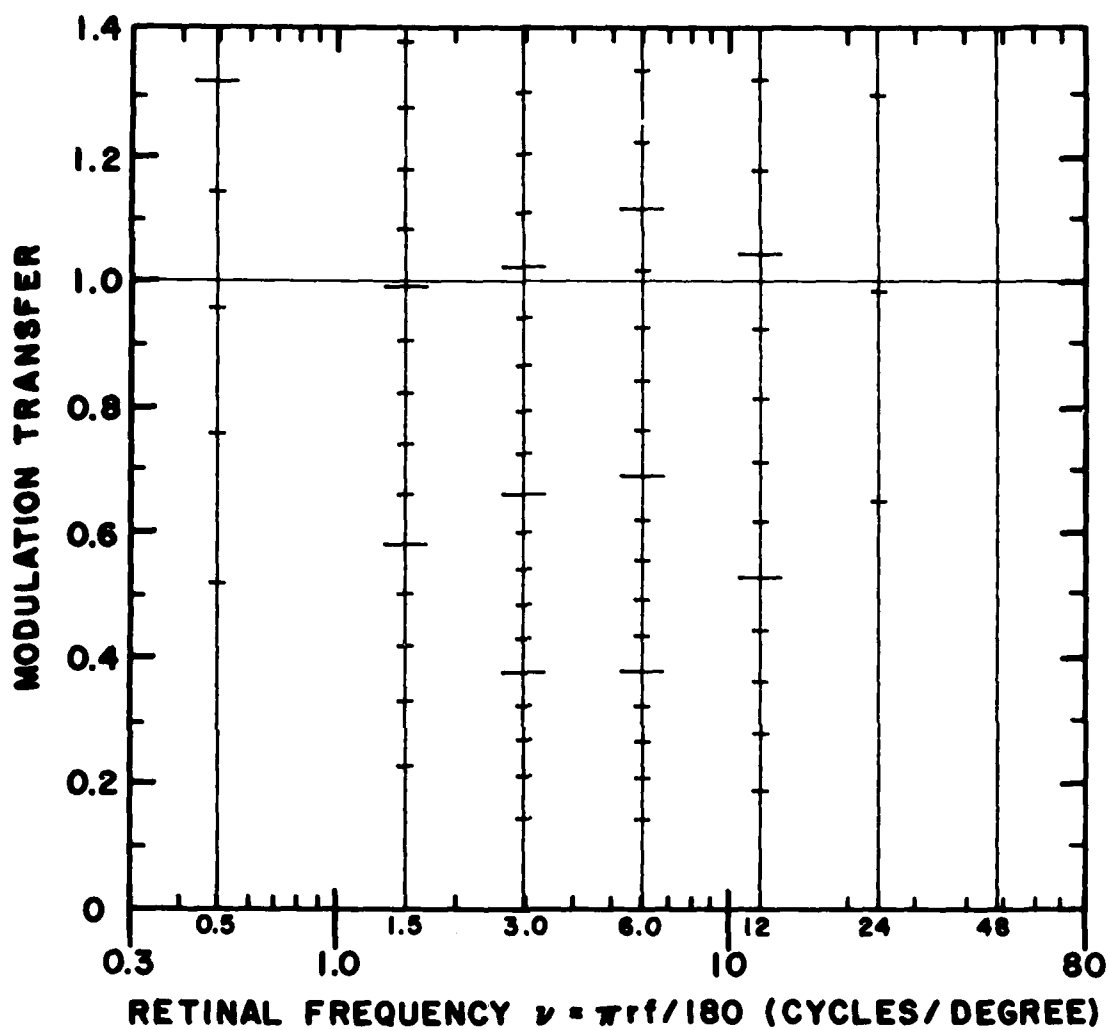
Figure 61. DDD No. 44. Discriminable Difference Diagram for noise on a uniform luminance analog display: r/w = 3, r = 200 cm, $\bar{I}$ = 35 mL, and $\sqrt{N(\bar{f})}/\bar{I}$ = 0.01.

98
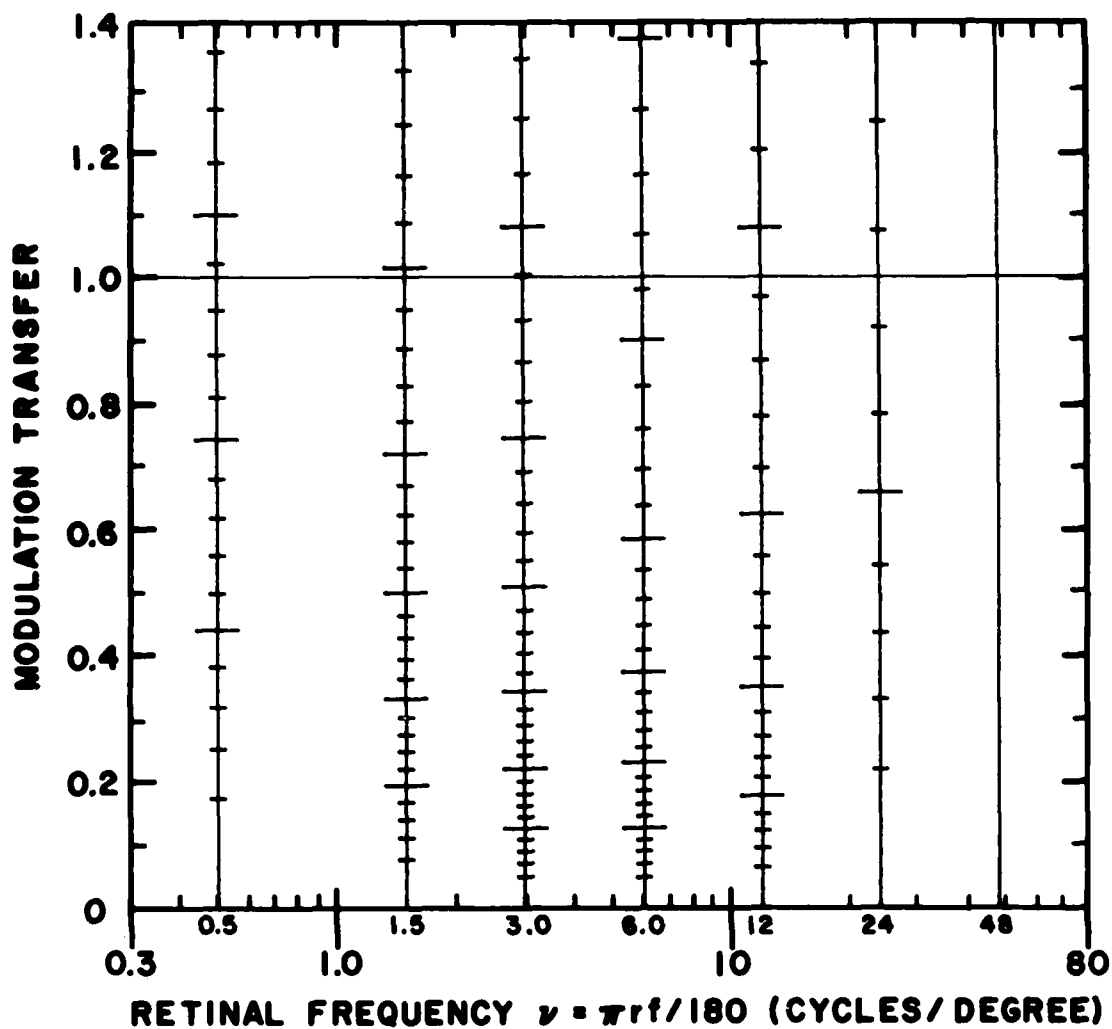
Figure 62. DDD No. 45. Discriminable Difference Diagram for noise on a uniform luminance analog display: $r/w = 3$, $r = 200$ cm, $\overline{I} = 35$ mL, and $\sqrt{N(f)}/\overline{I} = 0.03$.

99
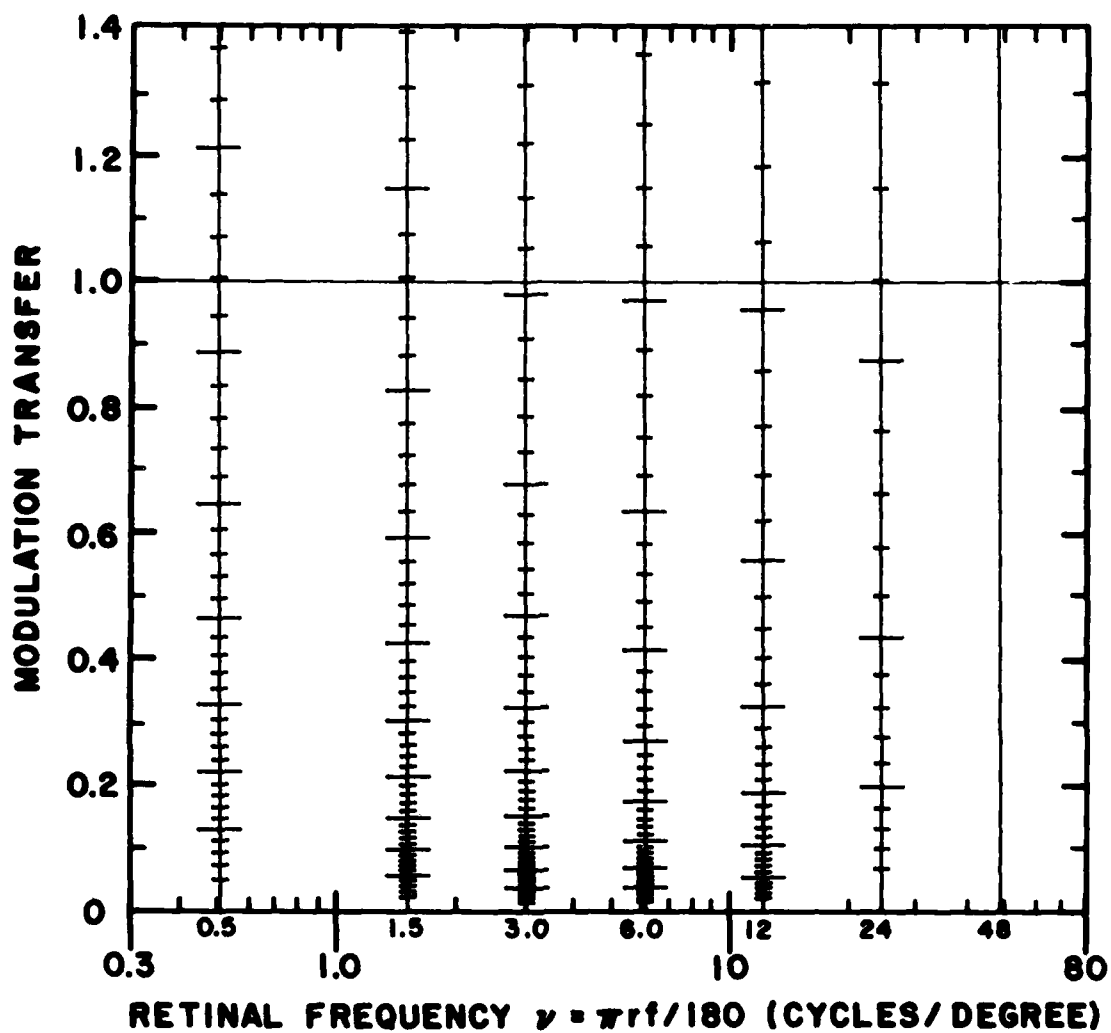
Figure 63. DDD No. 46. Discriminable Difference Diagram for noise on a
uniform luminance analog display: $r/w = 3$, $r = 200$ cm,
$\overline{I} = 35$ mL, and $\sqrt{N(f)}/\overline{I} = 0.1$.

100
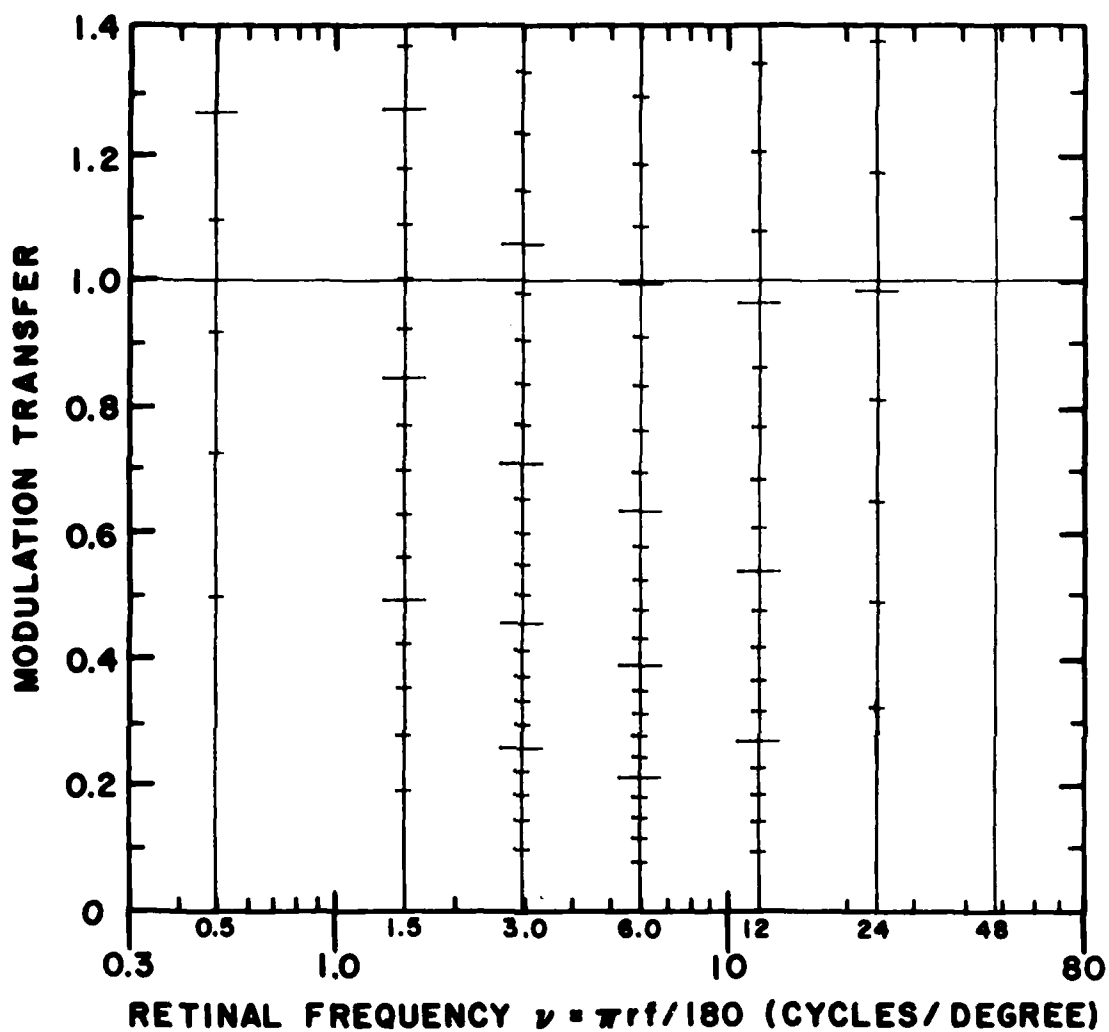
Figure 64. DDD No. 47. Discriminable Difference Diagram for noise on a uniform luminance analog display: r/w = 10, r = 50 cm, $\bar{I}$ = 35 mL, and $\sqrt{N(\bar{f})}/\bar{I}$ = 0.1.

101
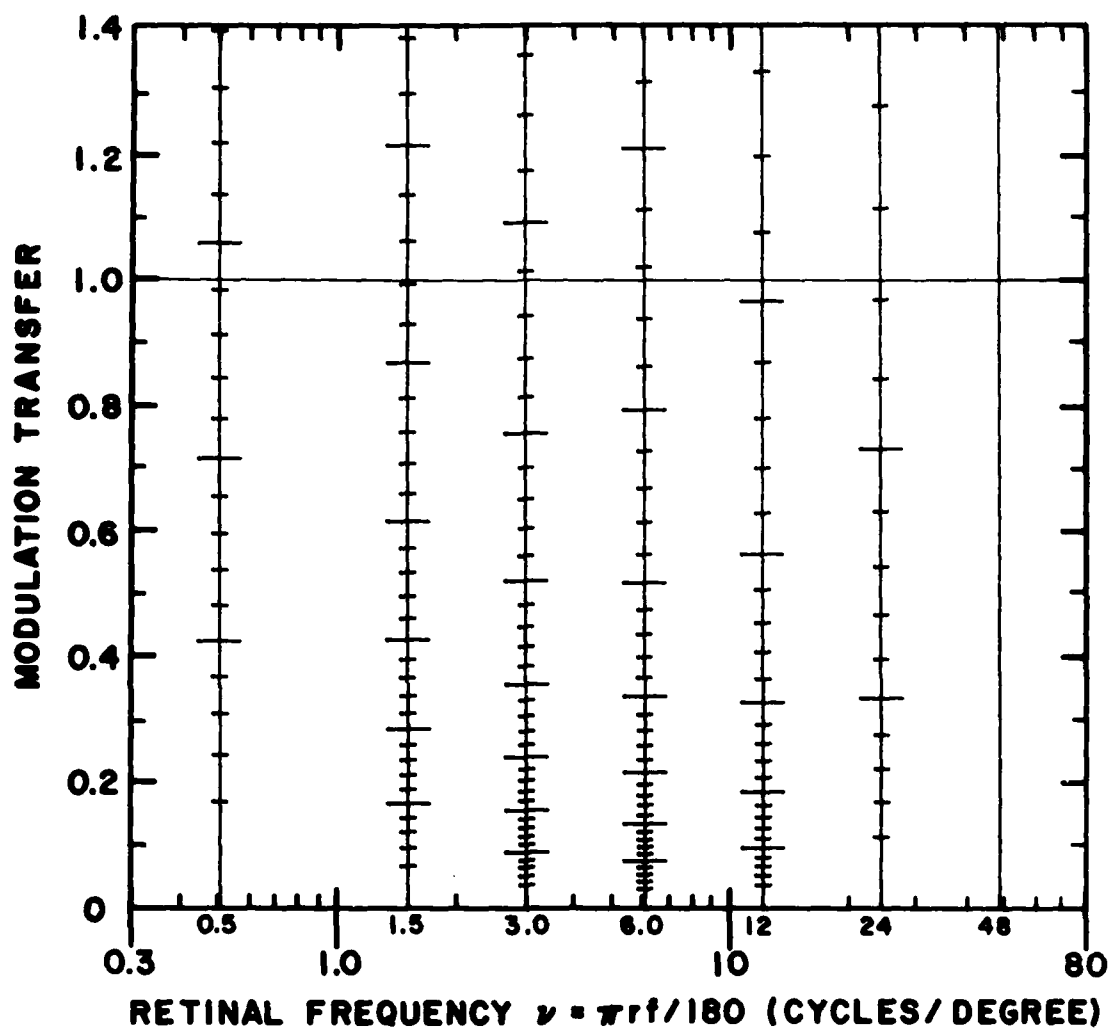
Figure 65. DDD No. 48. Discriminable Difference Diagram for noise on a uniform luminance analog display: r/w = 10, r = 50 cm, $\overline{I}$ = 35 mL, and $\sqrt{N(f)}/\overline{I}$ = 0.3.
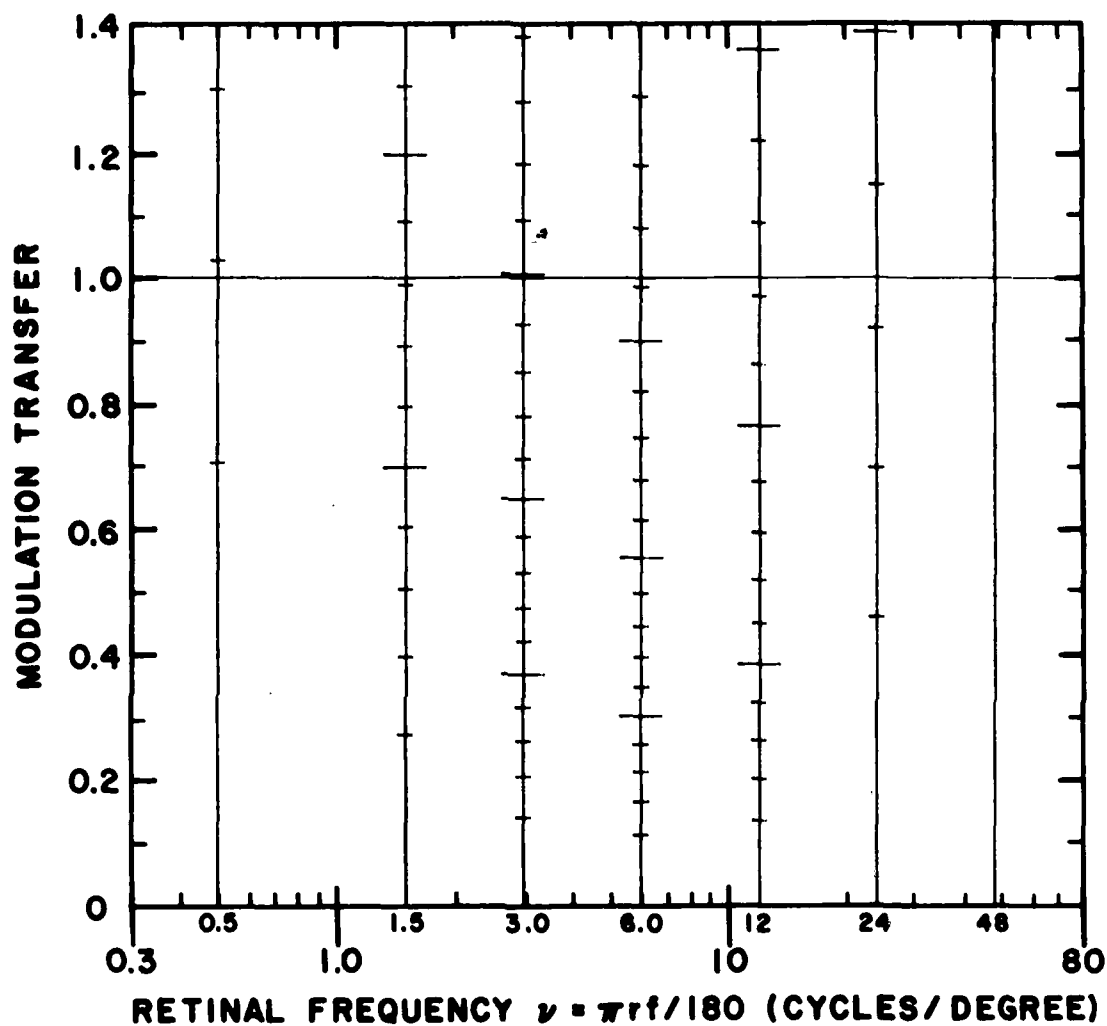
Figure 66.   DDD No. 49.   Discriminable Difference Diagram for noise on a uniform luminance analog display: $r/w = 10$, $r = 100$ cm, $\overline{I} = 35$ mL, and $\sqrt{N(f)}/\overline{I} = 0.1$.
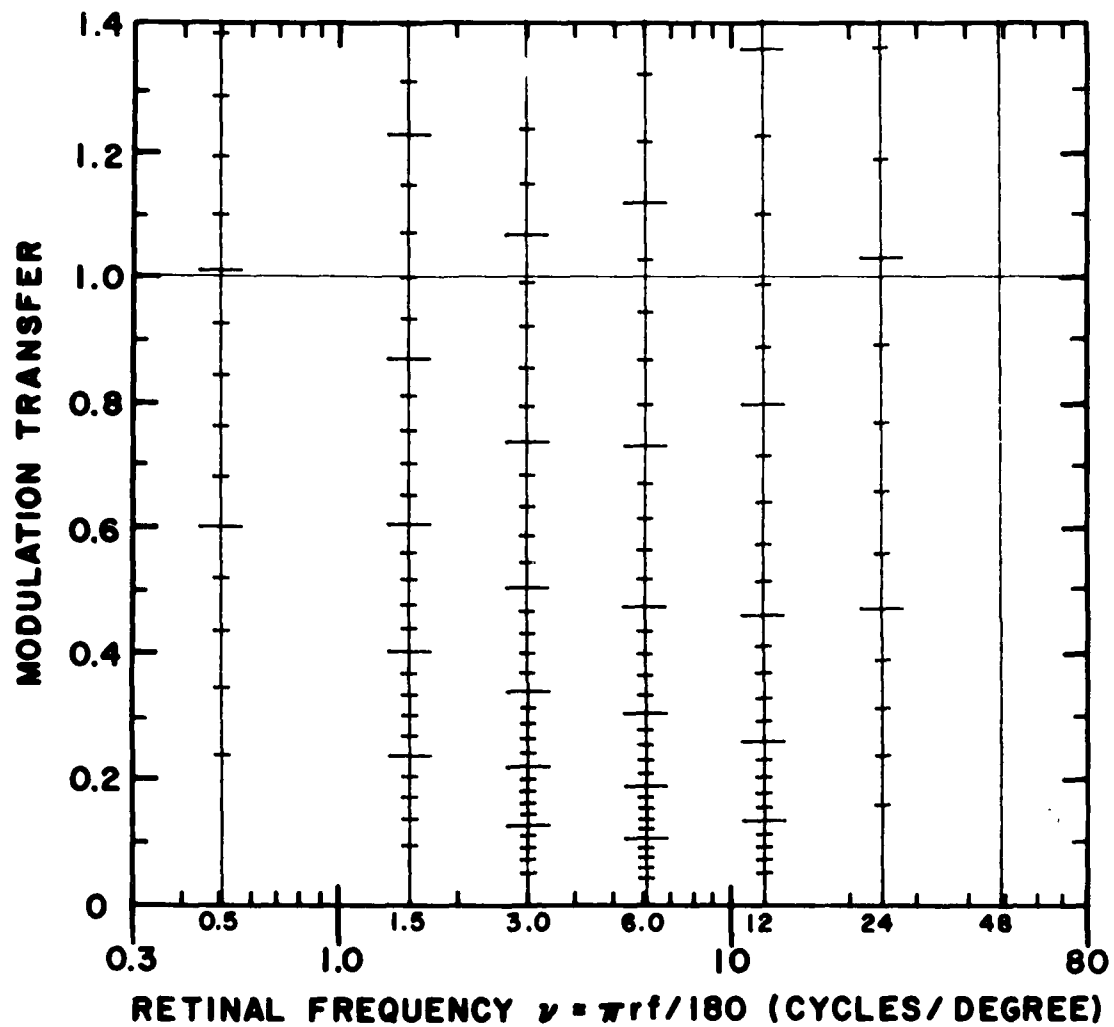
Figure 67. DDD No. 50. Discriminable Difference Diagram for noise on a uniform luminance analog display: r/w = 10, r = 100 cm, $\overline{I}$ = 35 mL, and $\sqrt{N(f)}/\overline{I}$ = 0.3.

104
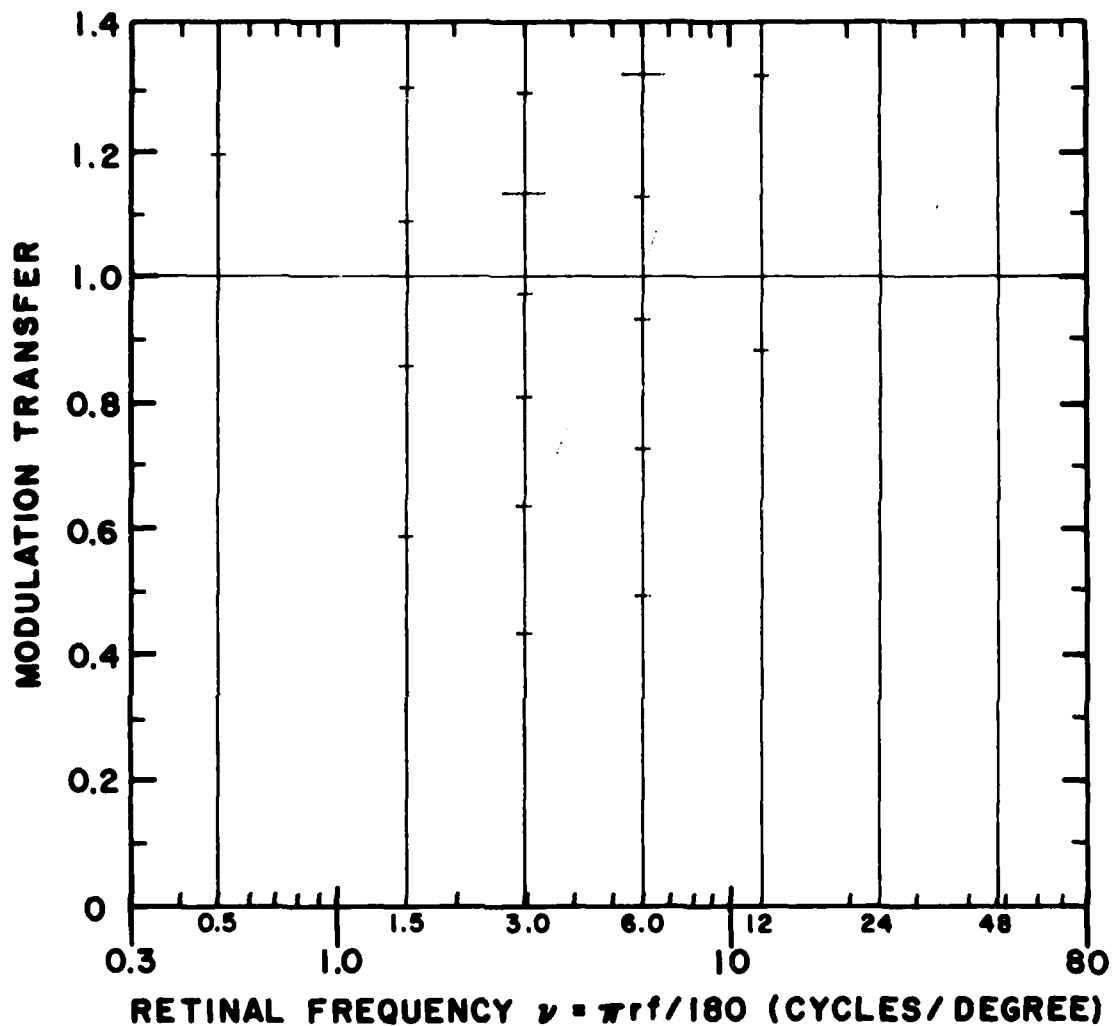
Figure 68. DDD No. 51. Discriminable Difference Diagram for noise on a uniform luminance analog display: $r/w = 10$, $r = 100$ cm, $\bar{I} = 1$ mL, and $\sqrt{N(f)}/\bar{I} = 0.1$.
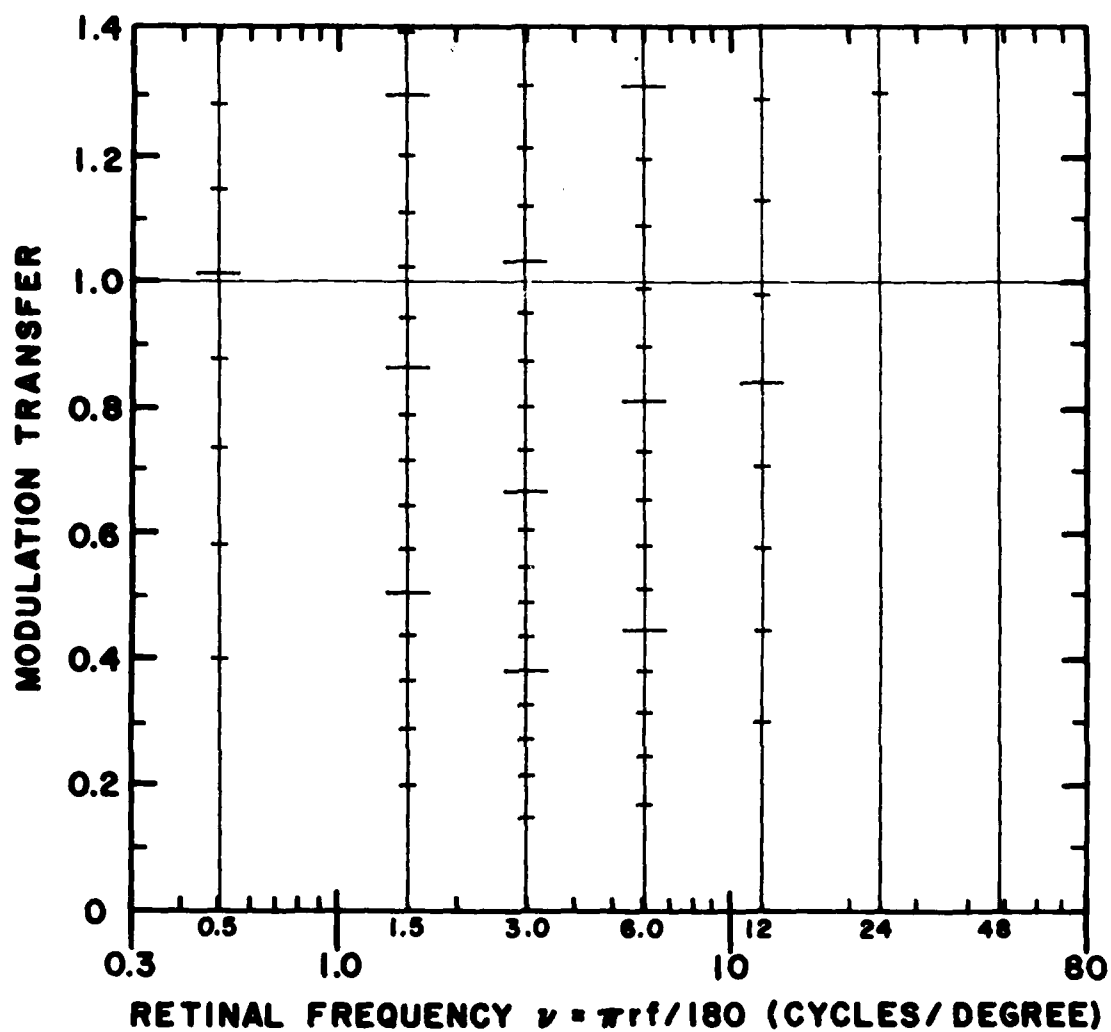
Figure 69. DDD No. 52. Discriminable Difference Diagram for noise on a uniform luminance analog display: $r/w = 10$, $r = 100$ cm, $\bar{I} = 1$ mL, and $\sqrt{N(f)}/\bar{I} = 0.3$.

106
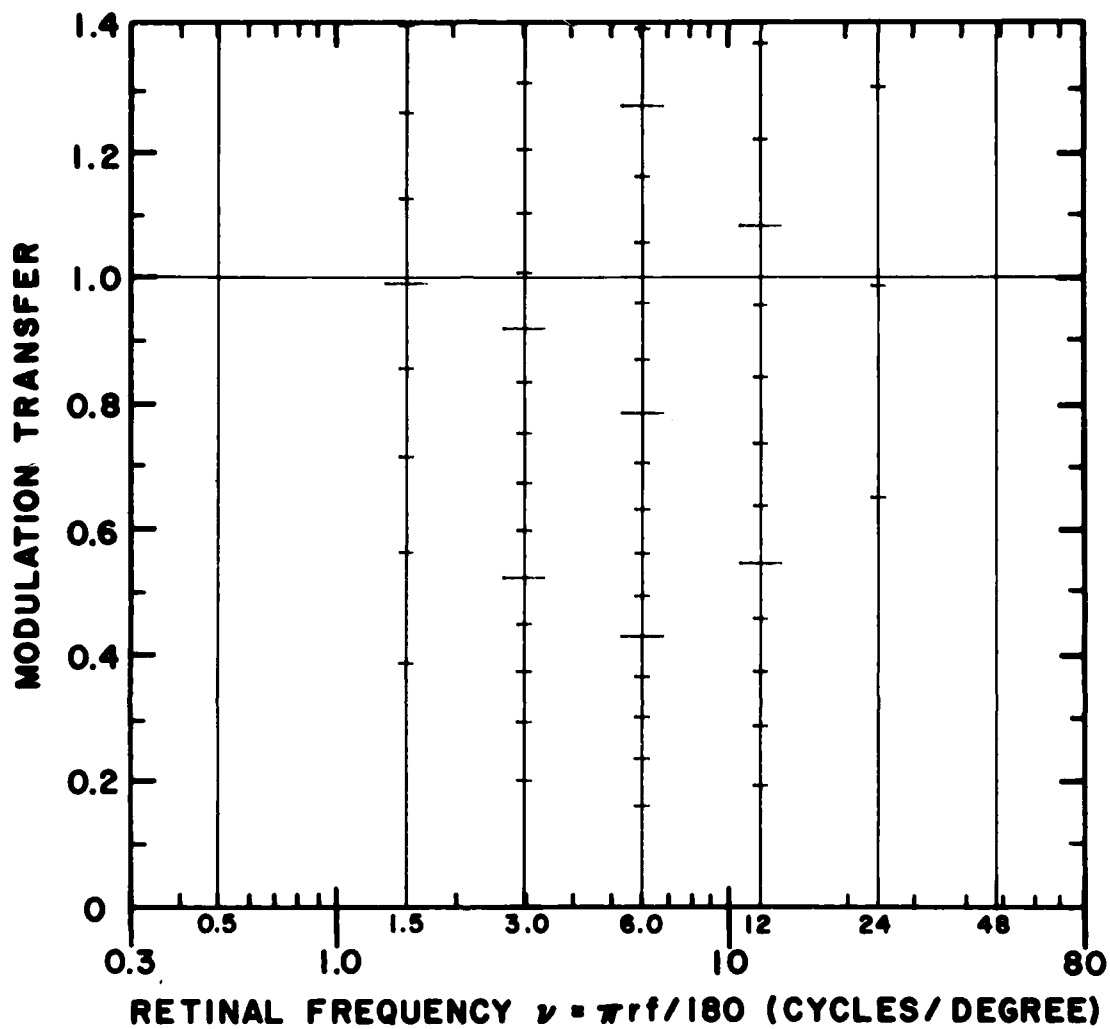
Figure 70. DDD No. 53. Discriminable Difference Diagram for noise on a
uniform luminance analog display: r/w = 10, r = 200 cm,
$\bar{I}$ = 35 mL, and $\sqrt{N(f)}/\bar{I}$ = 0.1.

107
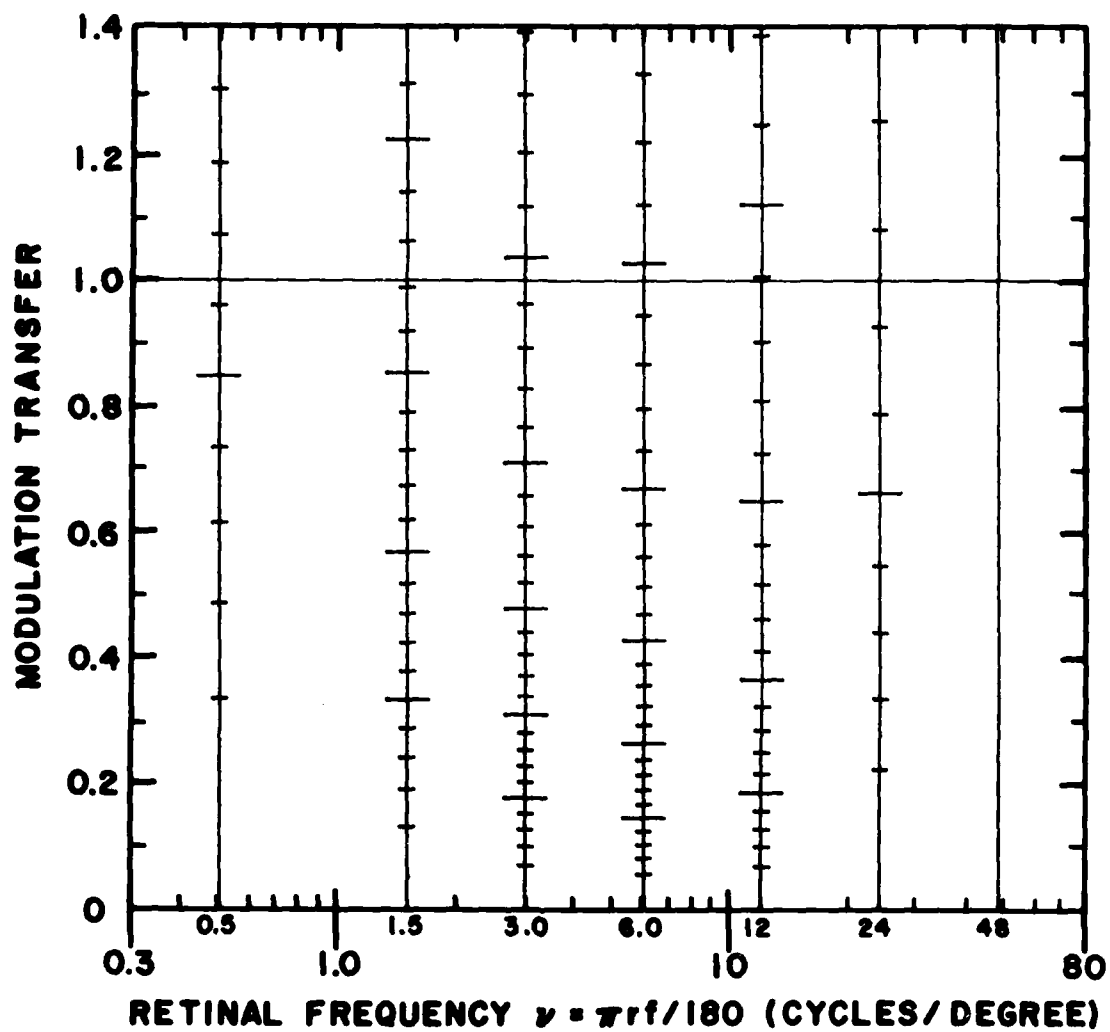
Figure 71. DDD No. 54, Discriminable Difference Diagram for noise on a uniform luminance analog display: $r/w = 10$, $r = 200$ cm, $\overline{I} = 35$ mL, and $\sqrt{N(f)}/\overline{I} = 0.3$.
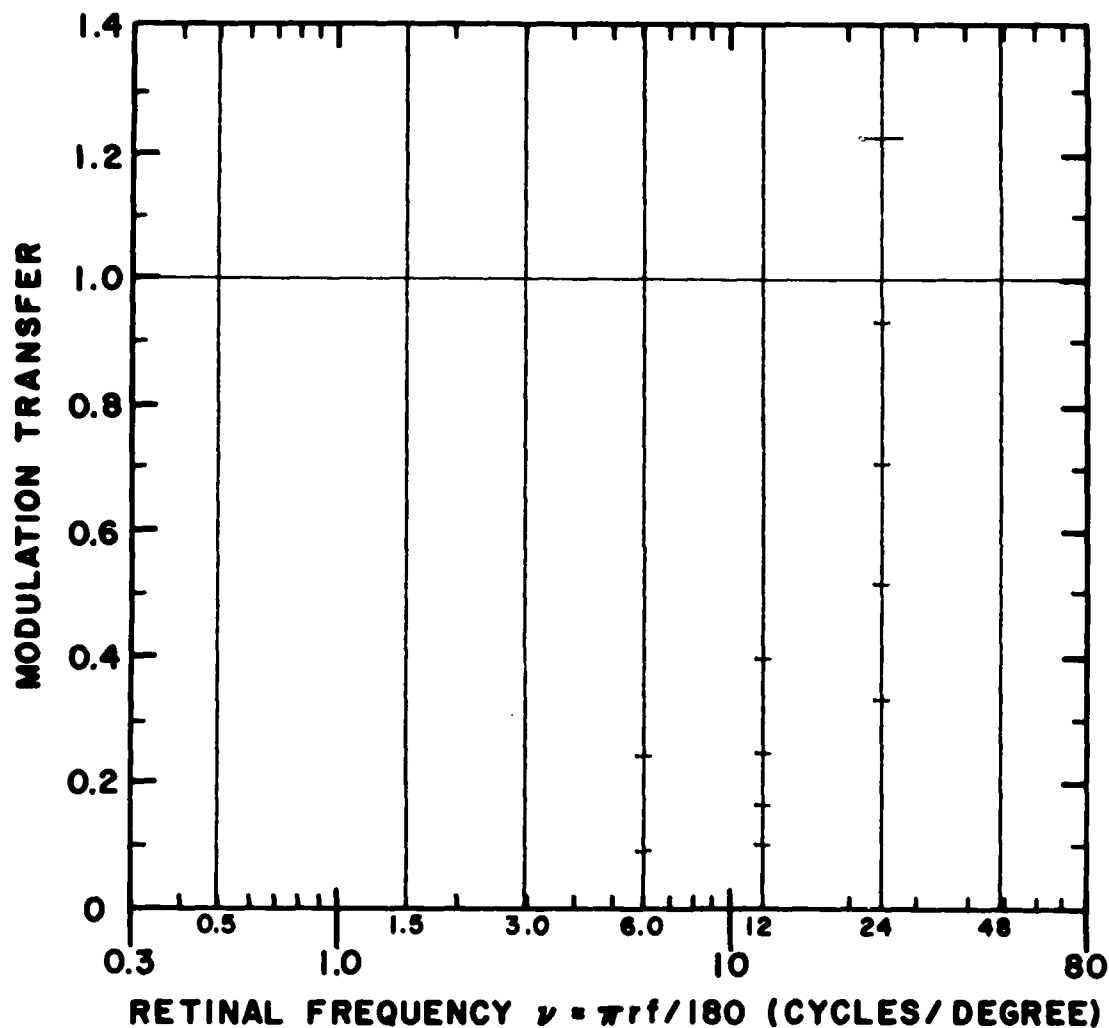
Figure 72. DDD No. 55. Discriminable Difference Diagram for noise in the presence of ensemble-averaged input pictorial information on an analog display: $r/w = 3$, $r = 50$ cm, $\bar{I} = 35$ mL, and $\sqrt{N(f)}/\bar{I} = 0.01$.
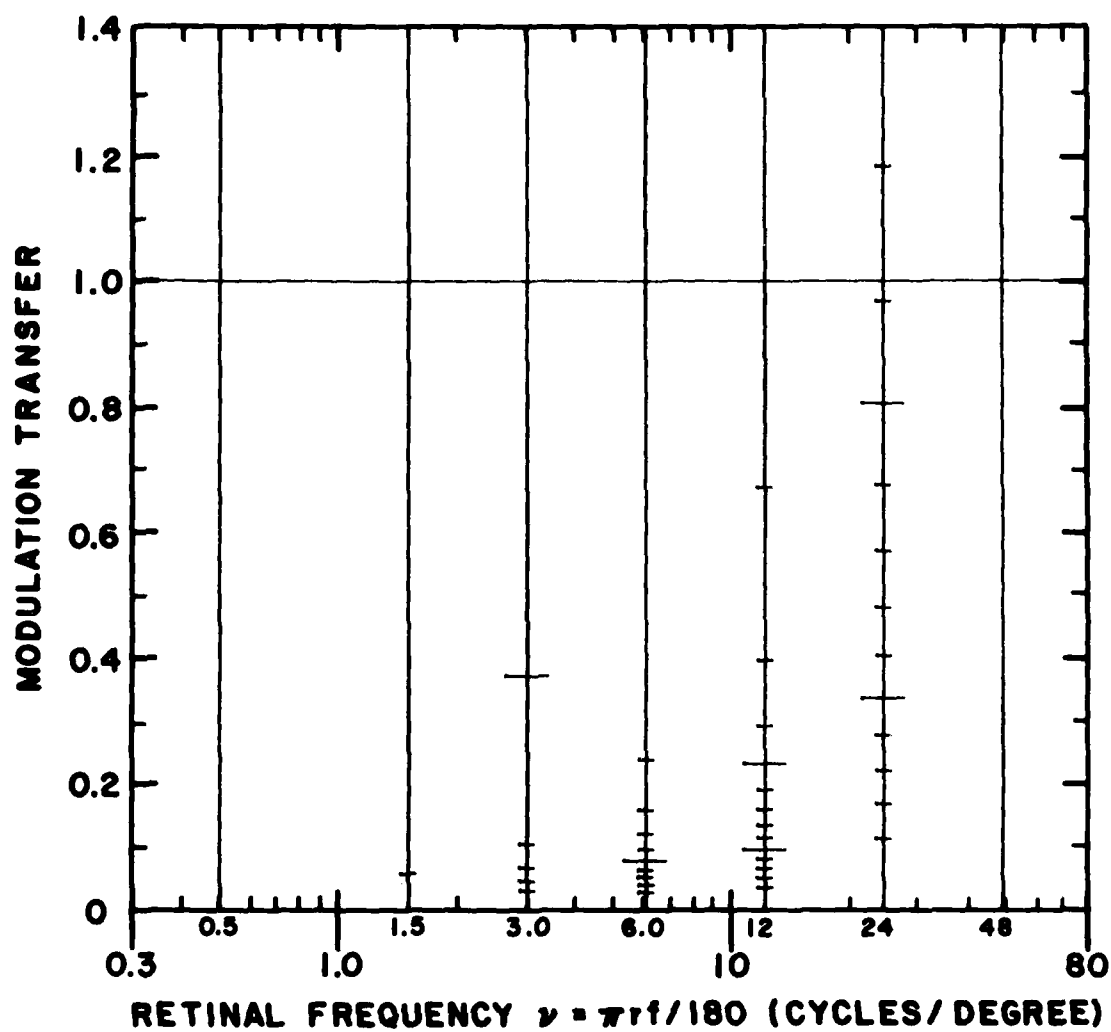
Figure 73. DDD No. 56. Discriminable Difference Diagram for noise in the presence of ensemble-averaged input pictorial informa-tion on an analog display: $r/w = 3$, $r = 50$ cm, $\bar{I} = 35$ mL, and $\sqrt{N(f)}/\bar{I} = 0.03$.

110
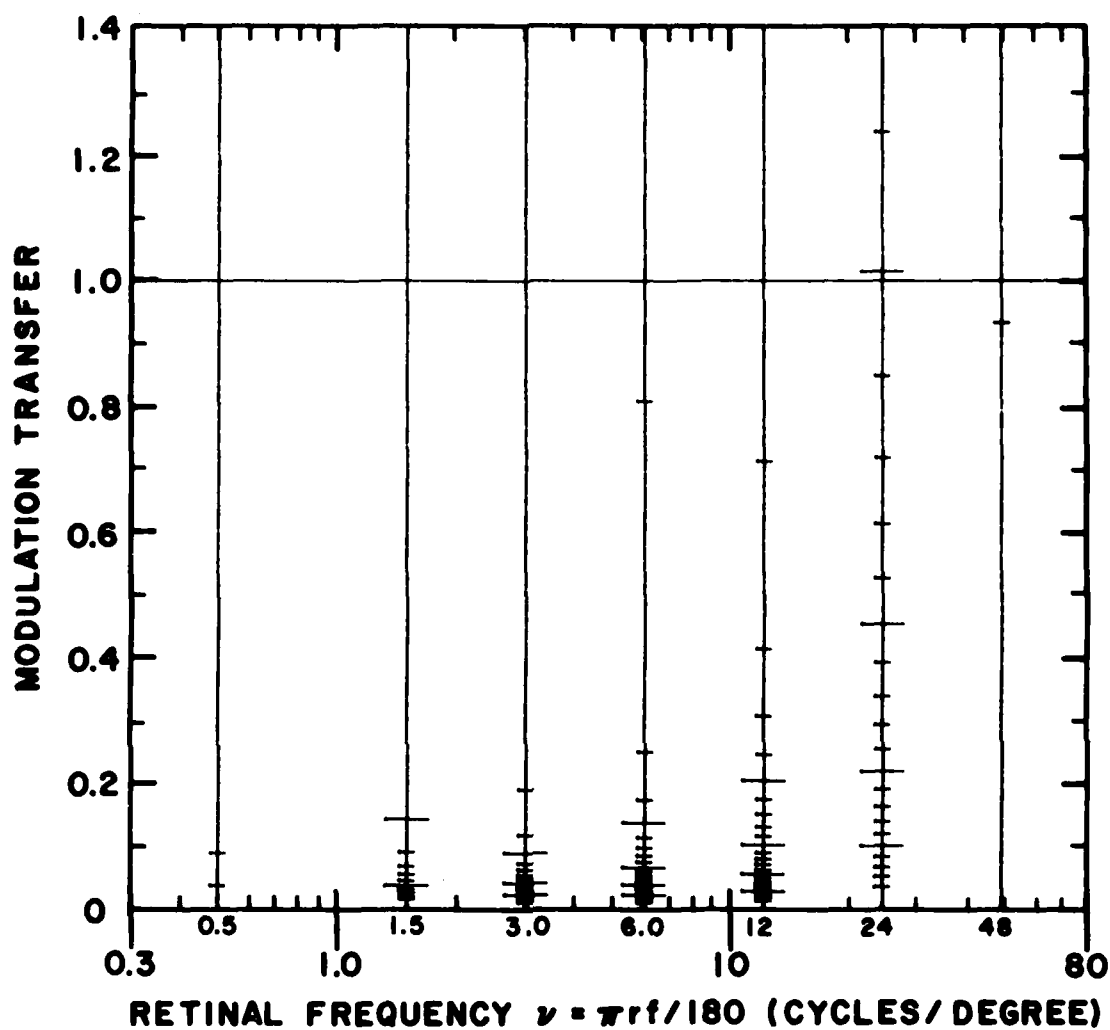
Figure 74. DDD No. 57. Discriminable Difference Diagram for noise in the presence of ensemble-averaged input pictorial information on an analog display: $r/w = 3$, $r = 50$ cm, $\bar{I} = 35$ mL, and $\sqrt{N(f)}/\bar{I} = 0.1$.
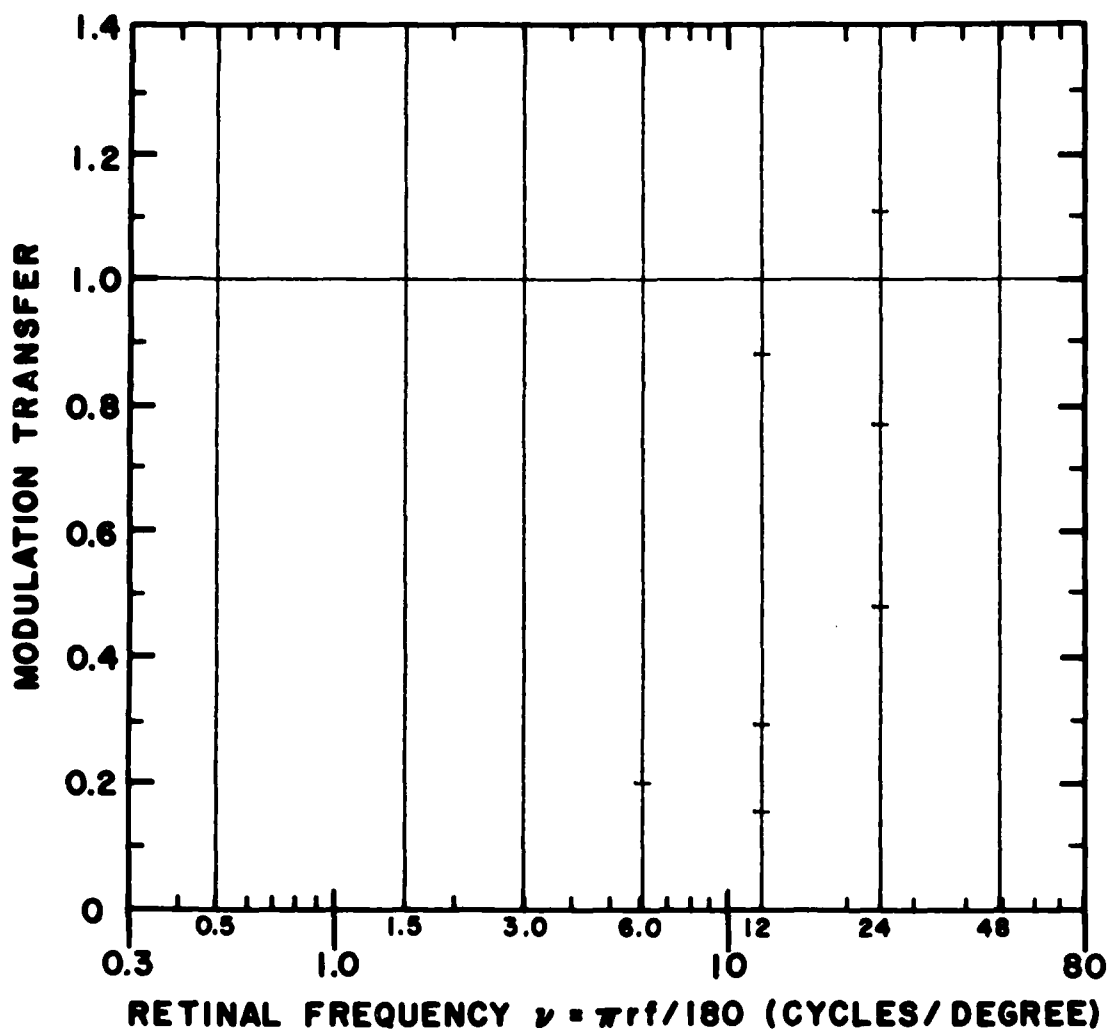
Figure 75. DDD No. 58. Discriminable Difference Diagram for noise in the presence of ensemble-averaged input pictorial information on an analog display: $r/w = 3$, $r = 100$ cm, $\bar{I} = 35$ mL, and $\sqrt{N(f)}/\bar{I} = 0.01$.

112
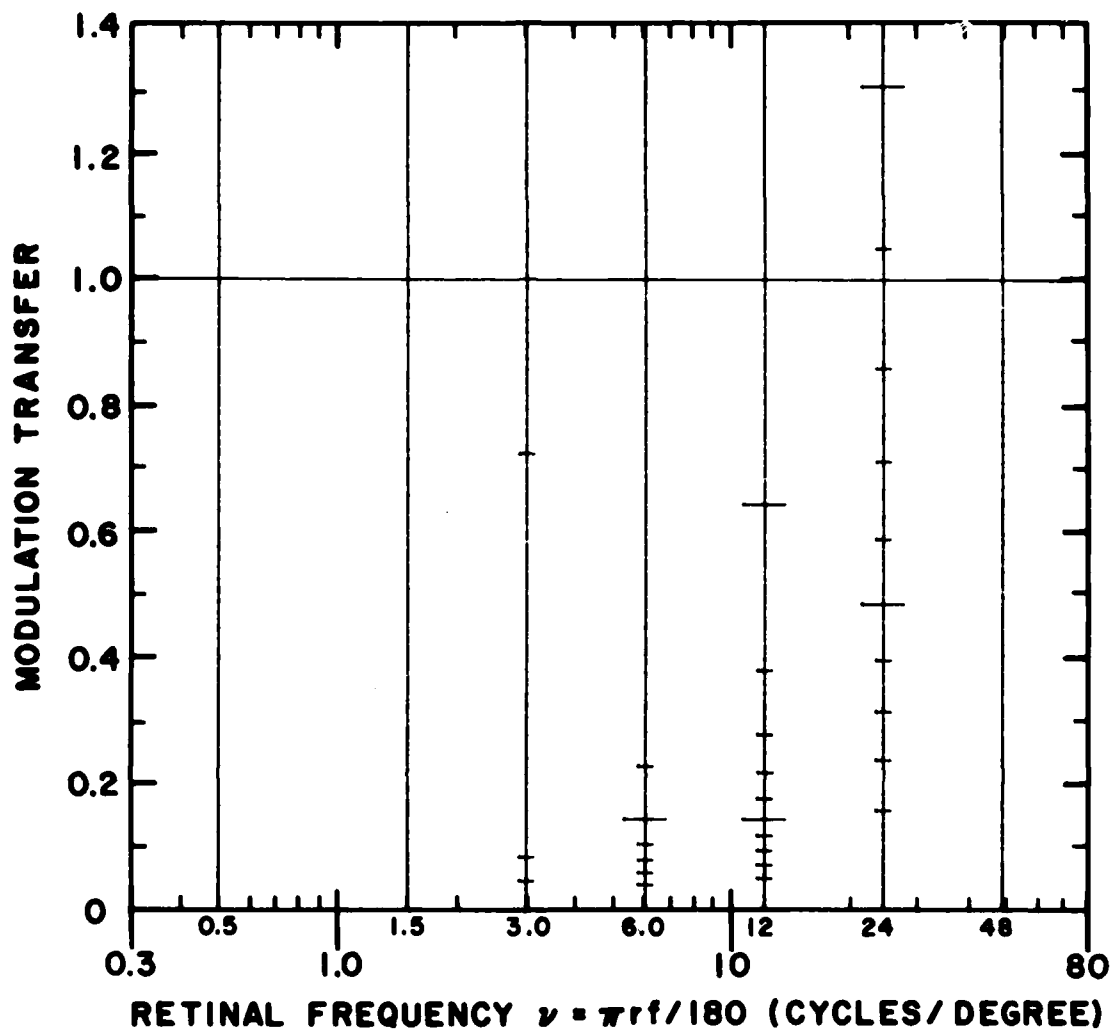
Figure 76. DDD No. 59. Discriminable Difference Diagram for noise in the presence of ensemble-averaged input pictorial information on an analog display: r/w = 3, r = 100 cm, $\bar{I}$ = 35 mL, and $\sqrt{N(f)}/\bar{I}$ = 0.03.
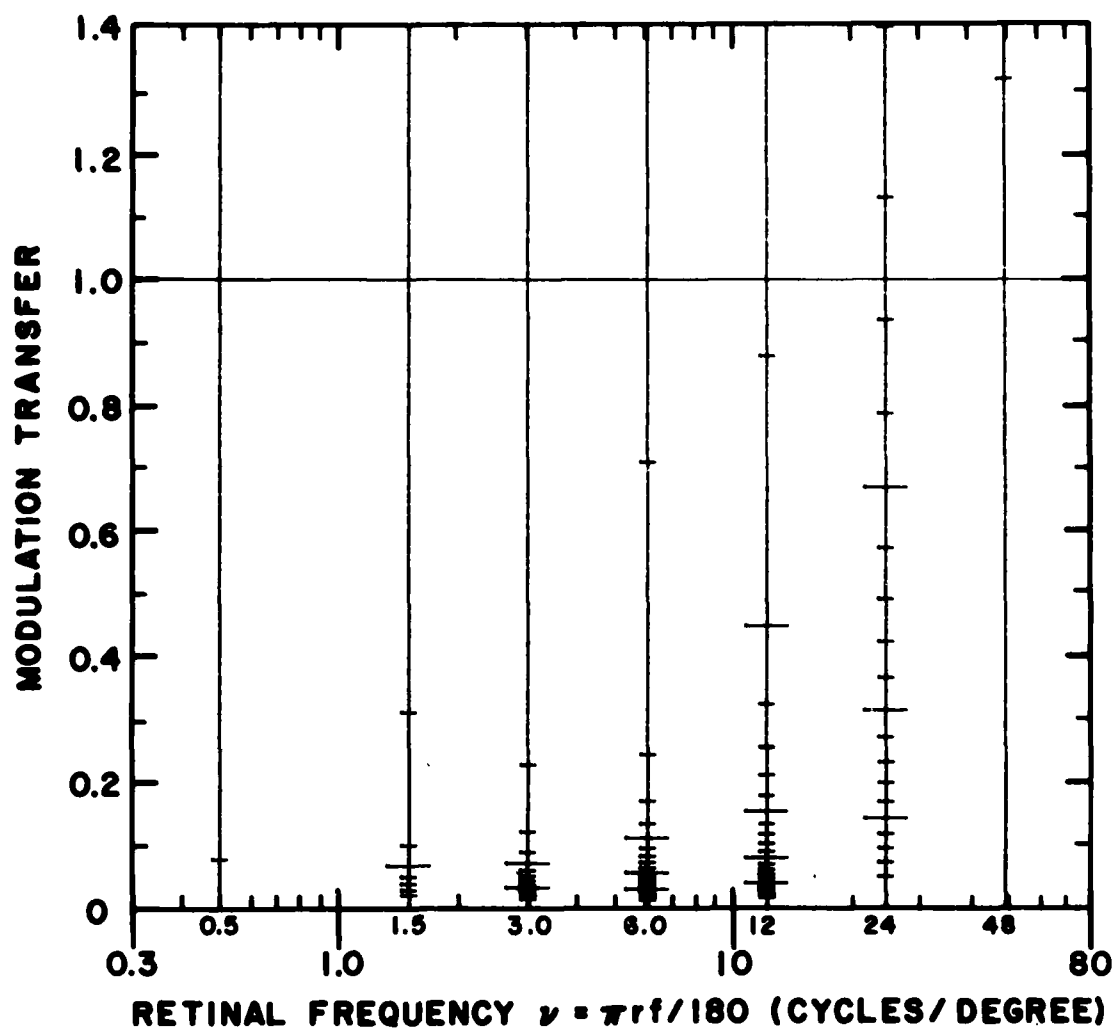
Figure 77. DDD No. 60. Discriminable Difference Diagram for noise in the presence of ensemble-averaged input pictorial information on an analog display: $r/w = 3$, $r = 100$ cm, $\bar{I} = 35$ mL, and $\sqrt{N(f)}/\bar{I} = 0.1$.

114
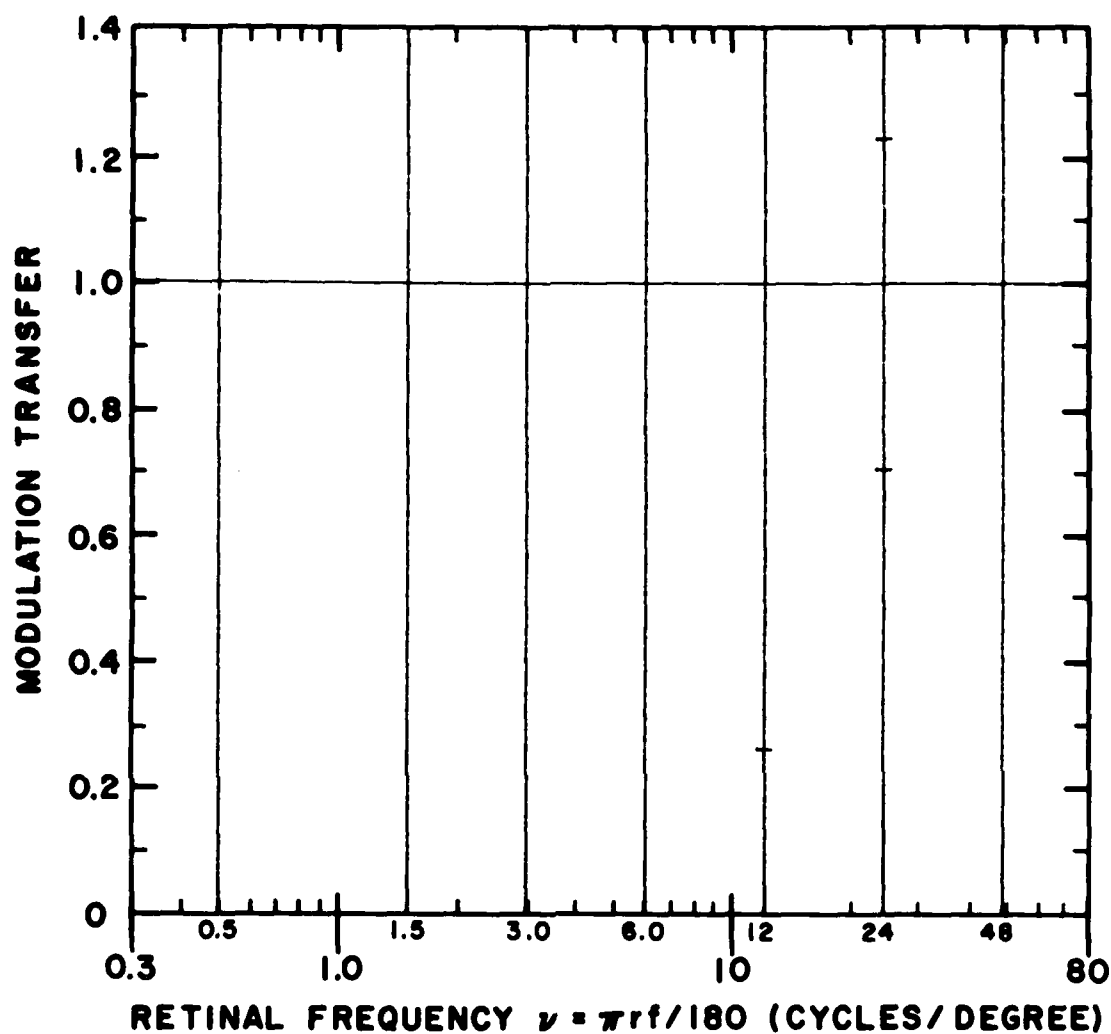
Figure 78.   DDD No. 61.   Discriminable Difference Diagram for noise in the presence of ensemble-averaged input pictorial information on an analog display: $r/w = 3$, $r = 200$ cm, $\bar{I} = 35$ mL, and $\sqrt{N(f)}/\bar{I} = 0.01$.
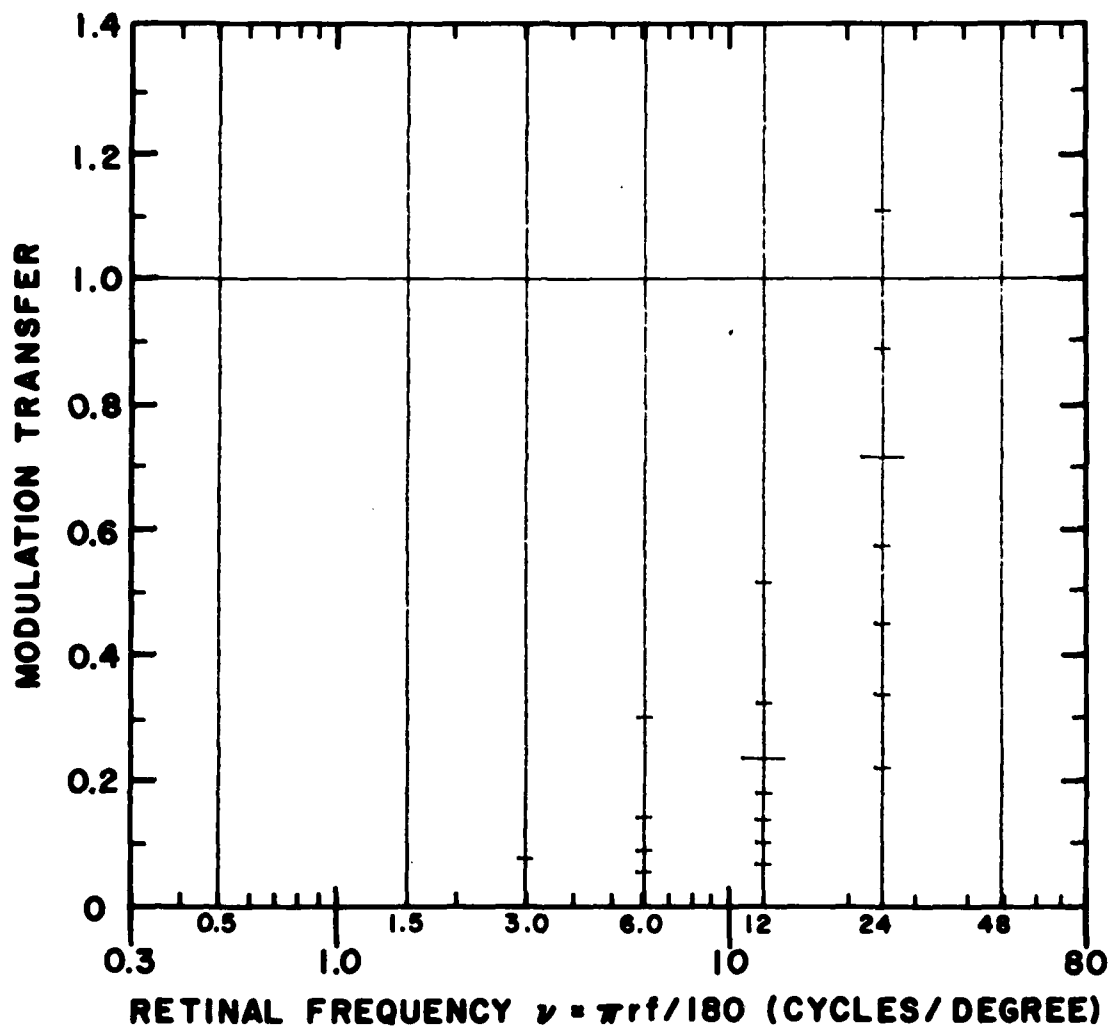
Figure 79. DDD No. 62. Discriminable Difference Diagram for noise in the presence of ensemble-averaged input pictorial information on an analog display: r/w = 3, r = 200 cm, $\bar{I}$ = 35 mL, and $\sqrt{N(f)}/\bar{I}$ = 0.03.
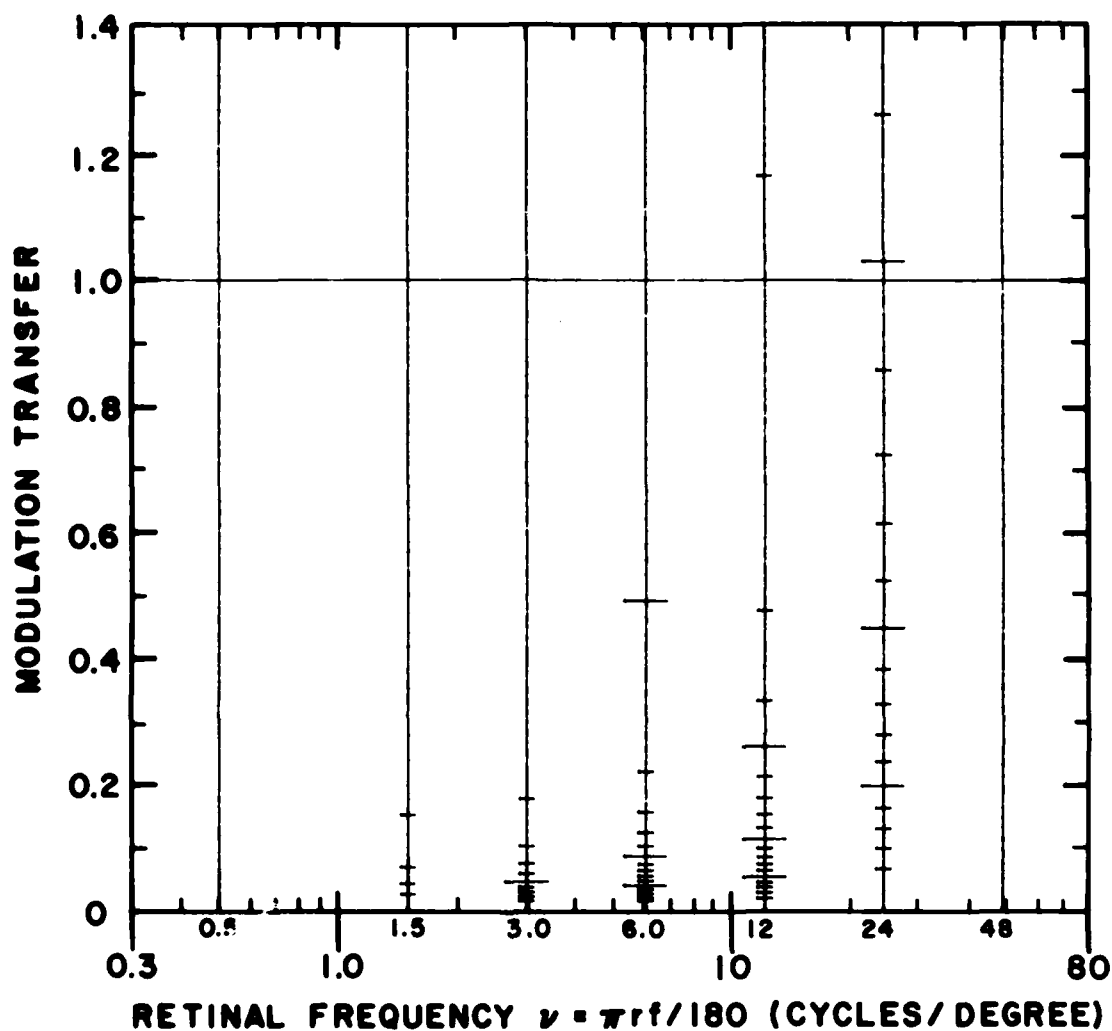
Figure 80. DDD No. 63. Discriminable Difference Diagram for noise in the presence of ensemble-averaged input pictorial information on an analog display: r/w = 3, r = 200 cm, $\bar{I}$ = 35 mL, and $\sqrt{N(f)}/\bar{I}$ = 0.1.

117
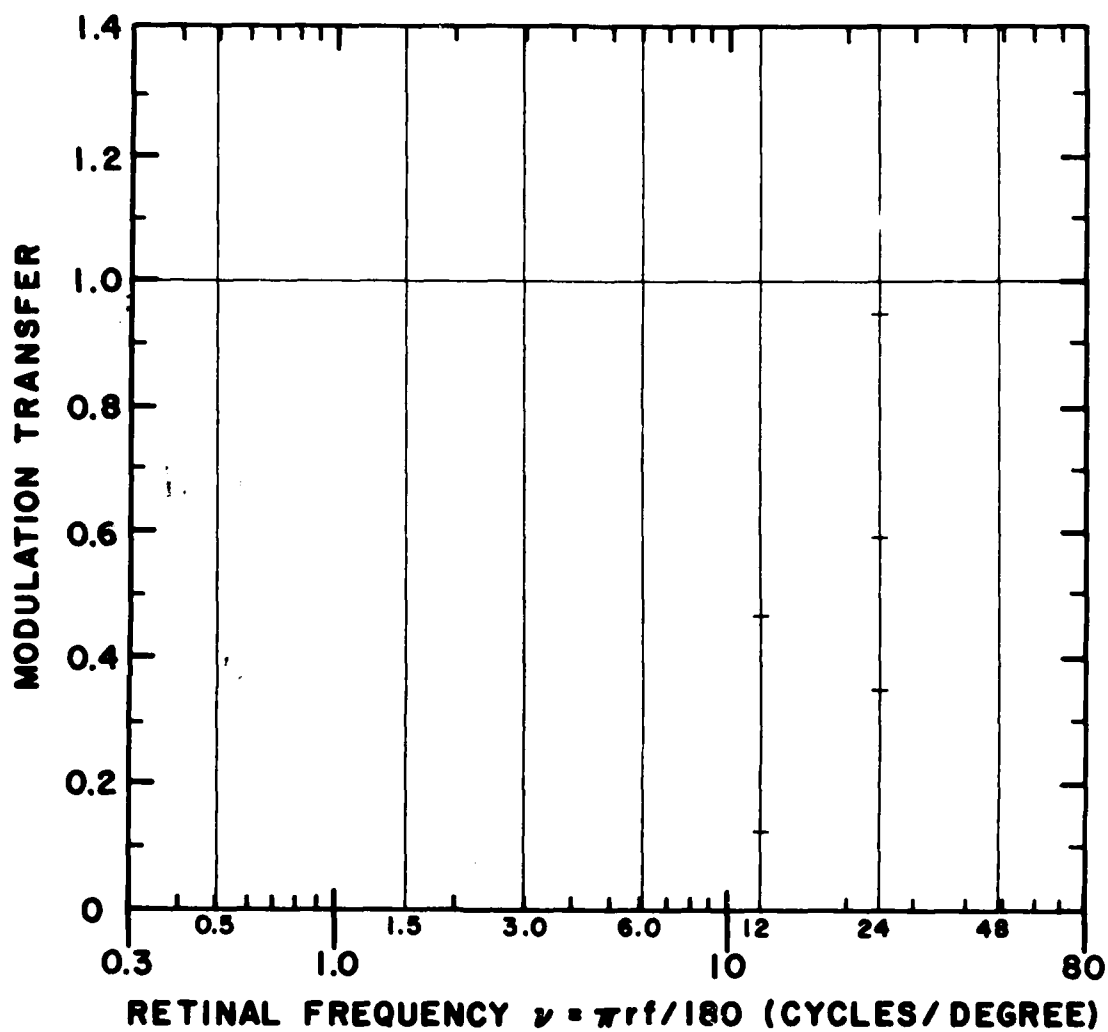
Figure 81. DDD No. 64. Discriminable Difference Diagram for noise in the presence of ensemble-averaged input pictorial information on an analog display: $r/w = 10$, $r = 50$ cm, $\bar{I} = 35$ mL, and $\sqrt{N(f)}/\bar{I} = 0.01$.
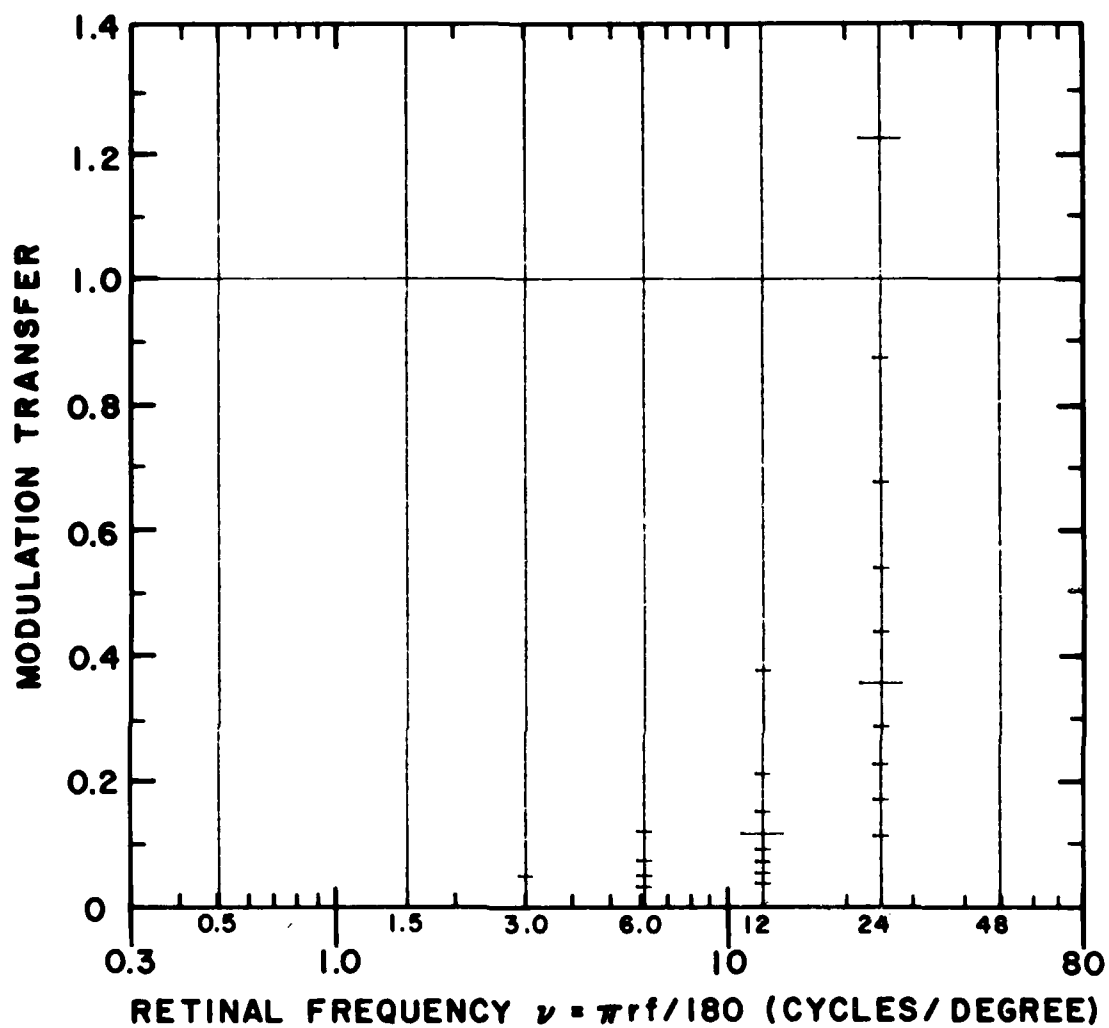
Figure 82. DDD No. 65. Discriminable Difference Diagram for noise in the presence of ensemble-averaged input pictorial information on an analog display: $r/w = 10$, $r = 50$ cm, $\bar{I} = 35$ mL, and $\sqrt{N(f)}/\bar{I} = 0.03$.

MODULATION TRANSFER

1.4
1.2
1.0
0.8
0.6
0.4
0.2
0

RETINAL FREQUENCY $\nu = \pi r f / 180$ (CYCLES/ DEGREE)

0.3   0.5   1.0   1.5   3.0   6.0   12   10   24   48   80
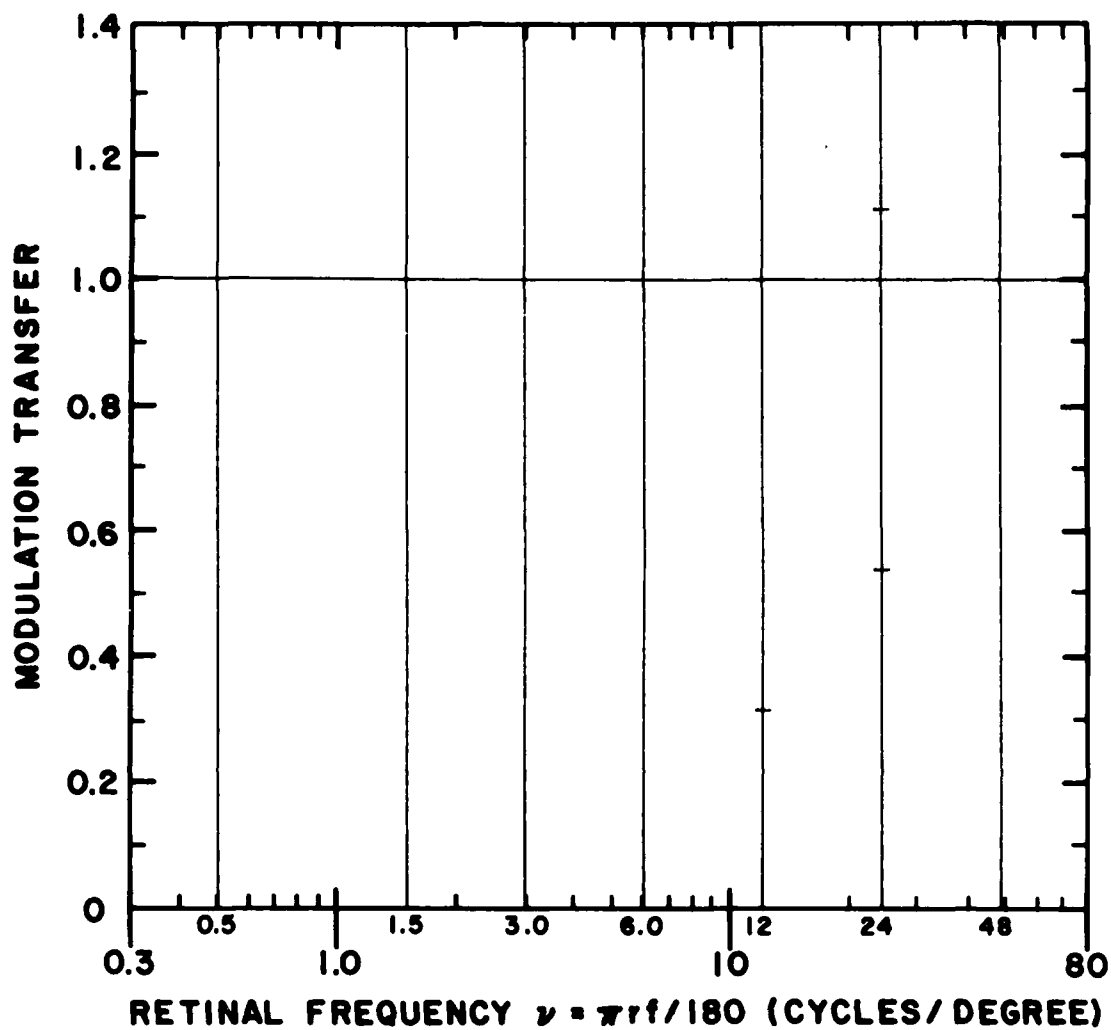
Figure 83.   DDD No. 66.   Discriminable Difference Diagram for noise in the presence of ensemble-averaged input pictorial information on an analog display: $r/w = 10$, $r = 100$ cm, $\bar{I} = 35$ mL, and $\sqrt{N(f)}/\bar{I} = 0.01$.

120
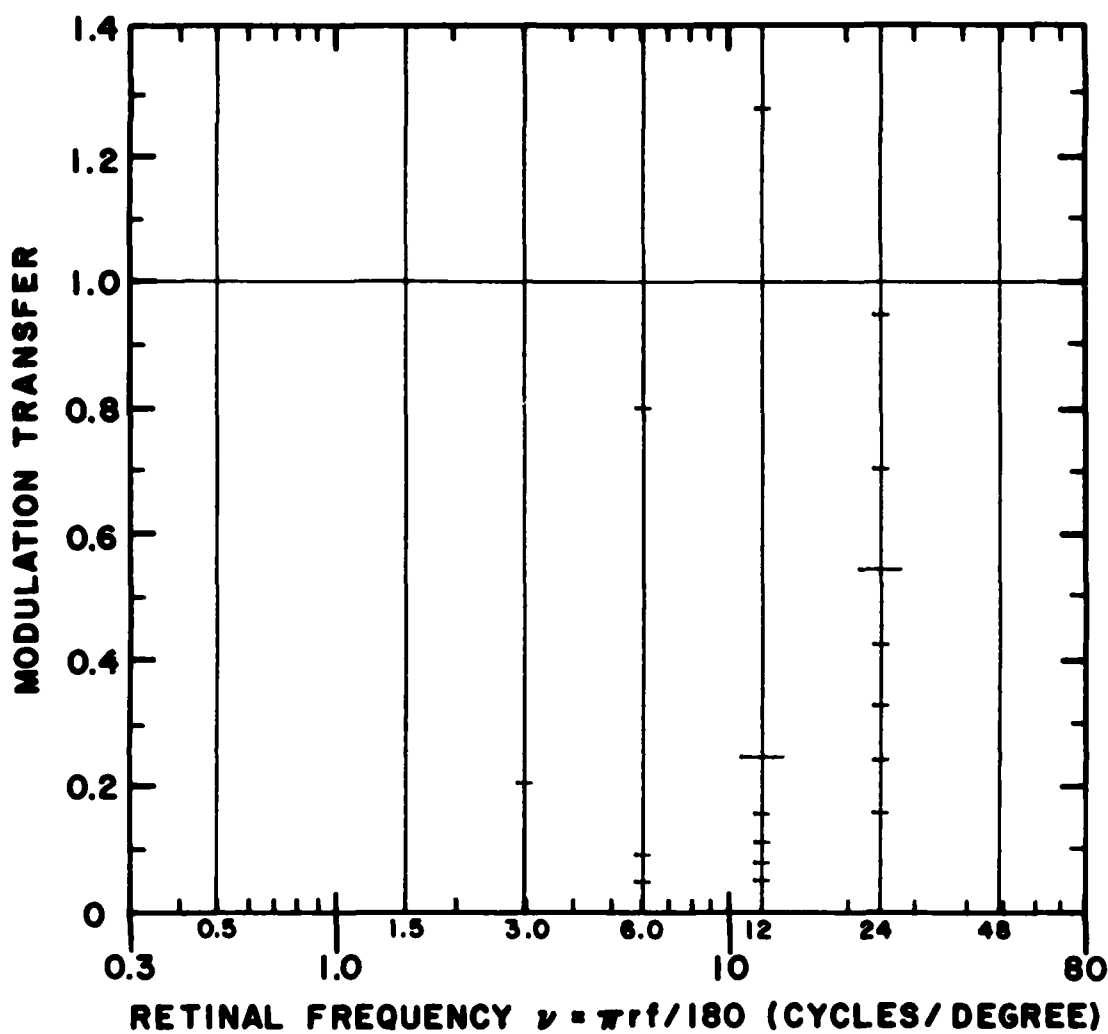
Figure 84. DDD No. 67. Discriminable Difference Diagram for noise in the presence of ensemble-averaged input pictorial information on an analog display: $r/w = 10$, $r = 100$ cm, $\bar{I} = 35$ mL, and $\sqrt{N(f)}/\bar{I} = 0.03$.

121
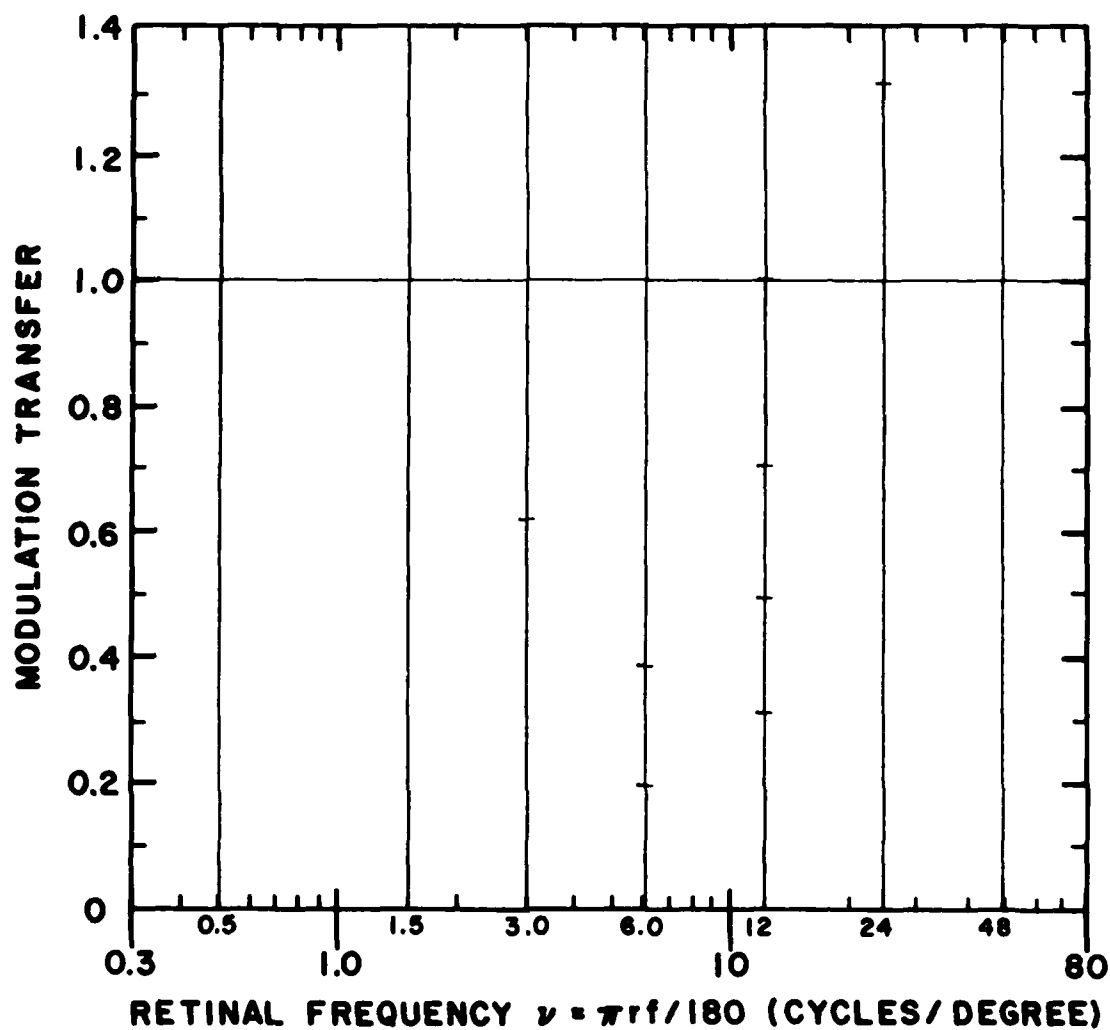
Figure 85. DDD No. 68. Discriminable Difference Diagram for noise in the presence of ensemble-averaged input pictorial information on an analog display: r/w = 10, r = 100 cm, $\bar{I}$ = 1 mL, and $\sqrt{N(f)}/\bar{I}$ = 0.03.

122
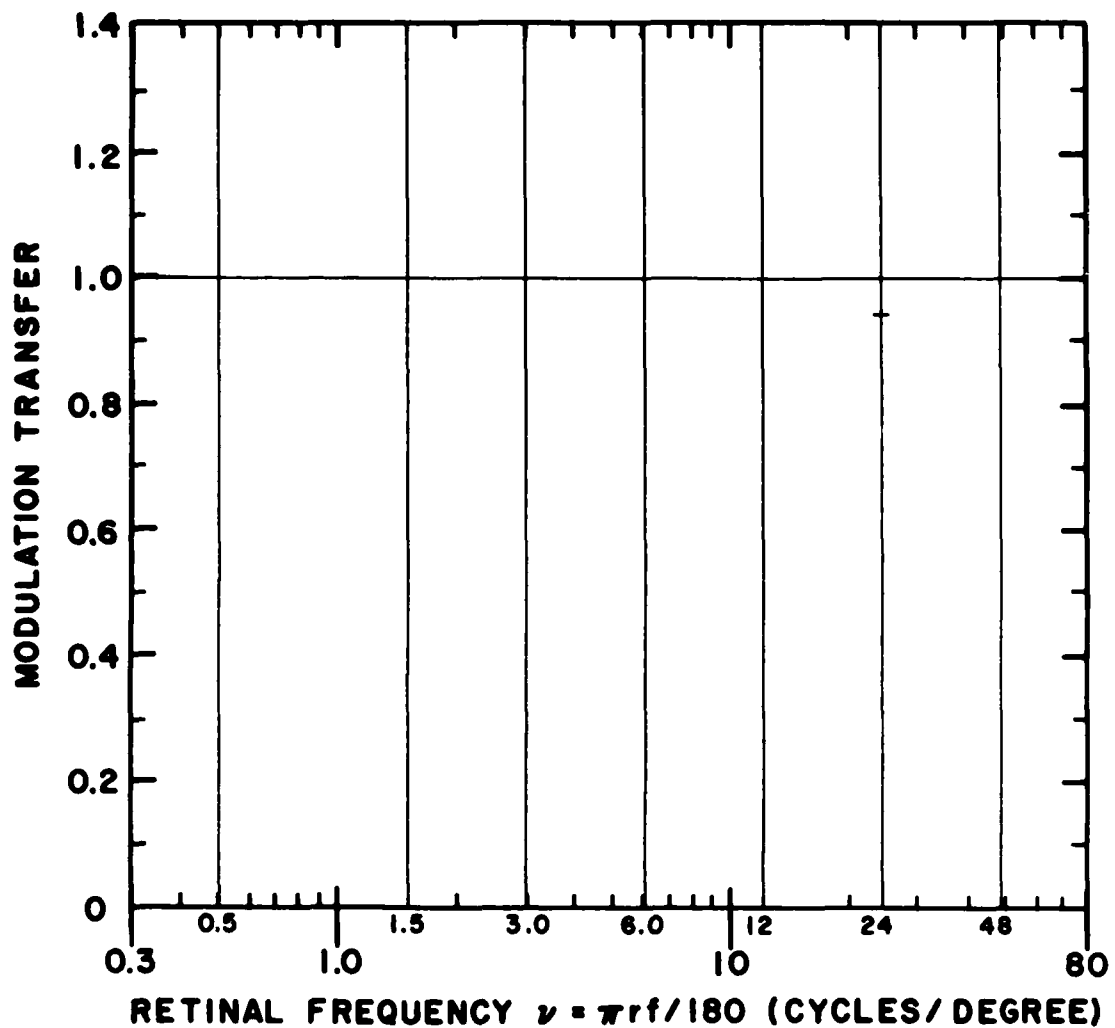
Figure 86. DDD No. 69. Discriminable Difference Diagram for noise in the presence of ensemble-averaged input pictorial information on an analog display: $r/w = 10$, $r = 200$ cm, $\bar{I} = 35$ mL, and $\sqrt{N(f)}/\bar{I} = 0.01$.

123
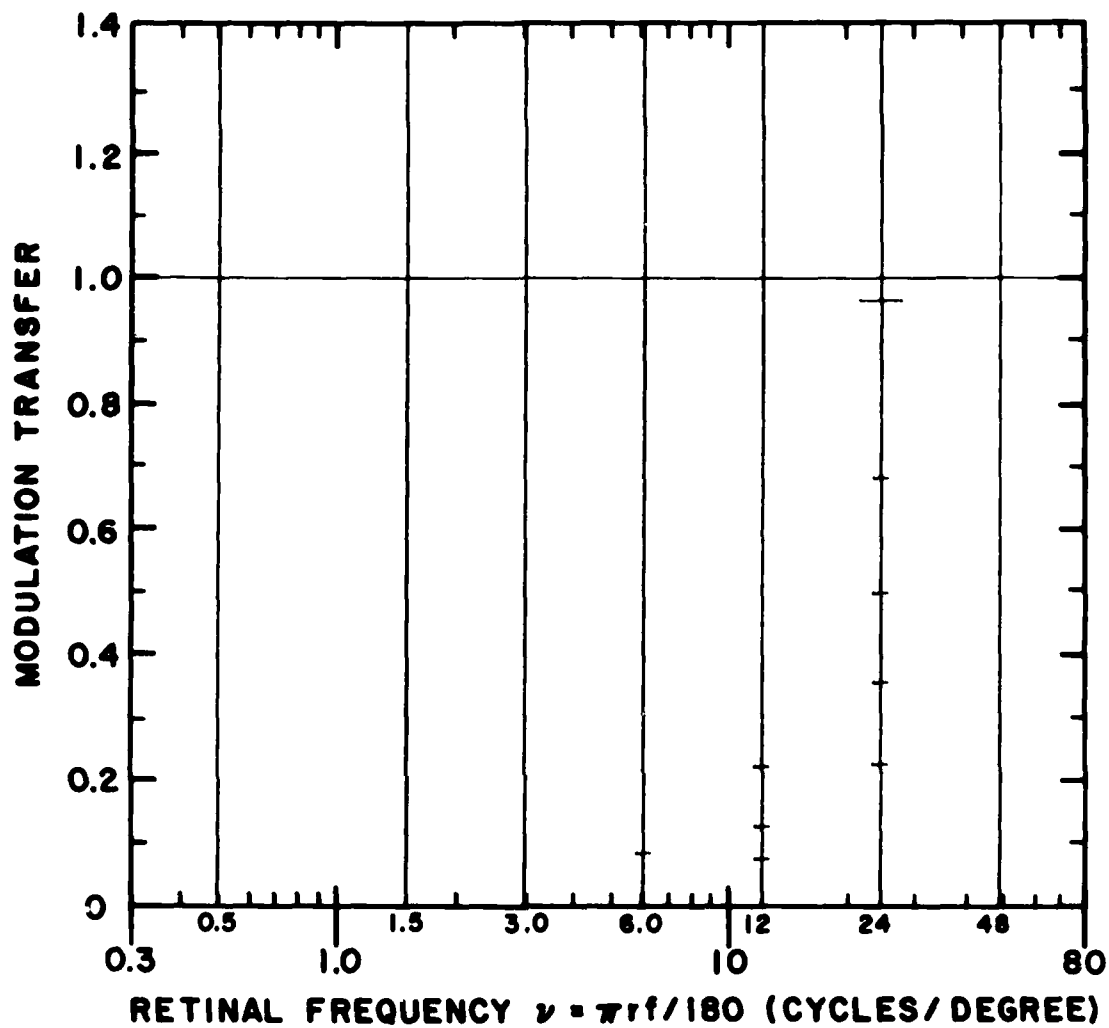
Figure 87. DDD No. 70. Discriminable Difference Diagram for noise in the presence of ensemble-averaged input pictorial information on an analog display: $r/w = 10$, $r = 200$ cm, $\bar{I} = 35$ mL, and $\sqrt{N(f)}/\bar{I} = 0.03$.
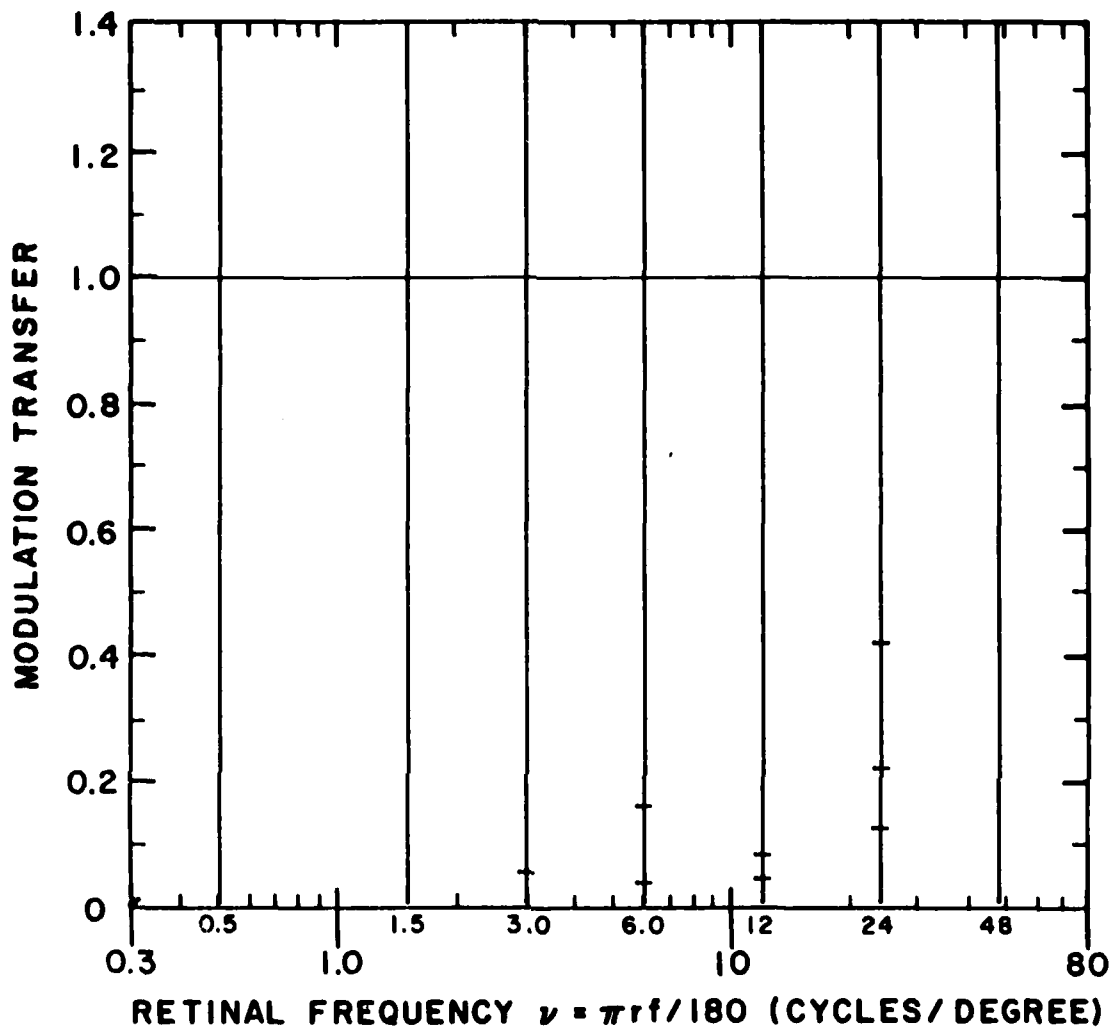
Figure 88. DDD No. 71. Discriminable Difference Diagram for noise in the presence of a 100% contrast luminance edge transition on an analog display: $r/w = 3$, $r = 50$ cm, $\bar{I} = 35$ mL, and $\sqrt{N(f)}/\bar{I} = 0.03$.

125
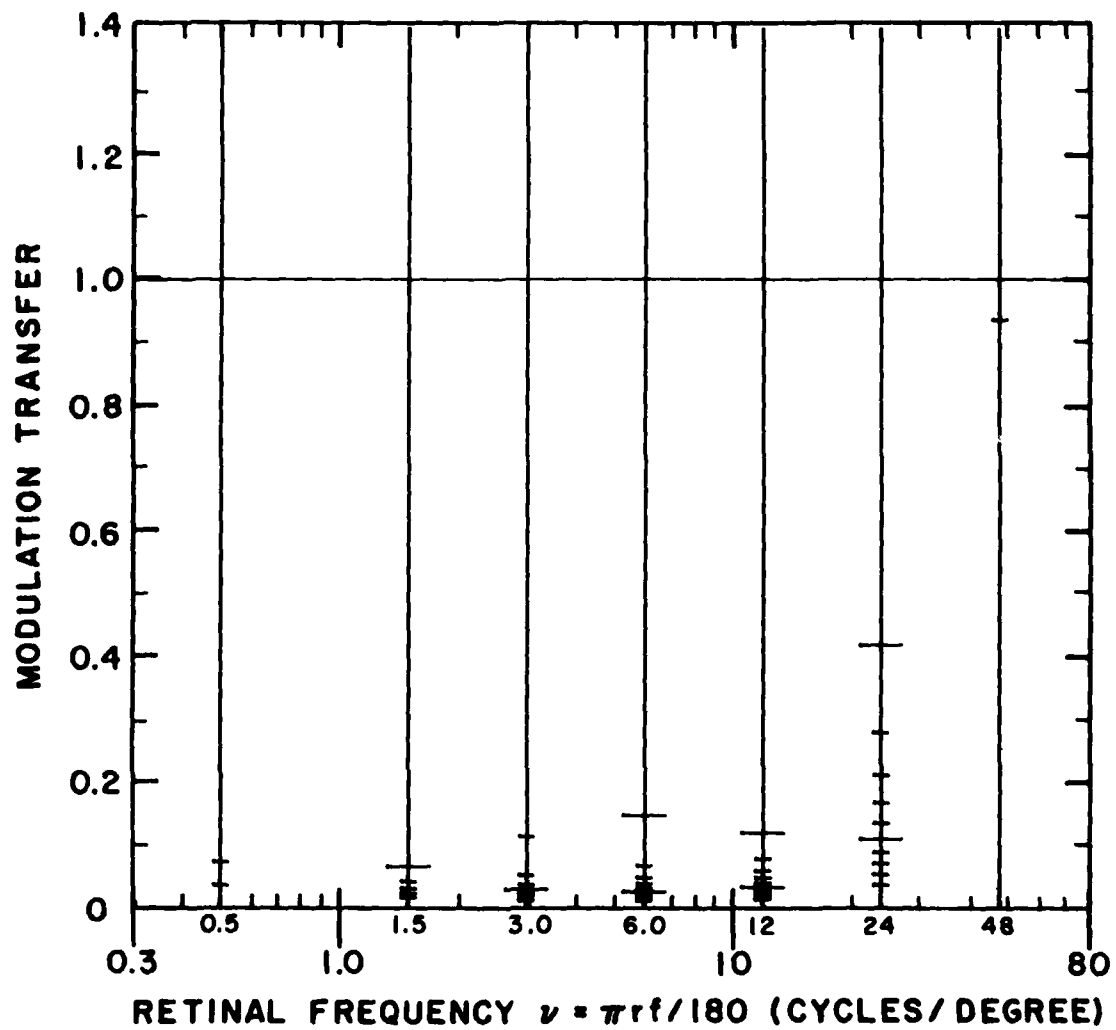
Figure 89. DDD No. 72. Discriminable Difference Diagram for noise in the presence of a 100% contrast luminance edge transition on an analog display: $r/w = 3$, $r = 50$ cm, $\bar{I} = 35$ mL, and $\sqrt{N(f)}/\bar{I} = 0.1$.
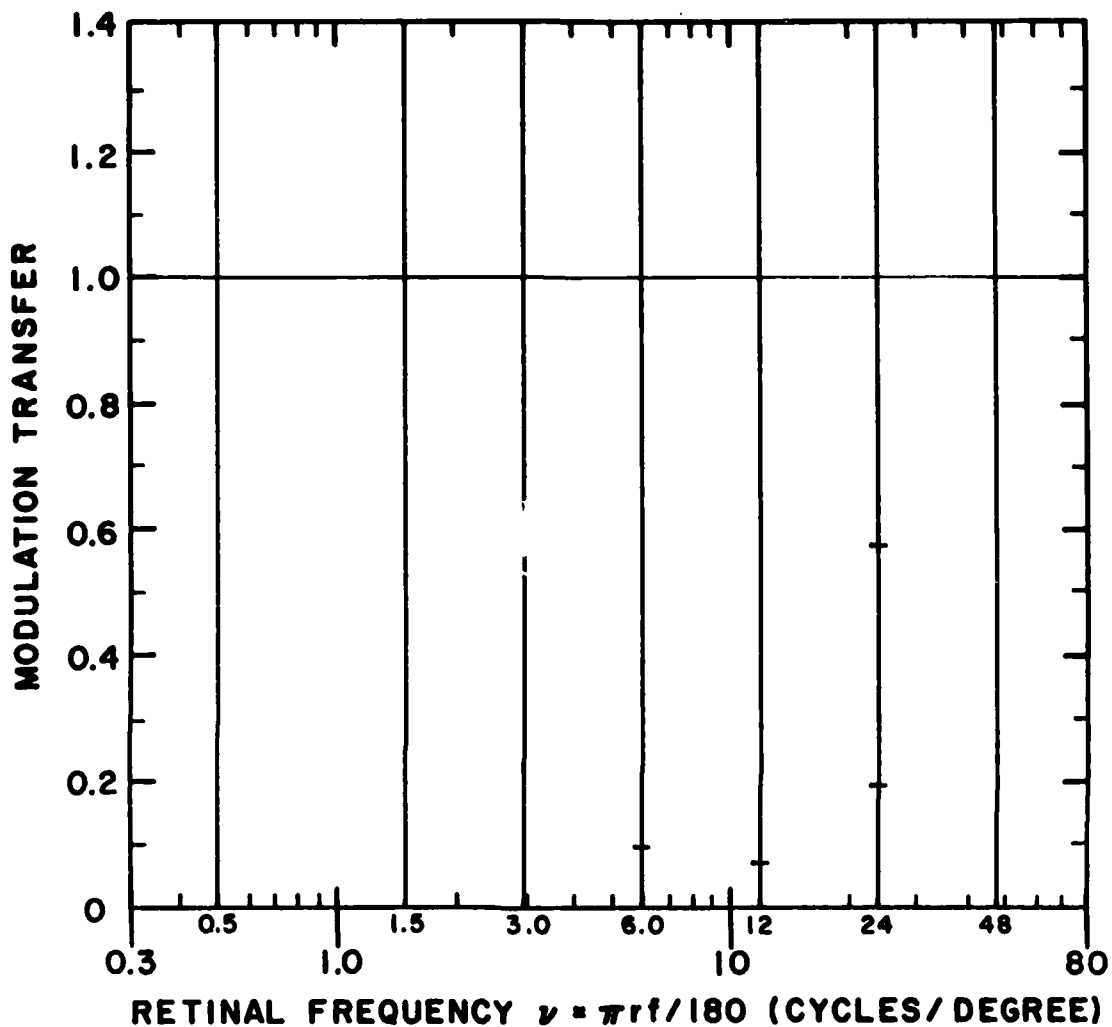
Figure 90. DDD No. 73. Discriminable Difference Diagram for noise in the presence of a 100% contrast luminance edge transition on an analog display: $r/w = 3$, $r = 100$ cm, $\bar{I} = 35$ mL, and $\sqrt{N(f)}/\bar{I} = 0.03$.

127
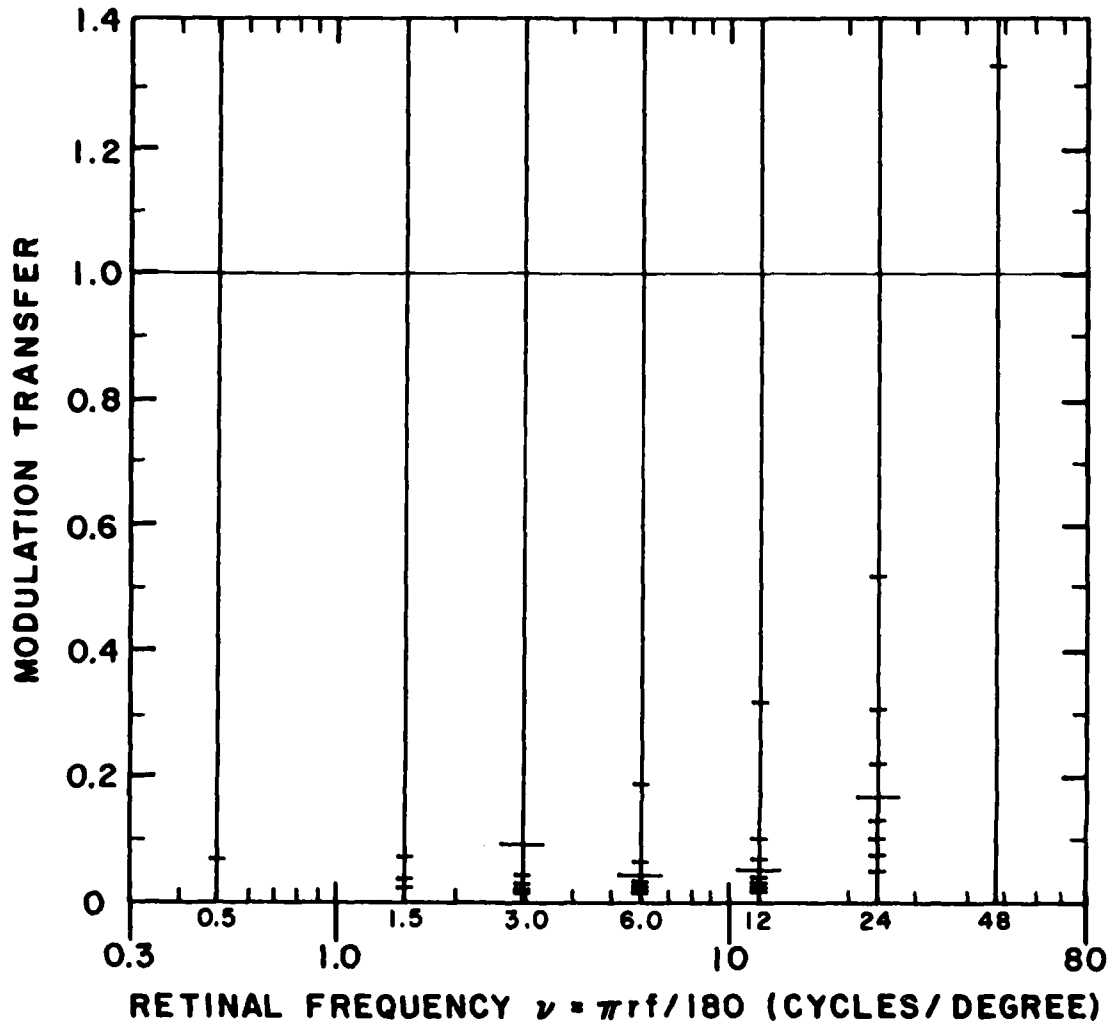
Figure 91. DDD No. 74. Discriminable Difference Diagram for noise in the presence of a 100% contrast luminance edge transition on an analog display: r/w = 3, r = 100 cm, $\bar{I}$ = 35 mL, and $\sqrt{N(f)}/\bar{I}$ = 0.1.

128
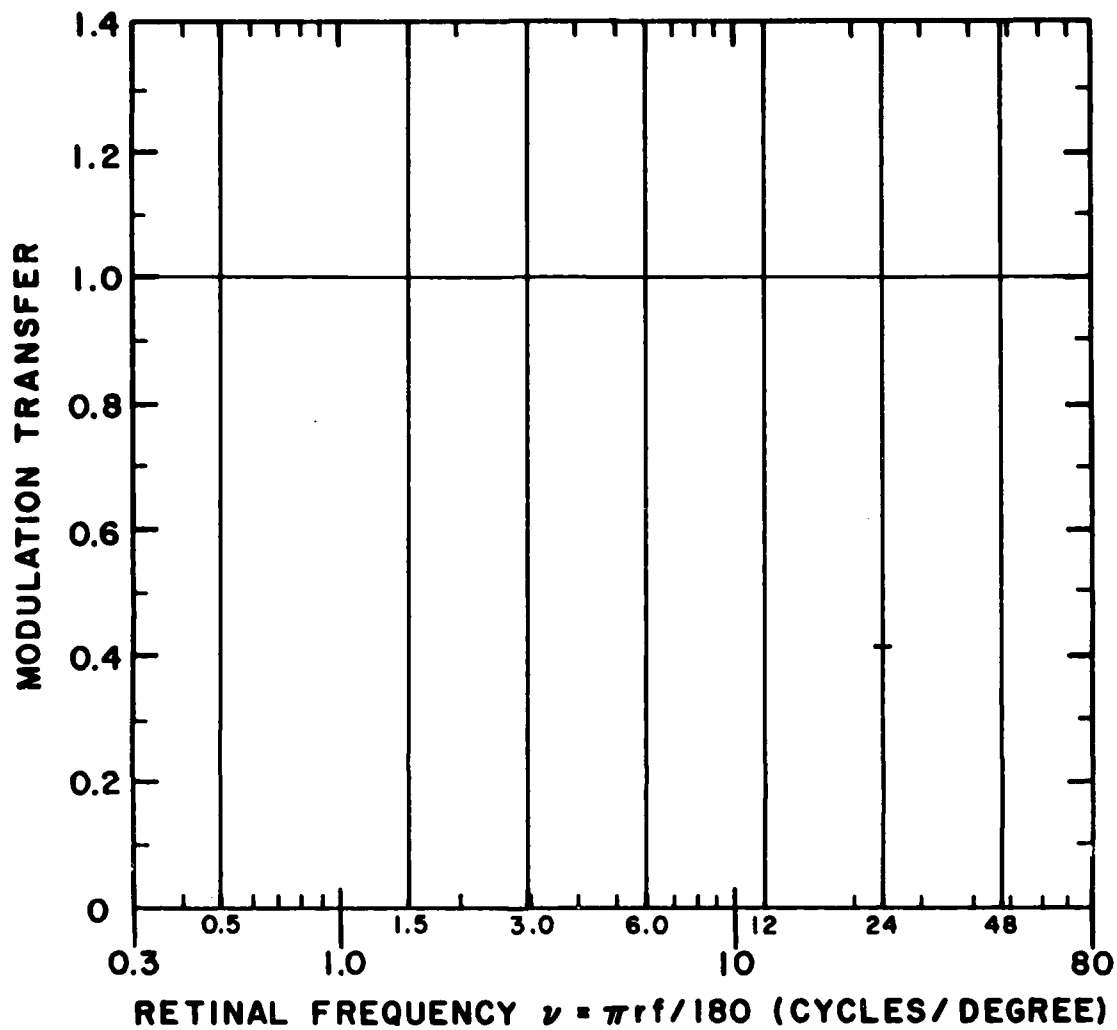
Figure 92. DDD No. 75. Discriminable Difference Diagram for noise in the presence of a 100% contrast luminance edge transition on an analog display: r/w = 3, r = 200 cm, $\bar{I}$ = 35 mL, and $\sqrt{N(f)}/\bar{I}$ = 0.03.
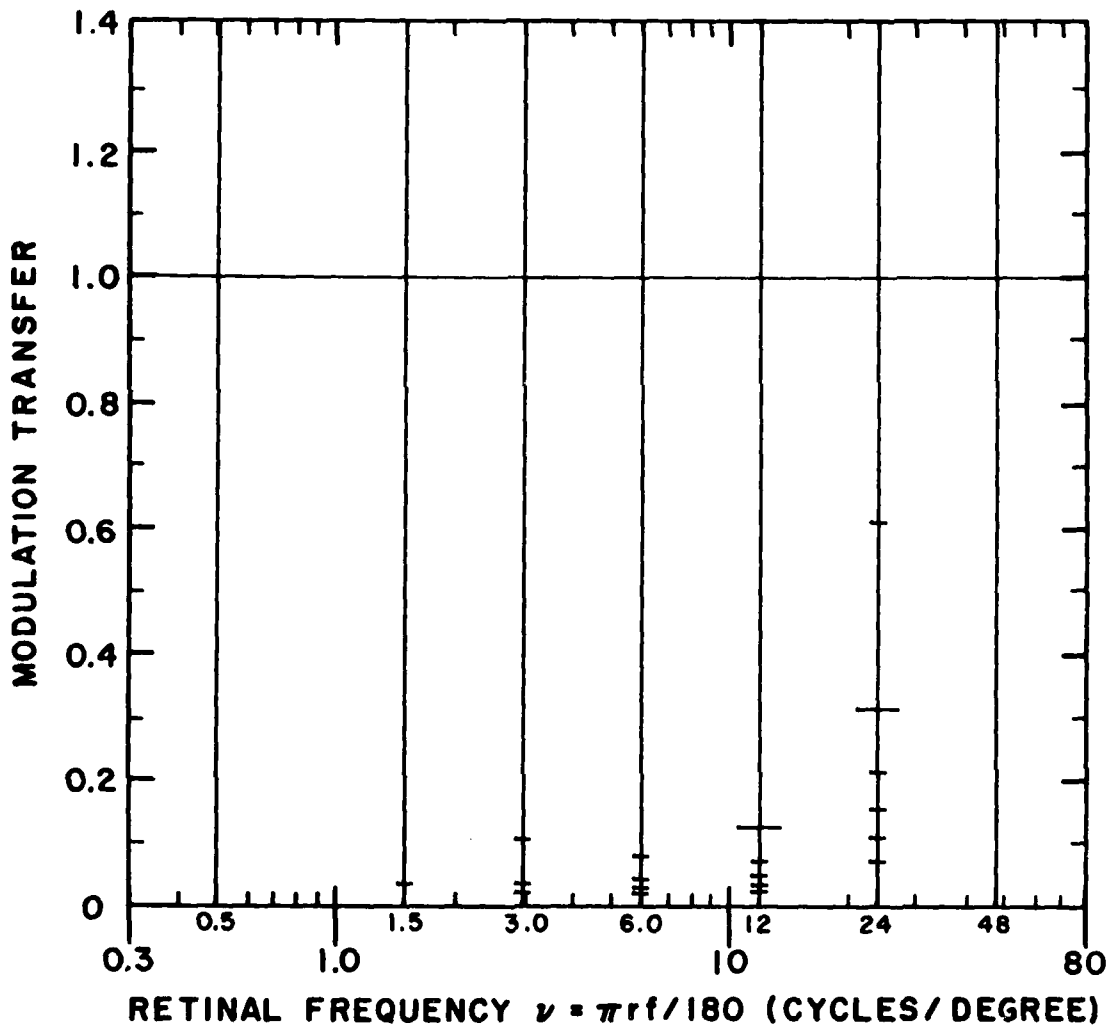
Figure 93. DDD No. 76. Discriminable Difference Diagram for noise in the presence of a 100% contrast luminance edge transition on an analog display: $r/w = 3$, $r = 200$ cm, $\bar{I} = 35$ mL, and $\sqrt{N(f)}/\bar{I} = 0.1$.

130
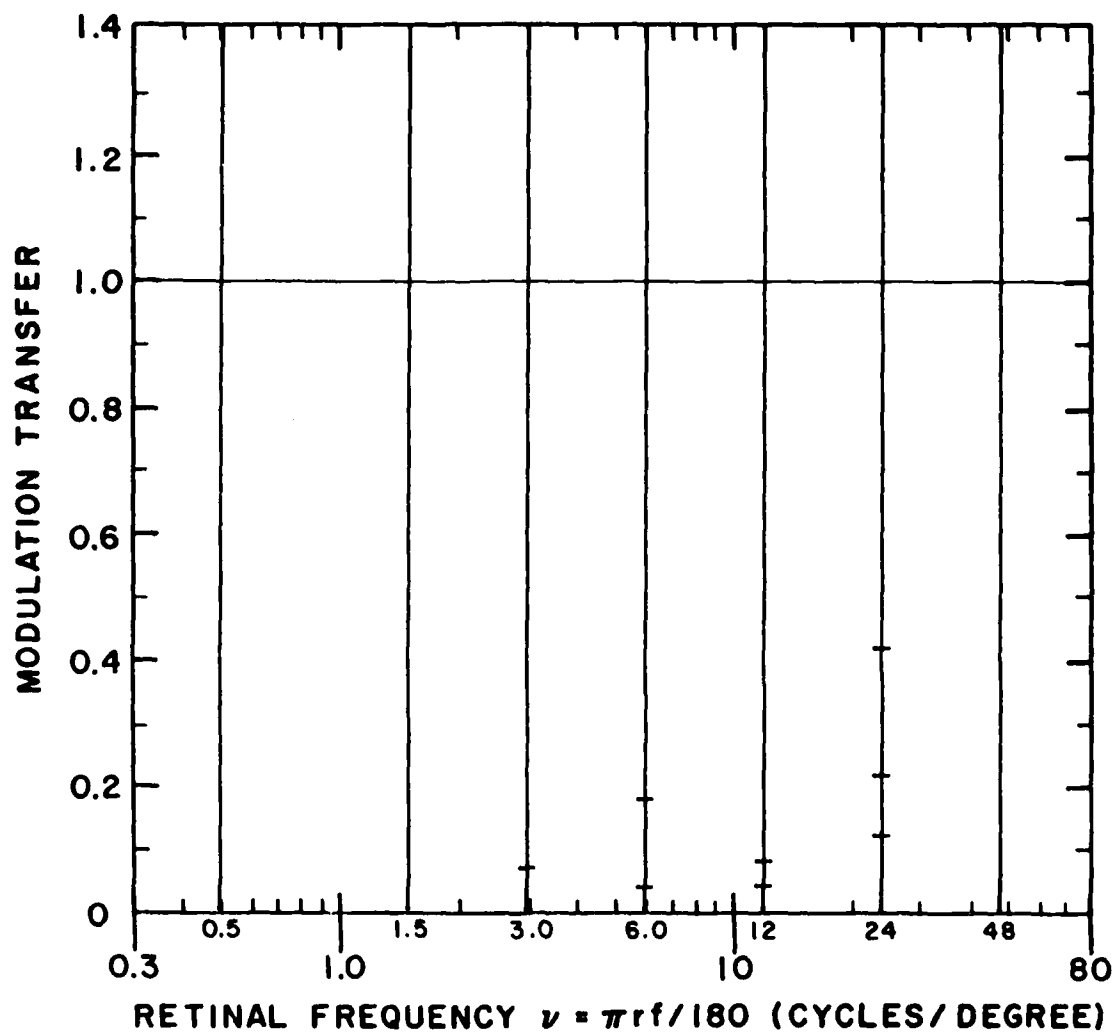
Figure 94. DDD No. 77. Discriminable Difference Diagram for noise in the presence of a 100% contrast luminance edge transition on an analog display: $r/w = 10$, $r = 50$ cm, $\bar{I} = 35$ mL, and $\sqrt{N(f)}/\bar{I} = 0.03$.

131
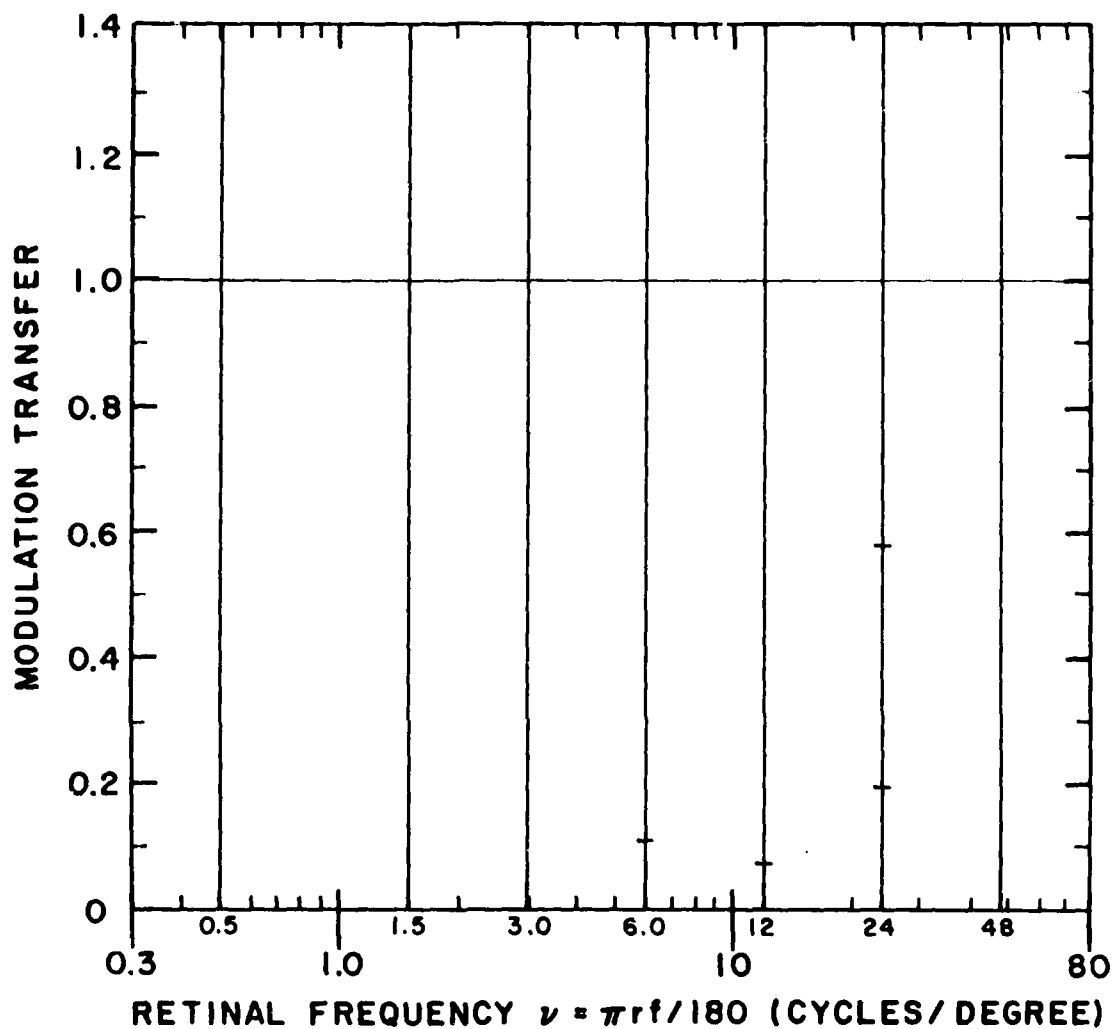
Figure 95. DDD No. 78. Discriminable Difference Diagram for noise in
the presence of a 100% contrast luminance edge transition
on an analog display: r/w = 10, r = 100 cm, $\bar{I}$ = 35 mL,
and $\sqrt{N(f)}/\bar{I}$ = 0.03.

132
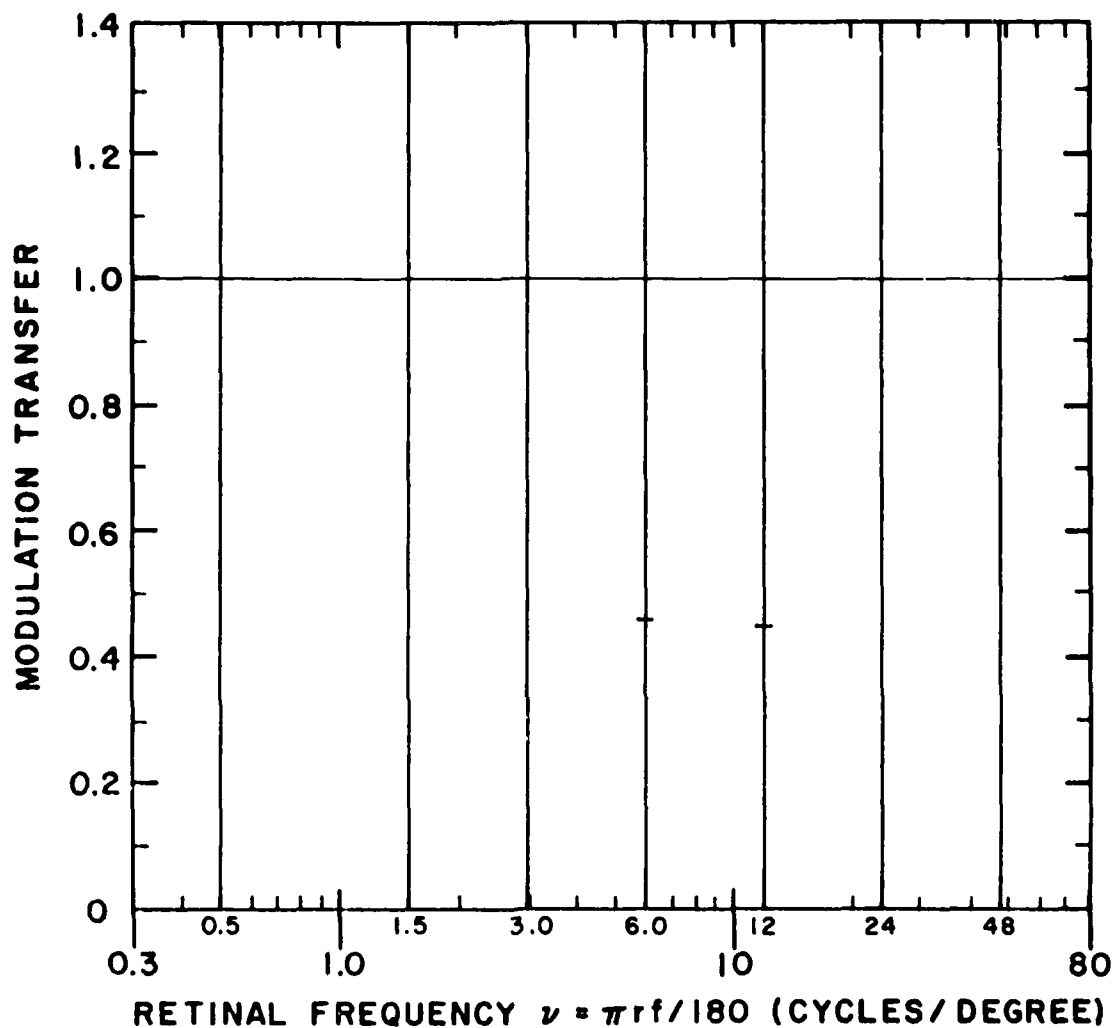
Figure 96. DDD No. 79. Discriminable Difference Diagram for noise in the presence of a 100% contrast luminance edge transition on an analog display: r/w = 10, r = 100 cm, $\bar{I}$ = 1 mL, and $\sqrt{N(f)}/\bar{I}$ = 0.03.
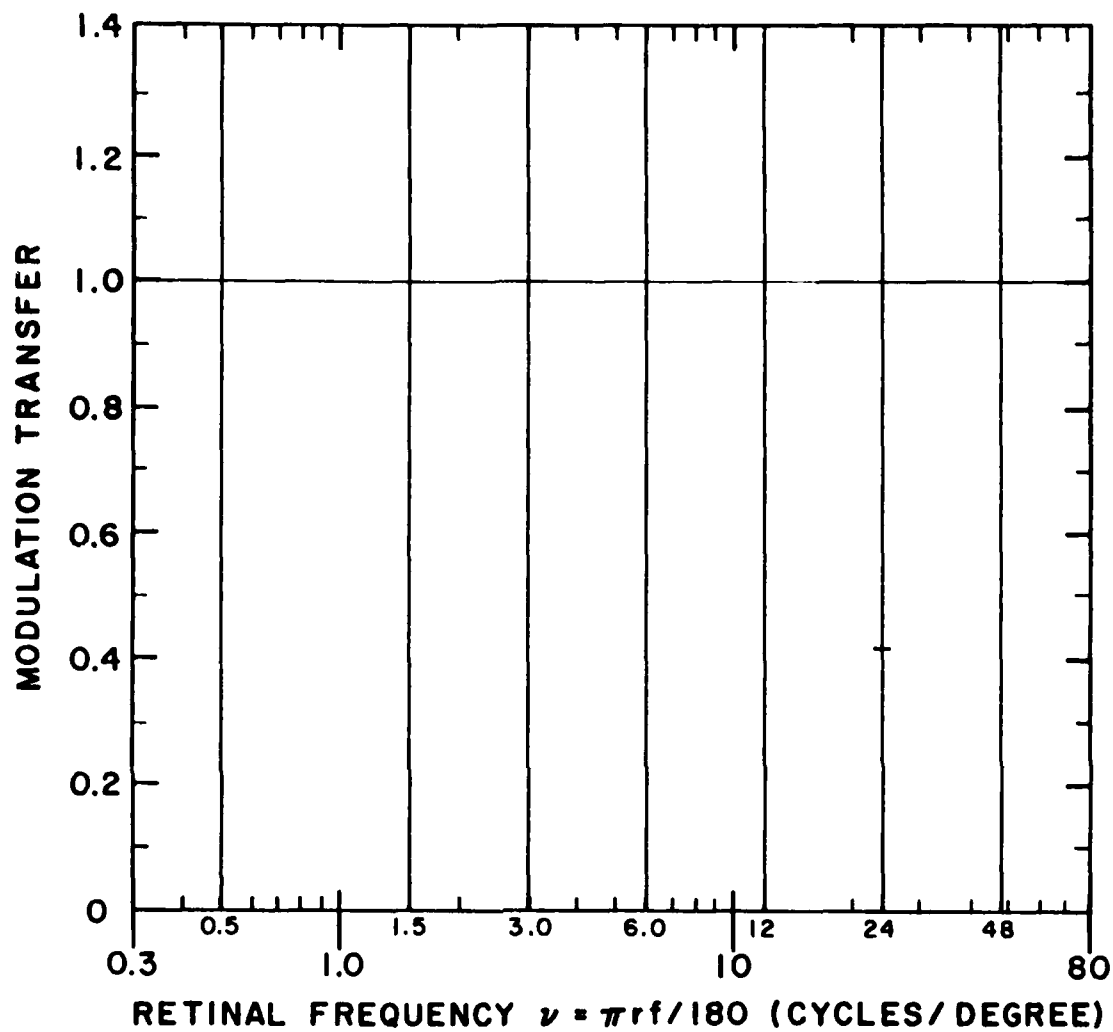
Figure 97. DDD No. 80. Discriminable Difference Diagram for noise in
the presence of a 100% contrast luminance edge transition
on an analog display: r/w = 10, r = 200 cm, $\bar{I}$ = 35 mL,
and $\sqrt{N(f)}/\bar{I}$ = 0.03.

134
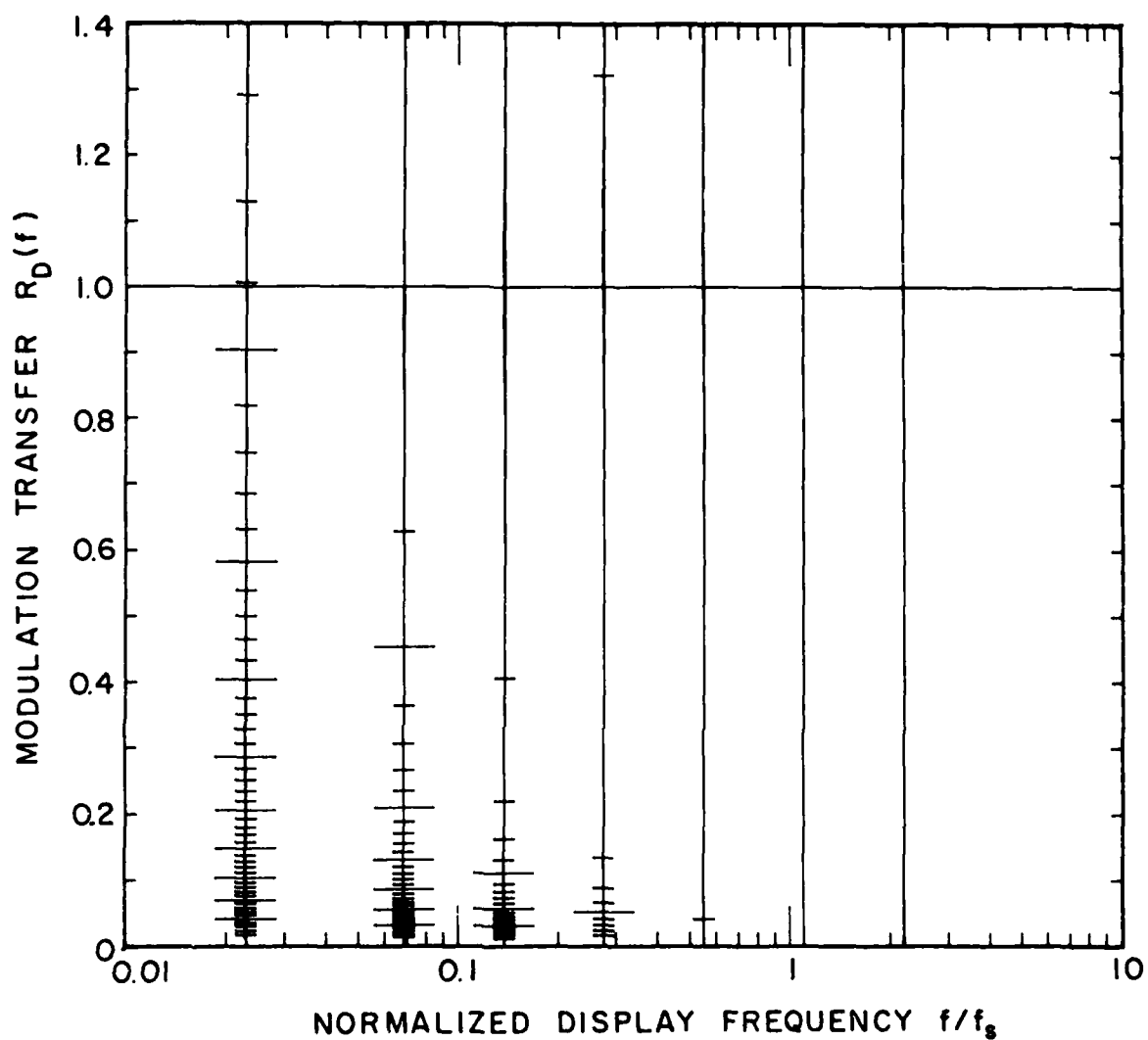
Figure 98. DDD No. 81. Discriminable Difference Diagram for signal
levels on a sampled/raster display: No prefilter,
$s = 0$, $N_s r/w = 1250$.

135
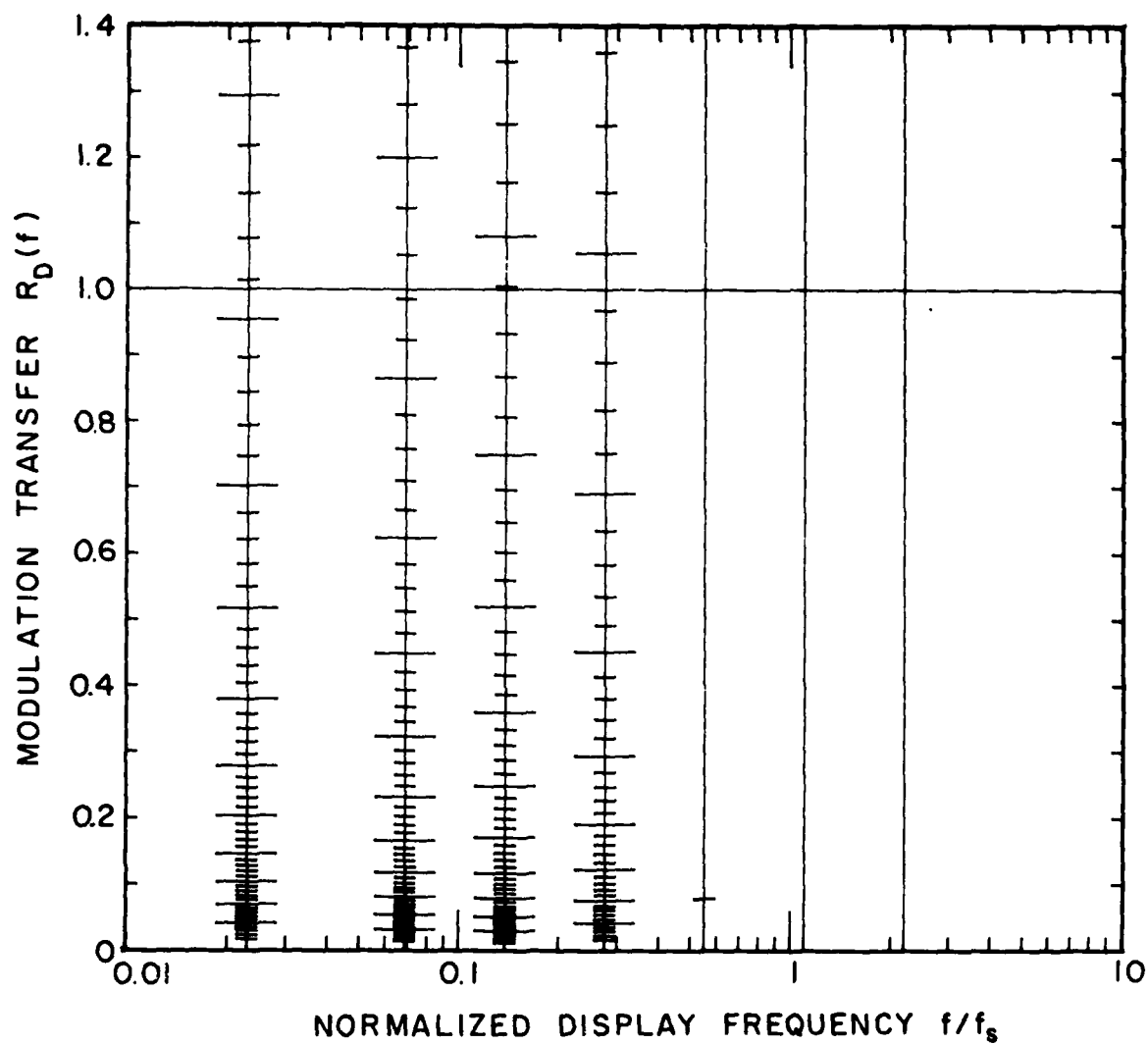
Figure 99. DDD No. 82. Discriminable Difference Diagram for signal
levels on a sampled/raster display: Nyquist prefilter,
s = 0, $N_s r/w$ = 1250.

136
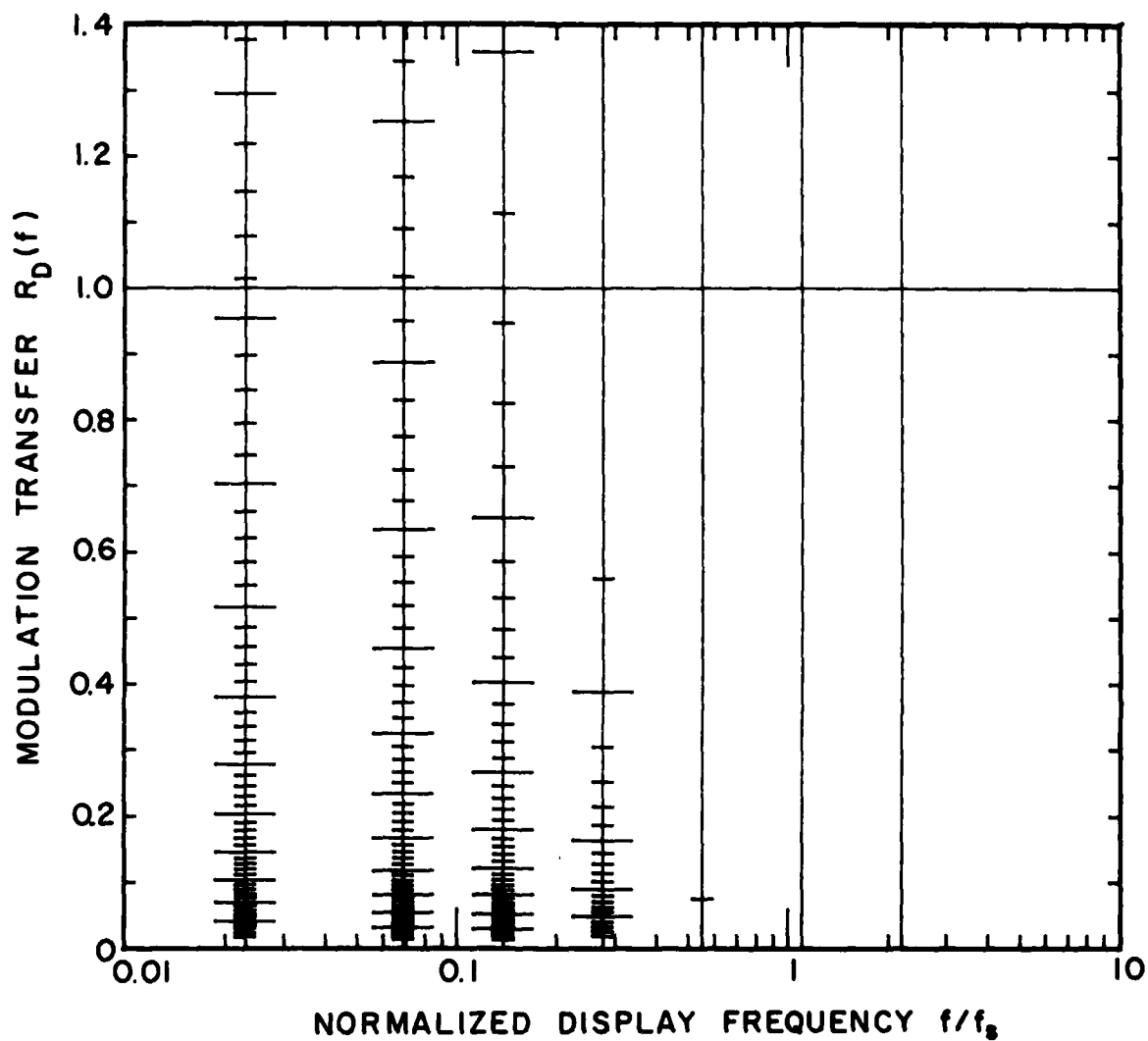
Figure 100. DDD No. 83. Discriminable Difference Diagram for signal levels on a sampled/raster display: No prefilter, s = 1, $N_s r/w$ = 1250.

137
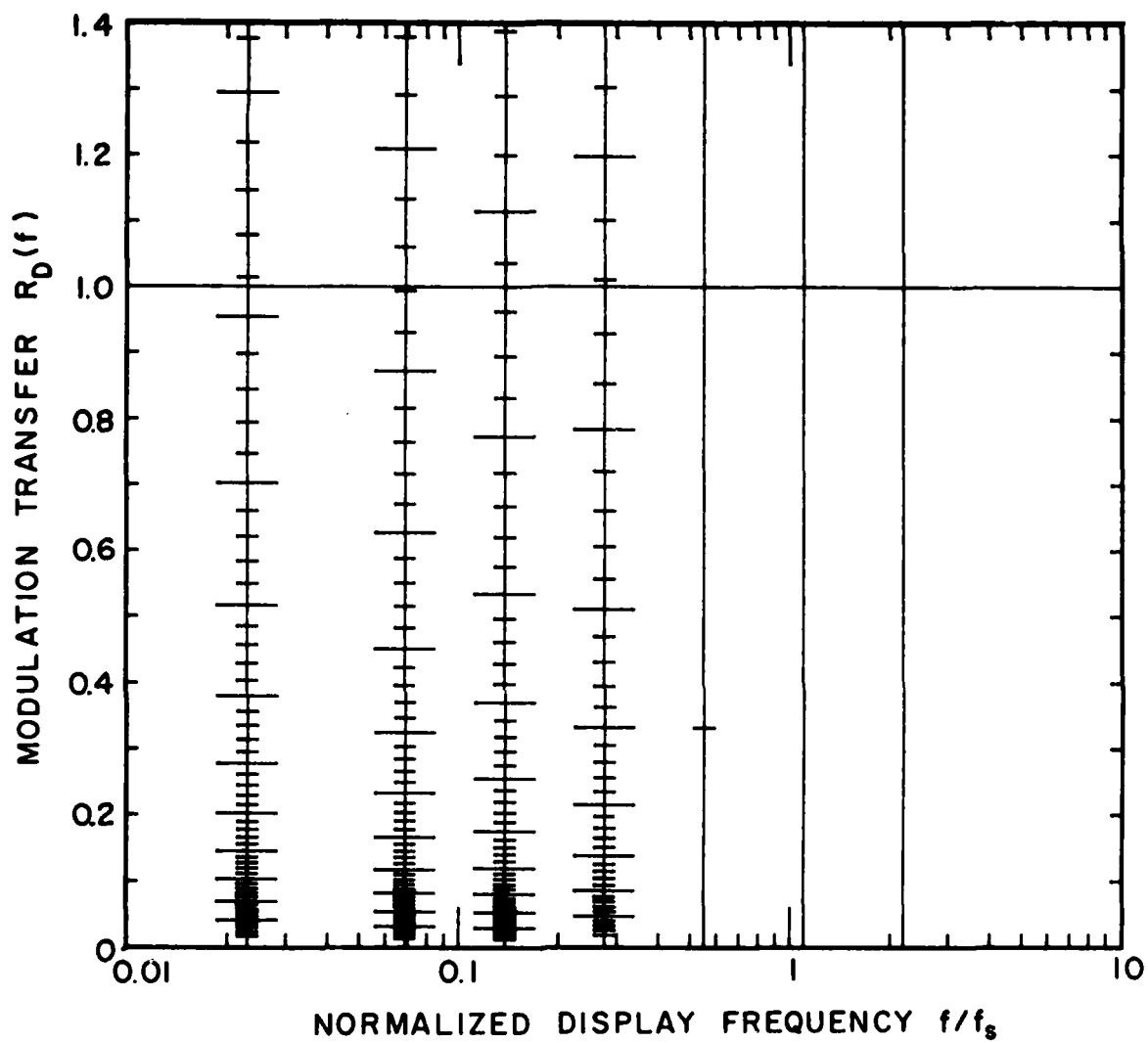
Figure 101.   DDD No. 84.   Discriminable Difference Diagram for signal
levels on a sampled/raster display: Nyquist prefilter,
$s = 1$, $N_s r/w = 1250$.

138
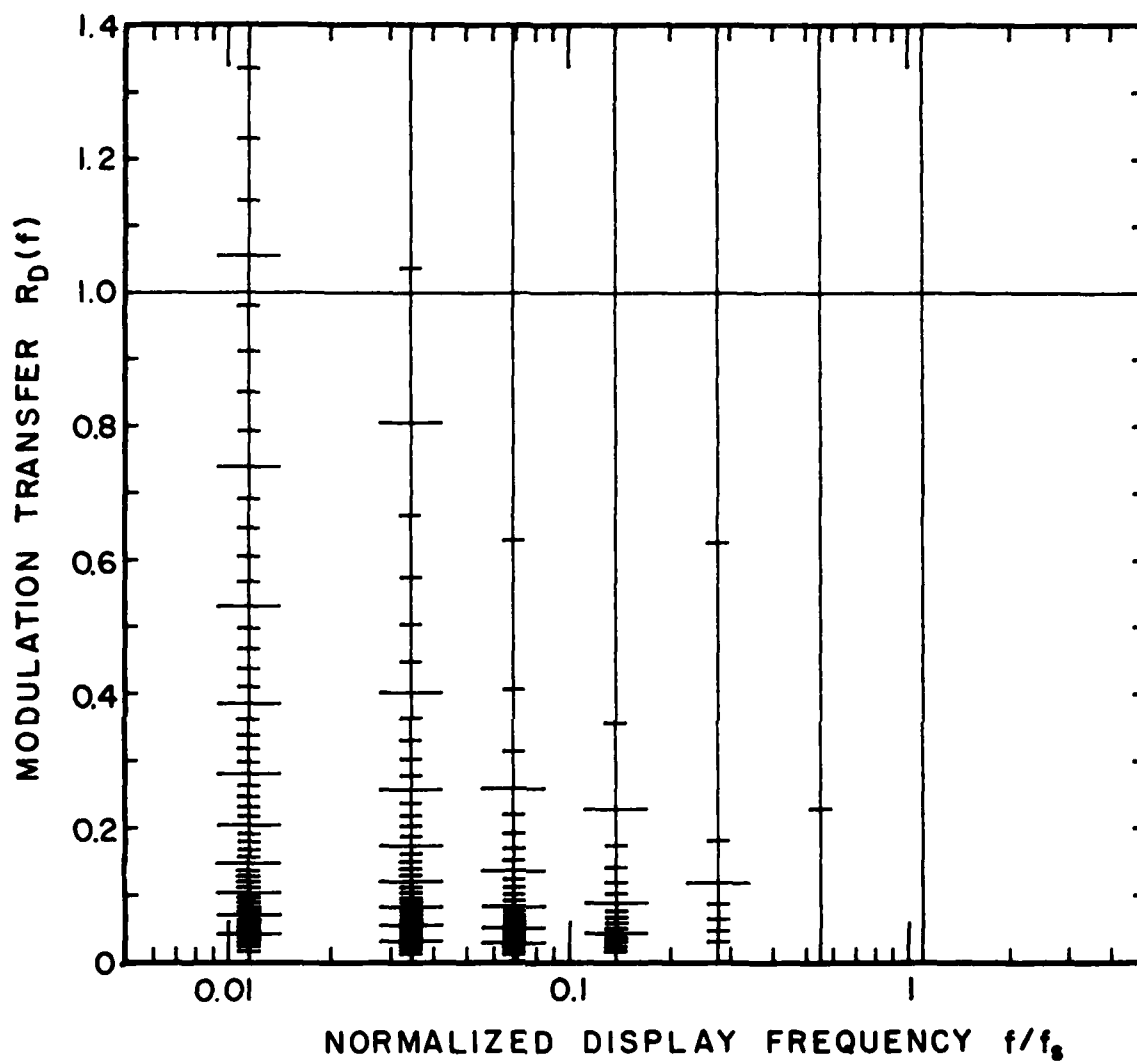
Figure 102. DDD No. 85. Discriminable Difference Diagram for signal
levels on a sampled/raster display: No prefilter, s = 0,
$N_s r/w$ = 2500.
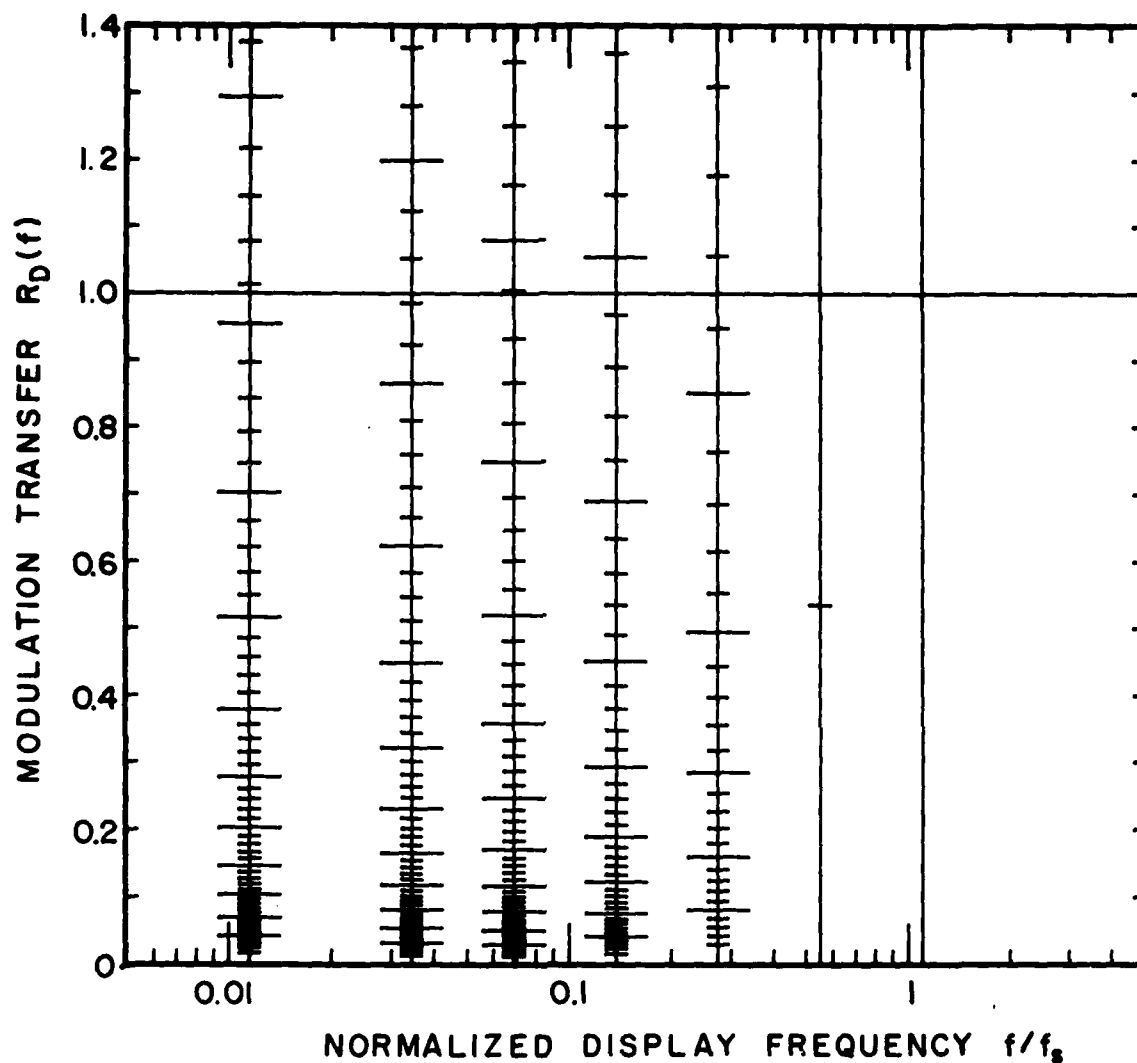
Figure 103. DDD No. 86. Discriminable Difference Diagram for signal
levels on a sampled/raster display: Nyquist prefilter,
$s = 0$, $N_s r/w = 2500$.

140
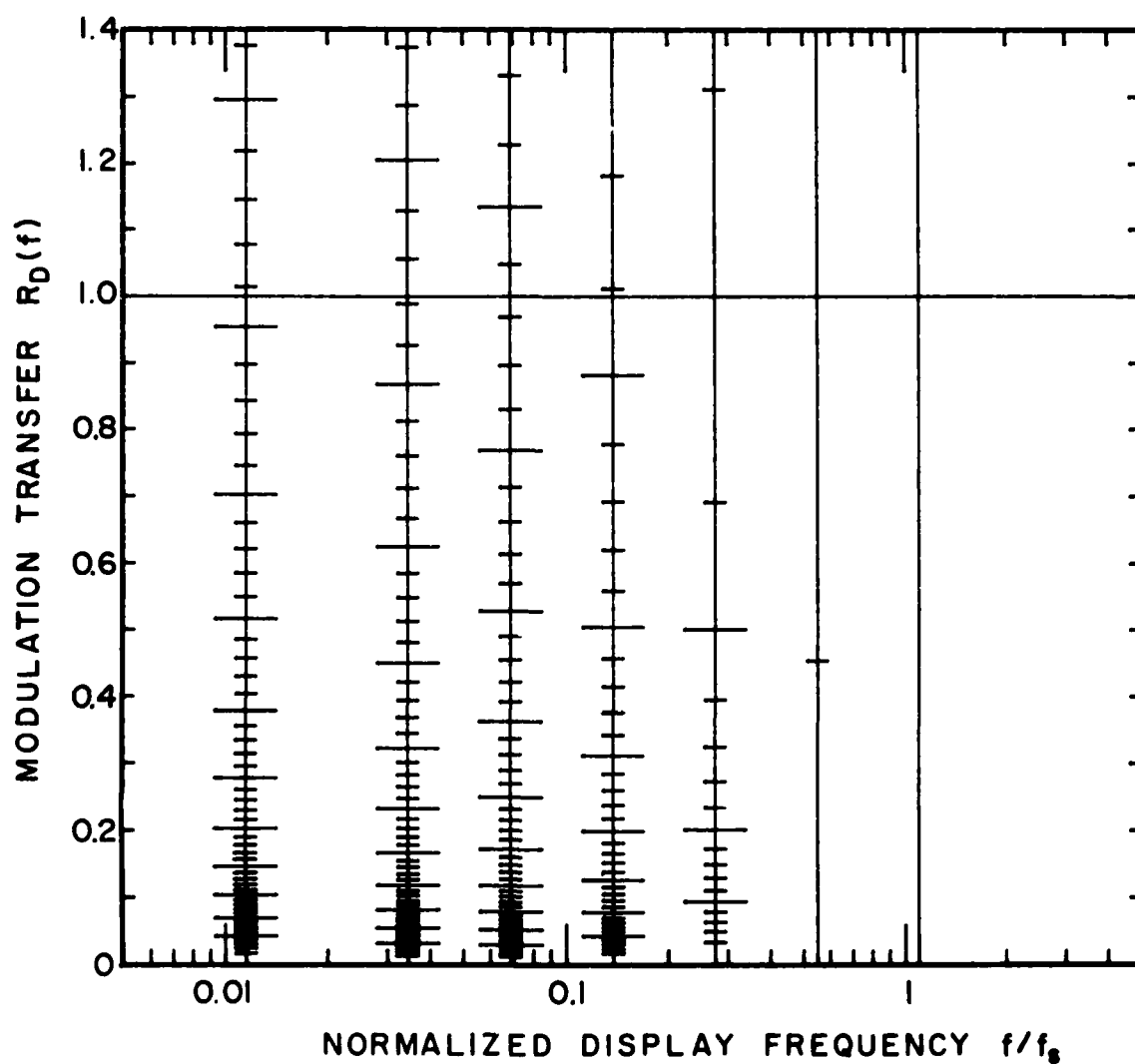
Figure 104. DDD No. 87. Discriminable Difference Diagram for signal
levels on a sampled/raster display: No prefilter, s = 1,
$N_s r/w = 2500$.

141
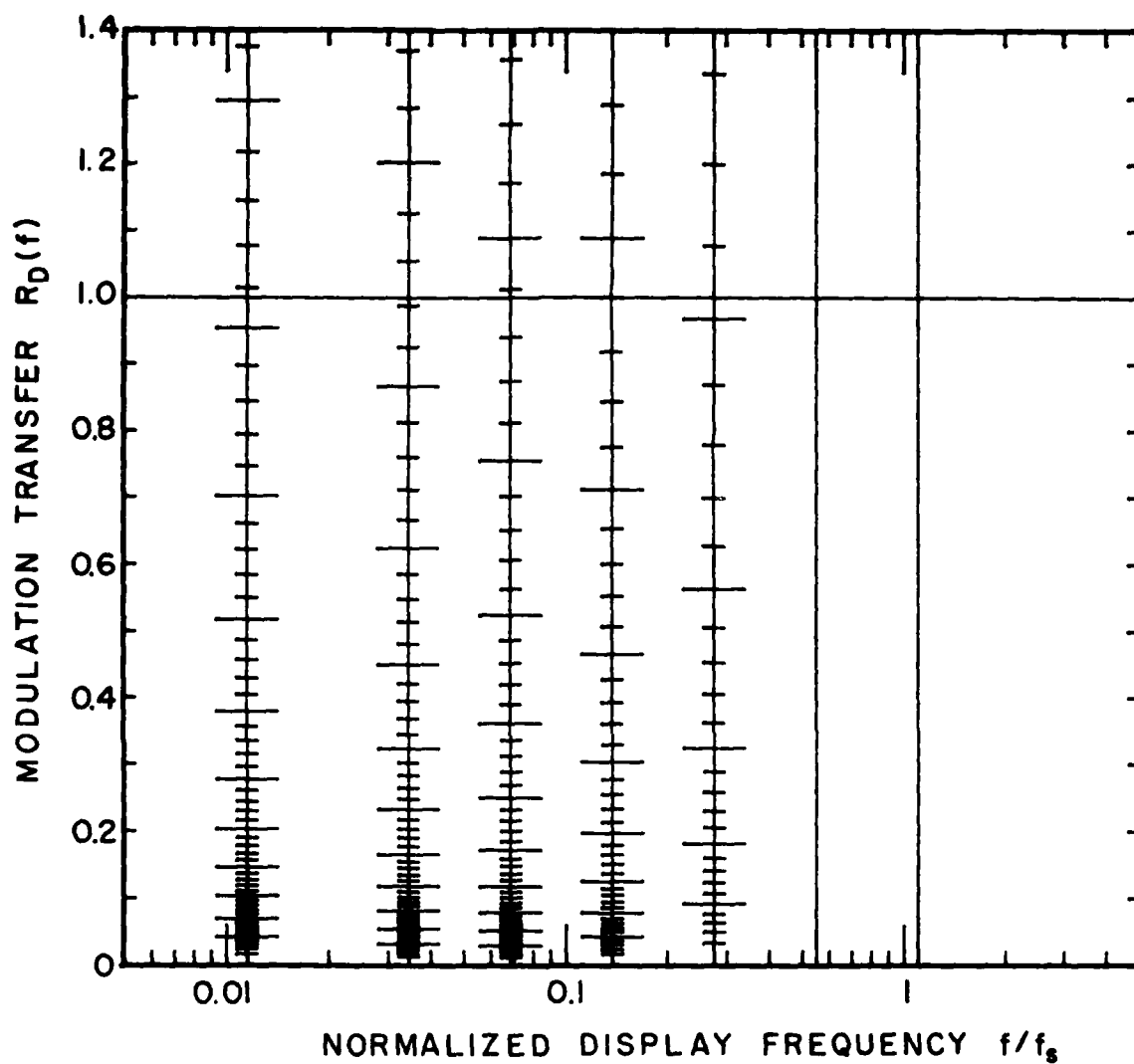
Figure 105. DDD No. 88. Discriminable Difference Diagram for signal
levels on a sampled/raster display: Nyquist prefilter,
$s = 1$, $N_s r/w = 2500$.

142
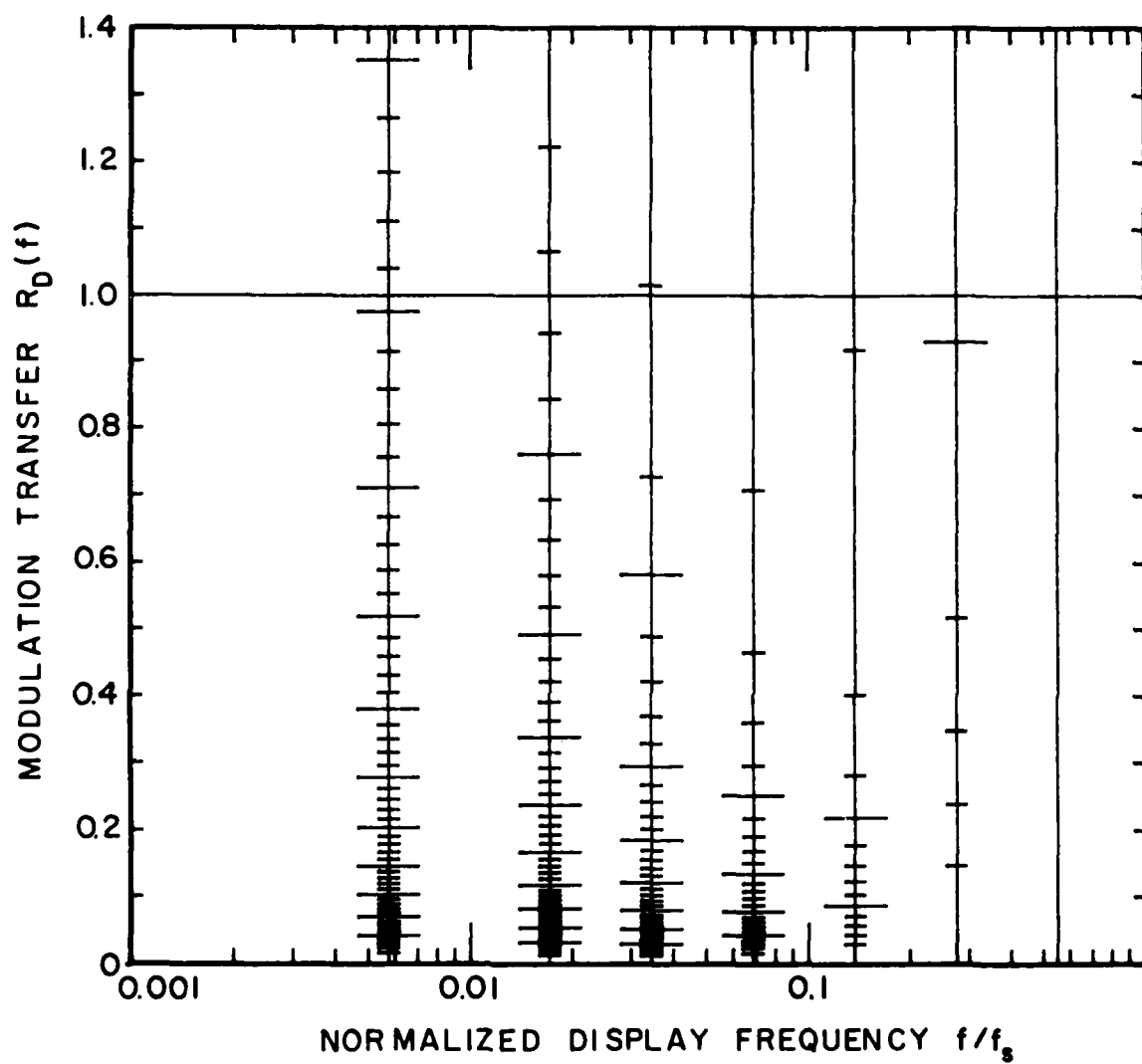
Figure 106. DDD No. 89. Discriminable Difference Diagram for signal levels on a sampled/raster display: No prefilter, s = 0, $N_s r/w$ = 5000.

143
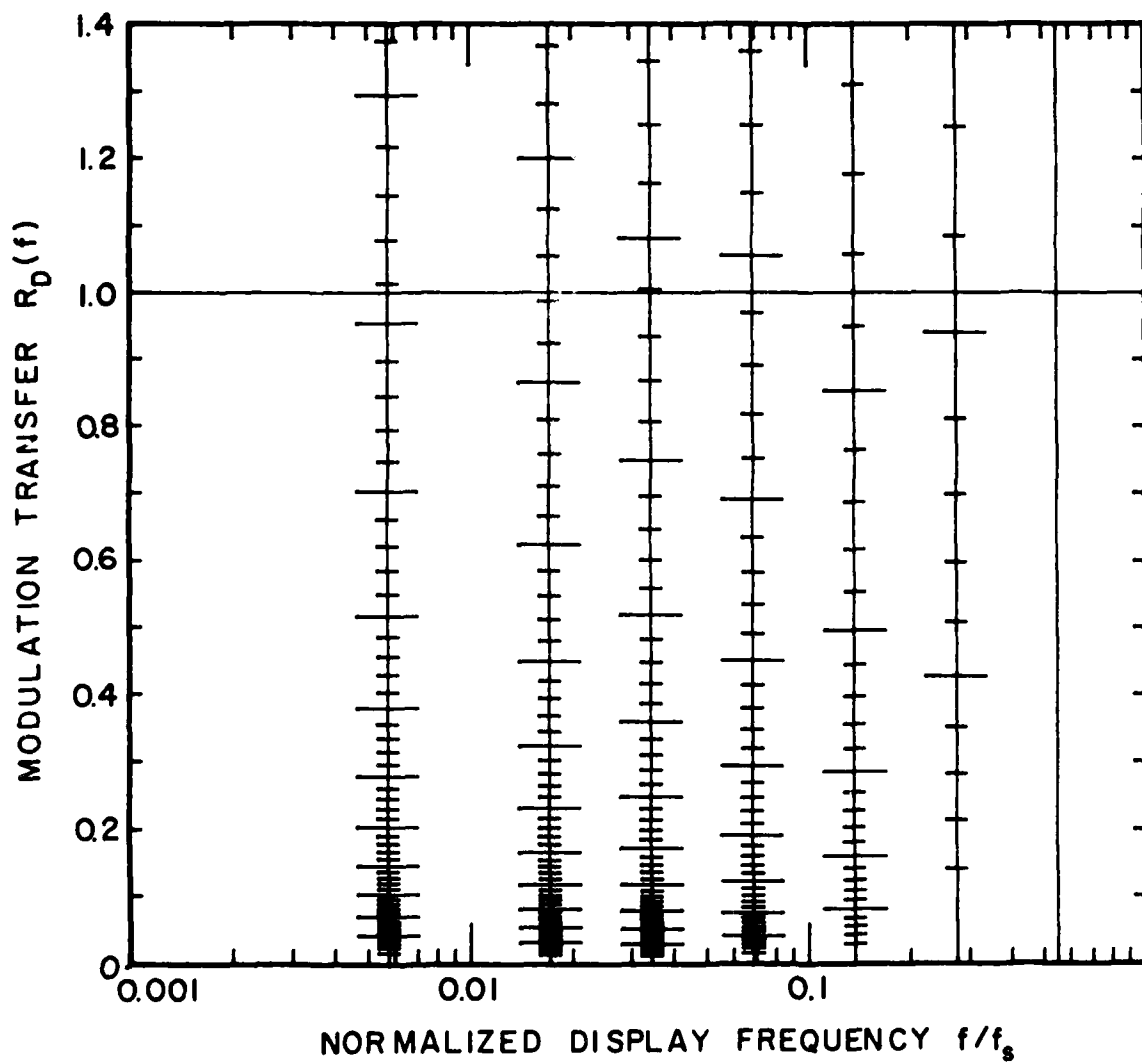
Figure 107. DDD No. 90. Discriminable Difference Diagram for signal
levels on a sampled/raster display: Nyquist prefilter,
$s = 0$, $N_s r/w = 5000$.

144
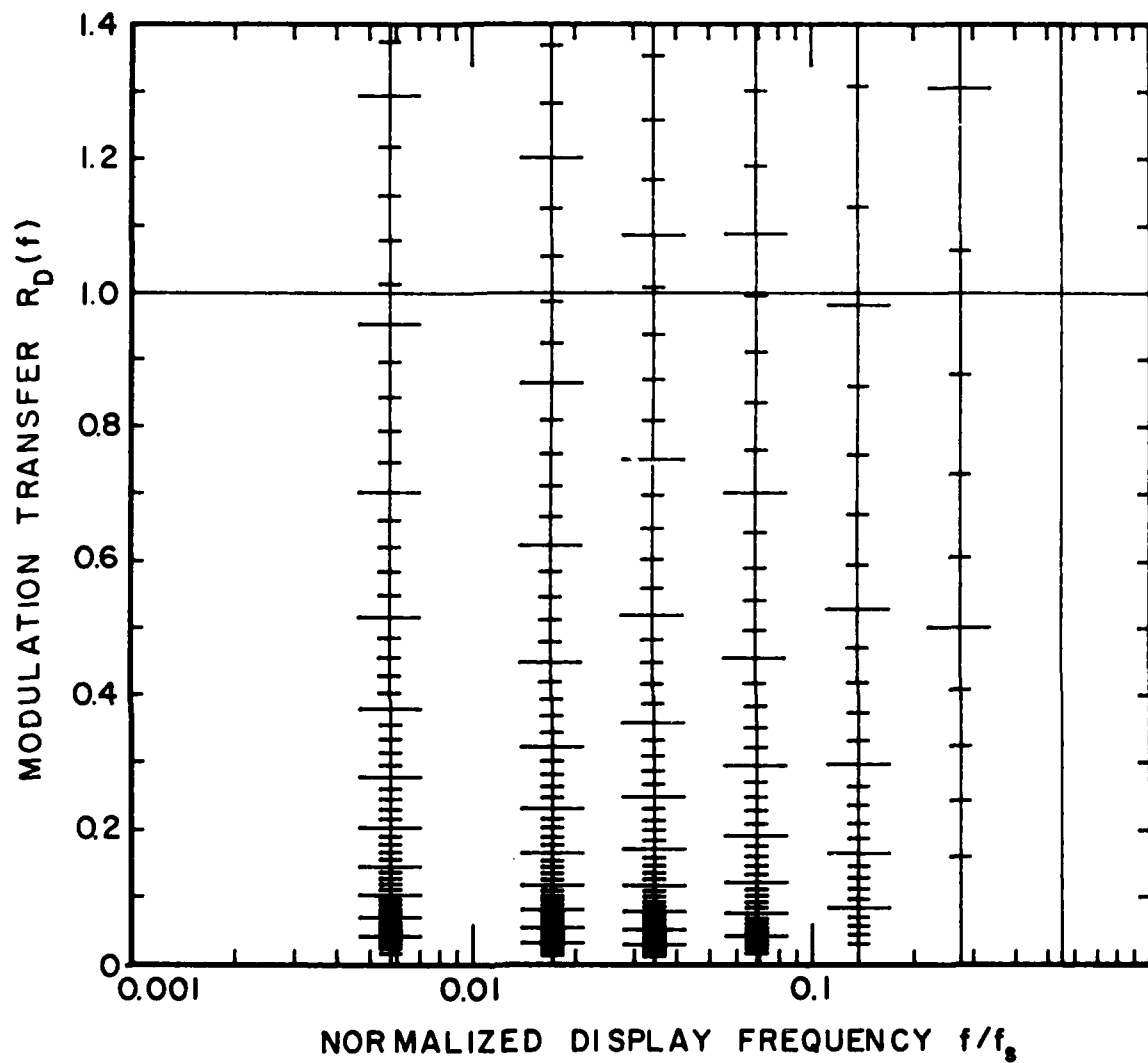
Figure 108. DDD No. 91. Discriminable Difference Diagram for signal
levels on a sampled/raster display: No prefilter, $s = 1$,
$N_s r/w = 5000$.

145
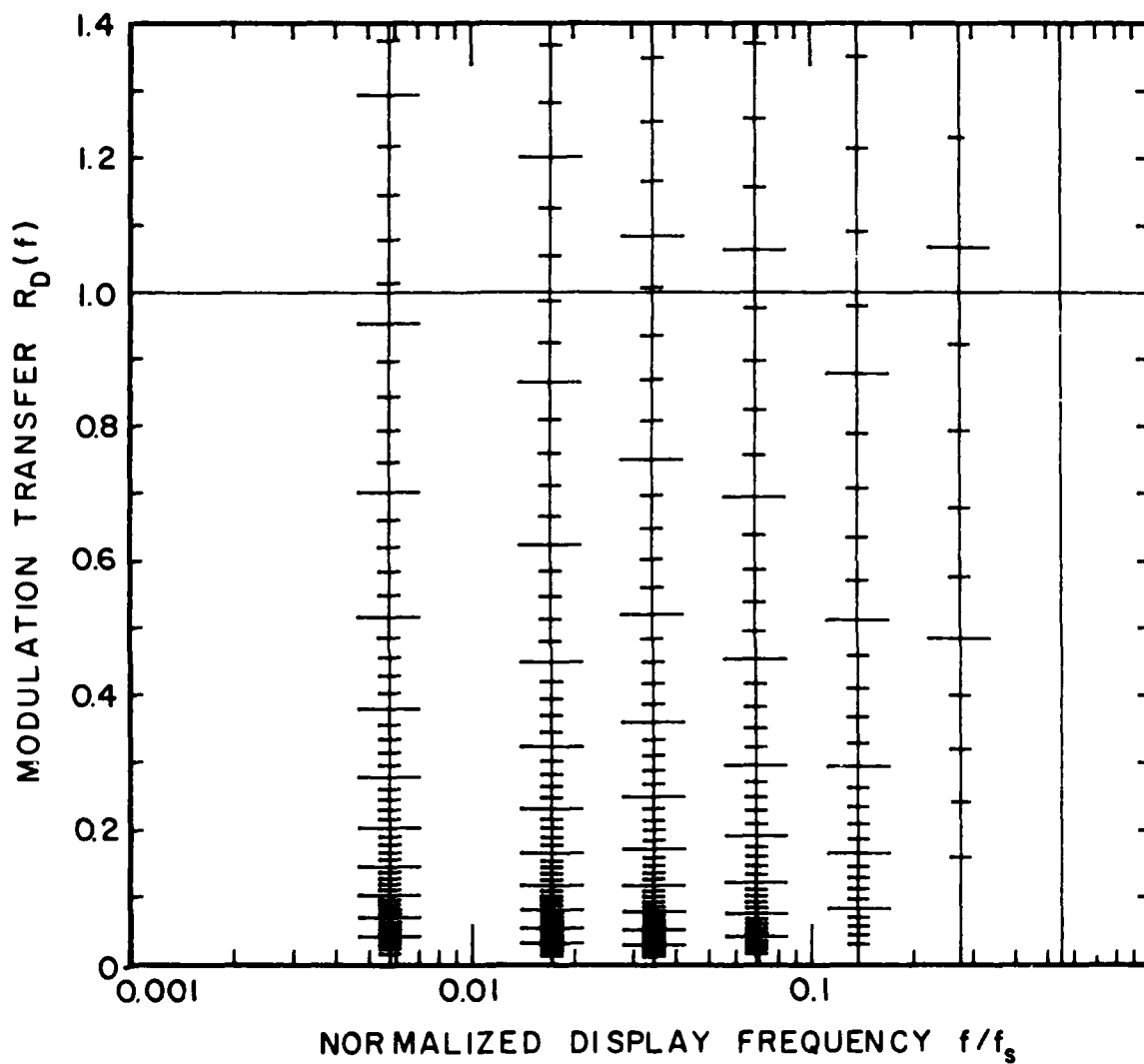
Figure 109. DDD No. 92. Discriminable Difference Diagram for signal
levels on a sampled/raster display: Nyquist prefilter,
$s = 1$, $N_s r/w = 5000$.

146
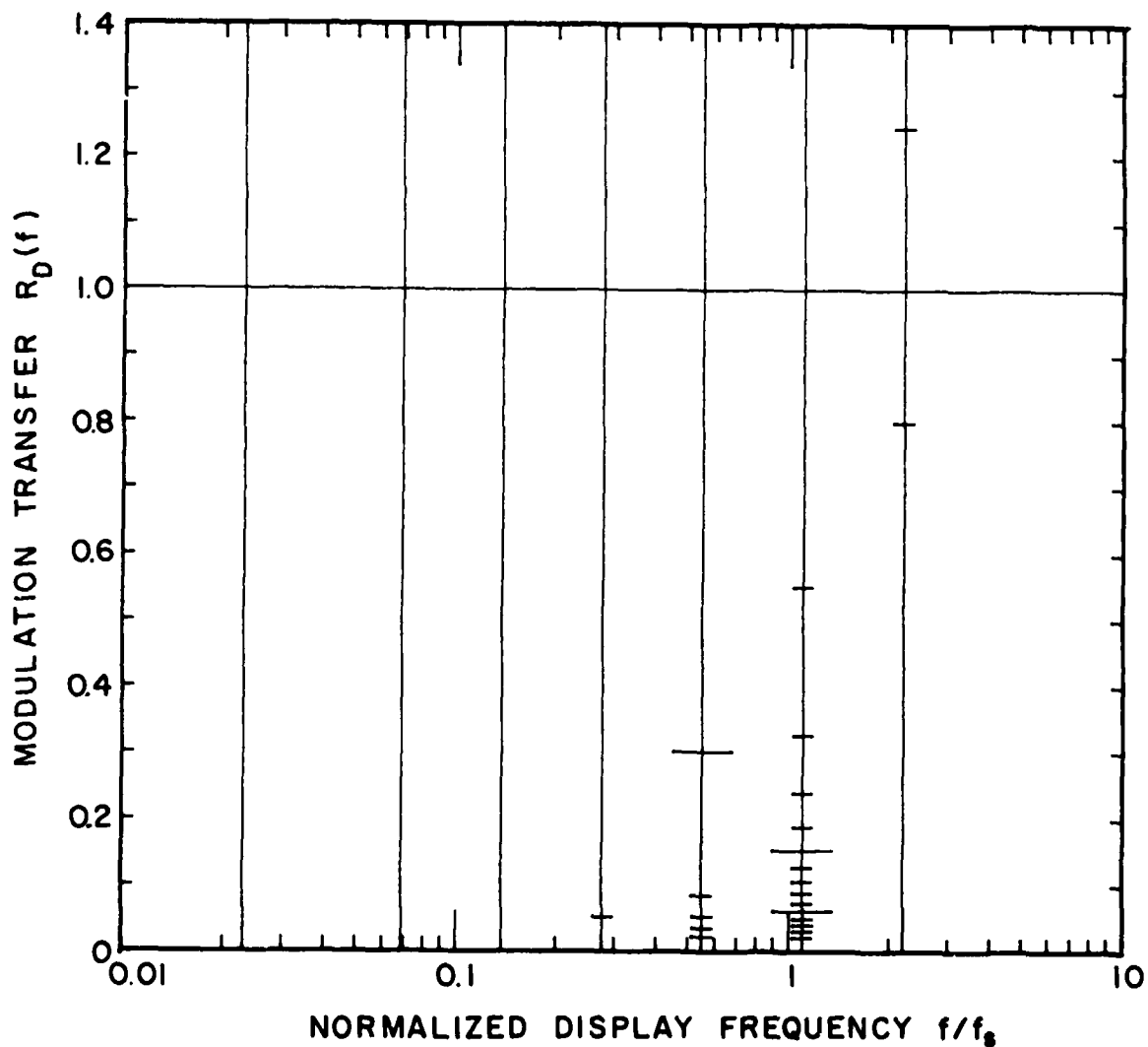
Figure 110. DDD No. 93. Discriminable Difference Diagram for noise
levels due to sampling on a sampled/raster display: No
prefilter, $s = 0$, $N_s r/w = 1250$.
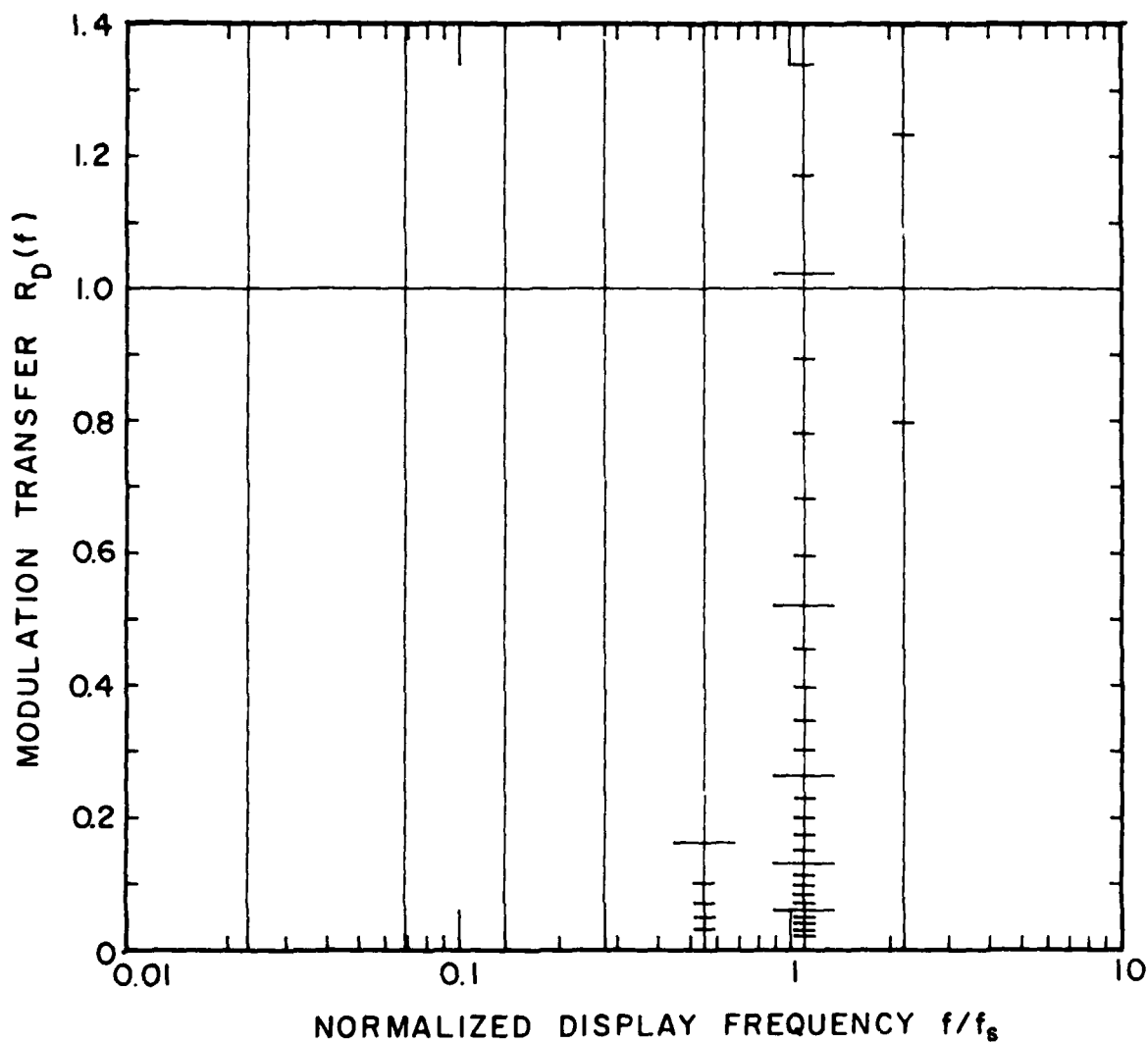
Figure 111. DDD No. 94. Discriminable Difference Diagram for noise
levels due to sampling on a sampled/raster display:
Nyquist prefilter, $s = 0$, $N_s r/w = 1250$.

148
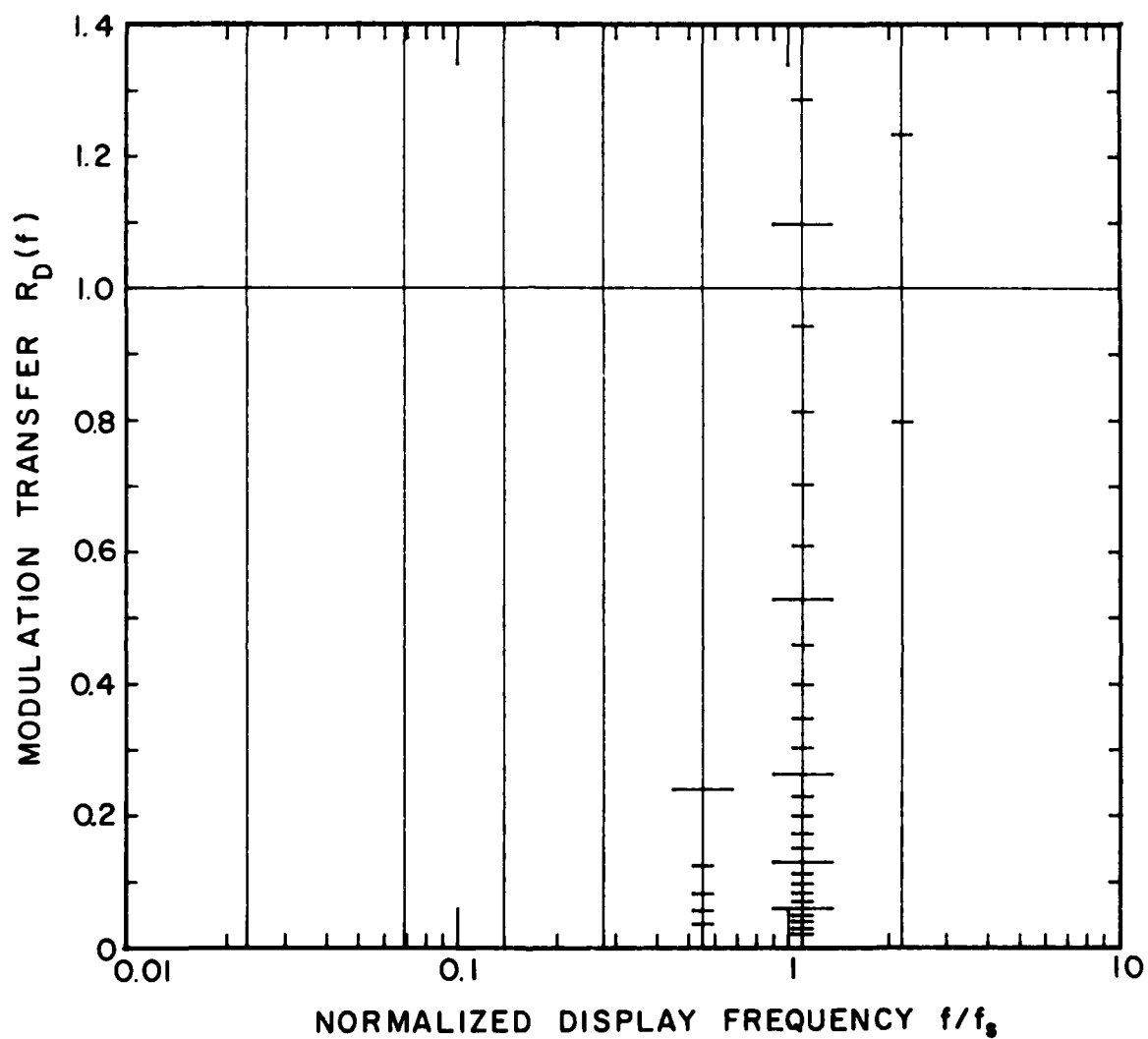
Figure 112.   DDD No. 95.   Discriminable Difference Diagram for noise
levels due to sampling on a sampled/raster display:
No prefilter, s = 1, $N_s r/w$ = 1250.

149
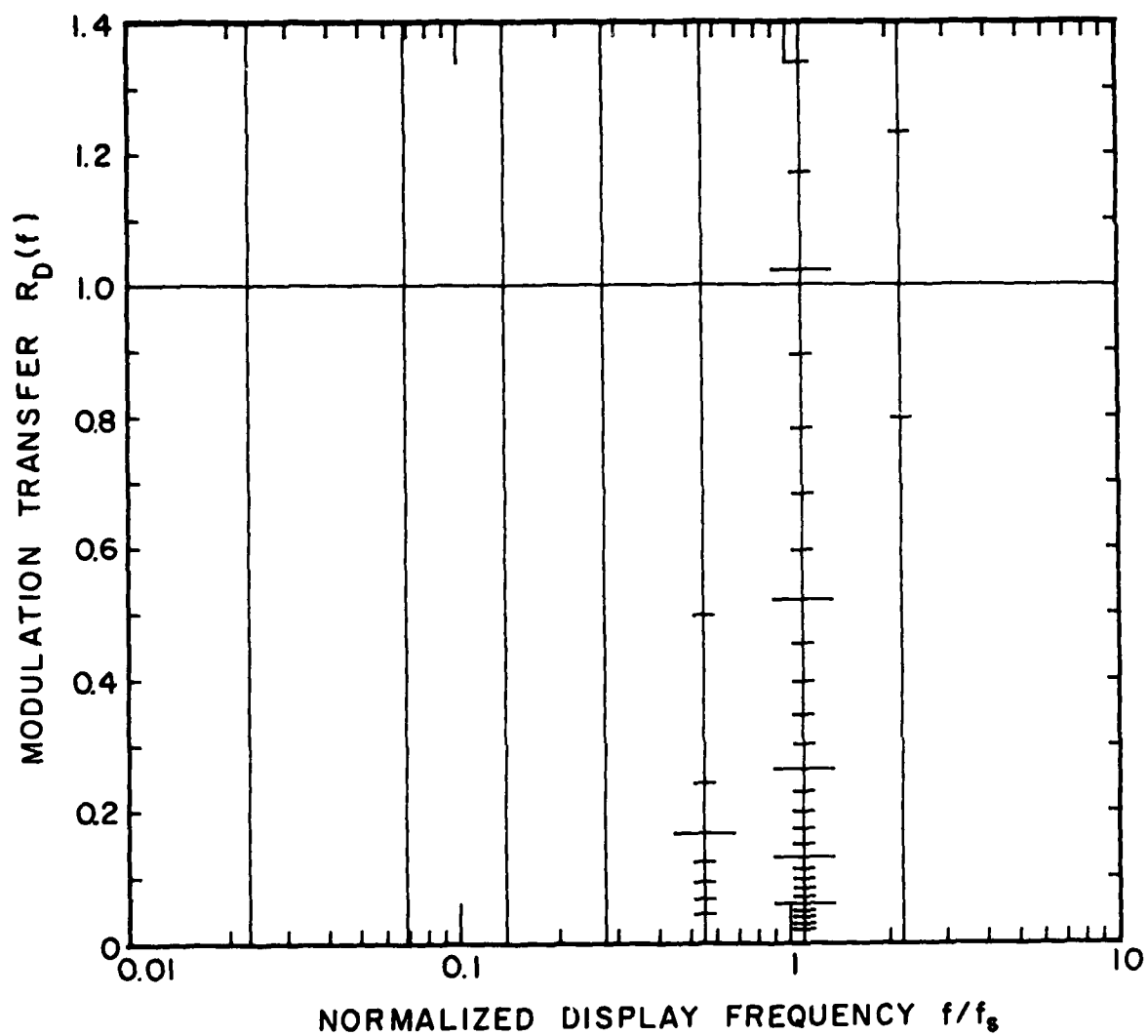
Figure 113. DDD No. 96. Discriminable Difference Diagram for noise
levels due to sampling on a sampled/raster display:
Nyquist prefilter, $s = 1$, $N_s r/w = 1250$.

150
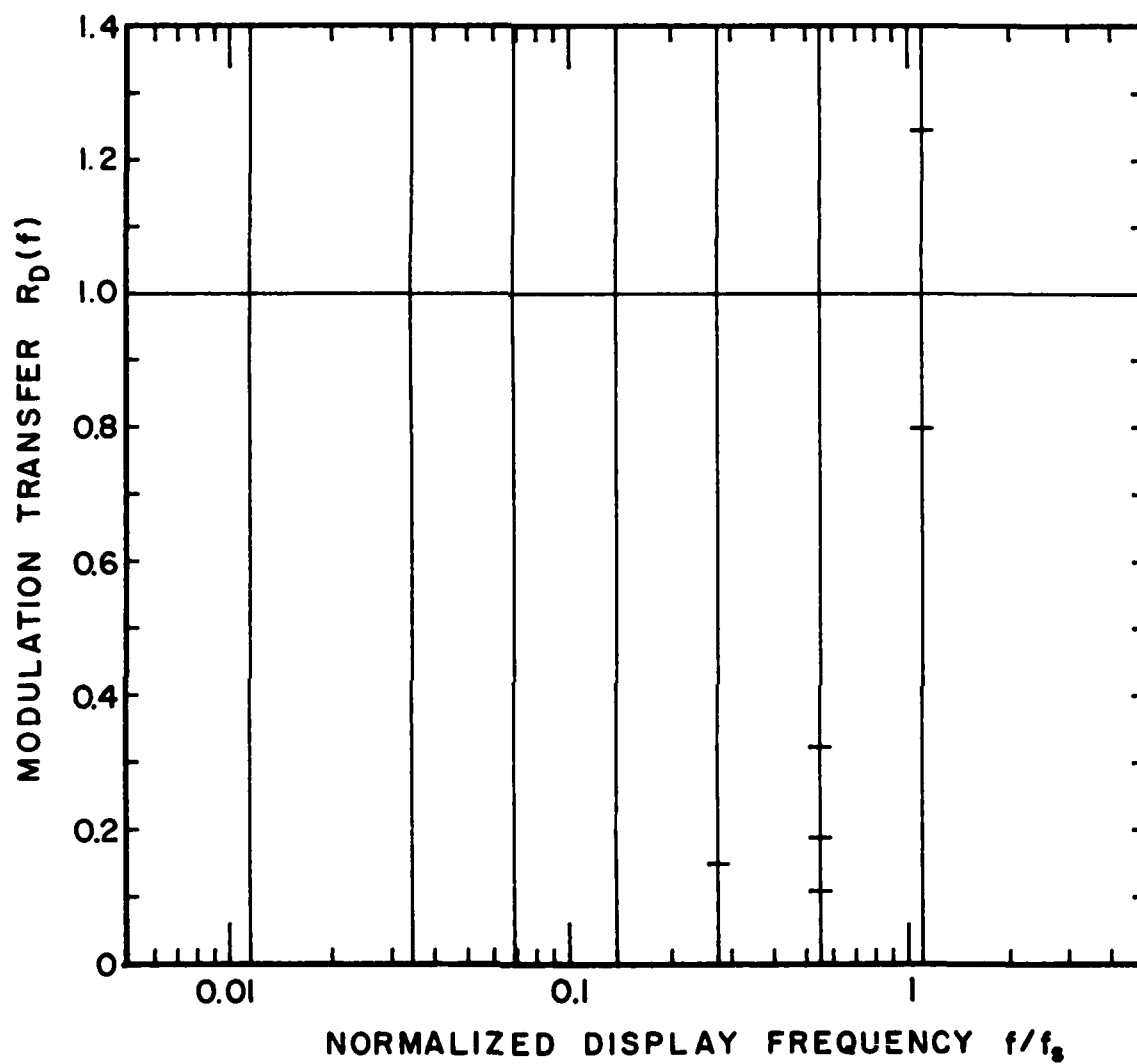
Figure 114. DDD No. 97. Discriminable Difference Diagram for noise levels due to sampling on a sampled/raster display: No prefilter, s = 0, $N_s r/w = 2500$.

151
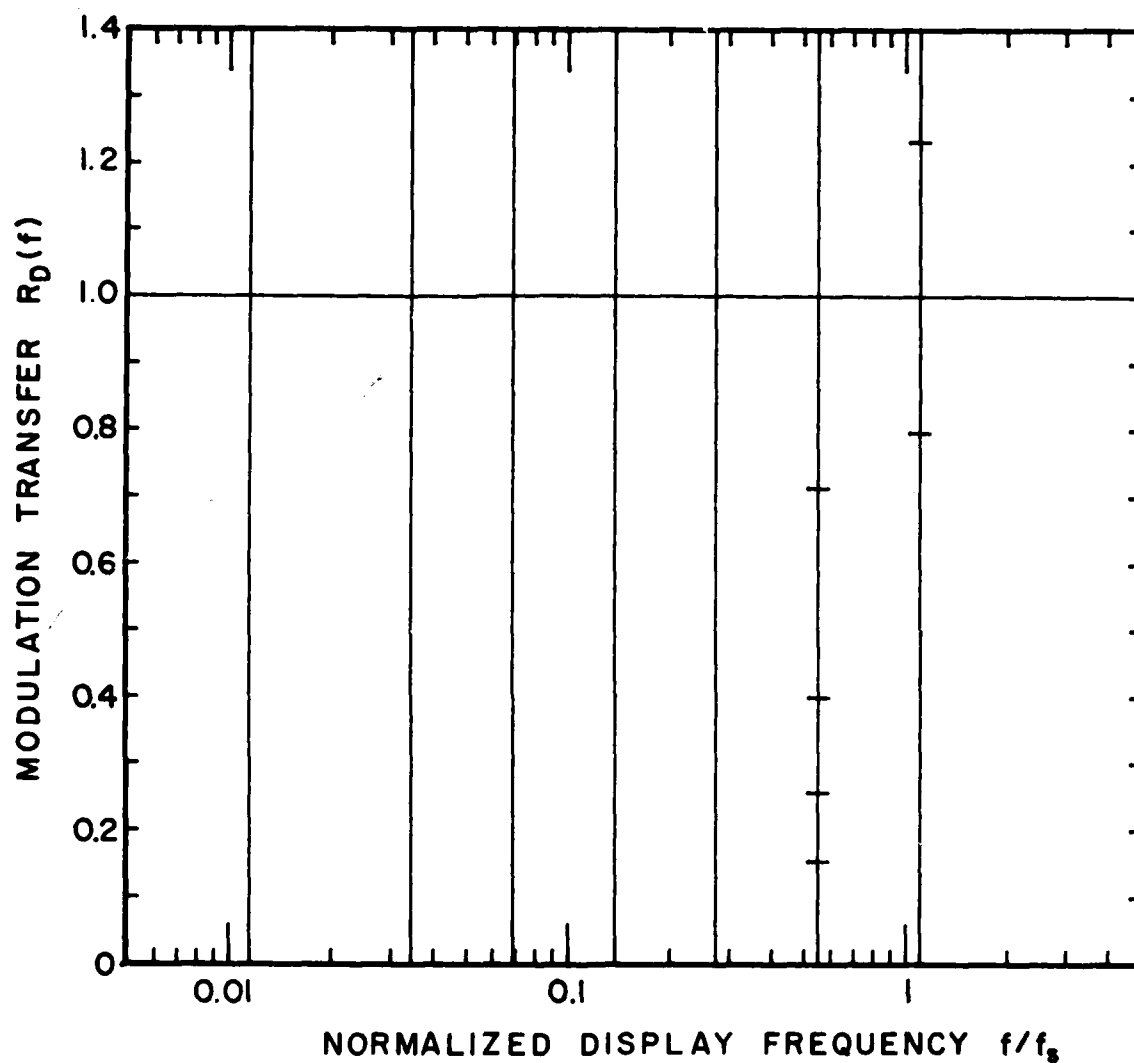
Figure 115. DDD No. 98. Discriminable Difference Diagram for noise levels due to sampling on a sampled/raster display: Nyquist prefilter, s = 0, $N_s r/w$ = 2500.

152
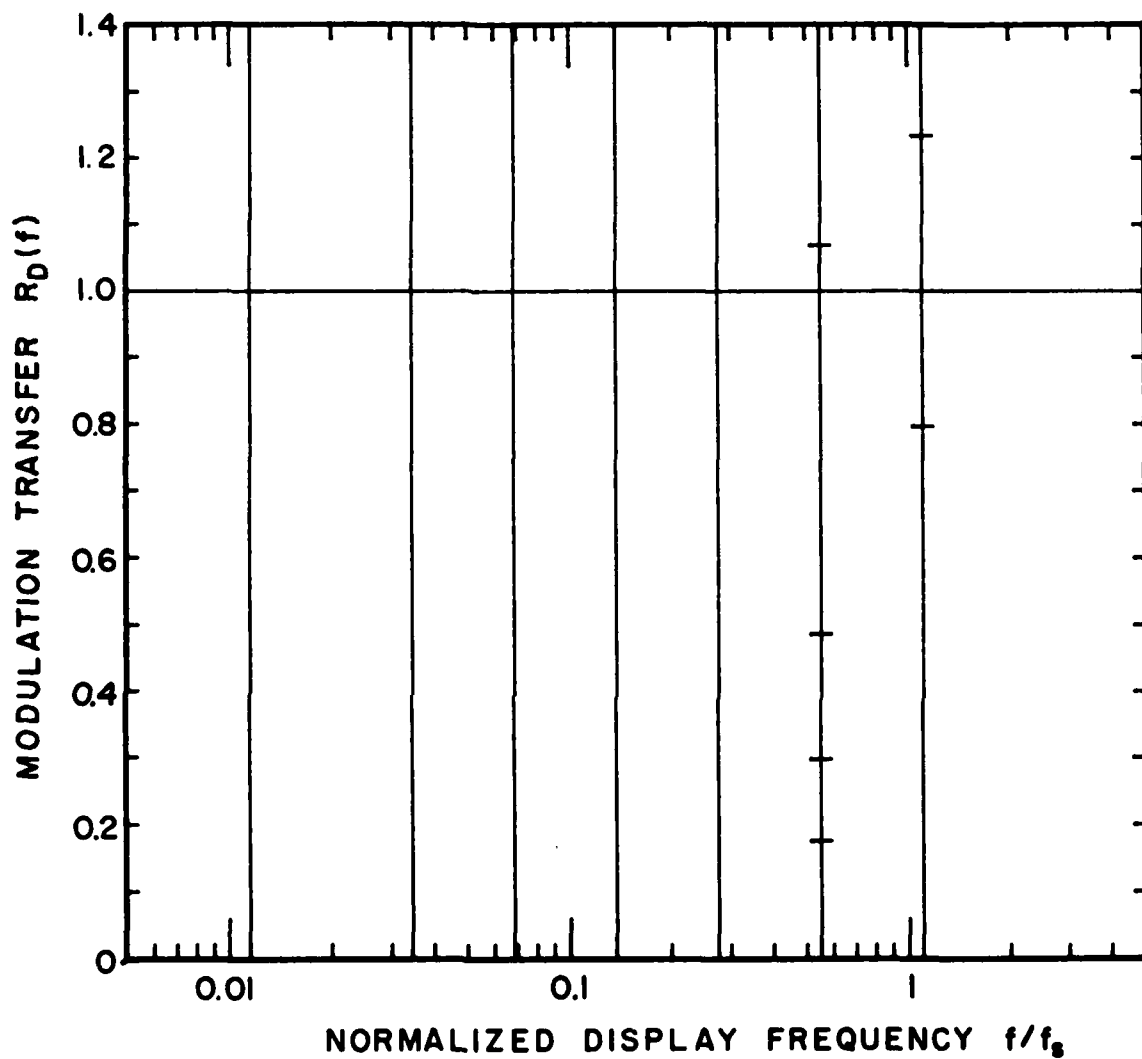
Figure 116. DDD No. 99. Discriminable Difference Diagram for noise
levels due to sampling on a sampled/raster display: No
prefilter, s = 1, $N_s r/w$ = 2500.

153
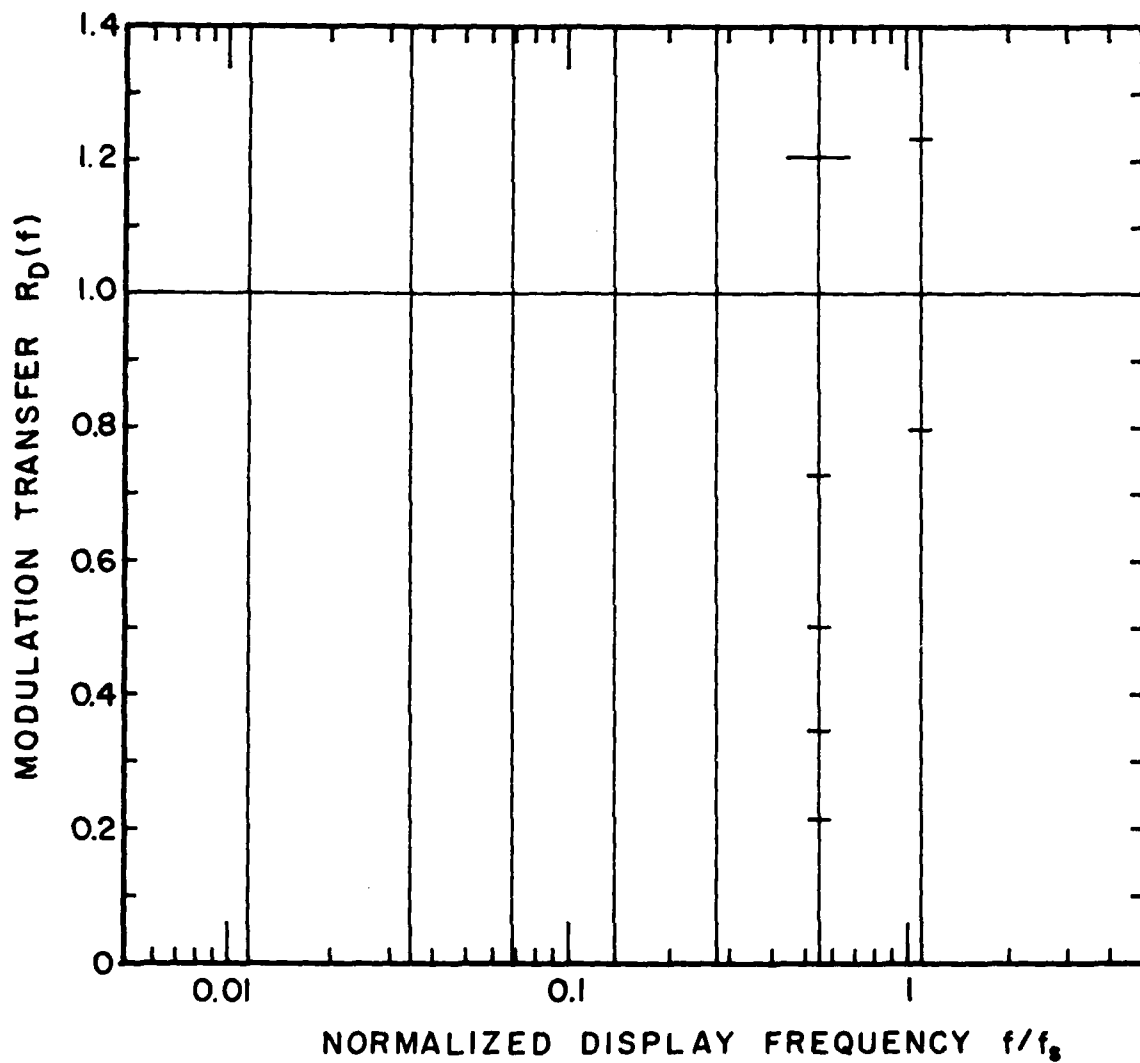
Figure 117. DDD No. 100. Discriminable Difference Diagram for noise
levels due to sampling on a sampled/raster display:
Nyquist prefilter, s = 1, $N_s r/w$ = 2500.

MODEL EMPLOYED FOR THE COMPUTATION OF DISCRIMINABLE DIFFERENCE DIAGRAMS

A. INTRODUCTION

In this section we outline those features of the display-observer system that are necessary to compute the Discriminable Difference Diagrams given in Section III. It will be seen that the core of this analysis is the quadratic detection model used to approximate detection processes in the visual system. The basic statement of this model is as follows: For a luminance change to be seen with a given probability, the change in the spatial sum of the square of the luminance signal, contained within relatively narrow bands of spatial frequencies, must be equal to a constant fraction of the interfering noise terms. Although, to our knowledge, this is the first application of a model of this type to the visual system, similar "energy detection" models have been used successfully to describe detection processes in audition [11].

In its simplest form the visual signal-detection model proposed here consists of four parts: a spatial frequency filtering element, various noise sources, a square-law device, and a spatial integrator. (1) The motivation for the filtering element is provided by the concept of independent frequency-specific channels* in the visual system [12]. It is argued that an arbitrary scene will first be decomposed by the visual system into relatively narrow, contiguous bands of spectral information. (2) Within each of the frequency-specific channels, there exist two distinct sources of visual noise that interfere with the perception of a signal. The first is physically identified as the "background" noise that sets the ultimate sensitivity of the visual system, while the second is a noise term proportional to the signal level, which gives a Weber's law-like behavior at high signal levels. (3) The motivation for the square-law element at the output of each frequency-specific channel is provided by our interpretation of basic contrast-detection experiments given here and in TR3. Although these experiments suggest a power function within each channel with exponent greater than unity, the actual choice of a square law is motivated, in part, by its mathematical simplicity. Nevertheless, it will be demonstrated that more complicated expressions are not

---

*In audition they are referred to as "critical bands" of temporal frequencies.

presently warranted. (4) Finally, the purpose of the spatial integrator is simply to sum the squared output from each channel.

In the succeeding paragraphs each of these elements will be described in detail and the expressions that relate them to the appropriate display variables will be given. Finally, the results of several experiments, which have been performed to test the validity of the model, will be presented. It will be shown that for the cases investigated, the model is in good agreement with the empirical results.

B. QUADRATIC SIGNAL-DETECTION MODEL

The general concepts of the signal-detection model will first be established by applying the model to the problem of predicting a just-noticeable difference (jnd) in contrast of a simple one-dimensional luminance sine-wave grating. It is shown that this relatively simple experiment not only verifies the functional correctness of the model, but also fixes two of the parameters in the model. Second, the model will then be generalized to predict a jnd in image contrast, or structure, for scenes with more complicated spectra. Later, in Section IV.H, the predictions of the model will be compared with measurements made with a wide range of different scenes.

1. Discrimination of Changes in Sine-Wave Grating Contrast

Consider the simple luminance pattern given by

$$I(x) = \overline{I}[1 + m_o \cos(2\pi f x)] \tag{17}$$

where $\overline{I}$ is the mean luminance on the display, m_o is the contrast of the grating,* f is the spatial frequency on the display, and x is the physical coordinate across the display. If an observer views this pattern from a distance r, the retinal frequency ν, in cycles/degree, seen by the observer is

$$\nu = \pi r f / 180 \tag{18}$$

---

*Note that m is equivalent to the conventional definition of contrast given by $(I_{max} - I_{min})/(I_{max} + I_{min})$.

156

Now, we ask the following question: For this stimulus, what change in contrast $\Delta m(\nu)$, from the initial starting contrast $m_o(\nu)$, is necessary so that an observer can see that change with a specified rate of accuracy? This question is empirically answered by the results of Nachmias and Sansbury [13].* Their data, at one spatial frequency (3 cycles/degree), are shown in Fig. 118 along with the predicted curve, which will be explained shortly. Consider first the case where the initial contrast $m(3)$ is zero: By definition, $\Delta m(3)$ is equal to the contrast $m_T(3)$ required for threshold detection of the grating. When $m_T(\nu)$ is measured at spatial frequencies throughout the bandpass of the visual system, it is commonly referred to as a contrast-sensitivity function. Such display attributes as mean luminance and angular size are included in the model through this function. Second, when the initial contrast is greater than zero, it may be seen that $\Delta m(3)$ first decreases from its initial value [i.e., $\Delta m(3) = m_T(3)$], goes through a minimum, and eventually approaches a Weber's law characteristic at high values of initial contrast where $\Delta m(3)$ is roughly proportional to $m_o(3)$.

We now show that the measured results given in Fig. 118 can be accounted for by a simple square-law detection model. The need for a power greater than unity to account for the initial decrease in $\Delta m(\nu)$ has been discussed previously [14,15] but, to our knowledge, has not been applied to an analysis of the results of the measurements of the jnd in contrast. Following the discussion in TR3, we assume that the relevant psychophysical stimulus in the sine-wave discrimination experiments is the change δI^2 in the mean-square luminance of the gratings.** Therefore, if the initial contrast of the sinusoid

---

*The authors define the jnd in contrast, $\Delta m(\nu)$, to be that change required to obtain a 79.4% correct response in a forced-choice experiment. Everywhere else in this report the jnd is defined at the 75% point.
**The physical power (or, where appropriate, energy) of a stimulus should not be confused with its information theory equivalent. It happens that in audition these quantities can be the same, but in the visual model proposed here they are not. Specifically, the luminance variations of an image (which are proportional to physical power) correspond to signal amplitude; the square of this quantity (which has no direct physical meaning) corresponds to signal power.
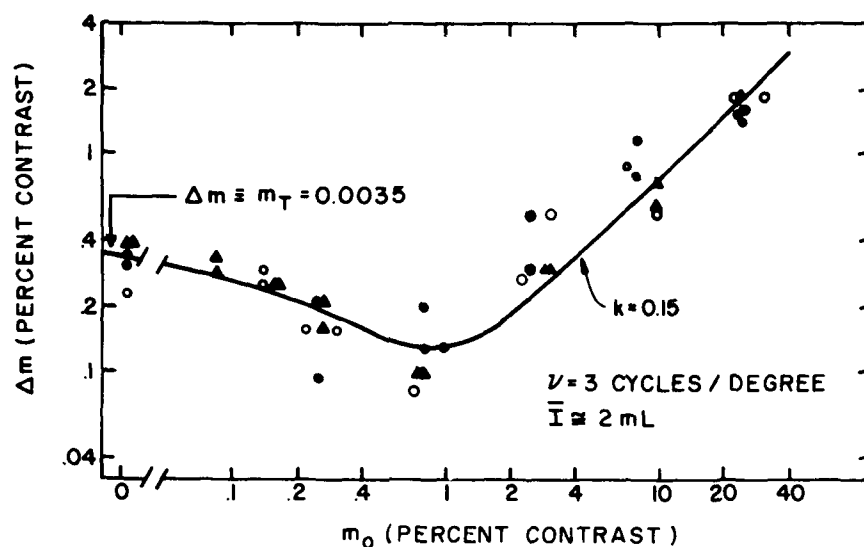
Figure 118. Required increase Δm in contrast of a 3-cycle/degree grating for 1 jnd as a function of the starting contrast m_0. The data points are taken from the experiments of Nachmias and Sansbury [13]. Different symbols represent different observers. The solid curve is the theoretical fit to the experimental points, based on the indicated values of the threshold contrast m_T and the fraction k. One jnd is defined here as a 79% correct response in a two-alternative forced-choice experiment.

is $m_0(\nu)$ and if this contrast is changed to $[m_0(\nu) + \Delta m(\nu)]$, then the change in the mean-square luminance is

$$\delta I^2 = \tfrac{1}{2}[m_0(\nu) + \Delta m(\nu)]^2 \bar{I}^2 R_\nu^2(\nu) + \tfrac{1}{2} m_0^2(\nu)\bar{I}^2 R_\nu^2(\nu) \qquad (19)$$

where $R_\nu(\nu)$ is the value of the physical MTF* of the visual system.

Equation (19) represents the perceived signal. However, in order for this signal to be seen with a given probability, we assume that it must be equal to a constant fraction of an interfering noise term. In general, the interfering signal consists of the sum of the contributions from visual noise,

---

*$R_\nu(\nu)$ includes both the effects of the physical optics of the eye and the sampling processes of the retinal mosaic.

random display noise, and the initial value of the mean-square luminance, but for the contrast discrimination experiments of Nachmias and Sansbury we assume that the display noise is zero. Therefore, the condition for the detection of a change in the contrast of the sinusoid is

$$\delta I^2 = k(\nu)[N_\nu(\nu)\Delta\nu + \tfrac{1}{2} m_o^2(\nu)\overline{I}^2 R_\nu^2(\nu)] \qquad (20)$$

where $k(\nu)$ is a constant fraction at each ν, $N_\nu(\nu)$ is the visual-noise spectral power per unit retinal frequency, and $\Delta\nu$ is the width of the spatial-frequency-specific channel centered about frequency ν [12] (the properties of these channels will be discussed shortly).

Now, since $\Delta m(\nu) \equiv m_T(\nu)$ when $m_o(\nu) = 0$, we can combine Eqs. (19) and (20) to give

$$m_T^2(\nu) = 2k(\nu)N_\nu(\nu)\Delta\nu/\overline{I}^2 R_\nu^2(\nu) \qquad (21)$$

Equation (21) relates the visual noise term $N_\nu(\nu)$ to the sine-wave contrast sensitivity function $m_T(\nu)$, a quantity that has been measured extensively (see Section IV.C.1). Finally, using Eq. (21) and solving Eqs. (19) and (20) for $\Delta m(\nu)$ we find that

$$\Delta m(\nu) = [(1 + k(\nu))m_o^2(\nu) + m_T^2(\nu)]^{1/2} - m_o(\nu) \qquad (22)$$

The parameter $k(\nu)$ can be determined from the measured results of Fig. 118. (Because of the importance of both $m_T(\nu)$ and $k(\nu)$ in the model, their properties are presented in detail in Section IV.C.)

We have plotted Eq. (22) on Fig. 118 with $k(3) = 0.15$ and $m_T(3) = 0.0035$. It may be seen that the theoretical curve is in good agreement with the experimental results.

For the case of small initial contrast, $m_o^2(\nu) \ll m_T^2(\nu)$, Eq. (22) reduces to $\Delta m(\nu) = m_T(\nu) - m_o(\nu)$, thereby predicting an initial decrease in observer discriminability as $m_o(\nu)$ is increased from zero. On the other hand, for the case of large initial contrast, $m_o^2(\nu) \gg m_T^2(\nu)$, Eq. (22) becomes $\Delta m(\nu) = [(1 + k(\nu))^{1/2} - 1] m_o(\nu)$, indicating a Weber's law behavior. As mentioned earlier, an analysis based on a linear detection model is incapable of

159

reproducing the observed initial decrease of $\Delta m(\nu)$. However, models based on powers higher than 2 can also predict the initial decrease in $\Delta m(\nu)$. Furthermore, the results of more recent and more detailed sine-wave contrast detection experiments [16,17] indicate that a power greater than 2 (but not greater than 4.0) gives a better fit to the experimental results. The effect of higher powers is to make the minimum in $\Delta m(\nu)$ somewhat smaller and to move the location of the minimum to a slightly lower value of $m_o(\nu)$. Mathematically, higher powers tend to increase the range of $m_o(\nu)$ over which the approximation $\Delta m(\nu) = m_T(\nu) - m_o(\nu)$ is valid. Powers greater than 2 need not, however, modify the predictions in the Weber's law regime. Finally, it has been experimentally determined that for $m_o^2(\nu) \gg m_T^2(\nu)$, the slope of $\Delta m(\nu)$ versus $m_o(\nu)$ is 1.0, as predicted by a Weber's law characteristic, only for spatial frequencies near 10 cycles/degree [17]. It will be shown in Section IV.C that for spatial frequencies less than 10 cycles/degree the slope is less than 1.0, and for higher spatial frequencies it is slightly greater than 1.0. However, it is felt that neither the use of power laws greater than two nor the correction of the Weber's law slope at different spatial frequencies is warranted for the purposes of this report. As Fig. 118 demonstrates, and as we will show later with more complicated stimuli, the success of the square-law, linear-slope Weber's law model in predicting answers to questions of interest justifies the use of this model.

2. Discrimination Model for Complex Scenes

Actual scenes, whether they be graphic, alphanumeric, or pictorial, have luminance spectra that are substantially more complicated than the sine-wave grating considered in the last section. Nevertheless, the quadratic signal-detection model can be easily formulated to apply to these scenes by invoking the concept of frequency-specific channels in the visual system [12]. This concept states that the visual system performs a primitive Fourier-like decomposition of a spectrally complex scene by partitioning the spectra into relatively narrow, adjacent bands of information. Each channel, or band of frequencies, is centered about a retinal frequency ν and has a bandwidth $\Delta\nu$, although the locations of the channels are not fixed at specific frequencies. Additionally we will assume that luminance information falling within a channel is processed independently of information falling within any other channel.

160

Although the degree of independence of the channels is still an area of active research, this approximation presently appears to be reasonable [18]. Also, neither the exact width nor the functional dependence of $\Delta\nu$ with contrast is well characterized, but for $\nu > 1.5$ cycles/degree, $\Delta\nu/\nu = 2/3$ represents a good estimate [19]. The actual values of $\Delta\nu$ used to compute the DDDs are given in Table 11.*

With the concept of independent frequency-specific channels in the visual system, the analysis of the previous section can be easily generalized to spectrally complex scenes. If $\Phi_i(f)$ and $\Phi_f(f)$ are, respectively, the initial and final perceived power spectra of the scenes under investigation (see Appendix A), then for the detection of this change within a channel ν of width $\Delta\nu$ we have

$$R_\nu^2(\nu)\left[\Phi_f(f) - \Phi_i(f)\right]\left(\frac{180\Delta\nu}{\pi r}\right) = k(\nu)\left[N_\nu(\nu)\Delta\nu + R_\nu^2(\nu)\Phi_i(f)\left(\frac{180\Delta\nu}{\pi r}\right)\right] \qquad (23)$$

where, as before, $R_\nu(\nu)$ is the physical MTF of the visual system, $N_\nu(\nu)$ is the visual-noise spectral power per unit retinal frequency, and $k(\nu)$ is the same proportionality constant that appears in Eq. (20). The quantities $\Phi_i(f)$ and $\Phi_f(f)$ are, in general, the sum of the signal and noise power spectra, as determined on the display screen. The frequency on the display f is related to the retinal frequency ν, in cycles/degree, through $f = 180\nu/\pi r$. Although Eq. (23) only applies to one-dimensional luminance patterns, the generalization to two dimensions is straightforward, as outlined in Section IV.G.

Equation (23) can be expressed in a more convenient form by writing the power spectra $\Phi_i(f)$ and $\Phi_f(f)$ in terms of an equivalent sine-wave contrast. Specifically, the quantity $\Phi_{i,f}(f)(180\Delta\nu/\pi r)$ can be replaced by the power associated with a single sine-wave grating of frequency f and equivalent contrast $m_{i,f}(f)$. Mathematically,

$$\tfrac{1}{2}m_{i,f}^2(f)\overline{I}^2 = \Phi_{i,f}(f)\ (180\Delta\nu/\pi r) \qquad (24)$$

---

*Table 11 is located in Section IV.E, page 184.

161

where the left-hand side of this equation is the mean-square signal power of a sine-wave grating of contrast $m_{i,f}(f)$. Then, using Eqs. (21) and (24), Eq. (23) can be rewritten as

$$m_f^2(\nu) - m_i^2(\nu) = m_T^2(\nu) + k(\nu)m_i^2(\nu) \tag{25}$$

where $m_f(\nu)$ and $m_i(\nu)$ are, respectively, the final and initial equivalent sine-wave contrasts of the displayed signal falling within the frequency-specific channel centered about ν.

Equation (25) is the form of the contrast-discrimination model that will be used throughout this report. Consider, as an example of its application, the contrast detection experiment described in the previous section, performed with a single frequency sine-wave grating. Here $m_f(\nu) = m_o(\nu) + \Delta m(\nu)$ and $m_i(\nu) = m_o(\nu)$. For this case Eq. (25) easily reduces to Eq. (22), as expected.

3. Equivalent Sine-Wave Contrasts for Signals and Noise

With the simplification of the model afforded by the definition of the equivalent contrast, the problem of applying the model is shifted to the calculation of the equivalent contrasts for various cases of interest. The method employed is to compute the spatial frequency spectrum of the "spatially summed power." The spatially summed power is defined as the spatial integral of the square of the luminance profile on the display screen. The integration is performed over a characteristic length $\ell(f)$, which represents the length over which the visual system can sum spectral information at a given spatial frequency. In a crude sense it reflects the fact that humans can only process luminance information displayed over a finite visual angle. It has been shown* [20] that $\ell(f)$ can be approximated by

$$\ell(f) = 14/f \tag{26}$$

for $\pi r f/180 \gtrsim 1$ cycle/degree.

The equivalent contrasts for various power spectra are derived in Appendix A. In Appendix B, the equivalent contrasts for the signal and noise components of an edge transition displayed on a sampled/raster display are calculated.

---

*The experiments used to determine $\ell(f)$ were performed with sine-wave gratings at threshold. It is not presently known if Eq. (26) varies with grating contrast.

162

In this section, we summarize the results of Appendix A. The perceptual significance of the various power spectra in actual scenes is discussed in Section IV.D.

a. *One-Dimensional Luminance Edge Transition* - A particular input "scene" of importance in this report is a one-dimensional luminance edge transition, as shown in Fig. 119. From Eq. (A-14) the equivalent sine-wave contrast for this pattern is

$$m_E^2(\nu) = \frac{1}{14\pi^2}\left(\frac{\Delta I}{\bar{I}}\right)^2\left(\frac{\Delta\nu}{\nu}\right) \tag{27}$$

where ΔI is the luminance edge height, $\bar{I}$ is the average display luminance, $\Delta\nu$ is the frequency-specific channel bandwidth, and ν is the center frequency of the channel. When $\nu \geq 1.5$ cycles/degree, $\Delta\nu/\nu = 2/3$, and when $\nu \leq 1.5$ cycles/degree, $\Delta\nu = 1$ cycle/degree (see Table 11).

DISTANCE ACROSS DISPLAY

$$\text{CONTRAST} = \frac{I_{max} - I_{min}}{I_{max} + I_{min}}$$
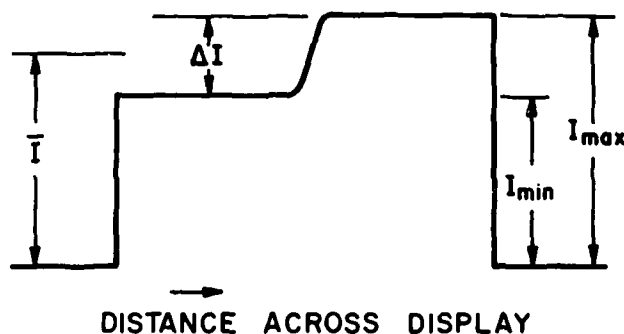
Figure 119.   Definition of the contrast of a one-dimensional luminance edge transition.

b. *Ensemble-Averaged Pictorial Information Input* - A second equivalent sine-wave contrast, $m_P(\nu)$, is obtained from the ensemble-averaged power spectra of a large number of pictorial scenes. We find from Eq. (A-15)[*]

---

[*]We have assumed here that $f^2 \gg f_L^2$ and that $f_L = 1/w$ (from Section IV.D.1).

163

$$m_P^2(\nu) = \frac{1}{45} \frac{\overline{I_m^2}}{\overline{I}^2} \left(\frac{r}{w}\right) \left(\frac{\Delta\nu}{\nu}\right) \left(\frac{1}{\nu}\right) \tag{28}$$

where r is the viewing distance, w is the width of the display, and $\sqrt{\overline{I_m^2}/\overline{I}}$ is the normalized rms luminance modulation depth of the images. We take $\sqrt{\overline{I_m^2}/\overline{I}} = 1/2$ in this report (see Section IV.D).

c. White Noise - For analog displays the noise added to the displayed images is assumed to be white.* Therefore, from Eqs. (A-10) and (A-16) we have for the equivalent sine-wave contrast for white noise

$$m_N^2(\nu) = \frac{N(f)}{\overline{I}^2} \left(\frac{360\Delta\nu}{\pi r}\right) \tag{29}$$

where N(f) is the noise power spectrum with units of mean-square luminance per cycle per cm. N(f) is related to the mean-square noise fluctuation N^2 on a display through Eq. (1).

4. Number of Distinguishable Contrast Levels

Equation (25) can be employed, as outlined in Appendix E, to predict the total number J(ν) of distinguishable contrast levels that can be seen at any retinal frequency when the contrast of a sinusoid is progressively increased from zero to a specified final value. For the specific case of interest here, where a spectrally complex scene with additive noise is presented on a display with MTF R(f), the total number of distinguishable contrast levels is

$$J_{S,N}(\nu) = \frac{\ell n \left[1 + \dfrac{k(\nu)m_{S,N}^2(\nu)R^2(180\nu/\pi r)}{m_T^2(\nu) + k(\nu)m_I^2(\nu)R^2(180\nu/\pi r)}\right]}{\ell n \left(1 + k(\nu)\right)} \tag{30}$$

where $m_{S,N}(\nu)$ represents the equivalent sine-wave contrasts for either the signal, $m_S(\nu)$, or noise, $m_N(\nu)$, respectively, and where $m_I(\nu)$ represents

---

*For sampled/raster displays the sampling process produces other noise terms. See Section II.C.

the equivalent sine-wave contrast for any additional signals on the display, the presence of which will interfere with the perception of $m_{S,N}(\nu)$.

As an example of the appropriate equivalent sine-wave contrasts, $m_{S,N}(\nu)$ and $m_I(\nu)$, that go into Eq. (30), consider the problem illustrated in the DDDs, of white noise added to a one-dimensional edge transition on an analog display. For this problem the number of discriminable noise levels $J_N(\nu)$ is predicted from Eq. (30) when $m_N(\nu)$ is given by Eq. (29) and when $m_I(\nu) = m_E(\nu)$ is given by Eq. (27).

In Fig. 120 we illustrate the use of Eq. (30) by plotting $J(\nu)$ as a function of ν for three cases of interest in this report: (1) for simple sine-wave gratings of 100% contrast (i.e., $m_S(\nu) = 1.0$), (2) for a one-dimensional luminance edge transition of 100% contrast [Eq. (27) with $\Delta I/\bar{I} = 2.0$], and (3) for random input pictorial information [Eq. (28) with $\sqrt{\overline{I_m^2}}/\bar{I} = 1/2$ and $r/w = 3.0$]. The required values of $m_T(\nu)$, $k(\nu)$, and $\Delta\nu/\nu$ were obtained from Table 11, assuming $\bar{I} = 35$ mL. In addition, we have taken $R(f) = 1.0$ and $m_I(\nu) = 0$. Thus, the values given in Fig. 120 represent the maximum number of discriminable contrast levels at each ν that can be seen for each case, each level being perceived with a 75% accuracy. These values may be compared with the values given in the DDDs when the assumptions given above are not made.

First, consider the predicted results for the 100% contrast sine-wave grating input. The number of distinguishable levels for this case represents the maximum that can be seen for any input. Thus, these values represent a standard by which the number of distinguishable levels produced by other inputs can be compared. The peak in $J(\nu)$ versus ν of 82 levels at roughly 1.5 cycles/degree is due primarily** to the minimum in the contrast sensitivity function $m_T(\nu)$ near this frequency, as shown in Fig. 122. Note that this peak value of $J(\nu)$ is roughly 7 times less than the number of discriminable levels predicted (incorrectly) by simply taking the reciprocal of the contrast sensitivity function at this retinal frequency (i.e., $1/m_T(1.5) \approx 600$). Second, for the one-dimensional edge input, the functional form of $J(\nu)$ versus ν is

---

*Table 12 is located in Section IV.E.
**$k(\nu)$ is slowly varying with ν, as shown in Table 11.
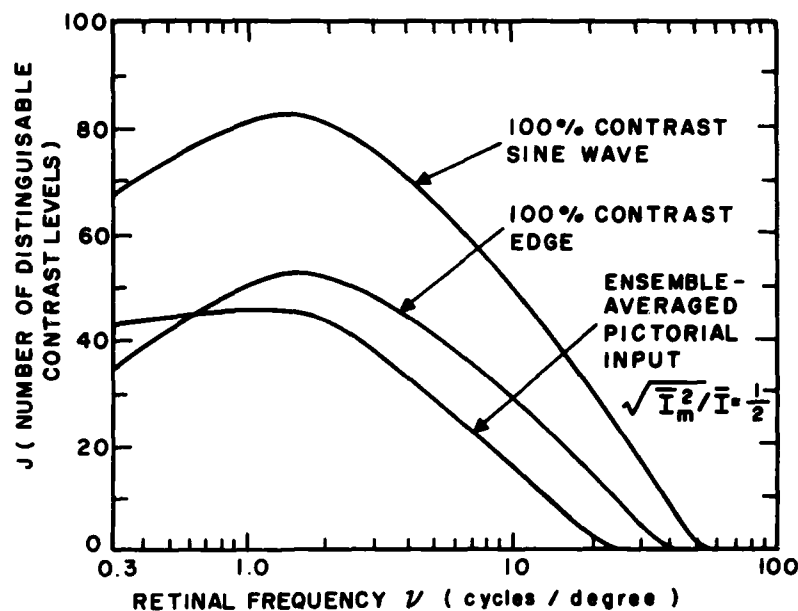
Figure 120. Computed number of distinguishable contrast levels as a
function of retinal frequency ν on a noise-free display
for three conditions: (1) a grating of 100% contrast,
(2) a 100% contrast luminance edge input, and (3) an
ensemble-averaged pictorial input.

similar to that of the sine-wave input, although the number of levels at each
retinal frequency is reduced. This functional similarity is due, once again,
to the $m_T(\nu)$ term in Eq. (30). Third, for the ensemble-averaged pictorial
input, the distribution of $J(\nu)$ versus ν is functionally different from the two
previous cases. At higher frequencies $J(\nu)$ rolls off more quickly, and at lower
frequencies $J(\nu)$ is more slowly varying. These properties are a result of the
$1/\nu$ term in Eq. (28).

We close this section with two additional expressions that can be derived
from Eq. (30). First, we give the fundamental equation that was used in
plotting the DDDs of Section III. This equation predicts the display MTF
$R_J(180\nu/\pi r)$ required to discriminate $J(\nu)$ contrast levels in the frequency-
specific channel centered about frequency ν. We have

$$R_J^2(180\nu/\pi r) = \frac{m_T^2(\nu)\left[\left(1 + k(\nu)\right)^J - 1\right]}{k(\nu)\left\{m_{S,N}^2(\nu) - m_T^2(\nu)\left[\left(1 + k(\nu)\right)^J - 1\right]\right\}} \tag{31}$$

166

where the variables all retain their earlier definitions. Second, the change in modulation transfer $\Delta R_J(180\nu/\pi r)$ necessary to produce one additional discriminable difference (i.e., 1 jnd) in the perceived luminance structure is determined from Eq. (31) with the following definition:

$$\Delta R_J(180\nu/\pi r) = R_{J+1}(180\nu/\pi r) - R_J(180\nu/\pi r) \qquad (32)$$

C. MODEL PARAMETERS $m_T(\nu)$ AND $k(\nu)$

The properties of the contrast-detection model parameters $m_T(\nu)$ and $k(\nu)$ are discussed in this section. It is through these parameters that the effects of selected display variables, such as mean display luminance and display size, are included in the model. In Table 11 are given the values of the parameters used in this report.

1. Sine-Wave Threshold Contrast Sensitivity $m_T(\nu)$

The parameter that determines the minimum contrast object that can be seen is the sine-wave threshold contrast-sensitivity function, $m_T(\nu)$. This quantity can be interpreted as representing an overall visual noise term that establishes the threshold of perception for sine-wave gratings, as shown in Eq. (23). Although it is possible to measure $m_T(\nu)$ under conditions where its value is determined solely by visual noise sources, such as those associated with photo-chemical conversion and neural processing, it is more typical for $m_T(\nu)$ to be measured under conditions where both visual and display noise sources are present, such as photon shot noise or the interfering "noise" associated with differences in display and surround luminance. This means that, for modeling purposes, we may consider the measured values of $m_T(\nu)$ as representing a parameter that includes the perceptual effects due to selected display and environmental variables. This approach, as contrasted with one that attempts to include separate terms in the model for each display variable (see, for example, Section V.C of TR3 and, for a different approach, ref. 21), greatly simplifies the model and guarantees that it will have maximum precision.

Since the first sine-wave contrast sensitivity measurements by Schade in 1956 [22], the properties of $m_T(\nu)$ have been extensively studied. It has been found that the contrast sensitivity function depends on many variables. They

167

include: mean display luminance [23], display size [TR2,20,24,25], retinal position [26], temporal modulation characteristics [27], drift rate [28], presentation time [29], surround luminance [TR2, 24], orientation [30], monocular versus binocular vision [31], pupil size [32], and experimental procedure [33]. However, $m_T(\nu)$ is remarkably constant from person to person if the viewing conditions are held constant [TR2]. Thus, although the details surrounding $m_T(\nu)$ are complicated, the last result indicates that $m_T(\nu)$ may indeed be considered a fundamental property of the visual system.

For the case of an observer looking at a display under normal viewing conditions, many of the aforementioned variables are not important. For example, we will only consider displays viewed foveally with binocular vision and natural pupils. Further, we will assume that $m_T(\nu)$ is isotropic,* that differences between the display luminance and the surround luminance are moderate,** and that all displayed images vary slowly with time.† Of these assumptions all but the last represent small changes in the predictions of the model, which, in any case, are easily included in the model. Even the quasi-static approximation is generally satisfied when applied to display *information*. It is only for time-varying display *noise* that this assumption is suspect. For time-varying noise, which is the dominant interfering signal in many display systems, such as commercial television, the visibility of the noise can be a strong function of both its temporal and spatial properties. In Appendix C this issue is briefly discussed with regard to pictorial information on a display.

As indicated, it is possible to represent selected display variables in the contrast-detection model through the contrast-sensitivity function, $m_T(\nu)$. In the DDDs of Section III we have done this for two display parameters: mean display luminance and display size. The values of $m_T(\nu)$ used to represent these cases are composites of data obtained from several sources. Although the relative accuracy of the values given is felt to be quite good (roughly ±20%), the absolute values of $m_T(\nu)$ can be expected to vary (roughly +100% to -20%) depending on the viewing conditions.

---

*For gratings running horizontally or vertically, $m_T(\nu)$ is roughly 50% less than for gratings running along the diagonals [30].
**For displays larger than roughly 2.0 degrees in diameter, contrast sensitivity varies slowly as long as the ratio of the mean display to mean surround luminance is between 10:1 and 1:5 [TR2].
†Approximately of the order of 0.1 second or longer [27].

In Fig. 121 we show, for a display 10 degrees in diameter, plots of $m_T(\nu)$ versus ν for the two mean luminances used in this report: 1 and 35 mL. Also shown on this figure, as a dotted line, is the maximum additional improvement in contrast sensitivity that occurs for even brighter displays. It may be seen that the improvement is relatively small. The 35-mL mean display luminance was selected because it is representative of values obtained on current high-quality displays, such as small-screen ($\leq$25-in.) home television. The 1-mL value represents the minimum practical luminance that can be used for reasonable quality pictorial displays, such as large-screen ($\sim$50-in.) television projection systems. For comparison we note that typical movie theaters [8] and better quality projection television systems* have mean display luminances between 5 and 15 mL.
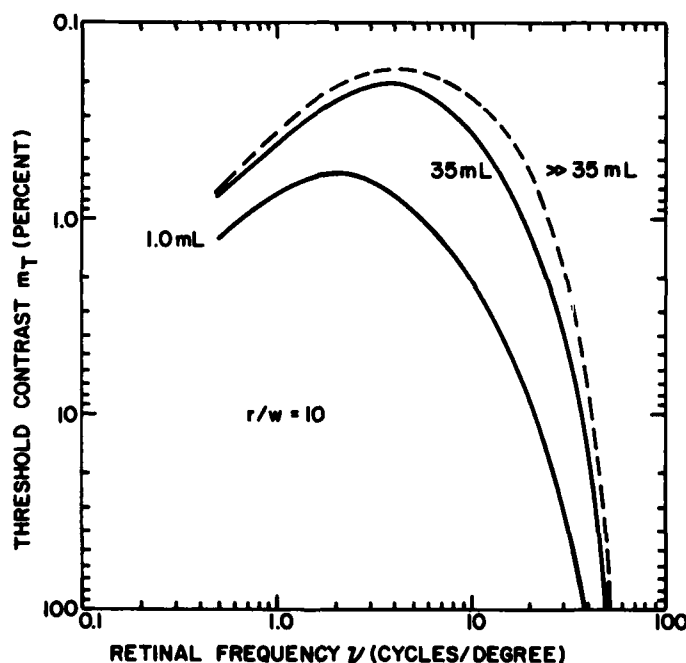
Figure 121. The solid curves show the sine-wave threshold contrast m_T as a function of retinal frequency ν for the two luminances of interest in this report: 1 and 35 mL. The dotted line shows, approximately, the decrease in m_T expected for even brighter displays. All the results given are for ratios of viewing distance r to display width w of 10. These curves reflect the experimental results of refs. 20 and 23.

*These results were obtained from measurements of the output screen luminance on a Matsushita Model TH6000 projection television, which was driven by a Model TV60 receiver.

169

Figure 122 shows the effect of angular display size on contrast sensitivity [TR2] for horizontal-running (see the inset on the figure) sine-wave gratings at a mean display luminance of 35 mL.* The results given as the solid lines are for the three ratios of viewing distance r to display width w used in this report: r/w = 3, 10, and 30. It may be seen that the primary effect of reducing display size is to reduce contrast sensitivity at the lowest spatial frequencies. This result is actually a consequence of the fact that, for spatial frequencies above approximately 0.3 cycle/degree, maximum contrast sensitivity is obtained when the display field contains roughly 14 cycles at any frequency. When the number of cycles is reduced from this value, which happens first at the lowest spatial frequencies for the smaller display sizes, contrast sensitivity is reduced [TR2,20,24,25]. Finally, it is also shown in Fig. 122 that for values of r/w less than 3, there is essentially no additional improvement in contrast sensitivity.

2. Weber's Fraction $k(\nu)$

The value of the proportionality constant $k(\nu)$, which sets the perceived signal-to-noise ratio in the contrast detection model [Eq. (25)], is obtained from the results of contrast discrimination experiments in the regime where $m_o(\nu) \gg m_T(\nu)$. With this restriction Eq. (22) can be solved to give $k(\nu) = [\Delta m(\nu)/m_o(\nu) + 1]^2 - 1$, which simplifies to $k(\nu) \simeq 2\Delta m(\nu)/m_o(\nu)$ for $\Delta m(\nu)/m_o(\nu) \ll 1.0$.

In Fig. 123 we show the regression line results from sine-wave contrast-discrimination experiments performed to determine $k(\nu)$. The straight-line regressions, computed on log-log coordinates, were fitted to the data in the regime where $m_o(\nu) \gg m_T(\nu)$. The value in parentheses beside each line is the slope of that line. These results were obtained using the apparatus and experimental procedure described in Section IV.H. The mean display luminance was 35 mL and the measured values of $\Delta m(\nu)$ were determined for a 75% correct response in a two-alternative forced-choice experiment.

---

*The extent of a sine-wave grating perpendicular to its periodicity (the vertical direction in the inset of Fig. 122) also influences its visibility. Although this property of $m_T(\nu)$ has not been extensively studied, it has been reported that this dimension must be about 1.0 degree for $m_T(\nu)$ to be a minimum [34, 35].
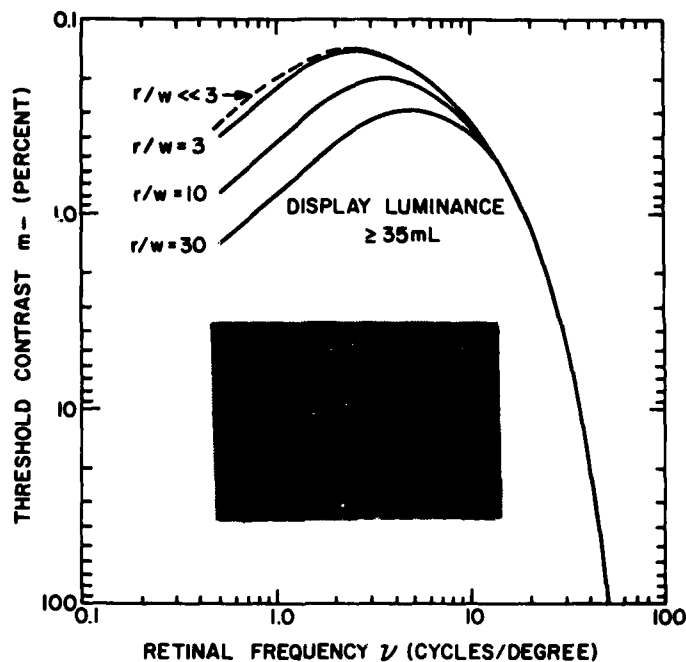
Figure 122.   The solid curves show the sine-wave threshold contrast m_T
as a function of retinal frequency ν for the three ratios
of viewing distances to display width of interest in this
report: r/w = 3, 10, and 30.   The dotted line shows, ap-
proximately, the decrease in m_T expected for even smaller
values of r/w.   All the results given are for mean display
luminances of 35 mL.   These curves reflect the experimental
results of refs. 20 and 28.   The inset shows a horizontal-
running sine-wave grating.

It may be seen from Fig. 123 that the slopes of $\Delta m(\nu)$ versus $m_o(\nu)$ are
not independent of retinal frequency.   Rather, the slope increases from about
0.44 at 0.4 cycle/degree to about 1.1 at 45 cycles/degree.   Only at spatial
frequencies near 12 cycles/degree does the slope approximate 1.0, in accord
with a perfect Weber's law characteristic.   Although the causes of these slope
differences are not presently known, it has been suggested that for spatial
frequencies below 3 cycles/degree, the decrease in slope might be, in part, a
consequence of transient mechanisms that are excited under the experimental
conditions used to perform the experiments [16].

The differences in slope shown in Fig. 123 were not included in the
contrast detection model.   Rather, in order to preserve mathematical simplic-
ity, all slopes were approximated as 1.0.   As Fig. 123 shows, this approxi-
mation is excellent for frequencies greater than roughly 10 cycles/degree.

171
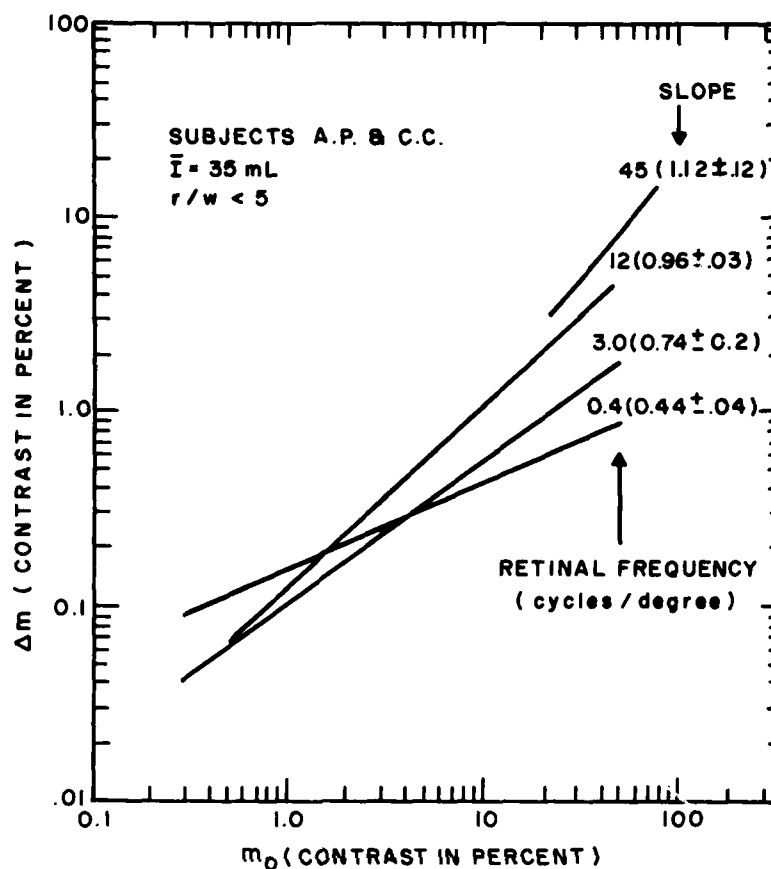
Figure 123. Required increase in sine-wave contrast Δm to produce a 1-jnd change from an initial contrast m_0, as a function of m_0 and with ν as a parameter. The regression lines represent the measured results at 0.4, 3.0, 12, and 45 cycles/degree, as given in ref. 17. One jnd is defined here as a 75% correct response in a two-alternative forced-choice experiment.

For frequencies much less than 10 cycles/degree it can lead to inaccuracies in some situations. However, for almost all practical display problems, the error incurred in approximating the slopes as unity will not be significant since their bandwidths are typically greater than 8 to 10 cycles/degree. The values of $k(\nu)$ used in the model were obtained from Fig. 123 at the approximate midpoints (on a log scale) between $m_o(\nu) = m_T(\nu)$ and 100% contrast. In Fig. 124 these values are plotted as a function of ν, and in Table 11 the values of $k(\nu)$ are given at the key frequency-specific channel locations used in the DDDs.
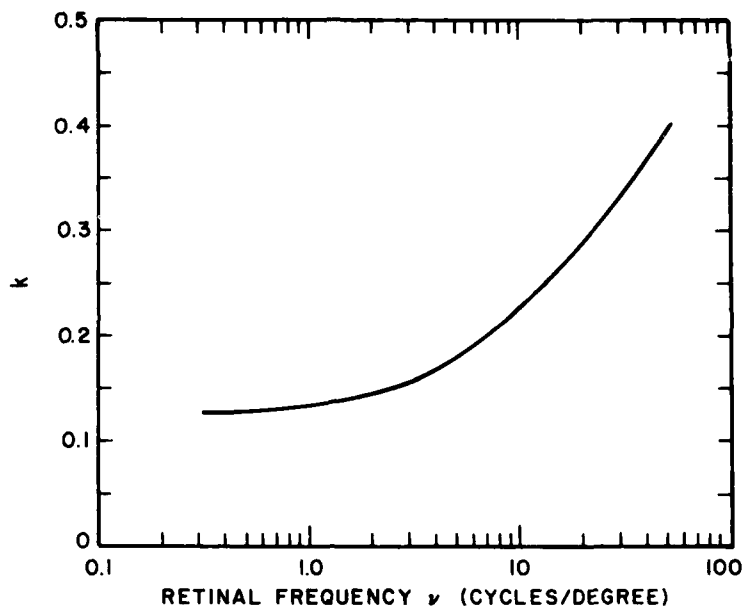
Figure 124. The values of the Weber's fraction k used in this report as a function of retinal frequency ν. These results were taken from Fig. 123 as explained in the test.

The data currently available indicates that $k(\nu)$ is slowly varying with changes in experimental condition and experimental procedure. In the two other studies in which $\Delta m(\nu)$ versus $m_o(\nu)$ was measured, the values obtained were very similar to those given in Fig. 123 [13, 16]. This is true even though there were significant differences in the experimental conditions between the studies. As an example of the constancy of $\Delta m(\nu)$ versus m_o, we show in Fig. 125 the regression lines from measurements at 3 cycles/degree for mean display luminances of 35 and 0.0035 mL. Although the display luminance has been decreased by a factor of 10^4 in going from 35 to 0.0035 mL, $\Delta m(\nu)$ has increased by a factor less than 3 at any value of $m_o(\nu)$. For comparison consider that $m_T(\nu)$ changes by a factor of roughly 40 over this range of luminance [23]. Finally, on the basis of experiments in progress, $k(\nu)$ also appears to be only weakly dependent on display size.

D. SOME PROPERTIES OF IMAGES

Images consist of many distinct features: textures, edges, one- and two-dimensional patterns, subtle shadings, periodic structures, and various

173
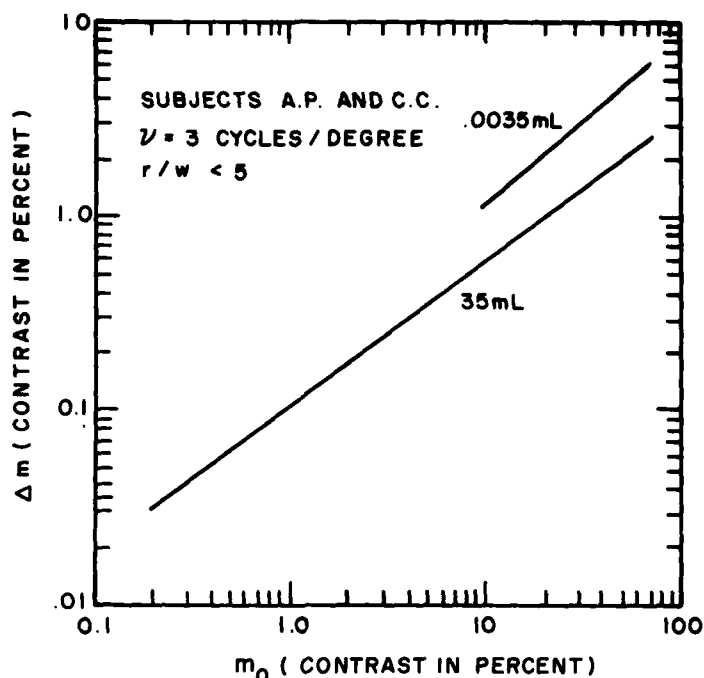
Figure 125. Required increase in sine-wave contrast Δm at 3 cycles/degree to produce a 1-jnd change from an initial contrast m_0, as a function of m_0 and with mean display luminance as a parameter.

length scales, to mention a few. In the previous section a model was developed that has, as one of its primary inputs, the perceived power spectra $\Phi(f)$ for the scenes under investigation. These power spectra must reflect the significant features of the scenes under investigation and, further, for the model to have wide utility, these spectra should apply to a large subset of images. In this section we will show that these objectives can be realized in a consistent fashion.

The emphasis in this section will be on pictorial scenes, but the concepts developed here and in Appendix A are readily generalized to subsets of images that have very different properties. For non-pictorial images such as alphanumerics and map displays, where the luminance information is highly modulated, it will be shown in Section IV.H that the quantities given here give good answers to many questions of interest. For very weakly modulated images, such as some x-ray negatives, the results given here are probably representative in form but not in magnitude. In these cases additional information about

174

their statistical properties is required to obtain the proper value of the scene modulation depth $\sqrt{I_m^2}$.

In the succeeding paragraphs the properties of two power spectra for pictorial scenes will be described. These power spectra can be identified with two distinct perceptual conditions. The first, which we call the power spectrum of pictorial scenes, represents a measure of an observer's overall impression of the displayed information. It is formed from the ensemble-averaged power spectra of a large number of pictorial scenes. The second power spectrum reflects the observation that luminance edges are a significant feature in pictorial images and that these edges are often used in image discrimination tasks. This spectrum will be given by a highly modulated one-dimensional luminance edge transition. In addition to these quantities several other statistical properties of scenes will be presented.

1. Power Spectrum of Pictorial Scenes

In most communications channels, such as commercial television, a unique prediction of the transmitted information is not possible since a fraction of the information is constantly changing in an unpredictable way. For these conditions it is only possible to describe the information in terms of its statistically averaged properties.[*] The quantity that is most important here in the description of the properties of the input information is the ensemble-averaged power spectrum. Because of the importance of this quantity both in the present work and in previous work, we have measured its properties in some detail [TR1 and TR3].

In our previous work [TR1-3], in which we applied the concepts of statistical communications theory to display design problems, the ensemble-averaged power spectrum represented a property of the most likely spectral input to the system. This meaning is retained in the present work, but it is also necessary to ask what meaning this spectra has for an observer looking at a display. Physically, it is the most likely spectrum an observer would see if he weighted equally all points of a large number of images. Thus, in this work it approximates a perceptual condition in which the observer obtains an overall impression of the displayed image. No one feature of the displayed image is given greater perceptual weight than any other feature.

---

[*]We assume here that these statistical properties are stationary [36].

The results of Buswell [37] indicate that the conditions under which we compute the ensemble-averaged power spectrum may be a reasonable approximation of what people see when they look at pictures. He studied the eye fixations and eye motions of many observers looking at a wide range of still pictures. Very roughly, his results show that objects of interest in a picture are visually inspected uniformly. That is, for example, the edges, textures, and uniform luminance areas within, say, a face are given roughly equal numbers of fixations of roughly equal duration. However, as expected, unmodulated areas of an image, such as a uniform background around an object, are given few or no fixations. Nevertheless, since no one distinct perceptual attribute, such as textures or edges, is of dominant interest in looking at pictures, the general functional form of the actual perceived power spectrum should be similar to the physical spectrum we have measured [TR1, 3].

Figure 126 shows a summary of the measured one-dimensional luminance power spectra for 29 different pictorial scenes. In this figure the results are organized into four general categories that reflect, in a rough sense, the amount of detailed structure in the scenes. A striking feature of these results is that, although the images in each classification were chosen for wide differences in their appearance, their measured power spectra are remarkably similar. This conclusion was also found to be true for the individual scenes within each category [Section III, TR3].

It may be seen from Fig. 126 that at high frequencies the power spectra for all the pictorial scenes roll off as [*†] $1/f^2$. The primary influence of increased scene detail is to increase the relative amount of power at high frequencies and to flatten the spectra at the lower spatial frequencies. The low-frequency cutoff f_L, above which the spectra roll off as $1/f^2$, is roughly proportional to the inverse of the dominant length scale of the images under investigation. For off-the-air video we have found $f_L \simeq 1/w$, where w is the width of the display, a result that reflects the dominance on commercial television of single large objects, such as faces [Section II, TR1].

---

*This functional dependence was also measured using an extremely large number of off-the-air commercial television scenes [Section II, TR1].
†Power spectra that roll off as simple power functions are not limited to pictorial scenes. Similar results have been found in many other modalities. For an interesting discussion of similar spectral properties in speech and music, see Voss and Clarke [38].
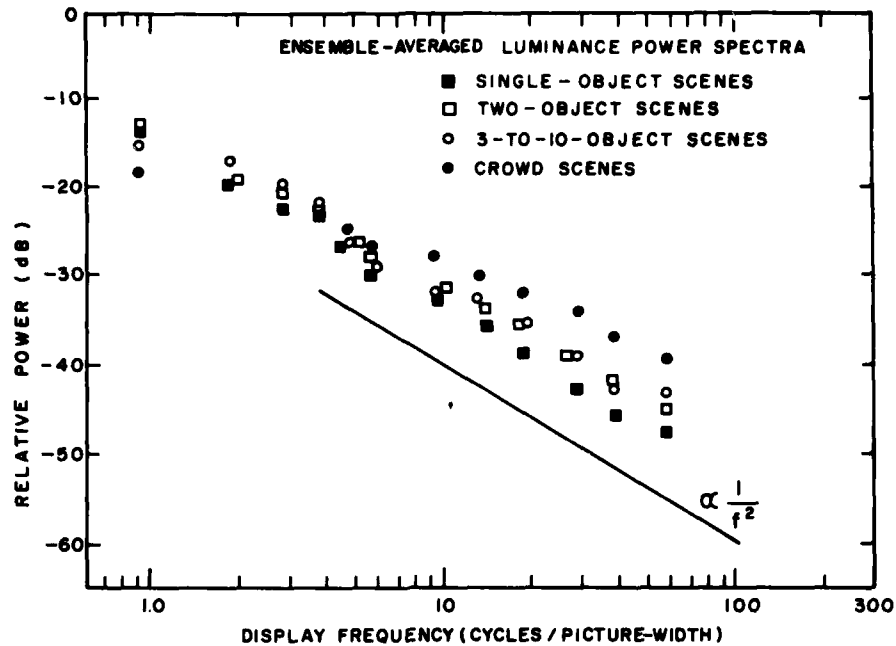
Figure 126. One-dimensional luminance-modulation power spectra obtained from 29 individual scenes. The images have been organized into four categories that reflect the amount of detail in the scenes. At high display frequencies all spectra roll off as $1/f^2$. We represent the one-dimensional luminance patterns in these scenes as $I(x) = \bar{I} + I_m(x)$, where $\bar{I}$ is the average scene luminance and $I_m(x)$ is the pictorial modulation about $\bar{I}$. These power spectra were obtained from the $I_m(x)$ term (TR3).

In Fig. 127 the one-dimensional luminance power spectra for the manikin and crowd scenes of Fig. 128 are shown. These spectra show in somewhat greater detail typical spectral variations between different scenes. They also clearly illustrate the $1/f^2$ rolloff at high spatial frequencies and the low-frequency cutoff f_L below which the spectra begin to flatten.

Mathematically, the spectral properties outlined above are well approximated by a Lorenzian of the form*

$$\Phi(f) = \frac{2}{\pi} \frac{f_L \overline{I_m^2}}{f^2 + f_L^2} \qquad (33)$$

------
*Note that Eq. (33) satisfies the following condition: $\displaystyle\int_0^{\infty} df \Phi(f) = \overline{I_m^2}$.
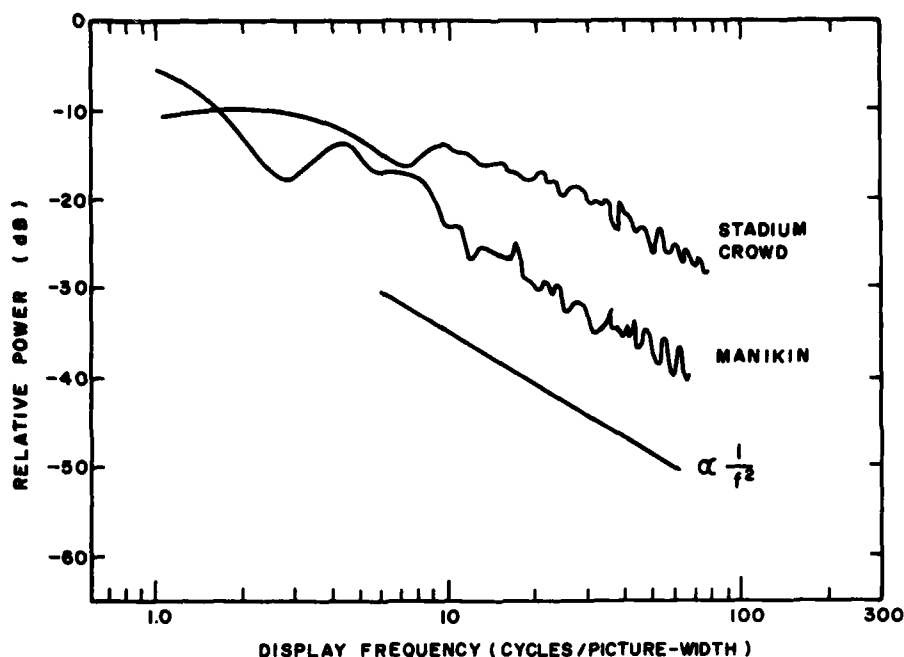
Figure 127. Average horizontal luminance-modulation power spectra for the manikin and crowd scenes shown in Fig. 128. At high spatial frequencies both spectra roll off approximately as $1/f^2$. As explained in the caption to Fig. 126, these spectra were obtained from the $I_m(x)$ term (TR3).

where f_L is the lower cutoff frequency and where $\overline{I_m^2}$ is the mean-square luminance fluctuations due to the image. That is, we consider the luminance pattern $I(x)$ of an image to be composed of two terms: a mean luminance term $\overline{I}$ and a modulated term $I_m(x)$, the latter representing the pictorial information. Now, since $I^2(x) = [\overline{I} + I_m(x)]^2 = \overline{I}^2 + I_m^2$, the contribution from the pictorial information to the mean-square luminance arises from the I_m^2 term, as shown in Eq. (33).

Table 10 is a list of measured normalized rms modulation depths $\sqrt{\overline{I_m^2}/\overline{I}}$ for a large number of pictorial scenes. It may be seen from the table that the measured values range from 0.28 to 0.87 with an average of 0.57, which indicates that pictorial scenes are highly modulated. In the calculations given in this report we always take $\sqrt{\overline{I_m^2}/\overline{I}} = 1/2$.

Figure 128. Photographs of two pictorial scenes used in the experiments described in this report. The top figure is referred to as the "manikin" scene and the bottom figure as the "crowd" scene.

179

TABLE 10.   LIST OF PICTORIAL SCENES AND THEIR RESPECTIVE
NORMALIZED RMS LUMINANCE MODULATION DEPTHS.

No.	Description	$\sqrt{\overline{I_m^2}/\overline{I}}$
1	Apartment building	0.87
2	Girl standing in room	0.86
3	Girl with RCA sign	0.86
4	Girl watching TV	0.80
5	Aeroplane and two people	0.76
6	Lady with checkerboard	0.76
7	Girl on striped blanket	0.72
8	Four people on beach	0.69
9	Man and women standing	0.66
10	Man and aeroplane	0.66
11	Red zinnia	0.66
12	Girl and dotted background	0.63
13	Crowd of Indians	0.60
14	Ten people	0.59
15	Girl and duck	0.57
16	Man and woman in room	0.56
17	Power lines	0.51
18	Girl in country	0.50
19	Stadium crowd	0.47
20	Fruit basket	0.47
21	Motel sign	0.47
22	Standing girl	0.47
23	Head of blond lady	0.45
24	Face of young girl	0.44
25	Manikin	0.43
26	Girl and tree	0.42
27	Soap box	0.42
28	Lady in kitchen	0.41
29	Fruit basket	0.39
30	Dog on grass	0.35
31	Four people	0.34
32	Aeroplane and mountains	0.31
33	Head of girl	0.28
		Average 0.56

2. The Importance of Luminance Edge Transitions

It is widely appreciated in the optical, photographic, and television in-
dustries that a good, quick test of the overall frequency response (or sharpness)
of an imaging system is obtained using a simple black-white edge transition
input. This choice is appropriate since edge transitions represent a signifi-
cant feature of most scenes and since the large modulation in a black-white
transition allows sensitive discrimination of small changes in display MTF.

In the previous section we demonstrated that at relatively high spatial frequencies, the power spectra of a large number of pictorial scenes roll off as $1/f^2$. We feel that this rolloff (as illustrated in Figs. 126 and 127) suggests that luminance edge transitions represent an important feature of pictorial scenes. This conclusion follows from the fact that the power spectrum for an ensemble of edges, randomly placed and with randomly distributed edge heights, will also have a high-frequency rolloff of the form $1/f^2$. The significance of luminance edges in pictorial scenes may also be established by simple observation of one's environment or by viewing on an oscilloscope the waveform of luminance signals from a television camera. In general, textural variations are of much lower modulation depth than are edge transitions.

Now, even if the luminance variations in a scene are dominated by luminance edge transitions, it does not immediately follow that these edges will be used by observers to discriminate small differences in image sharpness or structure. We assume that edges will be used for this purpose only if they represent the object in a scene that allows the most sensitive discrimination of small changes in display MTF. Although it has not yet been proved that edges represent such an object, the contrast-detection model of this report indicates that they are an excellent choice for this purpose. Specifically, for a 100% contrast edge the effective sine-wave contrast in any frequency-specific channel above 1.5 cycles/degree is 14% [Eq. (27)]. Since it is relatively rare that periodic structure in a pictorial scene will have a contrast that exceeds this value, and since the discrimination of a *modulation transfer* change in a channel is a minimum when the contrast in that channel is the largest, we conclude that a high contrast edge is a good pattern to choose when performing modulation transfer discrimination tasks.* Of course, there are occasional scenes, such as a football referee's shirt, where the fundamental frequency of a periodic pattern has a contrast close to 100 percent. In cases like this, depending on the retinal frequency of the pattern and the changes in MTF, these patterns can give smaller discrimination values than those obtained with a high contrast edge.

If our conclusion about the presence and perceptual significance of highly modulated edge transitions is correct, it then follows that scenes composed

---

*MTF changes usually occur over more than one frequency-specific channel, which may make the effectiveness of edges in discrimination tasks somewhat greater. See Section IV.F.

only of high-contrast edge transitions should produce not only similar ~~ ~er spectra, but also similar perceptual results in MTF discrimination experiments. In TR3 we showed that this conclusion is indeed true. The measured results of discrimination experiments performed with pictorial scenes and a one-dimensional high-contrast luminance-edge transition were found to be equivalent. (These results are reproduced in this report in Section IV.H.) For these reasons we have assumed that the appropriate input signal for use in the contrast-detection model of Section IV.B is the power spectrum of a highly modulated luminance edge transition. With this input the model accurately predicts the measured results of the discrimination experiments of Section IV.H. We note, in advance, that the results presented there cannot be predicted using the ensemble-average power spectrum of pictorial scenes (see Section IV.D.1). We interpret these findings as additional evidence for the perceptual importance of edges in contrast-discrimination tasks performed with pictorial images.

3. Distribution of Luminance Levels in Pictorial Scenes

In observing the video waveforms of typical off-the-air television it can be seen that the distribution of luminance levels is not nearly uniform from black to maximum white. In general, the highlight portions of most scenes occupy a significantly smaller fraction of the total area of the scenes than do the lowlights. We are not aware of any systematic attempt to study the distribution of luminance levels in a large number of pictorial scenes, but the skewed nature of the distribution is well known [39].

As typical examples we show two results obtained by Stockham [39], re-plotted in Fig. 129 (a) and (b). For television signals, the ratio of the mean luminance to the peak luminance has been reported to be roughly 0.13 [40], which is in good agreement with the values obtained from the distributions shown in Fig. 129.* Since the distribution of luminance signals is highly skewed, it is expected that corrections to the predictions of display descriptors based only on a few statistical quantities, such as $\overline{I}$ and $\overline{I_m^2}$, will occasionally be necessary. In Appendix C we consider such a situation: the visibility of noise on a display.

---

*The average of the ratios given in ref. 40, as measured in the video signal processing channel, was 0.40. We assume here a kinescope gamma of 2.2 in order to convert this voltage ratio to a luminance ratio on the display.
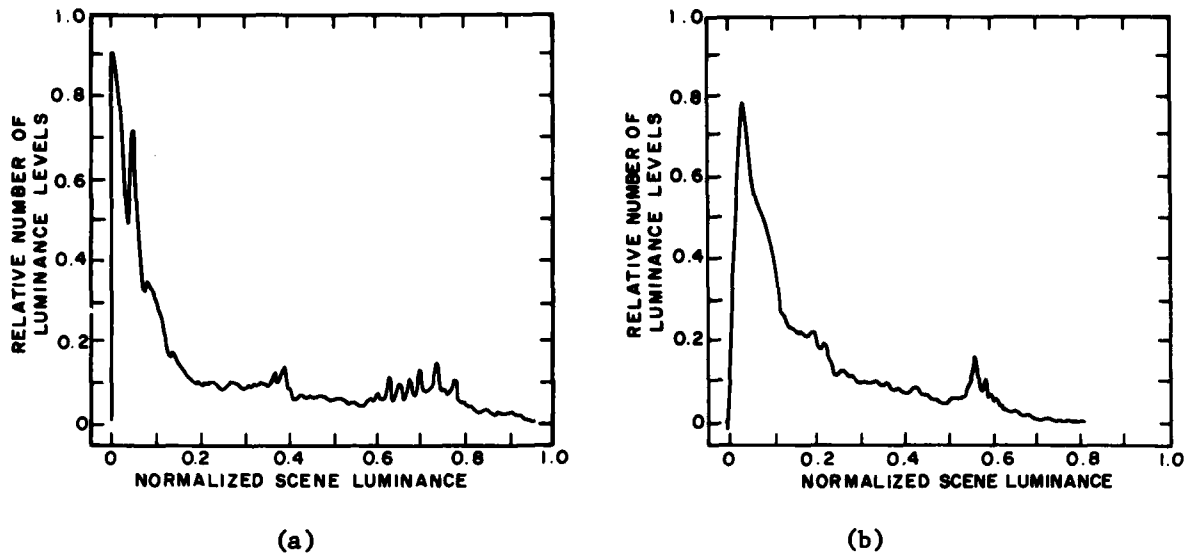
Figure 129. Luminance histograms from images digitized to 340 by 340 samples
and with 12 bits/sample (after T. G. Stockham, Jr. [39]).
(a) was formed from three wide-dynamic range scenes;
(b) was formed from two scenes of less dynamic range.

E. PARAMETERS AND ASSUMPTIONS USED IN COMPUTING THE DDDs

Table 11 lists the parameters and Table 12 lists the equations that were
used in Eq. (31) to compute the Discriminable Difference Diagrams given in
Section III. For the DDDs for both analog and sampled/raster displays, the
perceived signal levels were computed assuming a 100% contrast, one-dimensional
luminance edge input. The DDDs giving the noise levels for analog displays
were computed assuming a white input noise spectrum and the four viewing con-
ditions summarized in Table 11. For sampled and raster displays, the DDDs for
noise levels were calculated assuming that the noise was due only to the
sampling processes.

In the construction of the DDDs, the center frequencies of the independent
frequency-specific channels were fixed at 0.5, 1.5, 3.0, 6.0, 12, 24, and
48 cycles/degree. This assignment of frequencies is reasonable as long as
rapid changes in either the modulation transfer or the spectral content of
the display images do not occur within a channel.

183

TABLE 11. MODEL PARAMETERS USED IN COMPUTING THE
DISCRIMINABLE DIFFERENCE DIAGRAMS

ν (cycles/ degree)	$\Delta\nu$ (cycles/ degree)	$k(\nu)$	$m_T(\nu)$			
			$\left[\begin{array}{l}\bar{I}=35\text{mL}\\ r/w=3\end{array}\right]$	$\left[\begin{array}{l}\bar{I}=35\text{mL}\\ r/w=10\end{array}\right]$	$\left[\begin{array}{l}\bar{I}=35\text{mL}\\ r/w=30\end{array}\right]$	$\left[\begin{array}{l}\bar{I}=1.0\text{mL}\\ r/w=10\end{array}\right]$
0.5	1.0	0.130	0.00391	0.00751	0.0152	0.0127
1.5	1.0	0.140	0.00170	0.00290	0.00545	0.00625
3.0	2.0	0.158	0.00153	0.00213	0.0034	0.00653
6.0	4.0	0.185	0.00211	0.00241	0.00305	0.0105
12.0	8.0	0.240	0.00395	0.00410	0.00442	0.0266
24.0	16.0	0.310	0.0194	0.0196	0.0197	0.166
48.0	32.0	0.400	0.794	0.796	0.796	-

$\Delta I/\bar{I} = 2.0$ [100% contrast edge]

$\sqrt{\bar{I}_m^2}/\bar{I} = 1/2$

$f_L = 1/w$

184

TABLE 12.   EQUATIONS USED IN CONJUNCTION WITH Eq. (31) TO
COMPUTE THE DISCRIMINABLE DIFFERENCE DIAGRAMS

	Analog Displays	Sampled/Raster Displays
Signal: $m_S(\nu)$	Eq. (27)	Eq. (B-14)
Interfering Term: $m_I(\nu)$	Eq. (29)	Eq. (B-15)
Noise: $m_N(\nu)$	Eq. (29)	Eq. (B-15)
Interfering Term: $m_I(\nu)$	Either $m_I(\nu) = 0$, Eq. (27), or Eq. (28)	Eq. (B-14)

F.   COMBINING jnd's FROM SEVERAL CHANNELS

Generally, changes in display modulation transfer result in jnd changes
in more than one frequency-specific channel. If it were known how this in-
formation is combined by the visual system, an overall, or equivalent, number
of jnd's could be computed that would represent the effect of a change in
modulation transfer. Unfortunately, this property of the visual system is not
well understood. Nevertheless, it is possible to propose simple criteria that
establish likely boundaries for combining jnd's. We will consider three:

    (1)   jnd's in different channels do not combine.

    (2)   jnd's in different channels combine according to the law
        of probability summation.

    (3)   jnd's in different channels combine by simple addition.

The first criterion assumes that an observer can only be attentive to one
channel at a time. Jnd's in other channels are ignored during the detection
task. The second criterion assumes that jnd changes, which occur in several
channels, are perceived independently and simultaneously. Since the jnd
change in each channel represents a fixed probability of detection, the over-
all probability of detecting the change is given by the joint probability
formed from all of the individual probabilities. When required, this prob-
ability can then be readily converted back to jnd units. The third criterion
states that the jnd's in each channel should be simply added to form an overall

equivalent number of jnd's. We cannot justify this criterion theoretically, but, as we will show, it leads to reasonable predictions. For this reason, and also because of its mathematical simplicity, this approach was used in the examples of Section II.

In the following subsections the concept of probability summation among independent frequency-specific channels is developed. Then, the three criteria mentioned above are applied to the data of Section IV.H and their predictions compared.

1. Probability Summation Among Independent Frequency-Specific Channels

An observer, looking at a display under a specified set of conditions, has a probability p_i of detecting an MTF change that occurs within the i'th independent frequency-specific channel. Now, if an MTF change occurs over q frequency-specific channels, and each of these channels has its own probability p_i of detecting that change, then the joint probability p of seeing the change due to all the channels is [41]

$$p = 1 - \prod_{i=1}^{q} 2^{q-1}(1 - p_i), \text{ where } 0.5 \leq p_i \leq 1.0 \tag{34}$$

For example, consider the case where four channels are changed by 1 jnd each. Then $p_i = 0.75$ in all four channels and from Eq. (34), p = 0.97. The visibility of this change has been increased greatly.

In order to use Eq. (34) in conjunction with the DDDs, the empirical relationship between p_i and the change in the number of jnd's ΔJ at each frequency-specific channel location must be known.* In Fig. 130 p_i is plotted versus ΔJ for the case where the number of jnd's in a particular channel is less than 1 (threshold). A similar curve is shown in Fig. 131 for the case where the number of jnd's is greater than 1 (suprathreshold). It may be seen from these figures that the transition of p_i, from chance detection to near-certain detection, is considerably more sudden at threshold (J ≤ 1.0) than above threshold (J > 1.0). Thus, if probability summation exists between channels, then its effects will be considerably less important at absolute threshold than at suprathreshold.

---

*Once again, a single jnd is defined as the change in contrast required for $p_i = 0.75$, so that ΔJ = 1 at $p_i = 0.75$. This definition establishes the scale for ΔJ; e.g., for ΔJ = 2 the change in contrast is twice that required to give $p_i = 0.75$.
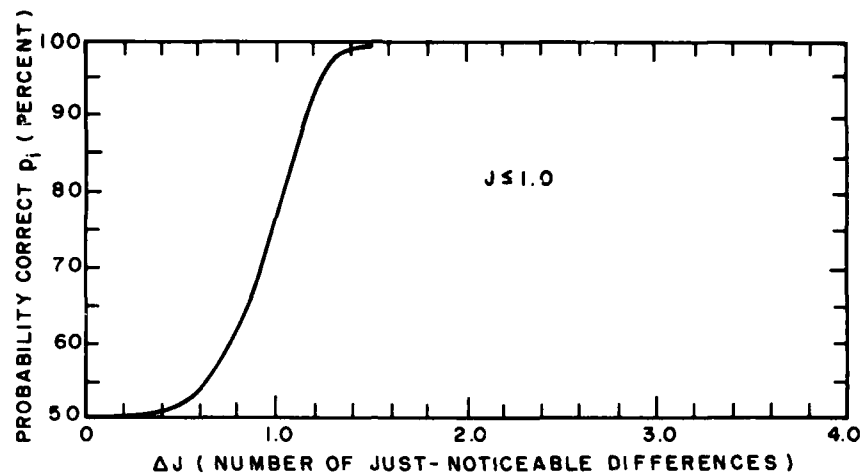
Figure 130.   Probability p_i of correctly detecting a change at threshold
(J $\leq$ 1.0) as a function of the change in the number of jnd's
ΔJ. After ref. 17.
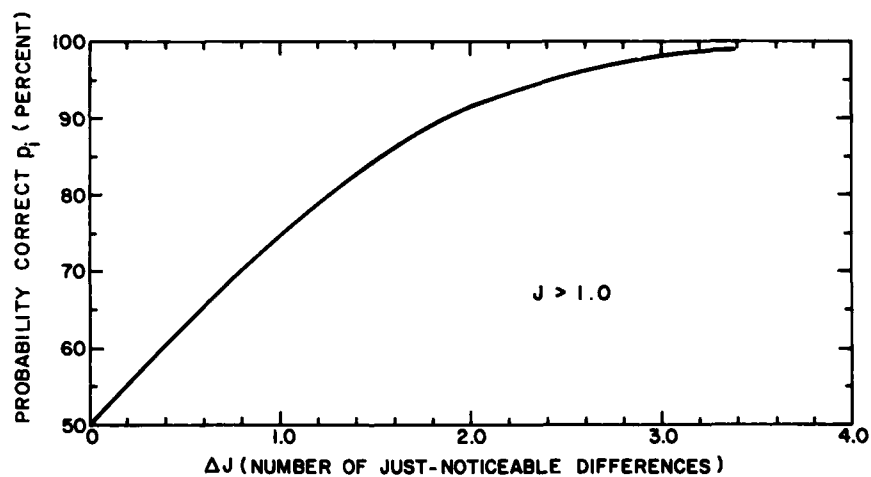
Figure 131.   Probability p_i of correctly detecting a change at suprathreshold
(J > 1.0) as a function of the change in the number of jnd's
ΔJ. After ref. 17.

With the aid of Figs. 130 and 131 and Eq. (34), the overall probability
p of detecting a change in display modulation transfer occurring over several
channels can be computed. With the aid of Figs. 130 and 131 this overall

187

probability p can be represented as an equivalent number of jnd's. For example, for the case given earlier, where a 1-jnd change (p_1 = 0.75) occurred over four channels, we determined from Eq. (34) that p = 0.97. If we now assume that these changes all occurred above threshold, then from Fig. 131 we find that this probability corresponds to approximately 2.9 jnd's. Said differently, we have determined that, due to probability summation, a 1-jnd change in four channels is equivalent to a 2.9-jnd change in one channel.

2. Comparison of Different Approaches

In Fig. 132 experimental results from Section IV.H are replotted. These results show the fractional change in bandwidth $(v_2 - v_1)/v_2$ necessary for an observer to perceive a single jnd change in the image structure of two pictorial scenes. Also shown on this figure are the predicted values obtained from the contrast-discrimination model using the three criteria outlined above. Curve 1 was obtained by assuming that only the most sensitive channel [i.e., the one that reaches 1 full jnd for the smallest change in $(v_2 - v_1)/v_1$] was responsible for producing the discriminable difference. Fractional changes in other channels were ignored. Curve 2 is the predicted result obtained by computing the joint probability [Eq. (34)] of seeing the change due to relatively small contributions from several channels. Finally, Curve 3 shows the predicted results obtained by simply adding fractional changes at each channel location to form 1 jnd.

From Fig. 132 it may be seen that, for these experimental conditions, the different criteria result in a range of roughly a factor of two between the predicted values* of $(v_2 - v_1)/v_2$. For v_1 < 10 cycles/degree, the results of criterion 3 agree best with the measured data. For 10 $\overset{<}{\sim}$ v_1 $\overset{<}{\sim}$ 40 cycles/degree, criteria 1 and 2 correspond somewhat better with the measured results, while for v_1 $\overset{>}{\sim}$ 40 cycles/degree, criterion 3 is once again superior. However, the spread in the data and the uncertainties in the values of the parameters in

---

*The MTF used in these experiments is given in Fig. 135. For MTFs that exhibit a more rapid roll-off, the differences between the three criteria decrease. In the limit of an ideal low-pass filter, the predictions of all three criteria are the same.

the model are sufficiently large to preclude a definite statement as to which of the three criterion is operating.*
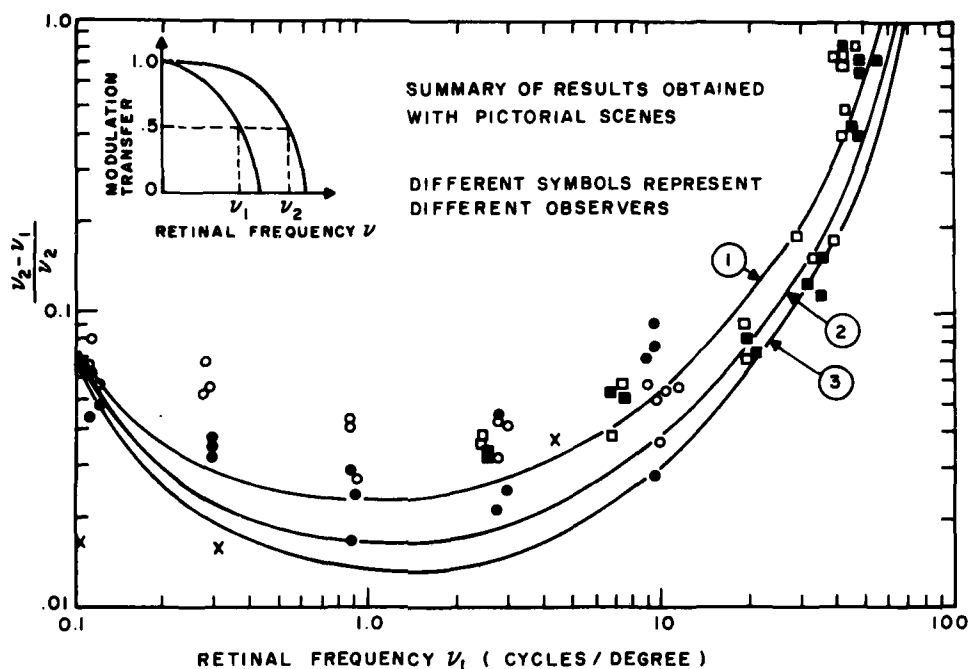
Figure 132. Comparison of the different methods of combining jnd changes that occur in more than one independent frequency-specific channel location. The measured results, which are taken from Section IV.H, are plotted with $(\nu_2 - \nu_1)/\nu_2$ as a function of ν_1. The bandwidths ν_1 and ν_2, where $\nu_2 > \nu_1$, are defined as the point where $R(\nu) = 1/2$. The change in bandwidth $\nu_2 - \nu_1$ is defined as the change in ν_2 from ν_1 necessary for an observer to see a change in bandwidth 75% of the time. Curve 1 shows the predicted results obtained from assuming that only the most sensitive frequency-specific channel is responsible for producing the discriminable difference. Curve 2 is the predicted result obtained by computing the joint probability of seeing the change due to relatively small contributions from several channels. Curve 3 is the predicted result obtained by simply adding fractional changes at each channel location to form 1 jnd.

*The results of Fig. 132 show that there are major differences in the measured results between the different observers, particularly at the lower bandwidths (i.e., $\nu_1 < 10$ cycles/degree). It is possible that this is due, in part, to the observers using different strategies in performing these detection tasks. That is, criterion 1 may apply to one observer and a combination of criteria 1 and 2 may apply to another. For a discussion of additional considerations regarding these results, see Section IV.H.

189

While the results of Fig. 132 do not resolve the question of how the visual system combines jnd's from different frequency-specific channels, the exercise is useful since it establishes the range of predicted values that can be expected in practical situations using the different procedures. Indeed there is only a relatively small difference between the predicted results using the three criteria. Thus, because of its mathematical simplicity, criterion 3, simple addition of jnd's, was used in the examples of Section II. The reader should be aware, however, that the correct procedure for combining jnd's that occur in more than one frequency-specific channel must be between the limits imposed by criteria 1 and 2.

G. APPLICATION OF THE CONTRAST DETECTION MODEL TO ANISOTROPIC MTFs

There are several aspects of the display-observer system that can exhibit anisotropy: the spectral properties of the information, the display MTF, and, to a small extent, the visual system, as mentioned in Section IV.C. In this report we have generally assumed that display changes occur isotropically. This assumption greatly simplifies the model and, in many discrimination tasks, represents only a small error in the predicted results. On the other hand, when the overall structural content presented by a display is computed, the effects of anisotropy can be important.

The effects of spatial anisotropy in the display-observer system are included in the one-dimensional contrast detection model of Section IV.B through the concept of independent orientation-specific channels in the visual system [42, 43]. The essence of this concept is that spectral information in a two-dimensional scene is broken down by the visual system into adjacent angular bands. Within these bands, each roughly 12 to 29 degrees wide, the spectral information in each frequency-specific channel can be summed, in a manner analogous to that described in Section IV.B, to form an equivalent sine-wave contrast for the information at that orientation and in that frequency-specific channel.

With a model that includes orientation specific channels, the general procedure in analyzing the perceivable effect of a change in display modulation transfer is: (1) divide the display into roughly 12 equal orientation specific bands and form the perceived power spectra within each band; (2) compute the

190

individual probabilities that result from modulation transfer changes in each frequency-specific channel within each orientation specific band,* and (3) form the overall joint probability of perceiving the modulation transfer change due to the contributions of the probabilities at each frequency-specific channel location within each channel location, as described in Section IV.F.**

In order to discuss the properties of this generalized model two conditions must be distinguished: (1) the <u>detection</u> of a change in a display property, which is the general problem addressed in this report, and (2) the overall <u>effect</u> on image structure that results from that change. Consider first the detection experiments of Section IV.H, where the observer's task was to detect <u>any</u> change in display modulation transfer. In this case the measured discrimination of a change in modulation transfer should not depend strongly on whether the change occurs isotropically or anisotropically. This conclusion follows from the results of Sections IV.D and IV.H, which imply that high-contrast one-dimensional edges are the most important attribute of scenes in performing these discrimination tasks. Thus, as long as an observer can locate one highly modulated edge whose power spectrum falls along the line of a change in display modulation transfer, it will not matter if the modulation transfer change occurs isotropically or anisotropically. Nevertheless, it is clear that, in general, isotropic and anisotropic changes in display modulation transfer will result in very different overall amounts of displayed image structure. For example, in some pictorial scenes there are, statistically, more vertical and horizontal edges than there are at other orientations. Therefore, for these images the statistical loss in image structure due to a fixed reduction in modulation transfer is less when it occurs at oblique orientations than when it occurs either horizontally or vertically.

H. EXPERIMENTAL VERIFICATION OF THE CONTRAST-DETECTION MODEL

1. Introduction

In Section IV.B it was shown that the contrast-detection model accurately predicts the measured results of discrimination experiments performed with

---

*That is, each orientation specific band would have its own DDD, which would indicate the structural distribution of the information at that orientation.
**We emphasize that it has not been empirically established that the visual system performs an operation similar to the probability summation described in Section IV.F. Thus, this procedure is, at present, hueristic.

spectrally complex scenes. Specifically, we will show that the contrast-detection model successfully predicts the measured results of experiments to determine the just-noticeable difference in display modulation transfer for both pictorial and non-pictorial images. Two sets of experiments are reported. The first set was performed on a display that presented the images sequentially; the second set was performed with two displays viewed side by side. Although these results represent the primary test of the model, we have also shown that the model predicts the functional form of several important visual characteristics, such as the Rose-DeVries law, Ricco's law, and Piper's law [44]. Furthermore, in preliminary experiments we have found that the model is reasonably accurate in predicting the threshold visibility of certain non-periodic luminance patterns, such as luminance edges.

2. Experimental Conditions: Sequential Presentation

In these discrimination experiments observers were asked to determine which of two images, presented sequentially and with different bandwidths, appeared to be the sharper.* The bandwidths of the images ν_1 and ν_2 (where $\nu_2 \geq \nu_1$) were defined at the point where** $R(\nu) = 1/2$. Images were viewed continuously with binocular vision, without artificial pupils, and with no fixation point on the screen. The order in which ν_1 and ν_2 were presented was randomized, and the observers were required to respond after each change from either ν_1 to ν_2 or ν_2 to ν_1. At selected values of ν_1 throughout the bandpass of the eye, the psychometric function $p(\nu_2-\nu_1,\nu_1)$, which is defined as the probability of correctly choosing the sharper of the two images at a specific value of ν_1 as a function of $\nu_2 - \nu_1$, was determined from roughly 200 data points. The just-noticeable difference was determined from this data at the point where $p(\nu_2-\nu_1,\nu_1) = 0.75$.

---

*We assume that there is no measurable difference between a just-noticeable difference in image sharpness and a just-noticeable difference in image structure or contrast. The observers were instructed to look for differences in image sharpness because this was ostensibly the task they were performing and because this concept was readily understood. When performing the experiments, however, they responded when they could detect any difference between the two images.

**The MTF of the display used to perform these experiments is given in Fig. 135.

The measurements were performed using the experimental conditions summarized in Fig. 133. The display, shown in Fig. 134, consisted of two parallel diffuser plates separated by a distance Δ. By varying Δ the MTF of the display was varied as shown in Fig. 135 [45]. In these experiments the displayed images were effectively noise-free. An important feature of this display was that it did not introduce spatial frequency phase shifts along with changes in the magnitude of the modulation transfer. This is necessary in these experiments since the discrimination of phase shifts is not included in the model,* and their presence might act as an additional clue for discrimination of differences

PARALLEL PLATE
DIFFUSERS

INPUT-IMAGE
PLANE

FILTERED IMAGE
PLANE

OBSERVER

PROJECTOR OR
LIGHT SOURCE

VIEWING DISTANCE, r
128 OR 400 cm

PLATE SPACING, Δ
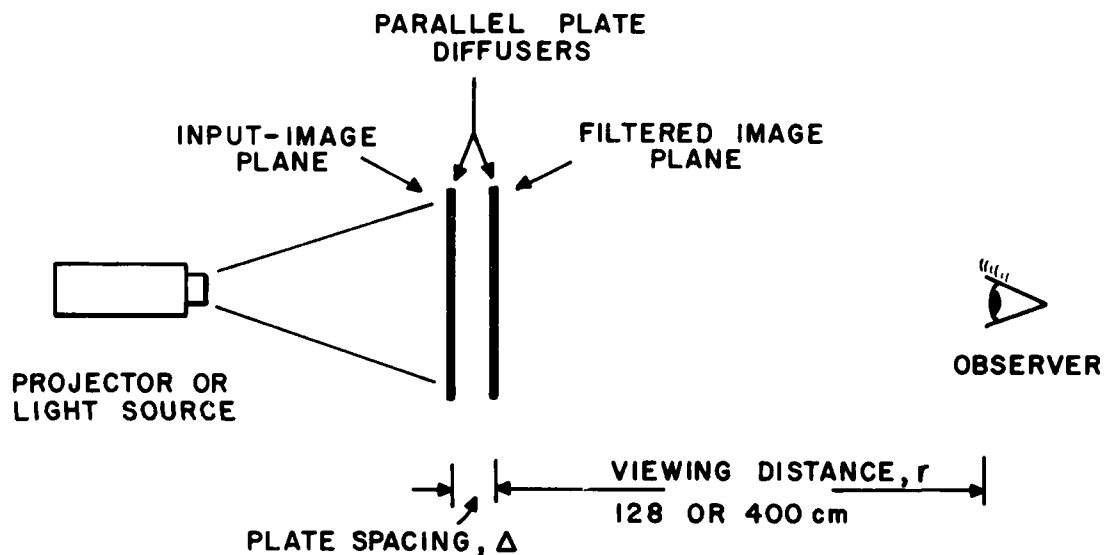
Figure 133. This figure shows the basic elements of the apparatus used to perform the modulation transfer discrimination experiments. Observers, sitting at viewing distances of either 128 or 400 cm, viewed images that were low-pass filtered by a display composed of two parallel diffusive plates. The MTF of the display was varied by varying the plate spacing Δ. Images were produced either by direct projection of 35-mm slides or by the back-illumination of images placed over the input plane of the display. The display was 59 cm wide by 43 cm high. For the cockpit display (Fig. 137) the mean display luminance was 2 mL, and for all the other images studied it was 35 mL.

---

*See, also, Section II.A for additional comments about this issue.
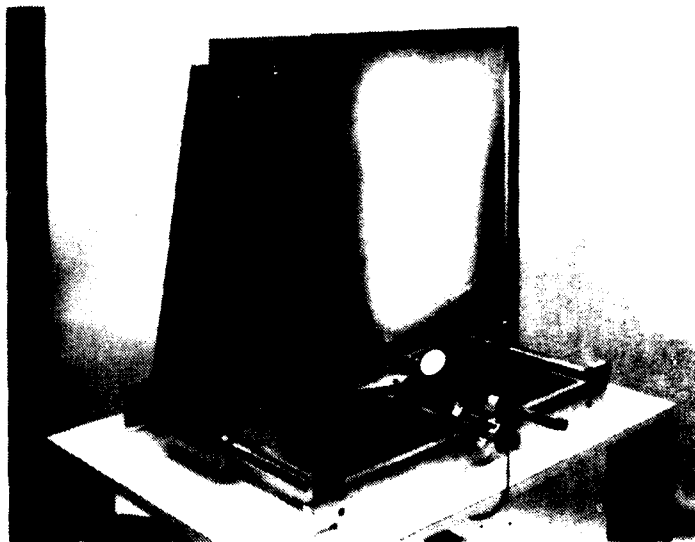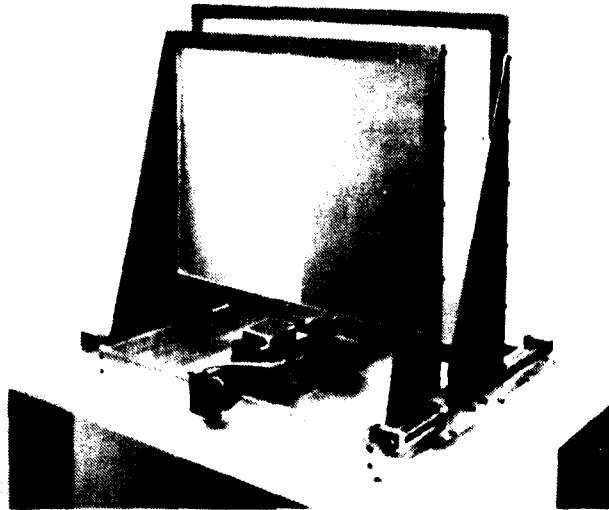
Figure 134. These two photographs show the diffuser display constructed to
perform the modulation transfer discrimination experiments.
The top photograph shows the input side of the display with a
superimposed luminance edge input. The bottom photograph shows,
from the observer's side, the same input edge after filter-
ing by the display. During the performance of the experiments
a large, white cardboard frame was placed around the display.

194
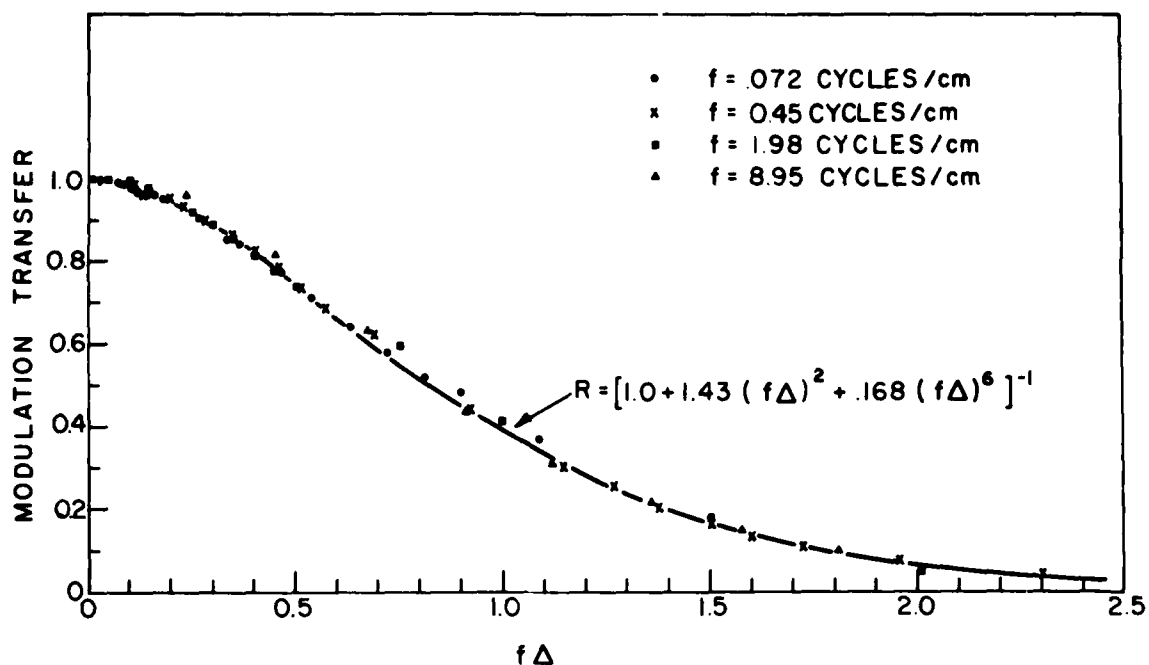
Figure 135. The measured MTF for the diffuser display discussed in Figs. 133 and 134 as a function of the spatial frequency on the display f times the diffuser plate spacing Δ. These results show that for all plate spacings the form of the MTFs is identical. The curve on the figure represents the approximate analytic expression for this MTF used in this report. Since $R(f\Delta) = 1/2$ when $f\Delta = 0.82$, and since $\nu = \pi r f/180$, the display MTF may be written as $R(\nu/\nu_{1,2}) = [1 + 0.951 (\nu/\nu_{1,2})^2 + 0.049 (\nu/\nu_{1,2})^6]^{-1}$, where $R(\nu/\nu_{1,2}) = 1/2$ when either $\nu = \nu_1$ or $\nu = \nu_2$.

in ν_1 and ν_2. All the experiments reported here (with the exception of the cockpit display for which $\bar{I} = 2$ mL) were performed with a mean display luminance of 35 mL and a mean surround luminance of roughly 5 mL. The experiments were conducted at viewing distances of 128 and 400 cm, which corresponded to display widths of 24 and 7 degrees, respectively. The parameters $m_T(\nu)$, $k(\nu)$, $\ell(\nu)$, and $\Delta\nu(\nu)$ used in the calculations are given in Table 11. The measured values of $m_T(\nu)$ for the observers of this study were in reasonably good agreement with those shown in Fig. 126 with $\bar{I} = 35$ mL, although for P.R. and B.S., $m_T(\nu)$ was somewhat larger than that shown in Fig. 122, particularly at the higher spatial

frequencies* [TR3], while for A.P. $m_T(\nu)$ was smaller for frequencies below roughly 1 cycle/degree [17]. The values of $k(\nu)$ used in the calculations were obtained from subjects A.P. and C.C. No data were taken to measure this quantity for either P.R. or B.S.

Five different scenes were used in this study: two pictorial scenes (Fig. 128), two edges (Fig. 136), and an aircraft cockpit display (Fig. 137). The pictorial scenes and the cockpit display were chosen to represent a diverse range of actual images; the one-dimensional luminance edge transitions were selected because of their relative mathematical simplicity and because, as described in Section IV.D, they represent a significant feature in many scenes. All edge contrasts were defined as $(I_{max} - I_{min})/I_{max} + I_{min})$, as shown in Fig. 119. The results for observers P.R. and B.S. have been given and discussed in part elsewhere [TR3, 6, 46, 47, 48]; the results for observers A.P. and C.C. are given here for the first time. Additional details regarding the apparatus, procedure, and experimental conditions used in this study can be found in refs. TR3, 17, and 47.

3. Results and Discussion: Sequential Presentation

In Figs. 138 through 143 the measured data points for a jnd change in image structure are shown, plotted as $(\nu_2 - \nu_1)/\nu_2$ as a function of ν_1. The solid line on each figure represents the predicted values from the contrast detection model of Section IV.B. For the one-dimensional edges the calculations were performed using the appropriate modulation depths $\Delta I/\bar{I}$ in Eq. (27), which was derived from the power spectrum of a one-dimensional luminance edge transition, as described in Appendix A. This equation was also used to obtain the predicted values for the pictorial scenes and the cockpit display,** but the edge modulation depth was taken as 100%. In all cases, jnd changes that occurred in more than one independent frequency-specific channel due to a change in modulation transfer

---

*The measured values of $m_T(\nu)$ for P.R. and B.S. were obtained using the method of adjustment, a procedure that can lead to larger values of $m_T(\nu)$ than those obtained using a two-alternative forced-choice procedure [33]. All the data given in this report were obtained using a two-alternative forced-choice procedure.

**Additional details regarding the meaning of this power spectrum when applied to pictorial or graphic images is given in Section IV.D.
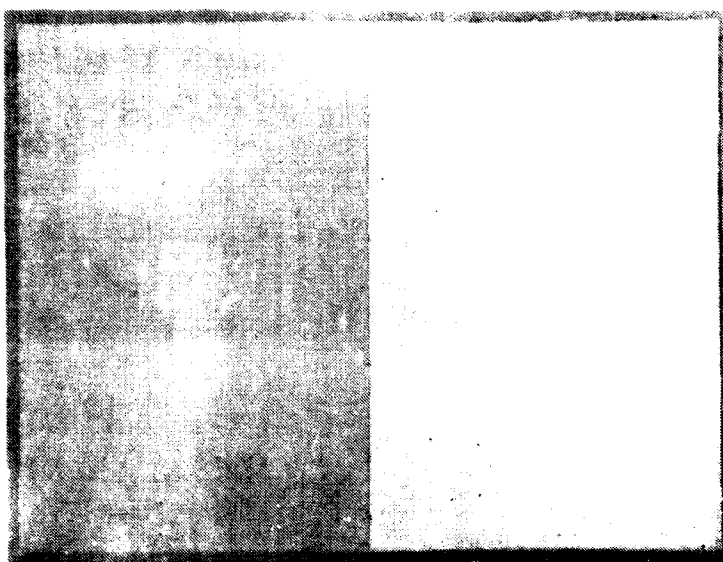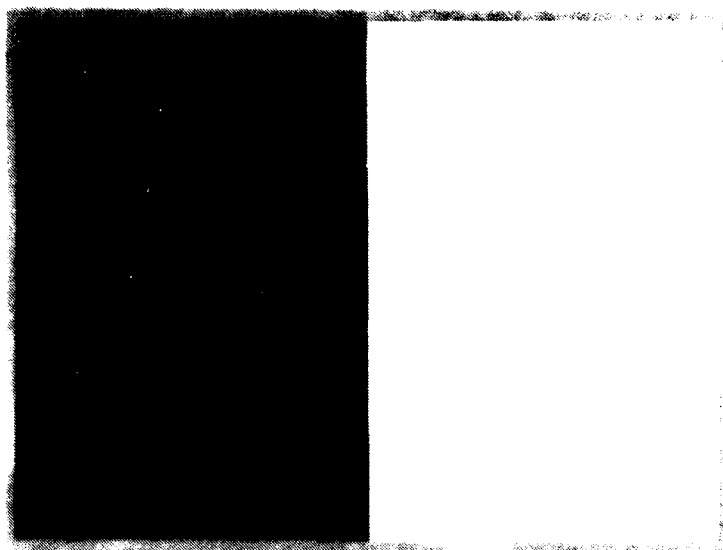
Figure 136. Approximate representations of the two luminance edge transitions used in the modulation transfer discrimination experiments. The top edge has a contrast of 82% and the bottom edge, 12%.
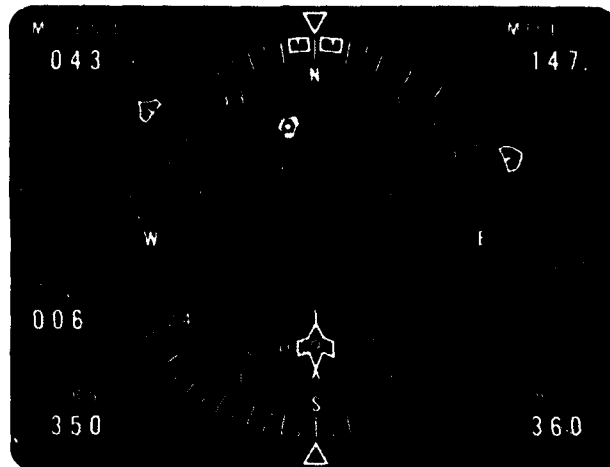
Figure 137. Photograph of the cockpit display image used in the modulation
transfer discrimination experiments (this is a copy of an image
from a Thomson-CSF Multi-color CRT display). This scene, viewed
from 400 cm, subtended 8° of visual angle horizontally. The
mean display luminance was 2 mL.

were combined using probability summation, as described in Section IV.F. The
frequency-specific channel locations were assumed to be freely adjustable above
1 cycle/degree in accord with current understanding of their properties
[Section IV.B]. That is, the center frequencies of the channels were adjusted
so that the predicted value of $(\nu_2 - \nu_1)/\nu_2$ at any ν_1 was a minimum.* This
procedure gave only slightly smaller values of $(\nu_2 - \nu_1)/\nu_2$ than those obtained
with fixed channel locations, as we have assumed in constructing the DDDs.

In Fig. 138 the measured and predicted results for the 12% contrast edge
are shown. The data points and the theoretical curve are in good agreement
for both observers at all but the intermediate spatial frequencies, where the

---

*In general, the display MTF $R(\nu/\nu_{1,2})$ and the power spectra of the input
scenes used in these experiments varied slowly with ν over each frequency-
specific channel. This allowed the average value of $R(\nu/\nu_{1,2})$ in each channel
to be approximated by the value of $R(\nu/\nu_{1,2})$ at the center of each channel.
However, for bandwidths $\nu_{1,2}$ less than roughly 0.8 cycle/degree, this approx-
imation for $R(\nu/\nu_{1,2})$ is not valid for the channel located at 0.5 cycle/degree.
Therefore, in this channel and for the lower bandwidths, $R(0.5/\nu_{1,2})$ was given
by $R(0.5/\nu_{1,2}) = \int_0^{\Delta\nu} d\nu \, R(\nu/\nu_{1,2})/\Delta\nu$, where $\Delta\nu = 1$ cycle/degree.

198
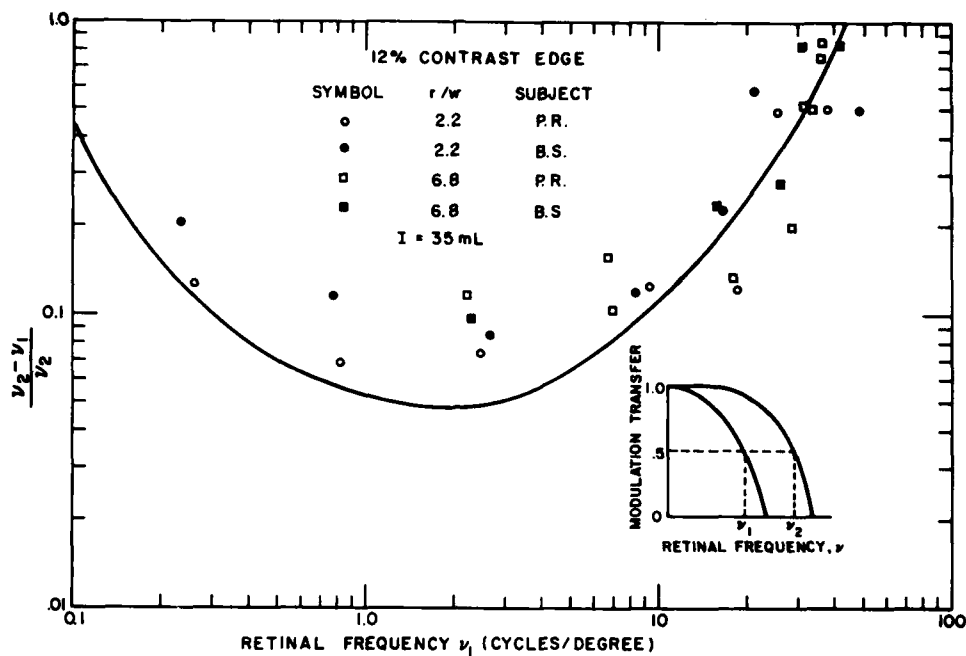
Figure 138. Measured results of modulation transfer discrimination experiments performed with a 12% contrast luminance-edge transition. The measurements are plotted with $(\nu_2 - \nu_1)/\nu_2$ as a function of ν_1, where ν_2 and ν_1 are defined in the inset on the figure. In these experiments the change in bandwidth, from either ν_2 to ν_1 or ν_1 to ν_2, was made instantaneously on the same display. The difference in bandwidth $\nu_2 - \nu_1$ was defined as that change from ν_1 necessary for an observer to see a change in the displayed image structure 75% of the time. The solid curve on the figure represents the predictions of the contrast-detection model assuming probability summation amoung independent frequency-specific channels, as explained in the text.
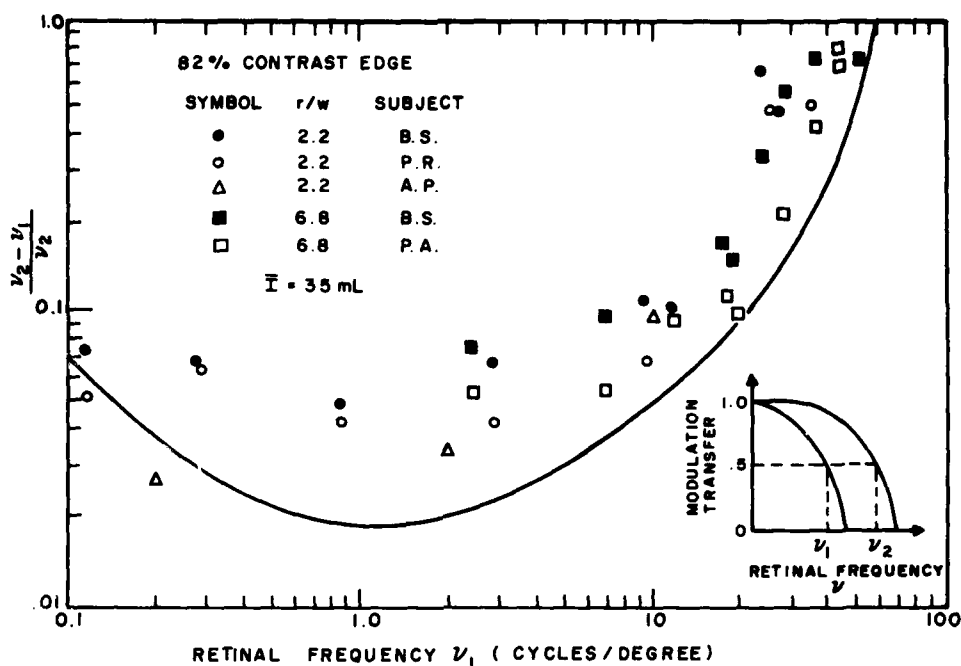
Figure 139. Measured results of modulation transfer discrimination experiments performed with an 82% contrast luminance-edge transition. The measurements are plotted with $(v_2 - v_1)/v_2$ as a function of v_1, where v_2 and v_1 are defined in the inset on the figure. In these experiments the change in bandwidth, from either v_2 to v_1 or v_1 to v_2, was made instantaneously on the same display. The difference in bandwidth $v_2 - v_1$ was defined as that change from v_1 necessary for an observer to see a change in the image structure 75% of the time. The solid curve on the figure represents the predicted results of the contrast-detection model assuming probability summation among independent frequency-specific channels, as explained in the text.

MANIKIN SCENE IN BLACK AND WHITE

SYMBOL	r/w	SUBJECT
o	2.2	P.R.
●	2.2	B.S.
□	6.8	P.R.
■	6.8	B.S.

$I = 35\,mL$

MODULATION TRANSFER

RETINAL FREQUENCY, ν

$\dfrac{\nu_2 - \nu_1}{\nu_2}$

RETINAL FREQUENCY ν_1 (CYCLES/DEGREE)

Figure 140. Measured results of modulation transfer discrimination experiments performed with the manikin scene of Fig. 128 in black and white. The measurements are plotted with $(\nu_2 - \nu_1)/\nu_2$ as a function of ν_1, where ν_2 and ν_1 are defined in the inset on the figure. In these experiments the change in bandwidth, from either ν_2 to ν_1 or ν_1 to ν_2, was made instantaneously on the same display. The difference in bandwidth $\nu_2 - \nu_1$ was defined as that change from ν_1 necessary for an observer to see a change in the image structure 75% of the time. The solid curve on the figure represents the predicted results of the contrast detection model assuming probability summation among independent frequency-specific channels, as explained in the text.

Figure 141. Measured results of modulation transfer discrimination experiments performed with the manikin scene of Fig. 128 in color. The measurements are plotted with $(\nu_2 - \nu_1)/\nu_2$ as a function of ν_1, where ν_2 and ν_1 are defined in the inset on the figure. In these experiments the change in bandwidth, from either ν_2 to ν_1 or ν_1 to ν_2, was made instantaneously on the same display. The difference in bandwidth $\nu_2 - \nu_1$ was defined as that change from ν_1 necessary for an observer to see a change in the image structure 75% of the time. The solid curve on the figure represents the predicted results of the contrast-detection model assuming probability summation among independent frequency-specific channels, as explained in the text.

Figure 142. Measured results of modulation transfer discrimination experiments performed with the crowd scene of Fig. 128 in color. The measurements are plotted with $(v_2 - v_1)/v_2$ as a function of v_1, where v_2 and v_1 are defined in the inset on the figure. In these experiments the change in bandwidth, from either v_2 to v_1 or v_1 to v_2, was made instantaneously on the same display. The difference in bandwidth $v_2 - v_1$ was defined as that change from v_1 necessary for an observer to see a change in the image structure 75% of the time. The solid curve on the figure represents the predicted results of the contrast-detection model assuming probability summation among independent frequency-specific channels, as explained in the text.

Figure 143. Measured results of modulation transfer discrimination experiments performed with the cockpit display of Fig. 137 in color. The measurements are plotted with $(\nu_2 - \nu_1)/\nu_2$ as a function of ν_1, where ν_2 and ν_1 are defined in the inset on the figure. In these experiments the change in bandwidth, from either ν_2 to ν_1 or ν_1 to ν_2, was made instantaneously on the same display. The difference in bandwidth $\nu_2 - \nu_1$ was defined as that change from ν_1 necessary for an observer to see a change in the image structure 75% of the time. The solid curve on the figure represents the predicted results of the contrast-detection model assuming probability summation among independent frequency-specific channels, as explained in the text.

predictions of the model appear to be dropping below the data. This trend is shown more convincingly for observers P.R. and B.S. in Fig. 139, which shows the results for the 82% contrast edge. Again the correlation between the predicted and measured values is acceptable for all observers at the higher and lower spatial frequencies, but, for observers P.R. and B.S., the predicted and measured values diverge from the predictions at intermediate spatial frequencies near 1 cycle/degree. There are several possible reasons for this behavior including the following: (1) incomplete probability summation among the frequency-specific channels, as discussed in Section IV.F, which can be an important effect in this frequency range; (2) interactions between the frequency-specific channels, especially at high equivalent contrast; and (3) differences in observer performance. For all subjects the experiments were considerably more difficult to perform at low v_1 due to the presence of strong after-images and the problem of visually localizing a highly smoothed edge (see also p. 85, TR3). This could result in slightly higher values of $(v_2 - v_1)/v_2$ at the lower bandwidths for observers with less than optimum discrimination procedures. It is our judgment that this possibility is greater for observers P.R. and B.S. than for subject A.P., a conclusion that is supported by the measured results. (4) Uncertainties in the model parameters $m_T(v)$, $\ell(v)$, $\Delta v(v)$, and $k(v)$. As discussed earlier in this section, it is possible that the actual values of $m_T(v)$ for observers P.R. and B.S. are somewhat larger than those used in the calculations, especially at the higher frequencies. This would increase the predicted values of $(v_2 - v_1)/v_2$. Increasing $\ell(v)$ would also increase the predicted values of $(v_2 - v_1)/v_2$, but the present values appear reasonable [20]. As outlined in Section IV.B, the correct values of $\Delta v(v)$, especially at low retinal frequencies, are not accurately known. If the values of $\Delta v(v)$ used in this report were too large by a factor of two for $v > 1.0$ cycle/degrees and if, in addition, we assume that there is no probability summation between the frequency-specific channels, the predicted values and the measured values given in Fig. 139 for $(v_2 - v_1)/v_2$ would then be very close. However, if there is probability summation, then a factor of two reduction in $\Delta v(v)$ has no significant effect on $(v_2 - v_1)/v_2$. Finally, for $v_1 < 10$ cycles/degree the exact values of $k(v)$ for this experiment are not independent of the contrast level, as discussed in detail

in Section IV.C.2. The reader will recall that we have simplified the model by assuming that $k(\nu)$ is independent of contrast; although for $\nu > 10$ this is a good approximation, for $\nu < 10$ cycles/degree this becomes a poorer approximation (see Fig. 123). The values of $k(\nu)$ used in the contrast-detection model represent average values that were selected to best represent the range of contrast of interest here. If, however, the variation of $k(\nu)$ with equivalent grating contrast is included in the model (from Fig. 123), the predicted and measured values of $(\nu_2 - \nu_1)/\nu_2$ are in somewhat better alignment.* For example, at $\nu_1 = 1$ cycle/degree for the 82% contrast edge, the predicted $(\nu_2 - \nu_1)/\nu_2$ is increased by roughly 50% over the values shown in Fig. 139.

Nevertheless, we consider the factors outlined above to be details that must be resolved in subsequent research. Figures 138 and 139 show that the model, which has <u>no</u> free parameters for adjusting the scale of $(\nu_1 - \nu_1)/\nu_2$, is in excellent functional agreement and in good quantitative agreement with the measured results. Furthermore, the decrease in $(\nu_2 - \nu_1)/\nu_2$ that results from changing the edge contrast from 12% to 82% is successfully predicted by the model.

Consider next the results of Figs. 141, 142, and 143, which were obtained using the manikin and crowd scenes. Now, however, the predicted results were obtained by approximating the pictorial input with a one-dimensional 100% contrast luminance edge. (Essentially the same predicted results can be obtained using DDD No. 1 with $R(\nu) = [1 + 0.951(\nu/\nu_{1,2})^2 + 0.045(\nu/\nu_{1,2})^6]^{-1}$.) In connection with these figures, we wish to make the following observations. First, it may be seen that the measured results for these images are functionally similar to the results obtained for the 82% contrast edge. This is an important finding since it represents additional indirect evidence that not only are luminance edge transitions an important feature of natural scenes, but they are also perceptionally significant in performing these discrimination tasks. The major difference between the edge and pictorial results is in the magnitude of $(\nu_1 - \nu_1)/\nu_2$, which is generally smaller for pictorial scenes than

---

*This correction for $k(\nu)$ is seldom required in practical display situations since the effective bandwidth of the system is rarely less than 8 to 10 cycles/degree. It is only in experiments such as those given here, where the range of ν_1 is entended to test the functional correctness of the model, that this consideration becomes important.

it is for the edge. In the model this can be due to two possibilities:
(1) probability summation among <u>orientation</u> specific channels, and (2) an
effective perceived power spectrum that is somewhat larger than that of a
single 82% contrast edge. It is for this latter reason that we have approxi-
mated the power spectrum for pictorial scenes as a 100% contrast one-dimensional
edge input. Second, the measured results for the manikin scene in either black-
and-white (Fig. 140) or color (Fig. 141) are indistinguishable. This result
means that the contrast-detection model can be applied to either black-and-
white or colored images without modification. Third, although the crowd and
manikin scenes were chosen to represent images with quite different subjective
properties, the measured results for observers P.R. and B.S. using these scenes
are essentially the same. This result might seem surprising, since the power
spectra for these scenes (Fig. 127) show that the crowd scene has substantially
more power at the higher spatial frequencies than does the manikin scene. This
high-frequency power is a direct consequence of the large number of luminance
edge transitions distributed throughout this picture. However, due to the
inhomogeneity of the visual system, as represented by Eq. (26) for the effec-
tive integration length of the visual system, much of the high-frequency
structure in these edges cannot be seen simultaneously. Thus, to the degree
that more than one high-contrast edge transition cannot be perceived simulta-
neously in either image, the measured results will be approximately the same.
At the lowest frequencies the visual system integrates over larger length
scales [Eq. (26)]; therefore, the measured spectra of Fig. 127 at low frequen-
cies should be a better indicator of the relative perceived signals. However,
since from this figure it may be seen that there is little difference in the
magnitude of the power spectra between the crowd and manikin scenes at the
lower frequencies, only minor differences are expected in the measured values
of $(\nu_2 - \nu_1)/\nu_2$ at these frequencies.

Figure 143 shows the measured and predicted results obtained with the
cockpit display of Fig. 137. These experiments were conducted under the same
conditions described above, with the exception that the mean display luminance
was 2 mL instead of 35 mL. Therefore, in the contrast-detection model the
values of $m_T(\nu)$ for this value of mean luminance were used (from Fig. 121).
It may be seen from the figure that the measured results for this image are
functionally similar to those given before. The primary difference is an

increase in the magnitude of $(\nu_2 - \nu_1)/\nu_2$ at all ν_1. Note, however, that in this case the predictions of the contrast-detection model are in particularly good agreement with the measured results. This result, when combined with the results given above, shows that the contrast detection model, and thus the DDDs, can be used successfully to describe changes in the properties of displays with remarkably dissimilar appearance.

4. Discrimination Experiments: Simultaneous Presentation

Observers were asked to determine, using a two-alternative forced-choice procedure, which of two images presented side by side on matched displays, but with slightly different bandwidths, appeared sharper. Both displays subtended 10 degrees and were separated by 4 degrees. The observers inspected each pair of images for up to 15 seconds and could use whatever inspection technique they found most suitable for performing the discrimination task. All other details involving the apparatus, experimental procedure, and experimental conditions are the same as those described earlier for the sequentially presented experiments.

5. Results and Discussion: Simultaneous Presentation

The measured and predicted results shown in Figs. 144 and 145 were obtained using the manikin and crowd scenes, respectively, of Fig. 128. As in the case of sequential presentation, there is no statistical difference between the measured results for the two scenes. Also, it may be seen that the measured results are once again in good agreement with the predicted curve. This is a significant finding; it establishes that, at least for display bandwidths down to roughly 10 cycles/degree, the computed results summarized in the DDDs are not strongly dependent on viewing procedure.*

---

*This result is actually predicted by the contrast-detection model. Of the inputs to the model, $k(\nu)$, $\Phi(f)$, $\Delta\nu$, $\ell(\nu)$, and $m_T(\nu)$, only $k(\nu)$ could change substantially with the changes in experimental conditions considered here. However, it is known from the results of experiments in similar situations that it does not [16,17]. Therefore, the measured values of $(\nu_2 - \nu_1)/\nu_2$ in both cases should be similar.

MANIKIN SCENE IN BLACK AND WHITE

SYMBOL	SUBJECT
•	A.P.
x	C.C.
▲	JM
□	JMc
+	M.F.

$I = 35\ mL$
$r/w = 5.2$

MODULATION TRANSFER

MODULATION TRANSFER

$\dfrac{\nu_2 - \nu_1}{\nu_2}$

RETINAL FREQUENCY, ν

RETINAL FREQUENCY, ν

RETINAL FREQUENCY ν_1 (CYCLES/DEGREE)
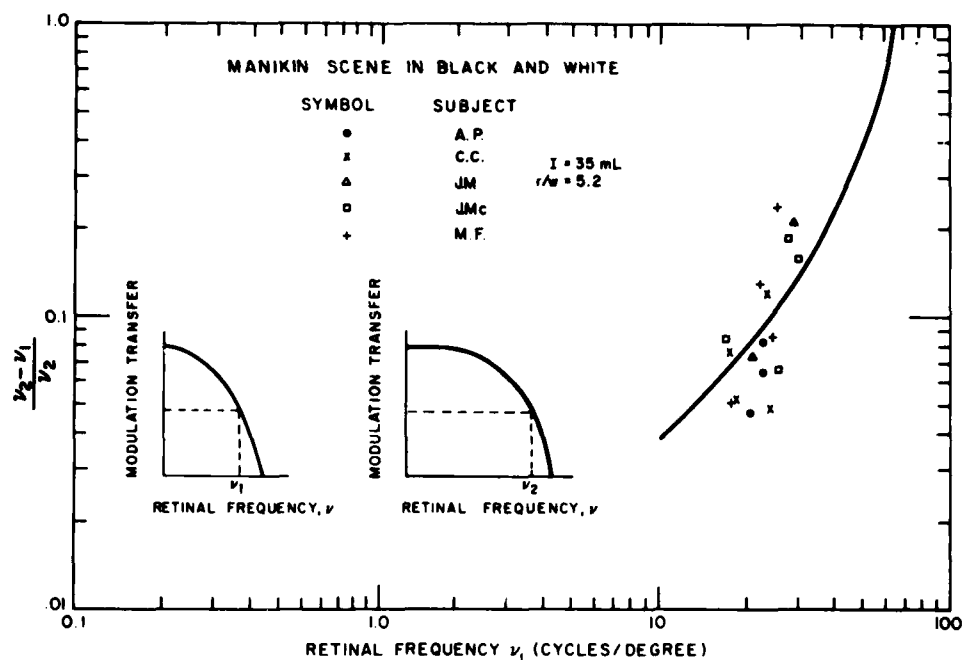
Figure 144. Measured results of modulation transfer discrimination experiments performed with the manikin scene of Fig. 128 in color. The measurements are plotted with $(\nu_2 - \nu_1)/\nu_2$ as a function of ν_1, where ν_2 and ν_1 are defined in the insets on the figure. These experiments were performed with two displays, each subtending 10° and separated by 4°. The observers inspected the two displayed images for up to 15 seconds and then stated which image had the higher bandwidth. The difference in bandwidth $\nu_2 - \nu_1$ was defined as that change from ν_1 necessary for an observer to detect the higher bandwidth image 75% of the time. The solid curve on the figure represents the predicted results of the contrast-detection model assuming probability summation among independent frequency-specific channels, as explained in the text.
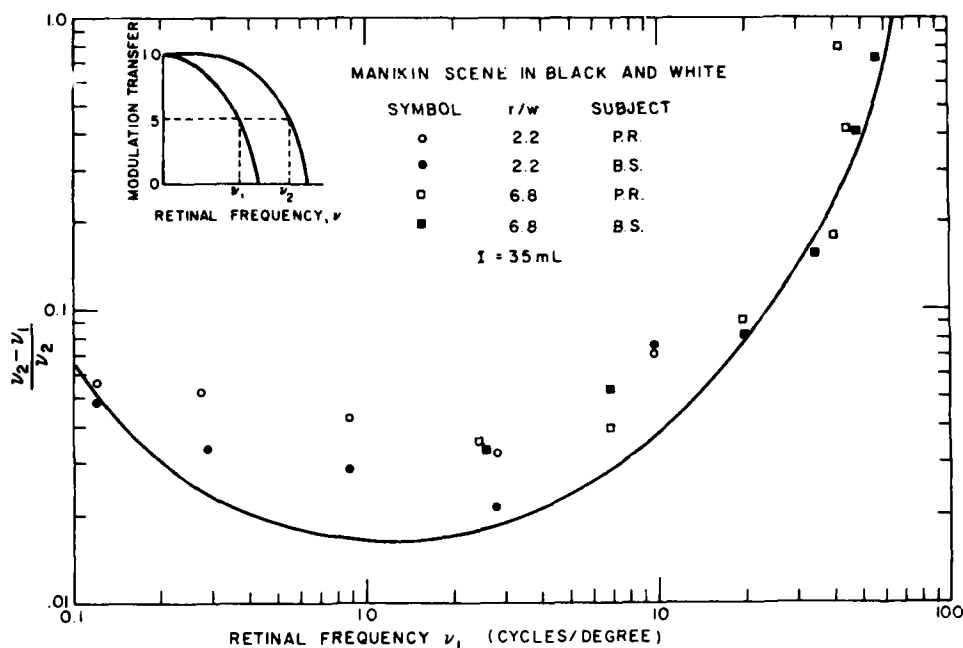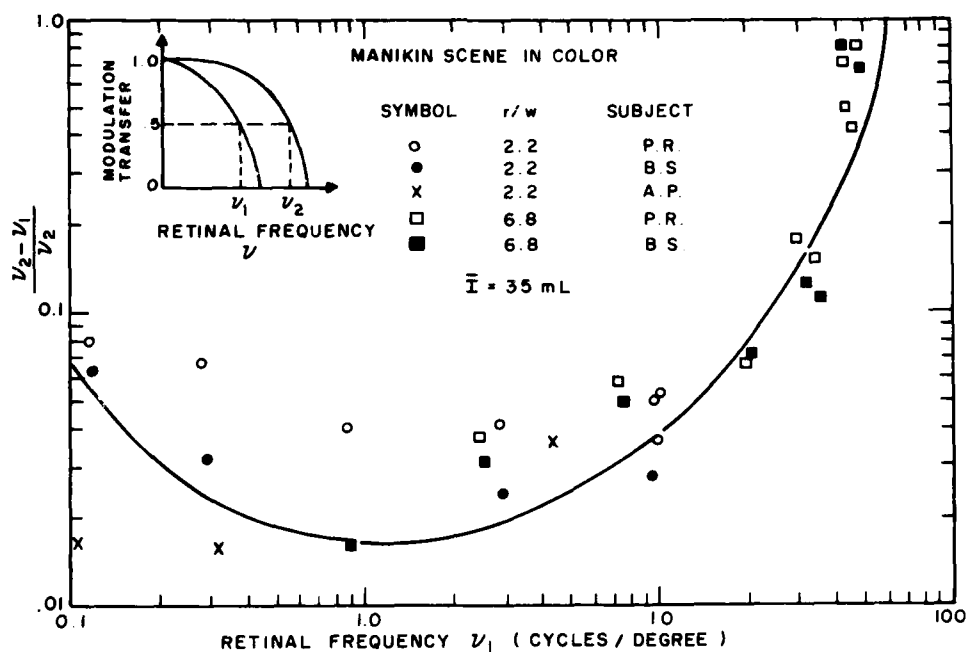
6. Conclusions

First, the results presented here have shown that the predictions of the contrast-detection model are in good agreement with experiments performed to determine the just-noticeable difference in image structure as a function of display modulation transfer. Second, the measured results using a high-contrast luminance edge transition, two different pictorial images, and an aircraft cockpit flight indicator, were found to be similar. These findings support the contention

209
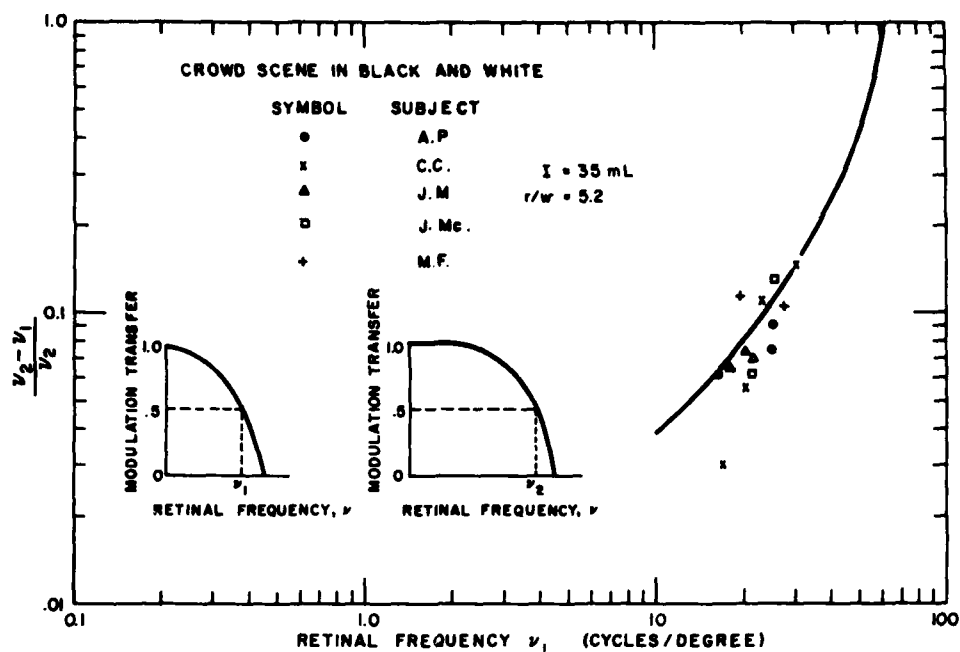
Figure 145. Measured results of modulation transfer discrimination experiments performed with the crowd scene of Fig. 128 in black and white. The measurements are plotted with $(v_2 - v_1)/v_2$ as a function of v_1, where v_2 and v_1 are defined in the insets on the figure. These experiments were performed with two displays, each subtending 10° and separated by 4°. The observers inspected the two displayed images for up to 15 seconds and then stated which image had the higher bandwidth. The difference in bandwidth $v_2 - v_1$ was defined as that change from v_1 necessary for an observer to detect the higher bandwidth image 75% of the time. The solid curve on the figure represents the predicted results of the contrast-detection model assuming probability summation among independent frequency-specific channels, as explained in the text.
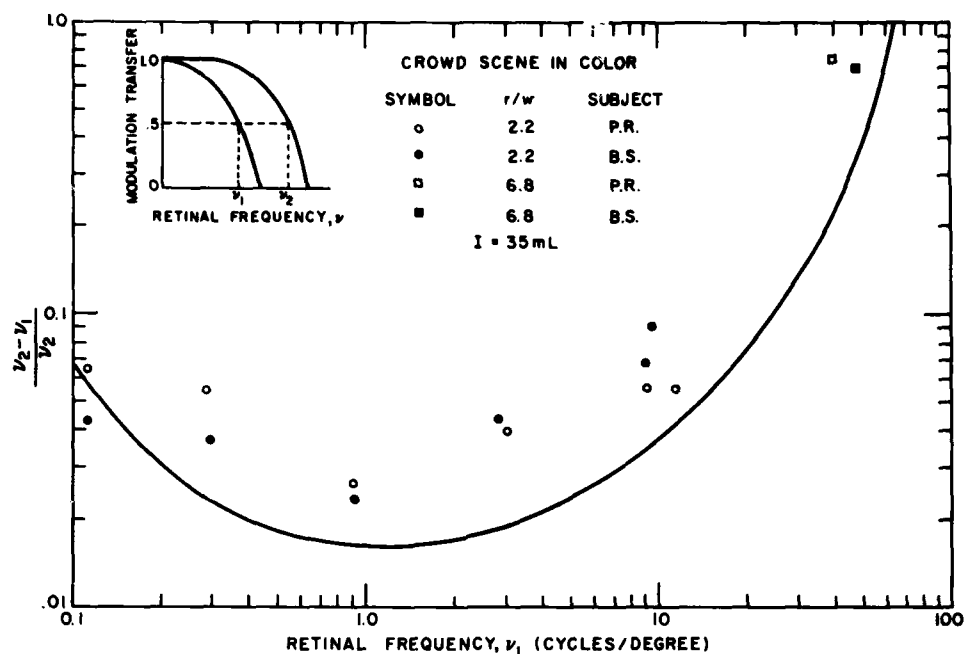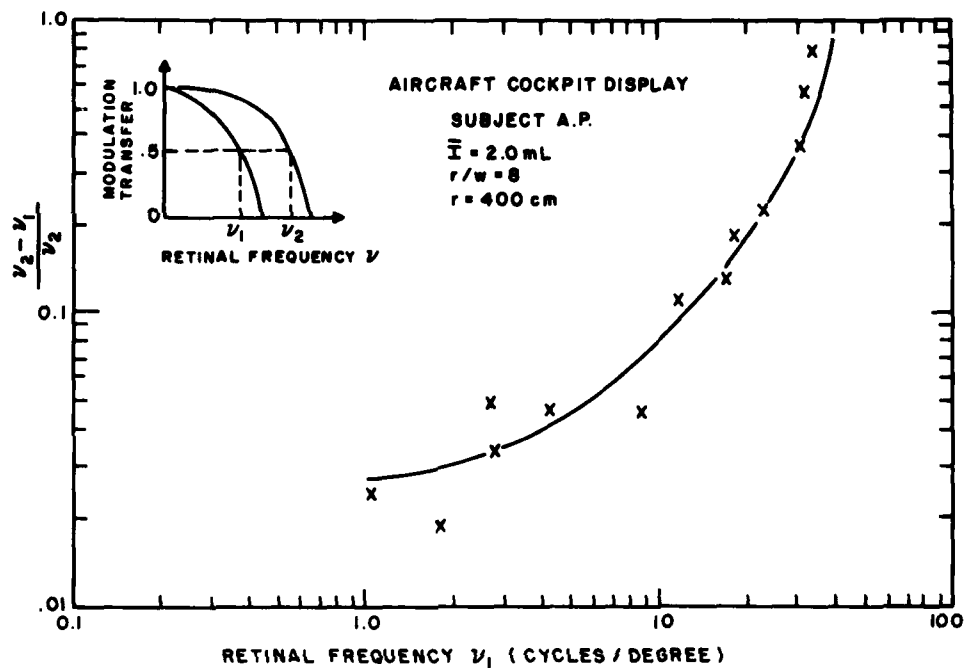
that edge transitions are an important feature of many images, and that the contrast-detection model, as summarized in the DDDs is readily applied to a diverse range of displayed images. Third, it was shown that discriminable differences in display bandwidth are independent of color in the images. Thus, the DDDs can be used without modification for either black-and-white or colored images. Finally, it was shown that for bandwidths above roughly 10 cycles/degree, the jnd in display modulation transfer between two images

210

does not depend strongly on whether they are examined sequentially on the same display or side-by-side on two different displays. Therefore, the DDDs given in this report can be applied directly to either situation.

APPENDICES

APPENDIX A

POWER SPECTRA FOR VARIOUS SIGNALS

In this Appendix the expressions for the perceived power spectra and the equivalent sine-wave contrasts for various input signals are derived. These expressions were employed in the calculation of the DDDs described in Sections II and III in the main body of the report. Two distinct cases are considered below: a single luminance edge transition located in the center of the display screen, and a random input of either pictorial scenes or white noise.

1. Spectrum of a Single Luminance Edge Transition

Consider a display with mean luminance $\bar{I}$ with a single luminance transition of magnitude ΔI, located at the center of the display screen, as shown in Fig. 119. The input luminance pattern $I_o(x)$ is then

$$
\begin{aligned}
I_o(x) &= \bar{I} - \tfrac{1}{2}\Delta I; \quad -\tfrac{1}{2}w \le x \le 0 \\
&= \bar{I} + \tfrac{1}{2}\Delta I; \quad\;\; 0 < x \le \tfrac{1}{2}w
\end{aligned}
\tag{A-1}
$$

The Fourier transform $\hat{I}_o(f)$ of this pattern is

$$
\hat{I}_o(f) = \int_{-\frac{1}{2}w}^{+\frac{1}{2}w} dx\, I_o(x)\exp(-2\pi i f x)
\tag{A-2}
$$

Inserting Eq. (A-1) into Eq. (A-2) and performing the elementary integrations yields

$$
\hat{I}_o(f) = (\bar{I}/\pi f)\sin(\pi f w) + (\Delta I/i\pi f)\sin^2(\pi f w/2)
\tag{A-3}
$$

In order to obtain the perceived power spectra for the input signals, we must compute the spatial sum of the square of the luminance profile $I_o(x)$. This quantity is called the "spatially summed power." As discussed in Section IV.B, the summation is performed over the characteristic integration length of the visual system ℓ. Thus, the spatially summed power is

$$
\int_{-\frac{1}{2}\ell}^{+\frac{1}{2}\ell} dx\, I_o^2(x) = \int_{-\frac{1}{2}\ell}^{+\frac{1}{2}\ell} dx \int_{-\infty}^{+\infty} df \int_{-\infty}^{+\infty} df'\; \hat{I}_o(f)\hat{I}_o(f')\exp[2\pi i(f + f')x]
\tag{A-4}
$$

213

The integration over x is performed first, yielding a factor $\sin[\pi(f + f')\ell]/[\pi(f + f')]$. Next, the integration over f' must be evaluated. We consider only the contribution from the second term in Eq. (A-3), since this term is due to the presence of the edge transition. After a straightforward application of the techniques of complex integration, we find

$$\int_{-\frac{1}{2}\ell}^{+\frac{1}{2}\ell} dx\, I_o^2(x) = \int_{-\infty}^{+\infty} df\, (\Delta I/2\pi f)^2 [1 - \cos(\pi f w)][1 - \cos(\pi f \ell)] \qquad (A-5)$$

For frequencies $f \gg 1/w$, the term $\cos(\pi f w)$ oscillates very rapidly. Therefore, for the purposes of computing the power within a relatively broad spectral band, it can be neglected. Similarly, since ℓ encompasses many wavelengths, the term $\cos(\pi f \ell)$ is also a rapidly oscillating phase factor that can be neglected. The final result for the spatially summed power is then

$$\int_{-\frac{1}{2}\ell}^{+\frac{1}{2}\ell} dx\, I_o^2(x) = \int_{0}^{+\infty} df\, P(f) \qquad (A-6)$$

where P(f) is the desired perceived power spectrum for positive frequencies:

$$P(f) = 2(\Delta I/2\pi f)^2 \qquad (A-7)$$

2. Spectrum of a Random Input

For a random input, Eq. (A-2) still applies, but in this case we do not have precise information as to the form of $\hat{I}_o(f)$. Instead we are given only the autocorrelation function of $\hat{I}_o(f)$:

$$\langle\, \hat{I}_o(f)\hat{I}_o(f')\, \rangle = \Phi(f)\delta(f + f') \qquad (A-8)$$

Here the brackets denote an average over an ensemble of random inputs, and $\Phi(f)$ is the power spectrum of the input (see Ref. 1, pp. 39-40). Next, we compute the spatially summed power as above. Because of the random nature of the input, this quantity must now be regarded as an average over many samples

214

from the statistical distribution of possible functions $\hat{I}_o(f)$. Using Eqs. (A-4) and (A-8), we again obtain Eq. (A-6), with

$$P(f) = \ell(f)\Phi(f) \tag{A-9}$$

In this equation, we have indicated the frequency dependence of ℓ explicitly.

We can now easily derive expressions for $P(f)$ for the cases of white noise and pictorial scenes. For white noise, we have $\Phi(f) = N(f) = $ constant, where $N(f)$ is the noise spectrum. The mean square noise fluctuation N^2 is given by

$$N^2 = \int_0^{f_{max}} df N(f) \tag{A-10}$$

where f_{max} is the maximum spatial frequency of the noise. From Eqs. (A-9) and (A-10), we obtain

$$P(f) = \ell(f) N^2 / f_{max} \tag{A-11}$$

For pictorial scenes, we have, from Eq. (33),

$$P(f) = \frac{2\ell(f) f_L \overline{I_m^2}/\pi}{f^2 + f_L^2} \tag{A-12}$$

where $f_L \cong 1/w$ is the lower cutoff frequency, and $\overline{I_m^2}$ is the contribution to the mean square luminance from pictorial information.

3. Equivalent Sine-Wave Contrasts

According to the discrimination detection model, a continuous spatial frequency spectrum may be regarded as equivalent to a single sine wave of appropriate contrast. This equivalent contrast is chosen so that the spatially summed power associated with the sine wave is equal to the spatially summed power of the continuous spectrum that is contained within a single frequency-specific channel of the visual system. Thus, the equivalent sine-wave contrast $m_{eq}(f)$ is defined by

$$\tfrac{1}{2} m_{eq}^2(f) \ \overline{I}^2 \ell(f) = P(f)(180\Delta\nu/\pi r) \tag{A-13}$$

215

where $\bar{I}$ is the mean luminance, and Δv is the width, in cycles/degree, of the frequency-specific channel corresponding to the display frequency f [$f = 180v/\pi r$]. We take one-octave-wide channels ($\Delta v/v = 2/3$) for $v \geq 3/2$ cycles/degree and $\Delta v = 1$ for $v < 3/2$. We also take $\ell(f) \overset{\sim}{=} 14/f$, as discussed in Section IV.B. From Eqs. (A-7), (A-11), and (A-12), we readily obtain the following expressions for the equivalent contrasts m_E, m_P, and m_N for a single-edge transition, pictorial scenes, and white noise, respectively:

$$m_E^2(f) = (1/21\pi^2)(\Delta I/\bar{I})^2; \qquad v \geq 3/2 \text{ cycles/degree}$$

$$= (1/14\pi^2)(\Delta I/\bar{I})^2(180/\pi r f); \quad v < 3/2 \text{ cycles/degree} \qquad \text{(A-14)}$$

$$m_P^2(f) = \frac{(8/3\pi)(\overrightarrow{I_m^2}/\bar{I}^2)f\ f_L}{f^2 + f_L^2}; \qquad v \geq 3/2 \text{ cycles/degree}$$

$$= \frac{(4/\pi)(\overrightarrow{I_m^2}/\bar{I}^2)(180/\pi r f)f\ f_L}{f^2 + f_L^2}; \quad v < 3/2 \text{ cycles/degree} \qquad \text{(A-15)}$$

$$m_N^2(f) = (4/3)(N^2/\bar{I}^2)f/f_{max}; \qquad v \geq 3/2 \text{ cycles/degree}$$

$$= 2(N^2/\bar{I}^2)(180/\pi r f_{max}); \qquad v < 3/2 \text{ cycles/degree} \qquad \text{(A-16)}$$

Equations (A-14) through (A-16), along with Eq. (31) for the distribution of discriminable levels and Table 11 for the required parameters, were employed in the construction of DDD Nos. 1 through 80 for analog displays.

APPENDIX B

EQUATIONS FOR SAMPLED AND RASTER DISPLAYS

In this Appendix, we present the equations that were utilized in the construction of Discriminable Difference Diagrams Nos. 81 through 100 for sampled/raster displays and in the individual examples described in Section II.C.2.

1. Displayed Intensity Pattern

From Section II.B of ref. 1, the displayed intensity pattern for a one-dimensional sampled display is

$$I(x) = \sum_{m=-\infty}^{+\infty} \int_{-\infty}^{+\infty} df R_D(f) R_P(f - mf_s) \operatorname{sinc}[s(f - mf_s)/f_s]$$

$$\times \hat{I}_o(f - mf_s) \exp(2\pi i f x) \tag{B-1}$$

where x is the coordinate on the display screen, m is an integer, and $\hat{I}_o(f)$ is the Fourier transform of the input scene $I_o(x)$:

$$\hat{I}_o(f) = \int_{-\frac{1}{2}w}^{+\frac{1}{2}w} dx \, I_o(x) \exp(-2\pi i f x) \tag{B-2}$$

The function $\operatorname{sinc}(y)$ is defined as

$$\operatorname{sinc}(y) = \sin(\pi y)/\pi y \tag{B-3}$$

As discussed in Section II.C of ref. 1, the term $m = 0$ in Eq. (B-1) is the information-bearing signal component of the displayed intensity pattern, whereas the terms $m \neq 0$ constitute a noise contribution. Thus, the signal contribution to the displayed intensity pattern is

$$I_S(x) = \int_{-\infty}^{+\infty} df \, R_D(f) R_P(f) \operatorname{sinc}(sf/f_s) \hat{I}_o(f) \exp(2\pi i f x) \tag{B-4}$$

217

and the noise contribution is

$$I_N(x) = \sum_{m \neq 0}^{\pm \infty} \int_{-\infty}^{+\infty} df \ R_D(f) R_P(f - mf_s) \text{sinc}[s(f - mf_s)/f_s]$$

$$\times \ \hat{I}_o(f - mf_s) \exp(2\pi i f x) \tag{B-5}$$

2. Equivalent Sine-Wave Contrasts

According to the discrimination detection model, a continuous spatial frequency spectrum may be regarded as equivalent to a single sine wave of appropriate contrast. The equivalent contrast is chosen so that the spatially summed power associated with the sine wave is equal to the spatially summed power of the continuous spectrum that is contained within a single frequency-specific channel of the visual system. Therefore, the first step in deriving the expressions for the equivalent sine-wave contrasts is to obtain the frequency spectrum of the spatially summed powers corresponding to $I_S(x)$ and $I_N(x)$. Using Eqs. (B-4) and (B-5), simple Fourier analysis gives

$$\int_{-\frac{1}{2}\ell}^{+\frac{1}{2}\ell} dx \ I_S^2(x) = \int_{-\infty}^{+\infty} df \ |R_D(f)|^2 |R_P(f)|^2 \text{sinc}^2(sf/f_s) |\hat{I}_o(f)|^2 \tag{B-6}$$

$$\int_{-\frac{1}{2}\ell}^{+\frac{1}{2}\ell} dx \ I_N^2(x) = \sum_{m,n \neq 0}^{\pm \infty} \int_{-\infty}^{+\infty} df \ |R_D(f)|^2 R_P(f - mf_s) R_P^*(f - nf_s)$$

$$\times \ \text{sinc}[s(f - mf_s)/f_s] \text{sinc}[s(f - nf_s)/f_s]$$

$$\times \ \hat{I}_o(f - mf_s) \hat{I}_o^*(f - nf_s) \tag{B-7}$$

where the asterisk denotes the complex conjugate, and ℓ is the spatial integration length of the visual system (see Section IV.B).

We treat the case of a single edge transition, of magnitude ΔI, located at a position $x = x_1$ on the display screen. For this case, we have $\hat{I}_o(f) = (\Delta I/2\pi i f)\exp(-2\pi i f x_1)$. We substitute this expression into Eqs. (B-6) and (B-7) and find, after averaging over possible values of x_1,

$$\int_{-\frac{1}{2}\ell}^{+\frac{1}{2}\ell} dx \ I_S^2(x) = \int_0^\infty df \ P_S(f)|R_D(f)|^2 \tag{B-8}$$

$$\int_{-\frac{1}{2}\ell}^{+\frac{1}{2}\ell} dx \ I_N^2(x) = \int_0^\infty df \ P_N(f)|R_D(f)|^2 \tag{B-9}$$

where

$$P_S(f) = 2(\Delta I/2\pi f)^2|R_P(f)|^2 \text{sinc}^2(sf/f_s) \tag{B-10}$$

$$P_N(f) = \sum_{m \neq 0}^{\pm\infty} 2(\Delta I/2\pi[f - mf_s])^2|R_P(f - mf_s)|^2$$

$$\times \ \text{sinc}^2[s(f - mf_s)/f_s] \tag{B-11}$$

The equivalent sine-wave contrasts for the edge signal $m_E(f)$ and for the noise $m_N(f)$ are defined by the expressions

$$\tfrac{1}{2} m_E^2(f)\bar{I}^2\ell(f) = P_S(f)(180\Delta\nu/\pi r) \tag{B-12}$$

$$\tfrac{1}{2} m_N^2(f)\bar{I}^2\ell(f) = P_N(f)(180\Delta\nu/\pi r) \tag{B-13}$$

where $\bar{I}$ is the mean luminance, and $\Delta\nu$ is the width, in cycles/degree, of the frequency-specific channel corresponding to the display frequency f. We take

219

$\ell \stackrel{\sim}{=} 14/f$ (see Section IV.B). We also take one-octave-wide channels ($\Delta v/v = 2/3$) for $v \geq 3/2$ cycles/degree and $\Delta v = 1$ for $v < 3/2$. Then Eqs. (B-10) through (B-13) become

$$m_E^2(f) = (1/21\pi^2)(\Delta I/\bar{I})^2 |R_p(f)|^2 \text{sinc}^2(sf/f_s); \quad v \geq 3/2 \text{ cycles/degree}$$

$$= (1/14\pi^2)(\Delta I/\bar{I})^2(180/\pi rf)|R_p(f)|^2 \text{sinc}^2)sf/f_s);$$

$$v < 3/2 \text{ cycles/degree} \tag{B-14}$$

$$m_N^2(f) = \sum_{m \neq 0}^{\pm\infty} (1/21\pi^2)(\Delta I/\bar{I})^2(f/[f - mf_s])^2 |R_p(f - mf_s)|^2$$

$$\times \text{sinc}^2[s(f - mf_s)/f_s]; \quad v \geq 3/2 \text{ cycles/degree}$$

$$= \sum_{m \neq 0}^{\pm\infty} (1/14\pi^2)(\Delta I/\bar{I})^2(180/\pi rf)(f/[f - mf_s])^2$$

$$\times |R_p(f - mf_s)|^2 \text{sinc}^2[s(f - mf_s)/f_s]; \quad v < 3/2 \text{ cycles/degree} \tag{B-15}$$

Equations (B-14) and (B-15), along with Eq. (31) for the distribution of discriminable levels and Table 11 for the required parameters, were employed in the contruction of DDD Nos. 81 through 100. For cases in which the channel frequency v corresponded to a display frequency sufficiently close to an integer multiple of f_s, Eqs. (B-14) and (B-15) give rise to values of m_N greater than unity. According to the channel hypothesis, the number of discriminable levels cannot exceed the value for a single sine-wave with 100% modulation. Therefore, when necessary, the value of m_N was cut off at $m_N = 1$.

APPENDIX C

NOISE VISIBILITY: THREE ISSUES

We are concerned here with three issues that can affect the predictions
given in the DDDs for analog noise. They are: (1) the display of temporally
dynamic noise, (2) the meaning of the visibility of noise when in the presence
of an "ensemble-averaged" pictorial scene, and (3) the influence on noise
visibility due to the distribution of luminance levels in pictorial scenes.
This last issue is illustrated by considering the effects of gamma changes
on the displayed signal-to-noise ratio. Each of these issues will be dis-
cussed briefly below.

Issue 1

The DDDs for analog noise given in this report were prepared for the case
of temporally static noise. Other diagrams can be constructed for cases in-
volving temporally dynamic noise by substituting the sine-wave contrast-
sensitivity function that represents the temporal properties of the noise in
the contrast-detection model used to construct the DDDs.* The relationship
between sine-wave contrast sensitivity and the predictions of the contrast-
detection model is discussed in Section IV, and in ref. 27 the results of
sine-wave contrast-sensitivity measurements are given for a wide range of
temporal frequencies. It follows from these results that, when displayed at
temporal frequencies below 30 Hz, temporally dynamic noise will generally be
more visible at lower spatial frequencies than temporally static noise but
less so at intermediate and higher spatial frequencies.

Although the issue of the visibility of static versus dynamic noise has
not been extensively investigated, a study performed by Mounts and Pearson
[49] with a television-like system found only moderate differences between
the visibility of static and dynamic noise. Using a 70-mL highlight luminance,
10-degree interlace-scanned display, they found that over a wide range of

---

*We assume here that $k(\nu)$ in Eq. (20) [in the main body of the text] is inde-
pendent of temporal frequency.

display signal-to-noise ratios, the visibility of stationary bandlimited white gaussian noise was less than 3 dB greater than for nonstationary noise.

Issue 2

The DDDs for analog noise in the presence of pictorial information given in this report were computed assuming an input scene whose spectral properties were obtained from the ensemble average of the power spectra from many different pictorial scenes. As explained in Section IV.D, we chose this input because it represents a perceptual condition where an observer obtains an overall impression of the displayed images. When noise is added to this ensemble-averaged input, the same meaning is retained for the noise. That is, the DDDs for analog noise represent a measure of the *average* number of jnd's of noise that an observer would see on a displayed image. Nevertheless, in practice, one must expect that there will be regions on an image where the actual number of jnd's of noise will be either larger or smaller than the number predicted by the DDDs. There are two reasons for this. First, images are not evenly modulated (there are regions of uniform luminance, areas of texture, edges, etc.). Thus, the amount of spatial frequency masking of the noise will vary according to the local properties of the image. This is easily verified by observing a noisy television picture. For regions at the same mean luminance, the noise will be much less visible in areas of texture than in areas of uniform luminance. Second, the number of jnd's of noise seen in an image will vary according to the local luminance. Since we have assumed that the noise is added to the luminance signal of the image, the *contrast* of the noise will vary inversely with the local image luminance. Therefore, for similar conditions, the number of jnd's of noise in the lowlight regions will be larger, and the number in the highlight regions lower, than the average number predicted by the DDDs. [This result is offset, somewhat, by the fact that contrast sensitivity is greater in highlights and smaller in lowlights (see Fig. 121).]

Issue 3

In this report we have represented the spatial properties of pictorial images by an ensemble-averaged power spectrum, as described in Section IV.D. This spectrum specifies one important property of pictorial information, but it does not uniquely specify the luminance properties of pictorial scenes. There are, for example, many different luminance patterns that have the same power spectrum. One additional measure of the statistical properties of images is the average distribution of luminance levels in those images. In computing the DDDs for analog noise in the presence of pictorial information we have implicitly assumed that the luminance fluctuations across the images are distributed symmetrically* about the mean luminance $\bar{I}$. However, as illustrated in Fig. 129, the actual distribution is highly skewed. In this section we consider a situation where the nonsymmetrical distribution of luminance values can affect the amount of noise seen ⁝ displayed image. These results imply that the predictions from the DDDs fₜₗ analog noise in the presence of pictorial information tend to underestimate the total number of jnd's of noise that would actually be seen.

In display applications, such as commercial television, where the video signal is transmitted to a remote receiver, the primary source of noise added to the video signal is often from the first rf amplifier of the receiver. For such cases it has been found experimentally that a savings of roughly 10 dB in the required video signal-to-noise ratio is obtained if the video voltage V is transmitted as $V^{1/\gamma}$, where $\gamma \simeq 2$, and then "gamma" corrected at the receiver by $(V^{1/\gamma})^{\gamma}$ to recover the original signal V [50]. The following paragraphs outline this process, demonstrating how this savings in signal-to-noise ratio can occur. Finally, we show that these savings are not completely predicted by assuming that the luminance signal is represented only by its average value.

---

*In the contrast-detection model, the spatial-frequency properties of the ensemble-averaged pictorial scenes are represented by a single value of equivalent sine-wave contrast at each frequency-specific channel location. A more complete characterization would include the distribution of equivalent sine-wave contrasts at each channel location. These distribution functions have yet to be measured.

Figure C-1 is a diagram of the process under consideration here. We begin with an image, whose luminance variations I (where $0 \leq I \leq I_0$) are converted to a video voltage V by an imaging device according to

$$V = \alpha I \tag{C-1}$$

where α is a proportionality constant and where $V_0 = \alpha I_0$. The voltage given in Eq. (C-1) is compressed by $1/\gamma$ to give

$$V_1 = V^{1/\gamma} V_0^{1 - 1/\gamma} \tag{C-2}$$

where V_1 has been normalized to a maximum voltage of V_0. Next, an rms noise voltage n is added to the video voltage, as shown in the figure. These signals are then gamma corrected to recover the original video voltage, which is now given by

$$V_2 = \left(V^{1/\gamma} V_0^{1-1/\gamma} + n \right)^{\gamma} V_0^{1-\gamma} \tag{C-3}$$

Finally, this voltage is presented on a display to obtain the original luminance signal, viz.,

$$I = \frac{1}{\alpha} V_2 \tag{C-4}$$

From Eq. (C-3) the signal-to-noise ratio on the display is given by

$$(S/N)_{\gamma} = \frac{V^{1/\gamma} V_0^{1-1/\gamma}}{\gamma \, n} \tag{C-5}$$

Since we wish to obtain a measure of the signal-to-noise ratio advantage realized when $\gamma > 1$, we form the ratio of $(S/N)_{\gamma}$ to $(S/N)_{\gamma=1}$ with the aid of Eq. (C-4) to give (in dB)

$$(S/N)_{\gamma} / (S/N)_{\gamma=1} = 20 \, \log \left[\frac{1}{\gamma} \left(\frac{I}{I_0} \right)^{1/\gamma - 1} \right] \tag{C-6}$$

In Fig. C-2 we have plotted Eq. (C-6) as a function of I/I_0 with $\gamma = 2.2$, which is the nominal gamma used in commercial television practice [5]. It may be seen from this figure that the effect of the 2.2 gamma, as compared with the 1.0 gamma, is to decrease the signal-to-noise ratio of the image highlights and to increase the signal-to-noise ratio of the image lowlights. The overall effect is to even out the perceived signal-to-noise ratio on the display.
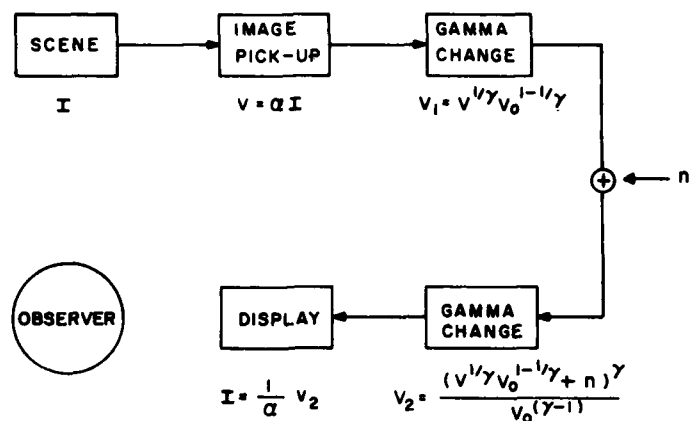
Figure C-1. Schematic diagram of an information channel that introduces a gamma compression before, and a gamma expansion after, the primary source of noise is added to the signal.
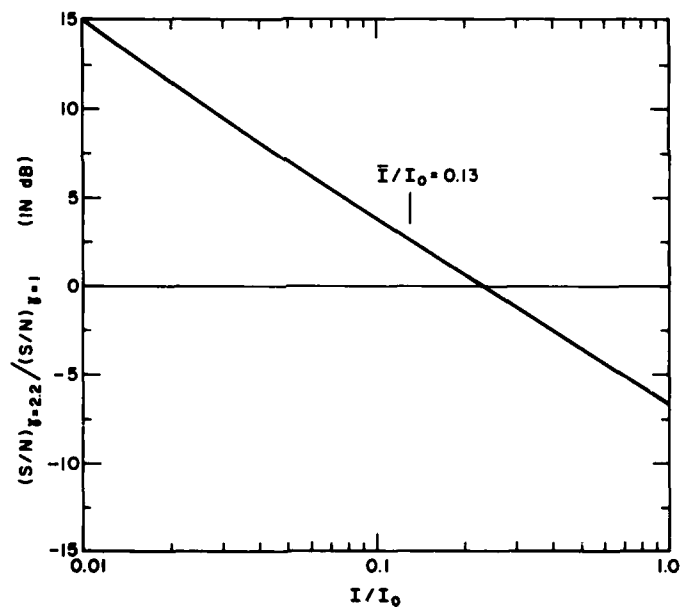
Figure C-2. Ratio of S/N for $\gamma = 2.2$ to S/N for $\gamma = 1$ versus I/I_o, where I represents the local luminance and I_o the maximum luminance in a displayed image.

225

Note, however, that for the average scene luminance $\bar{I} = 0.13\ I_o$ (as discussed in Section IV.D) the gain in S/N is only 2.4 dB, which is substantially less than the 10-dB improvement actually measured. This result can be understood by observing that the distribution of luminance levels in pictorial scenes is highly skewed (see Fig. 129) toward the lower luminance levels where the gain in S/N is more significant.

In summary, this example illustrates that the visibility of noise on a display can be significantly influenced by the distribution of luminance levels in pictorial scenes, which is skewed in favor of the lowlight levels. Since the DDDs for analog noise in the presence of pictorial information given in this report do not include this effect, we conclude that they may underestimate, somewhat, the number of jnd's of noise seen when viewing actual pictorial images.

226

APPENDIX D

IMAGE QUALITY AND THE DDDs

1. Introduction

This Appendix distinguishes between those display problems to which the contrast-detection model (used in computing the DDDs) is expected to apply, and those to which it is not expected to apply. We begin by observing that, in quantifying the performance of a display, two types of problems often arise: those that involve image *quality* and those that involve image *visibility*. Image quality is defined here as those attributes of an image that affect its appearance. Specific image quality issues are image sharpness [TR1,6] and image noisiness. Image visibility is defined here as those attributes of an image that affect its perceived information content. Specific image visibility issues are discrimination of a change in a display variable (the central issue of this report), detection and recognition of objects in an image, and specification of the total amount of perceived information in an image [TR3].

Analytically, the distinction between these two classes of problems is that image quality problems require the perceived amplitude of the displayed information to be specified, while image visibility problems require the perceived signal-to-noise ratio to be specified. This point can be clarified by considering, as a specific case, the contrast-detection model. As explained in Section IV, this model predicts the change in equivalent sine-wave contrast, formed over a band of spatial frequencies, necessary for an observer to see that change with a given error rate. However, the model contains no information about what that change in equivalent contrast will look like. Said differently, the contrast-detection model predicts the required signal-to-noise ratio for the detection of changes in spatial information, but it makes no prediction about the perceived amplitude or strength of those changes. By analogy, it is as if one were to specify the signal-to-noise ratio of a video voltage without specifying its amplitude.

Thus, in general, we expect the contrast detection model to apply to problems of image visibility and not to problems of image quality. As an example, the DDDs address one image visibility problem. They predict the probability with which a change in display modulation transfer can be seen. They can not, however, be expected to make predictions about what such a change will look like. For this problem to be addressed, additional information is required about the perceived amplitude of the information as a function of spatial frequency. Unfortunately this property of the visual system is not well understood. As a result, problems of display image quality are currently modeled with the aid of simple heuristic display descriptors. Although, in selected applications, several descriptors have proven useful [TR1-3], their range of application is inherently limited since they are not founded on fundamental psychophysical properties of the visual system. Furthermore, none of the proposed descriptors systematically incorporates all the relevant display variables, such as display signal-to-noise ratio and spectral properties of the displayed scenes.

In the following paragraphs we present the results of an image quality experiment where observers were required to equate the overall appearance of two displays with different modulation transfer functions (MTFs). The measured results are compared with the predictions of several previously proposed display descriptors. In addition, predictions are made using results obtained from the DDDs. It is shown, in support of the statements made above, that the DDDs do not directly predict the results of this image quality experiment.

2. Description of the Experiment

The objective of this experiment was to determine when two displays with different MTFs were perceived as equivalent. During the experiment the observers' task was to choose which of the two displays they preferred to watch. (In trial experiments observers were first asked to compare the two displays for (1) overall image quality and (2) overall image sharpness. All four observers found these criteria to be vague, and they were dropped in favor of the simple preference criterion, which the observers readily understood. It is interesting to note, however, that the measured results obtained using the two original criteria were within the spread of the results obtained using the eventual preference criterion.)

The two displays used in these experiments were similar in all respects to the one shown in Fig. 134. They subtended 10 degrees horizontally and were situated side by side, 4 degrees apart. The viewing distance was 305 cm, the mean screen luminances were 35 mL, and the displayed images were free of visible spatial frequency noise. Two still, colored images were used: the crowd and manikin scenes shown in Fig. 128. All experiments were conducted, however, with the same image on both displays. At the start of each experiment the displays were carefully matched for magnification, color temperature, and mean luminance. The initial MTFs for both displays were given by $R(\nu) = [1 + 0.951(\nu/\nu_1)^2 + 0.049(\nu/\nu_1)^6]^{-1}$, where ν_1 is the bandwidth parameter (see Fig. 135). At the start of each experiment the bandwidths were set at $\nu_1 = 21$ cycles/degree. Small differences in MTF between the displays were eliminated by preliminary matching experiments with each observer.

The MTFs of the two displays were modified from their initial values as illustrated in Fig. D-1. First, the MTF of display A, whose original MTF is shown as $R_o(\nu)$, was reduced at all spatial frequencies by the addition of uniform white light to the displayed scene. Letting I_S represent the mean luminance of the original scene and I_A the luminance of the light added, the fraction of modulation transfer remaining after adding the light was $\mu = I_S/(I_S + I_A)$ for spatial frequencies whose mean luminance was I_S. In all cases $I_S + I_A = 35$ mL. Thus, after the addition of the white light on the display, an overall effective MTF for display A was given by $R_A(\nu) = \mu R_o(\nu)$. Second, the MTF of display B, whose original MTF was also $R_o(\nu)$, was changed to $R_B(\nu)$ by simply reducing the bandwidth of the display from $\nu_1 = 21$. The form of the MTF was unchanged.

The experimental procedure used consisted of adding a specified amount of white light to display A. Then, using a forced-choice procedure, the observers were required to select the display they preferred to watch, A or B. The bandwidth of display B was changed, in a quasi-random order, to establish the bandwidth that gave an equal preference match to display A. Roughly 50 observations were made to obtain a data point for each image, quantity of white light added, and observer. For each observation the observers were
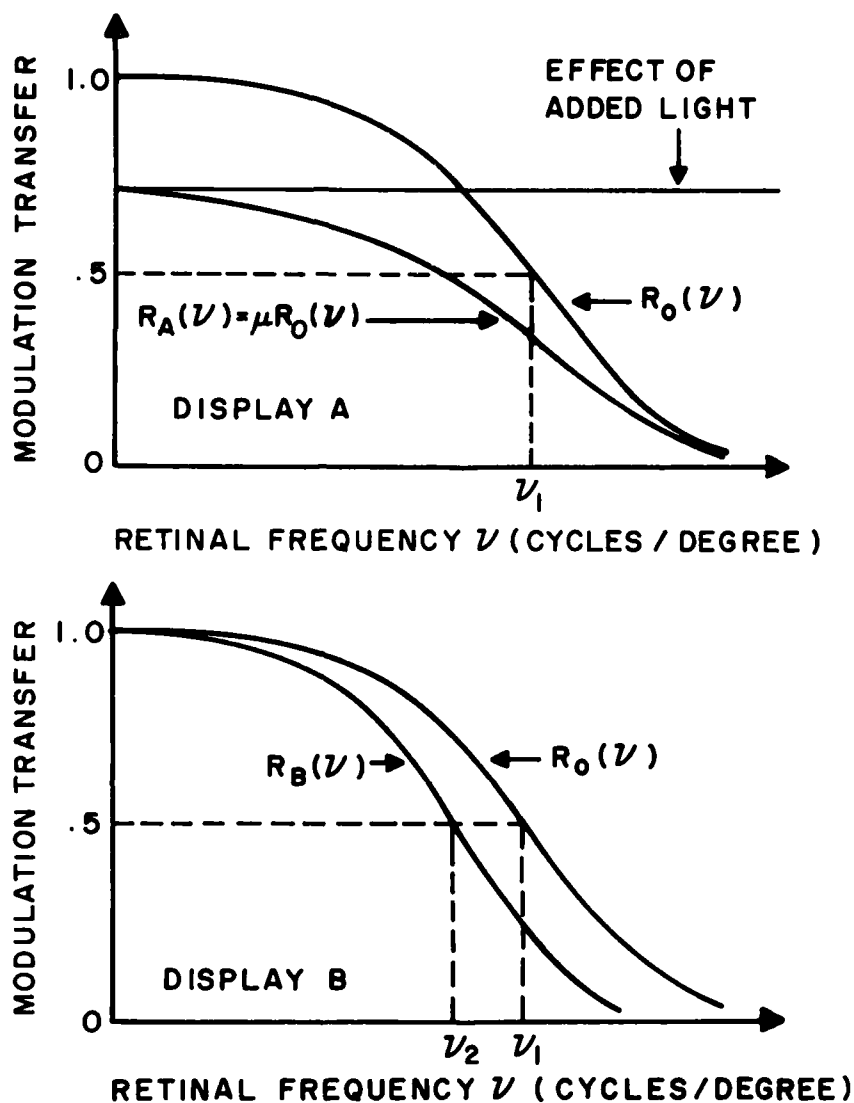
Figure D-1. Schematic representation of how the MTFs for the two displays used in this investigation were changed from their initial values. For both displays $R_0(\nu) = [1 + 0.951(\nu/\nu_1)^2 + 0.049(\nu/\nu_1)^6]^{-1}$, where $\nu_1 = 21$ cycles/degree.

allowed up to 15 seconds to make their choice. Using these procedures we estimate that the accuracy of the match between the two displays for each observer was within $\pm 5\%$.

In summary, the experiment described here consisted of matching, for preference, display A, whose MTF had been reduced at all spatial frequencies, to display B, whose MTF was reduced only at the highest spatial frequencies. A representative example of the images displayed is shown in Fig. D-2. Figure D-2(a) shows the original scene (with ν_1); Fig. D-2(b) shows the same scene with white light added; and Fig. D-2(c) shows the original scene after additional low-pass filtering ($\nu_2 < \nu_1$) to form an equal preference match with Fig. D-2(b). (Note that the results given here are only approximate due to the vagaries of the photographic processes involved in making these figures.)

3. Results

The results of the experiments are shown in Fig. D-3, plotted with fractional bandwidth ν_2/ν_1 versus percent white light added to the scene $I_A \times 100/(I_S + I_A)$. That is, we have plotted the reduction in bandwidth of display B required to form an equal preference match with display A, to which a specified quantity of white light had been added. It may be seen that the measured results obtained from the different images are not significantly different (a similar result was obtained with the modulation transfer discrimination experiments, reported in Section IV).

The solid lines on Fig. D-3 represent the predicted results obtained from four display descriptors. Each of these descriptors will now be discussed according to its letter designation on the figure.

(a) <u>MTFA</u> – The Modulation Transfer Function Area given by $\int_0^{\nu_{max}} d\nu\, (R(\nu) - m_T(\nu))$, where $R(\nu)$ is the display MTF, $m_T(\nu)$ is the sine-wave threshold contrast sensitivity function (Fig. 122), and ν_{max} is the frequency where $R(\nu) = m_T(\nu)$ [51, 52]. Although the MTFA is generally considered to be an image visibility descriptor (using the definition of this appendix), it gives the best correspondence to the measured results. What

(a) ORIGINAL

(b) LIGHT ADDED

(c) FILTERED

Figure D-2. Examples of the images produced by the modulation transfer
            processes illustrated in Fig. D-1. (a) represents the
            original image, (b) represents the original image after
            the addition of white light (Display A), and (c) repre-
            sents the original image after additional low-pass
            filtering (Display B) to form an equal preference
            match with 1(b). (The results given here are only
            approximate due to losses in the photographic proc-
            esses used in producing the figures.)
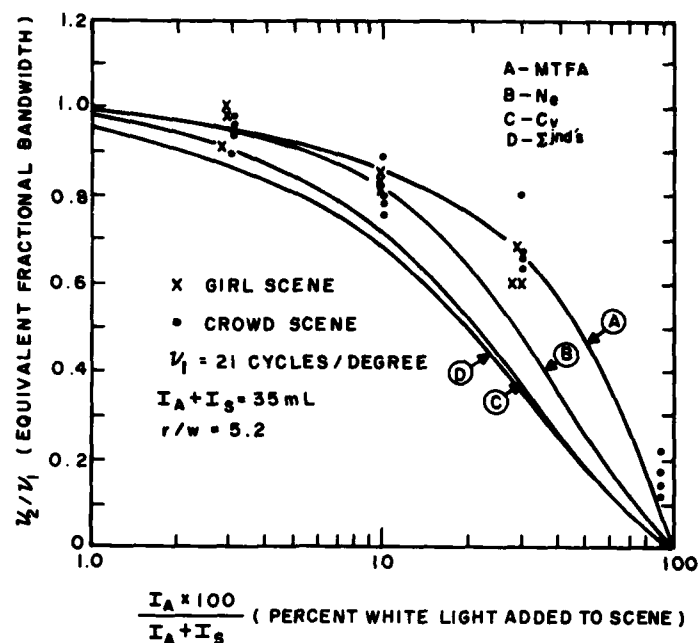
Figure D-3. Measured results obtained from the preference matching experiments plotted with fractional equivalent bandwidth v_2/v_1 versus the percent white light added to the scene $I_A \times 100/(I_S + I_A)$. The solid lines on the figure are the predicted results from several display descriptors, as explained in the text.

separates this descriptor from the others considered here is that it weights the higher spatial frequencies more heavily. The need for such weighting has been reported earlier [53].

(b) N_e – The Noise Equivalent Bandwidth given by $N_e = \int_0^\infty dv R^2(v)$, where $\overline{R(v)}$ is the display MTF in retinal units [54].

(c) C_v – The Visual Capacity given by $C_v = \int_0^\infty dv R^2(v) 0^2(v)$, where $R(v)$ is the display MTF and $0(v)$ is an MTF for the visual system [TR1]. $0(v)$ was formed here using the sine-wave threshold contrast sensitivity results of Fig. 122 (with $\bar{I} = 35$ mL and $r/w = 10$) by taking $0(v) = m_T(3.0)/m_T(v)$, where $m_T(3.0)$ is the minimum value of $m_T(v)$ for these conditions.

(d) The equivalent number of jnd's given by $\sum_{1}^{7} J(i)$, where i represents the index for the seven independent frequency-specific channels, as located in the DDDs (see Table 11), and where J(i) represents the total number of jnd's at each channel location, as given in the DDDs. Thus, this descriptor is based on the assumption that image preference is determined by the total number of jnd's in each image. The predicted results given here were obtained from DDD No. 18. It may be seen from Fig. D-3 that this descriptor does not accurately predict the measured results of this experiment, in agreement with the arguments made earlier in this Appendix.

APPENDIX E

DERIVATION OF THE EQUATION FOR THE

TOTAL NUMBER OF DISCRIMINABLE CONTRAST LEVELS

Equation (30) gives the total number of contrast levels $J(\nu)$ that can be distinguished over the range of sine-wave contrasts from zero to a final value $m(\nu)$. In this appendix we derive Eq. (30). We assume that the signal contrast $m(\nu)$ is displayed in the presence of a second, interfering signal, of contrast $m_I(\nu)$.

We begin by determining the change in contrast $\Delta m(\nu)$ from $m(\nu)$ necessary to perceive an increase of 1 jnd in the contrast of the signal. From Eq. (25) we have

$$[m(\nu) + \Delta m(\nu)]^2 - m^2(\nu) = m_T^2 + k(\nu)[m^2(\nu) + m_I^2(\nu)] \qquad \text{(E-1)}$$

Solving Eq. (E-1) for $\Delta m(\nu)$, we obtain

$$\Delta m(\nu) = \left[\left(1 + k(\nu)\right)m^2(\nu) + k(\nu)m_I^2(\nu) + m_T^2(\nu)\right]^{1/2} - m(\nu) \qquad \text{(E-2)}$$

To solve this equation for the contrast $m_J(\nu)$, associated with the J'th discriminable level, we must first write Eq. (E-2) as a difference equation. Letting $m(\nu) = m_J(\nu)$ and $\Delta m(\nu) = m_{J+1}(\nu) - m_J(\nu)$ gives

$$m_{J+1}(\nu) = \left[\left(1 + k(\nu)\right)m_J^2(\nu) + k(\nu)m_I^2(\nu) + m_T^2(\nu)\right]^{1/2} \qquad \text{(E-3)}$$

Equation (E-3) is readily solved by assuming a solution of the form $m_J^2(\nu) = (ab^J + c)$, where a, b, and c are constants to be determined, subject to the initial condition $m_1^2(\nu) = ab + c = m_T^2(\nu) + k(\nu)m_I^2(\nu)$. Substituting this form into Eq. (E-3) allows the identification of the undetermined constants. The result for $m_J^2(\nu)$ is then

$$m_J^2(\nu) = \left[\left(m_T^2(\nu) + k(\nu)m_I^2(\nu)\right)/k(\nu)\right]\left[\left(1 + k(\nu)\right)^J - 1\right], \quad J = 0, 1, 2 \ldots \qquad \text{(E-4)}$$

Finally, we rearrange Eq. (E-4) and drop the subscript on $m_J(\nu)$, to obtain the total number of discriminable contrast levels $J(\nu)$ for a given signal contrast $m(\nu)$.

$$J(\nu) = \frac{\ln \left[1 + \dfrac{k(\nu)m^2(\nu)}{m_T^2(\nu) + k(\nu)m_I^2(\nu)} \right]}{\left(1 + k(\nu) \right)} \qquad (E-5)$$

When the signals are presented on a display with MTF $R(\nu)$, $m^2(\nu)$ and $m_I^2(\nu)$ are replaced, respectively, by $m^2(\nu)R^2(\nu)$ and $m_I^2(\nu)R^2(\nu)$. This substitution gives Eq. (30).

REFERENCES

1. R. W. Cohen, I. Gorog, and C. R. Carlson, "Image Descriptors for Displays," Technical Report to the Office of Naval Research, Contract No. N00014-74-C-0184, Jan. 1975. (Referred to in the text as TR1.)

2. R. W. Cohen, C. R. Carlson, and G. D. Cody, "Image Descriptors for Displays," Technical Report to the Office of Naval Research, Contract No. N00014-74-C-0184, Jan. 1976. (Referred to in the text as TR2.)

3. J. J. Mezrich, C. R. Carlson, and R. W. Cohen, "Image Descriptors for Displays," Technical Report to the Office of Naval Research, Contract No. N00014-74-C-0184, Jan. 1977. (Referred to in the text as TR3.)

4. D. E. Pearson, *Transmission and Display of Pictorial Information* (John Wiley & Sons, Inc., New York, 1975), p. 87.

5. L. E. Weaver, *Television Measurement Techniques* (Peter Peregrinus Lts., London, 1971), p. 32.

6. C. R. Carlson, "Thresholds for Perceived Image Sharpness," SPSE Journal $\underline{22}$, March/April, 69 (1978).

7. R. W. Cohen, "Applying Psychophysics to Display Design," SPSE Journal $\underline{22}$, March/April, 56 (1978).

8. D. G. Fink, "Color Television vs. Color Motion Pictures," J. SMPTE $\underline{64}$ (1955).

9. See, for example, G. M. Jenkins, and D. G. Watts, *Spectral Analysis and its Applications* (Holden-Day, Inc., San Francisco, 1968), pp. 51-53.

10. See, for example, D. Langmuir, Proc. IRE $\underline{25}$, 977 (1937), or A. M. Morrell, H. B. Law, E. G. Ramberg, and E. W. Herold, *Color Television Picture Tubes*, Advances in Image Pickup and Display, Supplement 1 (Academic Press, Inc., New York, 1974), pp. 23-25.

11. D. M. Green and J. A. Swets, *Signal Detection Theory and Psychophysics* (John Wiley & Sons, Inc., New York, 1966), pp. 209-232.

12. M. B. Sacks, J. Nachmias, and J. G. Robson, "Spatial-Frequency Channels in Human Vision," J. Opt. Soc. Am. $\underline{61}$, 1176 (1971).

13. J. Nachmias and R. V. Sansbury, "Grating Contrast: Discrimination May Be Better Than Detection," Vision Res. $\underline{14}$, 1039 (1974).

14. J. Nachmias, "Signal Detection Theory and Its Application to Problems in Vision," in *Handbook of Sensory Physiology* (Edited by L. M. Hurvich and D. Jameson, Vol. VII/Part 3, Springer, Berlin, 1972), pp. 71-72.

15. J. Nachmias and E. Vocher, "Visual Detection and Discrimination of Luminance Increments," J. Opt. Soc. Am. $\underline{60}$, 382 (1970).

16. J. J. Kulikowski, "Effective Contrast Constancy and Linearity of Contrast Sensation," Vision Res. $\underline{16}$, 1419 (1976).

17. C. R. Carlson and A. Pica, "Sine-Wave Contrast Discrimination Results: Evidence for a Non-Linear Transducer Function in the Visual System," to be published.

18. R. Sansbury, "Some Properties of Spatial Channels Shown by Pulsed Simultaneous Masking," Ph.D. Thesis, Psychology Dept., Univ. of Penn. (1974).

19. N. Graham, "Visual Detection of a Periodic Spatial Stimuli by Probability Summation Among Narrowband Channels," Vision Res. 17, 637 (1977).

20. C. R. Carlson, "Sine-Wave Threshold Contrast Sensitivity Function: Dependence on Display Sizes," accepted for publication, J. Opt. Soc. Am.

21. A. D. Schnitzler, "Theory of Spatial-Frequency Filtering by the Human Visual System. I. Performance Limited by Quantum Noise. II. Performance limited by Video Noise," J. Opt. Soc. Am. 66, 608 (1976).

22. O. H. Schade, Sr., "Optical and Photoelectric Analog of the Eye," J. Opt. Soc. Am. 46, 721 (1956).

23. F. L. Van Ness and M. A. Bowman, "Spatial Modulation Transfer in the Human Eye," J. Opt. Soc. Am. 57, 401 (1967).

24. R. L. Savoy and J. J. McCann, "Visibility of Low-Spatial-Frequency Sine-Wave Targets: Dependence on Number of Cycles," J. Opt. Soc. Am. 65, 353 (1975).

25. J. Hoekstra, D. P. van der Goot, G. van den Brink, and F. A. Bilsen, "The Influence of the Number of Cycles Upon the Visual Contrast Threshold for Spatial Sine-Wave Patterns," Vision Res. 14, 365 (1974).

26. R. Hilz and C. R. Cavonius, "Functional Organization of the Peripheral Retina: Sensitivity to Periodic Stimuli," Vision Res. 14, 1333 (1974).

27. J. G. Robson, "Spatial and Temporal Contrast-Sensitivity Functions of the Visual System," J. Opt. Soc. Am. 56, 1141 (1966).

28. D. J. Tolhurst, C. R. Sharpe, and G. Hart, "The Analysis of the Drift Rate of Moving Sinusoidal Gratings," Vision Res. 13, 2545 (1973).

29. H. W. Schober and R. Hilz, "Contrast Sensitivity of the Human Eye for Square Wave Gratings," J. Opt. Soc. Am. 55, 1086 (1965).

30. F. W. Campbell, J. J. Kulikowski, and J. Levinson, "The Effect of Orientation on the Visual Resolution of Gratings," J. Physiol. (London) 187, 427 (1966).

31. F. W. Campbell and D. G. Green, "Monocular Versus Binocular Visual Acuity," Nature 208, 191 (1965).

32. J. M. Woodhouse, "The Effect of Pupil Size on Grating Detection at Various Contrast Levels," Vision Res. 15, 645 (1975).

REFERENCES (Continued)

33. D. H. Kelly and R. E. Savoie, "A Study of Sine-Wave Contrast Sensitivity by Two Psychophysical Methods," Percept. Psychophys. 14, 313 (1973).

34. J. M. Findlay, "A Spatial Integration Effect in Visual Activity," Vision Res. 9, 157 (1969).

35. T. W. Coltman and A. E. Anderson, "Noise Limitations to Resolving Power in Electronic Imaging," Proc. IRE 48, 858 (1960).

36. J. B. Thomas, An Introduction to Statistical Communication Theory (John Wiley & Sons, Inc., N. Y., 1969).

37. G. T. Buswell, How People Look at Pictures (Univ. of Chicago Press, Chicago, Ill., 1975).

38. R. F. Voss and J. Clarke, "'1/f Noise' in Music: Music from 1/f Noise," J. Acoust. Soc. Am. 63, 258 (1978).

39. T. G. Stockham, Jr., "Image Processing in the Context of a Visual Model," Proc. IEEE 60, 828 (1972).

40. S. F. Quinn and P. M. Newman, "Distribution of Average Picture Levels in Television Programs," Electron. Lett. 1, 261 (1965).

41. See, of example, Introduction to Mathematical Statistics, Third Ed., R. V. Hogg and A. T. Craig (Macmillan Co., London, 1970).

42. C. R. Carlson, R. W. Cohen, and I. Gorog, "Visual Processing of Simple Two-Dimensional Sine-Wave Luminance Gratings," Vision Res. 17, 351 (1977).

43. F. W. Campbell, "The Transmission of Spatial Information Through the Visual System," from Neurosciences Third Study Program, F. O. Schmitt and F. G. Worden, ed., (MIT Press, Cambridge, Mass., 1974), pp. 95-103.

44. See, for example, E. C. Carterette and M. P. Friedman, ed., Handbook of Perception, Vol. V. Seeing, (Academic Press, N. Y., 1975).

45. C. R. Carlson and P. Heyman, "A Large-Format Optical Display for the Generation of Generalized Psychophysical Stimuli," accepted for publication in Vision Res.

46. C. R. Carlson, R. W. Cohen, I. Gorog, and P. M. Heyman, "Subjective Sharpness of Displayed Images as a Function of the Display Modulation Transfer Function," Digest of Tech. Papers from the SID International Symposium held in Boston, Mass., April 1977.

47. C. R. Carlson, R. W. Cohen, and I. Gorog, "Development of an Absolute Scale of Image Sharpness," Proc. 30th Annual Conf. of the SPSE held in North Hollywood, Calif., May 1977.

48. C. R. Carlson and R. W. Cohen, "A Model for Predicting the Just-Noticeable Difference in Image Sharpness as a Function of Display Modulation Transfer," Digest of Tech. Papers from the SID International Symposium held in San Francisco, Calif., April 1978.

REFERENCES (Continued)

49. F. W. Mounts and D. E. Pearson," Apparent Increase in Noise Level When
    Television Pictures are Frame-Repeated," Bell Syst. Tech. J. 48, 527
    (1969).

50. K. McIlwain and E. E. Dean, eds., *Principles of Color Television*
    (John Wiley & Sons., Inc., N. Y., 1965) p. 208.

51. H. C. Borough, R. F. Fallis, T. H. Warnock, and H. J. Britt, "Quantitative
    Determination of Image Quality," Boeing Tech. Report D2-114058-1, May
    1967.

52. H. L. Snyder, "Image Quality and Observer Performance," in *Perception
    of Displayed Information,* L. M. Biberman, ed., (Plenum Press, N. Y.,
    1973) pp. 37-118.

53. C. N. Nelson and G. C. Higgins, "Image Sharpness," in *Advances in the
    Psychophysical and Visual Aspects of Image Evaluation,* R. P. Dooley,
    ed., (Summary of the Proceedings of an SPSE Tech. Conf., Rochester,
    N. Y., Oct. 1977) pp. 72-75.

54. O. H. Schade, Sr., *Image Quality* (RCA Laboratories, Princeton, N. J.,
    1975).

DISTRIBUTION LIST

Chief of Naval Research
800 North Quincy Street
Arlington, VA 22217
Attn: Codes 221   6
               455   1

Defense Documentation Center
Cameron Station
Alexandria, VA 23314   12

Director
Naval Research Laboratory
Washington, DC 20390
Attn: Code 2627   1

Office of Naval Research
   Branch Office
New York Area Office
715 Broadway (5th Floor)
New York, NY 10003   1

Director
Office of Naval Research
   Branch Office
1030 East Green Street
Pasadena, CA 91106   1

Office of Naval Research
   Branch Office
495 Summer Street
Boston, MA 02210   1

Director
Office of Naval Research
   Branch Office
536 Clark Street
Chicago, IL 60605   1

Office of the Chief of Naval
   Operations
Department of the Navy
Washington, DC 20350
Attn: OP-986D   1
       OP-987   1

Headquarters
Department of the Navy
Naval Material Command
Washington, DC 20360
Attn: Systems Effectiveness
       Branch MAT 08T23   1

Commander
Naval Air Systems Command
Washington, DC 20360
Attn: AIR 5335   1
            5313   1
            340D   1
            340F   1
            360A   1
            03PA   1

Commander
Naval Sea Systems Command
Washington, DC 20360
Attn: NSEA 03416   1

Commander
Naval Electronic Systems Command
Washington, DC 20360
Attn: ELEX 320   1
            330   1

Commanding Officer
U.S. Naval Air Development Center
Warminster, PA 13974
Attn: Codes 20P4   1
             607   1
             5023   1

Commander
Naval Ocean Systems Center
San Diego, CA 92152
Attn: Code 7113   1

Commander
Naval Weapons Center
China Lake, CA 93555
Attn: Code 3175   1

Commander
Naval Surface Weapons Center
Dahlgren Laboratory
Dahlgren, VA 20910
Attn: Technical Library   1

Commander
Naval Avionics Facility
6000 E. 21st Street
Indianapolis, IN 46218
Attn: Technical Library   1

Naval Training Equipment Center
Orlando, FL 32813
Attn: Technical Library   1
      N-71   1

Dean of Research Administration
Naval Postgraduate School
Monterey, CA 93940   1

Commander
Naval Underwater Systems Center
Department SB 324
Newport, RI 02840   1

Director, U.S. Army Research
  Institute
1300 Wilson Boulevard
Arlington, VA 22209   1

Commanding General
U.S. Army Electronics Command
Fort Monmouth, NJ 07703
Attn: AMSEL-VL-E   1
      AMSEL-TL-BD   1
      AMSEL-VL-I   1

Commandant, U.S. Marine Corps
Headquarters, U.S. Marine Corps
Washington, DC 20591
Attn: RD-1   1

Commandant
U.S. Coast Guard Headquarters
400 7th Street, NW
Washington, DC 20591
Attn: GDST/62 TRPT   1

Commanding General
U.S. Army Material Command
Washington, DC 20315
Attn: AMCRD-HA   1

Director
Human Engineering Labs
Aberdeen Proving Grounds, MD 21005
Attn: AMXRD-HEL   1

Air Force Avionics Laboratory
Air Force Systems Command
Wright-Patterson AFB, OH 45433
Attn: AFAL/RWI   1

Aerospace Medical Research
  Laboratory
Wright-Patterson AFB, OH 45433
Attn: AMRL/HEA   1

Air Force Office of Scientific
  Research
Bolling Air Force Base
Washington, DC 20332   1

Headquarters, Rome Air
  Development Center
Air Force Systems Command
Griffiss Air Force Base, NY 13441
Attn: RBRAC   1

Federal Aviation Agency
NAFEC Bldg. 10
Atlantic City, NJ 08405
Attn: Code ANA-230   1

Defense Advanced Research Project
  Agency
1400 Wilson Boulevard
Arlington, VA 22209   1

Institute for Defense Analysis
400 Army-Navy Drive
Arlington, VA 22204
Attn: L. Biberman   1

University of Illinois
2-113 Coordinated Sciences
  Laboratory
Urbana, IL 61801
Attn: Dr. G. Slottow   1

Virginia Polytechnic Institute
Dept. of Industrial Engineering
Blacksburg, VA 24061
Attn: Dr. H. L. Snyder   1

Honeywell, Inc.
Systems and Research Division
2600 Ridgway Parkway
Minneapolis, MN 55413
Attn: Dr. A. Kanarick   1

General Electric
Research and Development
Box 43
Schenectedy, NY 12301
Attn: J. E. Bigelow   1

Magnavox Company
Advanced Technology Group
Fort Wayne, IN 46804
Attn: Dr. C. Craighead   1

Kaiser Aerospace and Electronics
  Corporation
1651 Page Mill Road
P.O. Box 11275 Sta. A
Palo Alto, CA 94306
Attn: G. Carroll   1

IBM Watson Research Center
P.O. Box 218
Yorktown Heights, NY 10598
Attn: Ifay Chang   1

North Hills Electronics
Alexander Place
Glen Cove, NY 11542
Attn: S. Sherr   1

Xerox Corporation
Palo Alto Research Center
3333 Coyote Hill Road
Palo Alto, CA 94304
Attn: B. Kazan   1

Tektronix, Inc.
P. O. Box 500
Beaverton, OR 97005
Attn: A. Silzars   1
      C. Infante   1
      K. Considine   1

Sperry Flight Systems
2111 N 19th Ave.
M/S 109-C
Phoenix, AZ 85302
Attn: J. R. Trimmier   1

Northrop Electronics Division
2301 W. 120th Street
Hawthorne, CA 90250
Attn: Walt Goede   1

Westinghouse Electric Corp.
Research and Development Center
Pittsburgh, PA 15235
Attn: Dr. Peter Brody   1

Xerox Corporation
Webster Research Center
800 Phillips Road W114
Webster, NY 14580
Attn: J. B. Flannery   1

Lucitron, Inc.
1918 Raymond Drive
Northbrook, IL 60062
Attn: Alan Sobel   1

Boeing Commercial Airplane Co.
P. O. Box 3707
M/S 47-09
Seattle, WA 98124
Attn: A. F. Norwood   1

Harris Corporation
Electronic Systems Division
MS1/1821
P. O. Box 37
Melbourne, FL 32901
Attn: Terry Riley   1

Delco Electronics
Department 3210
7929 South Howell Ave.
Oak Creek, WI 53129
Attn: Earl Strandt   1

Hewlett Packard
1000 NE Circle Boulevard
Corvallis, OR 97330
Attn: Paul Van Loan   1

Aeronautical Systems Division
Air Force Systems Command
Wright-Patterson AFB, OH 45433
Attn: ASD/RW   1
       ASD/AERS   1

Sperry Univac DSD Research Lab
Univac Park
P. O. Box 3525 - UOP16
St. Paul, MN 55165
Attn: R. A. Erickson   1

Control Data Corporation
Research and Advanced Design Lab.
4290 Fernwood Street
Arden Hills, MN 55112
Attn: D. B. Bonstrom   1

Boeing Aerospace Company
Research and Engineering Division
P. O. Box 3999
Seattle, WA 98124
Attn: Crew Systems   1